Assembly of the Bacterial Flagellum

How *Salmonella* Exports Flagellar Proteins and Controls Hook Length

Dissertation

zur Erlangung des akademischen Grades des
Doktors der Naturwissenschaften (Dr. rer. nat.)

an der Universität Konstanz
Mathematisch-naturwissenschaftliche Sektion
Fachbereich Biologie

vorgelegt von
Marc Erhardt

Tag der mündlichen Prüfung: 07. April 2011

1. Referent: Prof. Dr. Winfried Boos, Universität Konstanz
2. Referent: Prof. Kelly T. Hughes, Ph.D., Université de Fribourg
3. Referent: Prof. Dr. Peter Kroth, Universität Konstanz

Table of Contents

List of Figures

List of Tables

Summary

Bacteria propel themselves through liquid environments using rotation of a propeller like organelle, the flagellum. Flagella are energized by the membrane ion gradient and enable bacteria to swim towards nutrients and away from harmful substances. This unique nanomachine shares structural and functional similarities to the needle-like injectisome complex that pathogenic bacteria employ to inject virulence factors into eukaryotic host cells. Bacterial flagella and injectisomes contain a specialized protein export system, termed 'type III secretion', that functions to deliver structural subunits and effector proteins to the outside of the cytoplasmic membrane. Type III secretion systems are made of multiple proteins, however, the function of individual subunits and the molecular mechanism of protein translocation is poorly understood.

The first part of this thesis reports that the flagellar type III secretion system functions as a proton-driven protein exporter and demonstrates that many components of the apparatus have a facilitating role and are dispensable for the actual protein translocation process. Treatment with a protonophore that disrupts the membrane proton gradient of the cell prevented export of flagellar substrates. In a mutant strain deleted for the flagellar-specific ATPase FliI, we observed weak swarming motility and rare formation of flagella. Hydrolysis of ATP had been considered to provide energy for protein translocation via the flagellar type III export apparatus but these findings demonstrate that flagellar secretion in *Salmonella enterica* requires the proton motive force while ATP hydrolysis is not essential.

For efficient export function of the flagellar type III secretion system, six integral membrane proteins (FliOPQR FlhAB), three soluble proteins (FliHIJ) and the rotor-switch complex (FliGMN) are needed. We sought mutants that allowed for export of a model substrate into the periplasm in the absence of the rotor-switch complex, the C-ring. We isolated mutants in known and unknown flagellar regulatory loci that resulted in at least two-fold increased expression of the flagellar master operon, *flhDC*. The increased *flhDC* expression coincided with elevated levels of hook-basal-body formation. These results indicate that the C-ring functions primarily as the rotor of the flagellum and provides a secondary, facilitating role during type III secretion as a affinity cup-like structure that enhances the specificity and efficiency of the export process.

We next measured export of a flagellar-specific model substrate in a battery of export-apparatus mutants. Export of a hook-β-lactamase fusion protein into the periplasm confers quantifiable ampicillin resistance. We found that the soluble components of the

flagellar type III secretion system, the cytoplasmic C-ring and the membrane protein FliO are dispensable for export. Overexpression of a single membrane protein, FliP, resulted in significant export of the reporter substrate, indicating that FliP forms the central channel of the secretion apparatus. Finally, we present the first molecular-level hypothesis for the organization and mechanism of the flagellar type III secretion system.

For efficient transmission of rotational energy from the flagellar basal-body to the rigid, extracellular filament, a flexible coupling structure is needed. The length of this flexible joint, the hook, is tightly controlled in *Salmonella enterica* by an intrinsic control mechanism. A molecular ruler, FliK, measures the length of the hook and transmits this information back to the FlhB component of the secretion apparatus at the base of the flagellum. Here, an interaction between the carboxy-terminus of FliK and FlhB induces a specificity switch in the flagellar type III secretion apparatus from secretion of rod-hook-type substrates to secretion of late substrates, including the filament subunits. Several models for the mechanism of length control have been proposed, including a 'static ruler' and a 'measuring cup', while failing to explain all published data on hook length control.

The second part of this thesis reports that FliK acts as an infrequent molecular ruler that is intermittently secreted during hook polymerization. We refuted the previous 'cup model' for flagellar hook length control by demonstrating normal hook length control in the absence of the rotor-switch complex that was thought to act as a 'measuring cup'. FliK deletion variants that were previously reported to control hook length without secretion were in fact secreted. By uncoupling hook polymerization from FliK expression, we demonstrated that secreted FliK immediately triggers the specificity switch if the ruler is secreted in elongated hooks greater than the physiological length. The probability of a productive interaction of FliK with FlhB, which results in the specificity switch, is an increasing function of hook length. The experimental hook length data displayed excellent agreement with a mathematical model of the Infrequent Ruler hypothesis. Finally, the velocity of FliK secretion correlated inversely with hook length, which provides a possible molecular mechanism for hook length control by FliK.

Deutsche Zusammenfassung

Bakterien benutzen die Rotation eines Propeller-ähnlichen Organelles, dem Flagellum, zur Fortbewegung in flüssiger Umgebung. Das Flagellum ermöglicht Bakterien zu Nährstoffen und weg von schädlichen Substanzen zu schwimmen. Die Rotation des Flagellums wird durch den Ionengradienten der Membran energetisiert. Das bakterielle Flagellum ist eine einzigartige Maschine im Nanomaßstab und vereint strukturelle und funktionelle Gemeinsamkeiten mit dem Injektisomkomplex von pathogenen Bakterien. Dieser Nadel-ähnliche Komplex wird von vielen Gram-negativen Bakterien verwendet um Virulenzfaktoren in eukaryontische Wirtszellen zu injizieren. Das Flagellum und der Injektisomkomplex beinhalten beide ein spezielles Proteintransportsystem, das sogenannte 'Typ III Sekretionssystem'. Dieser Transportapparat transportiert strukturelle Untereinheiten und Virulenzfaktoren über die Barriere der inneren Membran nach aussen. Typ III Sekretionssysteme sind aus mehreren Untereinheiten aufgebaut, aber über die Funktion einzelner Untereinheiten und den molekularen Mechanismus des Proteintransports ist wenig bekannt.

Der erste Teil dieser Dissertation zeigt, dass Proteintransport durch das Typ III Sekretionssystems des Flagellums unter Zuhilfenahme des Membran-Protonengradienten ermöglicht wird und dass viele Untereinheiten des Transportssystems nicht für den eigentlichen Transportprozess nötig sind, sondern eine unterstützende Funktion inne haben. Proteintransport durch das Typ III Sekretionssystem wurde durch Zugabe eines Protonophors inhibiert. Deletionsmutanten der Flagellum-spezifischen ATPase FliI waren begrenzt zur Fortbewegung fähig und bildeten manchmal komplette Flagellen. Bislang wurde davon ausgegangen, dass die Hydrolyse von ATP die Energie für den Proteintransport bereitstellt. Unsere Ergebnisse zeigen jedoch, dass der Protonengradient und nicht Hydrolyse von ATP für den Proteintransport durch das Typ III Sekretionssystem des Flagellums nötig ist.

Das Typ III Sekretionssystem des Flagellums benötigt sechs Membranproteine (FliO, FliP, FliQ, FliR, FlhA, FlhB), drei cytoplasmatische Proteine (FliH, FliI, FliJ) und einen cytoplasmatischen Ring (FliG, FliM, FliN) für effizienten Proteintransport. Wir führten eine positive Selektion für Mutanten durch, die in der Lage waren auch ohne den cytoplasmatischen Ring, den sogenannten C-Ring, ein Modelsubstrat in das Periplasma zu sekretieren. Wir fanden Mutationen, die in bekannter oder unbekannter Weise Einfluss auf die Genexpression des Flagellums haben. Alle Mutationen führten dazu, dass das Operon des Hauptregulator des Flagellums, *flhDC*, mindestens doppelt so stark exprim-

iert wurde. Die verstärkte Expression des Hauptregulators führte zur erhöhten Bildung von Basalkörpern des Flagellums. Zusammengenommen weisen diese Ergebnisse darauf hin, dass der cytoplasmatische C-Ring hauptsächlich als Drehkörper des Flagellums fungiert. Eine sekundäre, unterstützende Funktion des C-Rings wäre die Bereitstellung einer Affinitätsbindestelle für Exportsubstrate des Typ III Sekretionssystems.

In einem weiteren Schritt erfassten wir die Transportskapazitäten von einer Vielzahl von Mutanten des Typ III Sekretionssystems des Flagellums. Quantifizierbare Ergebnisse lieferte der Transport eines Modelsubstrates bestehend aus einer Fusion des flagellären FlgE-Proteins als Sekretionssignal und der β-Laktamase. Nur wenn dieses Fusionsprotein in das Periplasma transportiert wurde, waren die Bakterien gegen Ampicillin resistent. Mit dieser Methode konnten wir zeigen, dass die cytoplasmatischen Komponenten des Typ III Sekretionssystems, der C-Ring des Flagellums und das Membranprotein FliO nicht für den Proteintransport essentiell sind. Die Überexpression eines einzelnen Membranproteins des Typ III Sekretionssystems, FliP, ermöglichte signifikanten Transport des Modellsubstrates. Dies deutet darauf hin, dass FliP den zentralen Kanal des Transportsystems bildet. Diese Ergebnisse ermöglichen es uns eine Hypothese über die Organisation und Funktion des Typ III Sekretionssystems des Flagellums auf molekularer Ebene vorzuschlagen.

Ein flexibles Gelenkstück verbindet den Basalkörper des Flagellums mit dem starren Filament ausserhalb der Zelle. Dieses Gelenkstück ist nötig für eine effiziente Übertragung der Rotationsenergie. Die Länge des Gelenkstücks wird in *Salmonella enterica* durch spezifische Mechanismen genau kontrolliert. Ein molekulares Maßband, das Protein FliK, misst die Länge des Gelenkstücks und überträgt diese Information an FlhB, welches Bestandteil des Typ III Sekretionssystems des Flagellums in der cytoplasmatischen Membran ist. Eine Interaktion zwischen dem Carboxy-Ende von FliK und FlhB induziert einen Wechsel in der Erkennungsspezifität des Typ III Sekretionssystems. Dieser Wechsel führt dazu, dass nicht mehr Komponenten des Basalkörpers, sondern sogenannte 'späte' Substrate, wie zum Beispiel die Untereinheiten des Filaments, transportiert werden. In der Literatur wurden mehrere Modelle über den Mechanismus der Längenkontrolle des Gelenkstück vorgeschlagen, die allerdings nicht alle publizierten Sachverhalte befriedigend erklären können.

Im zweiten Teil dieser Dissertation zeigen wir, wie die Länge des flagellären Gelenkstücks durch das molekulare Maßband FliK festgelegt wird. FliK wird hierbei konstant, aber abwechselnd mit FlgE-Untereinheiten des Gelenks während dessen Aufbaus sekretiert und legt die Länge des Gelenkstücks durch einen statistischen Mechanismus fest. Unsere Ergebnisse widerlegen ein früheres Modell, wonach der C-Ring als Becher fungiert und ein Becher voller FlgE-Untereinheiten die Länge des Gelenkstücks festlegt. Wir überprüften dieses Model, indem wir die Länge des Gelenkstücks in einer Mutante untersuchten, die keinen C-Ring mehr produziert. Die Länge des Gelenkstücks des Flagellums in dieser Mutante war jedoch vergleichbar mit dem Wildtyp. Ein anderes Model besagte, dass FliK die Länge des Gelenkstücks im Cytosol reguliert, weil bestimmte Deletionsmutanten von FliK zwar zu einer Verringerung der Länge des Gelenks führten, aber anscheinend nicht nach aussen transportiert wurden. Wir konnten jedoch zeigen, dass

diese Deletionsmutanten instabil waren, aber dennoch nach aussen sekretiert wurden. Indem wir die Biosynthese des Gelenks von der Expression von FliK abkoppelten, waren wir weiterhin in der Lage unser Modell eines unregelmässig sekretierten, molekularen Maßbands zu beweisen. In Abwesenheit von FliK wird die Biosynthese des Gelenkstücks weit über die physiologische Länge fortgesetzt. Wir konnten zeigen, dass jedoch in diesem Fall der erstmalige Export von FliK sofort den Wechsel in der Sekretionsspezifität auslöst. Dies ist konsistent mit unserem Modell, wonach die Wahrscheinlichkeit einer erfolgreichen Interaktion zwischen FliK und FlhB eine ansteigende Funktion der Länge des Gelenkes ist. Unsere Messungen der Gelenklänge zeigten weiterhin eine hervorragende Übereinstimmung mit einem mathematischen Modell des hier vorgeschlagenen Mechanismus, welcher ein unregelmässig sekretiertes, molekularen Maßband vorschlägt. Zum Schluss schlagen wir einen potentiellen, molekularen Mechanismus vor, der beschreibt wie FliK in der Lage ist die Länge des Gelenkstücks zu kontrollieren. Bei diesem Modell bestimmt die Geschwindigkeit mit der FliK sekretiert wird, ob es zu einer erfolgreichen Interaktion mit FlhB kommt. Wir zeigen in dieser Arbeit, dass die Geschwindigkeit der FliK Sekretion invers mit der Länge des Gelenkstücks korreliert.

Dans la vie, rien n'est à craindre,
tout est à comprendre.[†]

[†]Marie Curie, 1867-1934

Introduction

Bacteria swim through liquid environments by rotating a rigid, helical organelle, the flagellum (18) (Figure 1). The flagellum enables bacteria to swim towards nutrients and away from harmful substances, a process known as chemotaxis (3). The flagellum is a sophisticated, molecular nanomachine made of about 25 different proteins. Flagellar synthesis is a highly regulated and coordinated process. To build a flagellum, more than two dozens proteins need to assemble in an ordered process. The accurate size and subunit composition of each sub-structure of this nanomachine is achieved by coordinated expression of flagellar genes during assembly and by other mechanisms that regulate the export of specific subunits (27, 91, 115, 151).

Evolutionary related to the flagellum is the type III injectisome, an organelle that allows Gram-negative bacteria to deliver effector proteins into eukaryotic host cells (32, 33, 55, 56). Common features of both the flagellum and the injectisome include a specific type III secretion system that is responsible for the export of most extracellular components through these machines and an intrinsic length-control mechanism that determines the length of the flagellar hook and injectisome needle.

Structure and assembly of the bacterial flagellum

The flagellum of *Salmonella enterica* is composed of three distinct sub-structures: i) the basal body as the rotary motor that traverses both cell membranes and houses the flagellar specific type III export apparatus (18, 173); ii) a flexible, universal joint, called the hook that couples the rotary motor to; iii) the rigid filament that functions as the propeller (38, 39) (Figure 2A).

Assembly of the flagellum initiates with the formation of the MS-ring (made of approximately 26 copies of FliF) in the inner membrane, followed by attachment of the

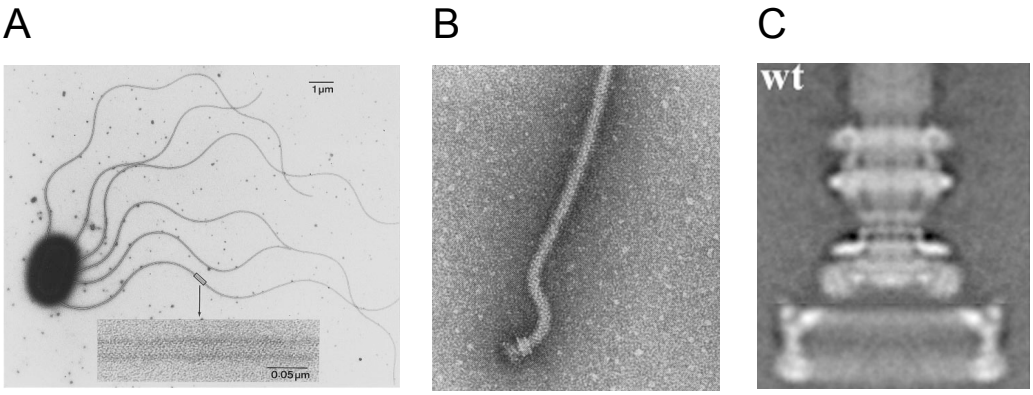

FIGURE 1

The bacterial flagellum. (A) Electron micrograph of negatively-stained *Salmonella typhimurium*. The magnified section shows a short segment of the flagellar filament. Image adapted from (151). (B) Isolated hook-basal-body with attached filament. The C-ring dissociated from the hook-basal-body during purification. Image adapted from (67). (C) Averaged electronmicroscopic image of basal bodies with attached C-ring. Image adapted from (187).

rotor/switch complex (FliG, FliM and FliN) at the cytoplasmic face of the MS-ring with an approximate stoichiometry of 25 (FliG), 34 (FliM) and 110 (FliN) copies, respectively (213, 214). The rotor/switch complex or C-ring forms a cup-like ring structure at the base of the organelle (19) (Figure 3). While the C-ring complex has been traditionally described as a static structure, recent evidence shows that its components can be highly dynamic and exchange constantly with cellular protein pools. In the flagellar system, FliM undergoes rapid turnover that is dependent on the presence of phosphorylated CheY, indicating that turnover is involved in the mechanism of motor-switching (37). FliG is known to interact with the MS-ring protein FliF and the stator proteins MotA and MotB (50, 101, 113), FliM is involved in the switching between clockwise and anticlockwise rotation by binding to phosphorylated CheY (189) and the FliN tetramer participates in rotation and switching (159), and provides binding sites for the cargo-delivery complex $FliH_2IJ$ (60, 127). The flagellar-specific type III secretion apparatus (consisting of FlhA, FlhB, FliH, FliI, FliJ, FliO, FliP, FliQ, FliR) is thought to assemble within the central pore of the MS-ring at the base of the basal body (5) and facilitates the proton motive force (PMF) dependent export of most extra-cytoplasmic components of the organelle (140, 158). Secretion through the flagellar filament occurs through a narrow channel with a diameter of approximately 2.5 nm (209), implying that substrates are translocated in an unfolded or partially folded state.

Rod, hook and filament subunits secrete through the narrow channel of the flagellum and self-assemble at the growing tip of the structure with the help of capping proteins. The rod cap FlgJ is an muramidase that digests the peptidoglycan layer to permit assembly of the rod structure (64). FlgD forms the cap for hook polymerization (154) and five FliD molecules assemble at the tip of the filament to form an annular pentameric cap structure with flexible leg domains that promotes flagellin self-assembly by a cap

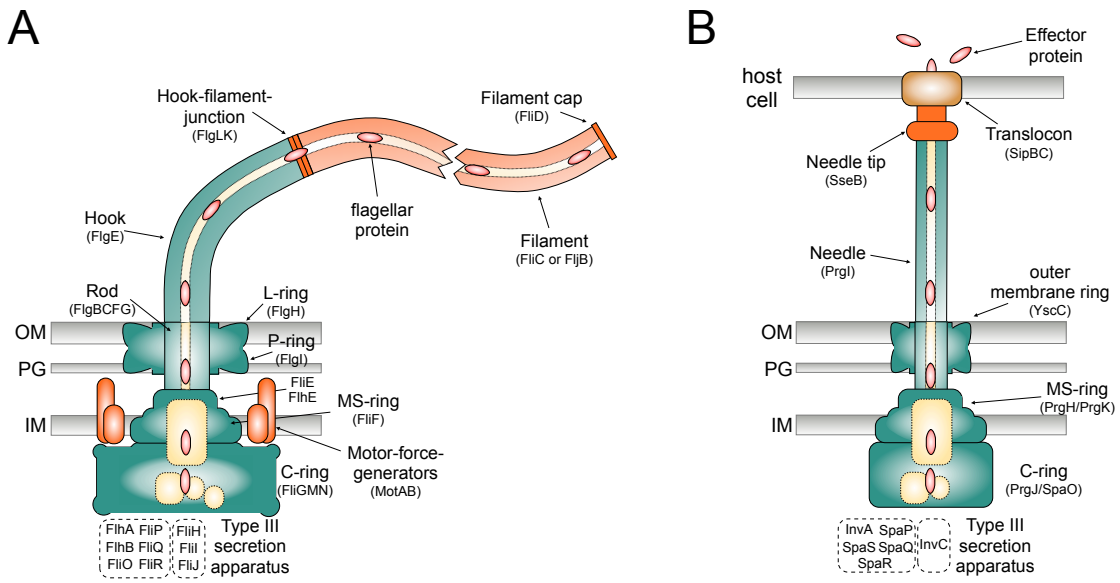

FIGURE 2

Schematic structure of the bacterial flagellum and type III injectisome. (A) Schematic overview of the bacterial flagellum. The structure of the flagellum consists of three parts: i) a basal body with a flagellar-specific type III secretion system within the inner membrane ring; ii) a flexible hook acting as a universal joint to iii) the rigid filament. Dashed boxes illustrate proteins with functions in flagellar type III secretion. Shaded in green are structural parts of the hook-basal-body and shaded in red are structural parts assembled after hook-basal-body completion. OM = outer membrane; PG = peptidoglycan; IM = inner membrane. (B) Schematic overview of the type III injectisome of *Salmonella*. Many components of the flagellum and injectisome are structurally and/or functionally related. The structure of the injectisome is divided in three main parts: i) the basal body with the type III secretion apparatus within the inner membrane ring; ii) a straight needle connecting the secretion system to iii) the translocon complex that forms a pore in the membrane of eukaryotic host cells. Shaded in green are structural parts of the needle complex and shaded in red are intermediate and late substrates (tip, translocon and effector proteins).

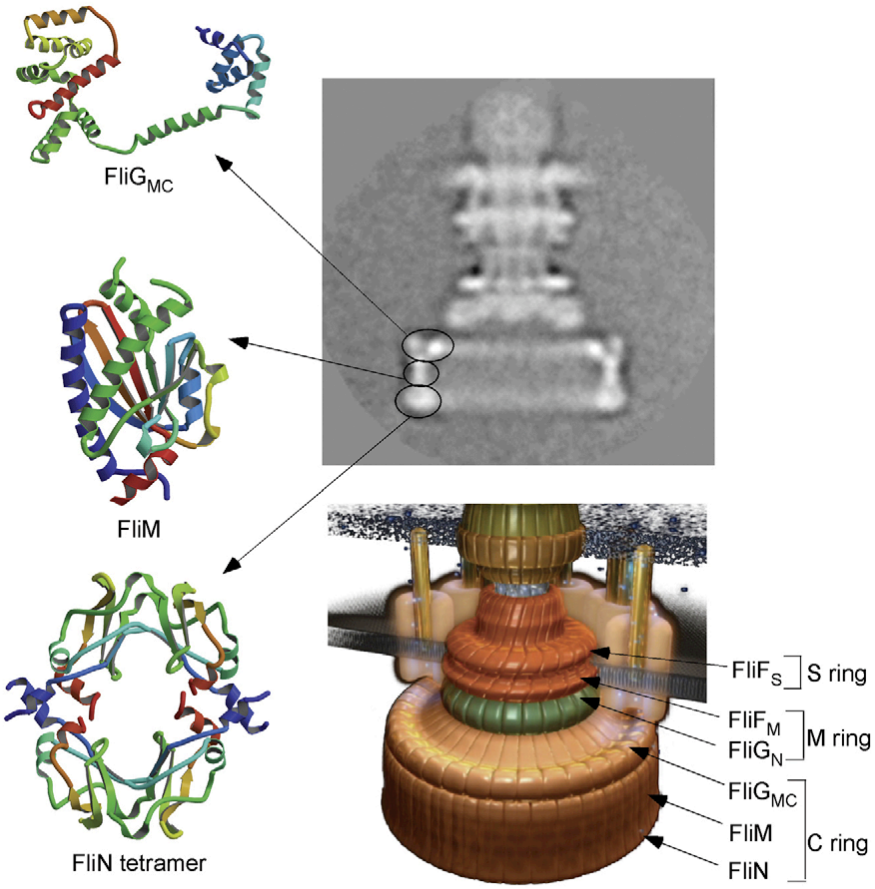

FIGURE 3

Structure of the C-ring. Left panel: Crystal structures of FliG$_{MC}$, the middle and C-terminal domains of FliG (top), FliM (middle), and the FliN tetramer (bottom). Upper right panel: Averaged cyro-electronmicroscopic image of a basal body complex in side view. Presumed locations of FliG, FliM and FliN are indicated. Lower right panel: Model for subunit organization in the MS- and C-ring. Figure adapted from (134).

rotation mechanism (208).

After assembly of the MS-ring and the type III secretion apparatus, the rod components FliE, FlgB, FlgC, FlgF (proximal rod) and FlgG (distal rod) secrete and assemble progressively as the next structural feature of the flagellum (144). The rod acts as a driveshaft that extends from the motor through the peptidoglycan layer to the outer membrane. While the distal rod protein FlgG is capable of continuous polymerization similar to the hook and filament, rod length seems to be controlled by an intrinsic stacking mechanism that only allows assembly of two stacks of FlgG terminating rod length at 22.5 nm (183). A bushing complex, made of the P-ring protein FlgI and the L-ring lipoprotein FlgH, then assembles around the distal rod and forms a pore in the outer membrane. FlgI and FlgH are not exported by the flagellar type III secretion system but via the Sec secretion pathway (70).

Upon completion of the rod and the PL-rings, the hook (composed of approximately 120 subunits of FlgE (91)) assembles to an approximate length of 55 nm, which is controlled by the molecular ruler FliK (67, 157). An interaction of the C-terminal domain of FliK with the FlhB component of the secretion apparatus flips a switch in secretion specificity from rod-hook-type substrates to late (filament)-type substrates (49, 130, 198). This switch in secretion specificity results in export of the anti-σ^{28} factor FlgM (73), which allows for σ^{28}-dependent expression of flagellar genes needed late in assembly (69). The last step of flagellar assembly is the polymerization of the filament that is made of as many as 20,000 subunits of a single protein (FliC or FljB in *Salmonella*) (27, 115), representing a significant amount of the cell's biosynthetic resources. The flagellar propeller assembles to about 10 µm length, yet is only 12 - 24 nm in diameter.

The stator complex proteins MotA and MotB mediate rotation of the flagellum. The stator complex assembles in the inner membrane and attaches non-covalently to the peptidoglycan layer via the C-terminal periplasmic domain of MotB (29, 180). The FliG component of the rotor interacts with MotA (113), which also forms the pathway for proton influx (21). Together, the stator (MotAB) and the rotor (C-ring) form the flagellar motor, whose rotation is energized by the proton motive force (27, 115). This rotary machine turns at hundreds of revolutions per second, utilizing both $\Delta\Psi$ and ΔpH (123, 126).

The flagellar transcriptional hierarchy

Flagellar gene expression is coupled to assembly of the flagellum in all bacteria where it has been studied. In gram-negative enteric bacteria the flagellar regulon includes more than 60 genes (54). In *Salmonella* these genes are organized into a transcriptional hierarchy of three promoter classes that are temporally regulated in response to the assembly state of the flagellar structure (80) (Figure 4).

At the top of the transcriptional hierarchy is a single Class I promoter that controls the fundamental decision whether and when to produce flagella. The Class I promoter transcribes the *flhDC* operon that encodes for the $FlhD_4C_2$ activator complex (197). Many

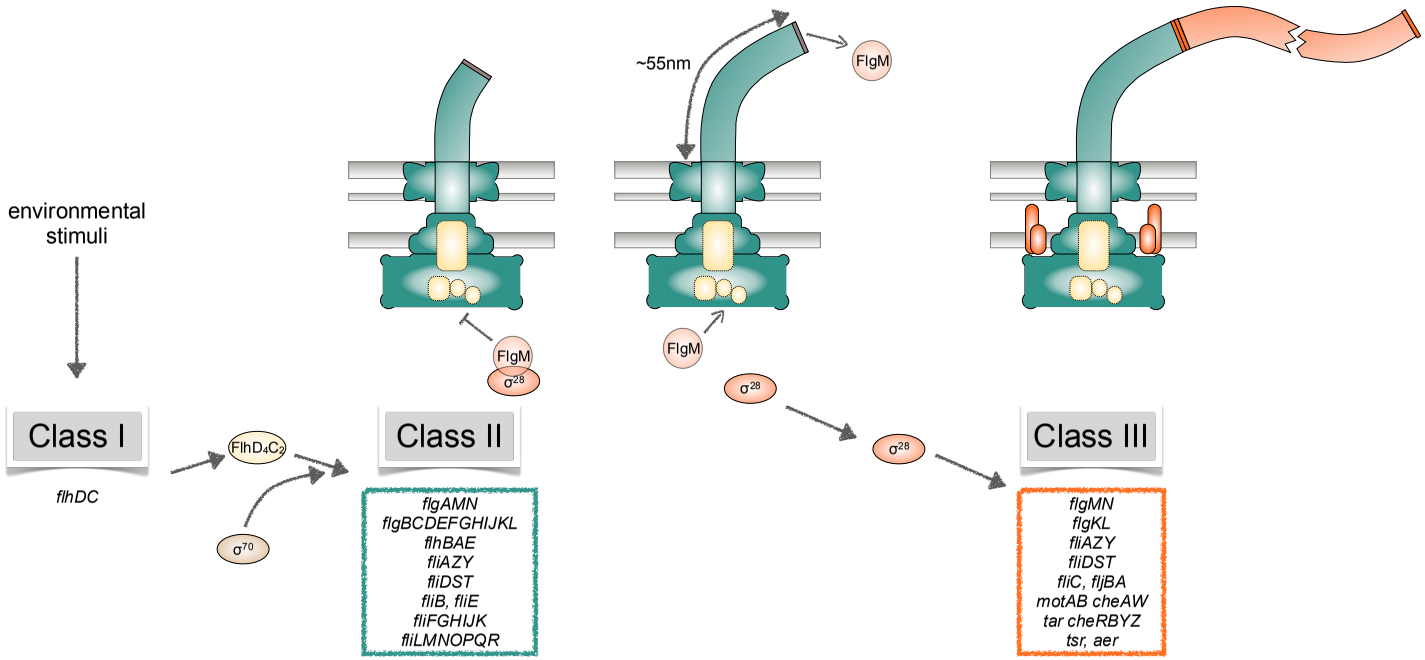

FIGURE 4

Schematic outline of the flagellar transcriptional hierarchy of *Salmonella*. The flagellar transcriptional hierarchy of *Salmonella enterica* is composed of three classes of promoters. The Class I promoter responds to a variety of environmental stimuli (see text for details) and transcribes the genes encoding for the master regulator of the flagellar transcriptional hierarchy, the $FlhD_4C_2$ complex. $FlhD_4C_2$ together with σ^{70} directs RNA polymerase to transcribe from Class II promoters. These genes encode structural components of the hook-basal-body complex (shaded in green), as well as regulatory proteins like the alternative, flagellar-specific σ-factor, σ^{28}, and its cognate anti-σ factor, FlgM. The hook-basal-body is completed as soon as the hook reaches an approximate length of 55 nm, upon which the molecular ruler FliK induces a switch in secretion specificity in the type III secretion apparatus to late-substrate secretion. The late substrate FlgM is exported out of the cell thus freeing σ^{28} to turn on transcription from Class III promoters. Class III gene products include the filament subunits, motor-force generators and the chemotactic system (shaded in red).

environmental signals are integrated at the level of the Class I promoter. For example more than ten DNA-binding proteins affect transcription of the *flhDC* operon. Chapter 2 extensively describes the factors and signals involved in activation or repression of the *flhDC* operon.

The heteromultimeric $FlhD_4C_2$ complex promotes σ^{70}-dependent transcription of Class II promoters (111). Genes transcribed from Class II promoters encode the structural components of the hook-basal-body complex, as well as regulatory proteins like the flagellar-specific σ-factor, σ^{28}, which is required for transcription from Class III promoters, and its cognate anti-σ factor, FlgM. Completion of the hook-basal-body is signaled by an interaction of the molecular ruler FliK and the FlhB component of the secretion apparatus, thereby inducing a flip in secretion specificity from rod-hook-type to late-substrate secretion (130). The anti-σ factor FlgM is then secreted from the cell as a late substrate. σ^{28} also functions as a type III secretion chaperone to facilitate FlgM secretion (11). The secretion of FlgM releases σ^{28} to initiate Class III promoter transcription (73). Class III genes encode the filament subunits, motor force generators and chemotaxis proteins. The σ^{28}/FlgM regulatory feedback system allows the cell to sense the completion of a functional hook-basal-body structure. While an advantage of this regulatory loop has not been determined experimentally, secretion of FlgM provides feedback to the flagellar transcriptional hierarchy, about when to start synthesis of filament subunits.

Another layer of regulation of flagellar gene expression occurs at the level of $FlhD_4C_2$ expression and activity. The $FlhD_4C_2$ complex is an auto-inhibitor of *flhDC* operon transcription (103), which likely occurs through $FlhD_4C_2$-dependent activation of a DNA-binding repressor of *flhDC* (203). FliT, the type III secretion chaperone of the filament cap FliD, binds to the $FlhD_4C_2$ complex and inhibits $FlhD_4C_2$-dependent activation of Class II promoters (206). Upon secretion of FliD as a late substrate, FliT is free to inhibit Class II transcription.

The hierarchy of flagellar gene expression in the process of flagellum assembly could be envisaged as follows. Class I transcription produces $FlhD_4C_2$, which activates Class II transcription and is the auto-inhibitor of Class I transcription. After hook-basal-body completion, FlgM and FliD are removed, freeing σ^{28} to transcribe Class III promoters and FliT to inhibit $FlhD_4C_2$, thus preventing it from auto-repression. This would allow for restoration of Class I transcription and re-initiation of a new round of flagellar gene expression. Therefore, the coupling of flagellum assembly and hook-basal-body completion to flagellar gene regulation allows for a hierarchical succession of the flagellar transcriptional cycle, where initiation of Class III gene expression coincides with re-initiation of a new round of hook-basal-body formation with the activation of Class I transcription.

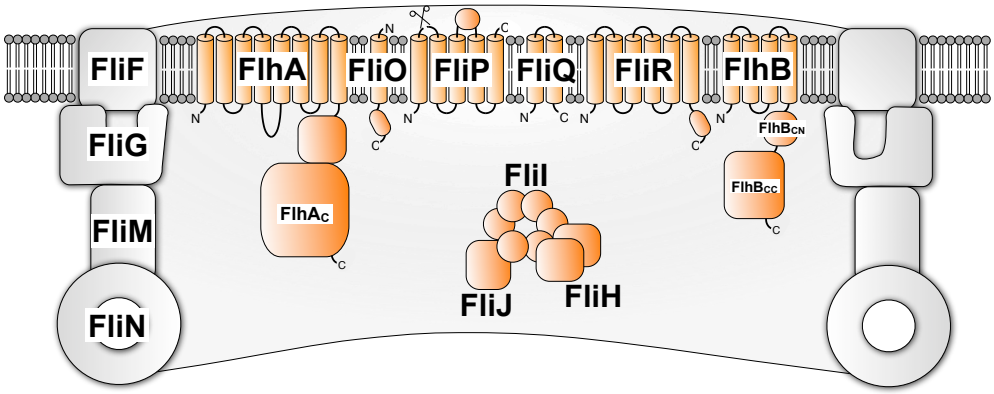

FIGURE 5

Schematic overview of components of the flagellar type III secretion apparatus of *Salmonella*. The flagellar type III secretion system of *Salmonella* consists of six integral membrane proteins; FlhA, FlhB, FliO, FliP, FliQ and FliR. The membrane components of the secretion apparatus are believed to assemble within a scaffold made of FliF, the MS-ring. The most probable number and topology of trans-membrane segments are indicated. FliI, the flagellar-specific ATPase, FliH, the regulator of FliI and FliJ, a general chaperone, are soluble components of the type III secretion system and make up the cargo-delivery complex. FliI forms a heterotrimer together with the homodimer FliH in the cytoplasm. It is presumed that after docking to the membrane components of the apparatus, FliI forms a functional hexamer. It is possible that ATP-hydrolysis by FliI provides energy for one or more steps in substrate delivery, such as disassembly or release of the substrate from the cargo-delivery complex. The actual protein translocation through the secretion apparatus is dependent on the proton motive force and substrates have to be secreted in an unfolded state through a narrow channel of about 2 nm in diameter.

The flagellar type III secretion apparatus

Many structural components of the flagellum assemble outside of the cytoplasmic membrane and must therefore be exported. With the exception of the P- and L-ring components, the flagellar-specific type III secretion apparatus exports at least 12 proteins. The export apparatus is believed to assemble within the MS-ring at the base of the flagellar basal body and consists of six integral membrane proteins (FlhA, FlhB, FliO, FliP, FliQ, FliR) and three cytoplasmic proteins (FliH, FliI, FliJ) (136). All components are essential for the export of rod-type, hook-type and filament-type secretion substrates (133, 136) (Figure 5).

FliH, FliI, and FliJ form the cargo-delivery complex that is thought to facilitate delivery and unfolding of secretion substrates prior to export. FliI is an ATPase (47) that forms a hexameric ring-shaped structure (30) and presumably couples ATP hydrolysis to some energy-utilizing step(s). FliI was initially thought to energize the transmembrane transport process, but other studies indicate that ATP hydrolysis energizes steps in substrate delivery instead, probably facilitating the unfolding of the substrate and its release from the cargo-delivery complex (9). Recent findings showed that the proton motive force energizes the actual transport process and does not require the ATPase FliI *per se* (140, 158). The two other components of the cargo delivery complex are the homodimer FliH, which regulates the ATP-hydrolyzing activity of FliI, and FliJ, a general chaperone for flagellar secretion substrates (136).

The integral membrane components FliOPQR of the export apparatus are relatively small (FliO, 13.1 kDa; FliP, 26.8 kDa; FliQ, 9.6 kDa; FliR, 28.9 kDa) and are predicted to have one to eight membrane spanning helices. Figure 5 depicts the likely orientation and the most probable number of trans-membrane helices of the membrane components of the flagellar secretion system. Little is known about possible functions of FliO, FliP, FliQ and FliR, respectively, however the proteins are required for export of early and late substrates (136). FlhA and FlhB are integral membrane proteins (75 kDa and 42 kDa, respectively) with large cytoplasmic domains that interact with the cargo delivery complex, $FliH_2IJ$ (138). The FlhB component controls the switch in substrate specificity that results in export of late structural subunits upon completion of the hook-basal-body complex (49). Although the major players in export have probably all been identified, the molecular mechanism of flagellar type III secretion is still poorly understood. A reasonable, general proposal for the mechanism is that $FliH_2IJ$ complexes bind to substrate proteins, shuttle the substrates to the base of the growing flagellar structure and present the unfolded substrates to the membrane-bound export apparatus for efficient PMF-dependent secretion (27). Translocation of the substrate across the inner membrane and into the channel uses energy from the electrochemical potential gradient of protons, the membrane potential $\Delta\Psi$ and the proton gradient ΔpH (140, 158). The export process itself is remarkable fast. About 10,000 amino acid residues per second are exported at early stages of filament assembly (74). In case of the type III injectisome, several thousand molecules of the effector protein SipA are transferred into a eukaryotic host cell within minutes (170).

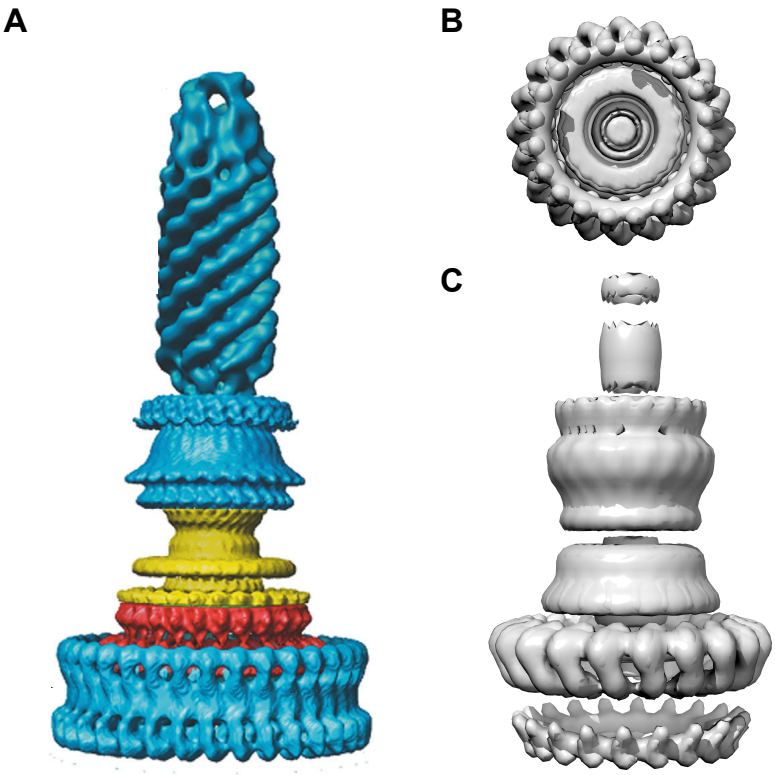

FIGURE 6

Electron micrograph reconstructions of basal-bodies of the flagellum and type III injectisome of *Salmonella*. (A) Structure of the flagellar hook-basal-body complex based on 3D-EM image reconstructions (40). (B, C) Surface renderings of the type III injectisome basal-body and needle structure based on 3D-EM reconstruction data from EmDep Database accession number EMD1100 (124). (B) View of the injectisome basal body complex from the cytoplasm and (C) side-view of the injectisome basal-body with attached needle. Figure adapted from (45).

Structural and functional similarities of the flagellum and type III injectisome

The bacterial flagellum and type III injectisome of Gram-negative pathogenic bacteria are evolutionary related on structural and functional levels. While the flagellum is an organelle used for locomotion of bacteria, the type III injectisome translocates virulence-effector proteins into eukaryotic host cells (22, 32, 56, 79, 98). The injectisome family is found in many Gram-negative plant and animal pathogens, including *Salmonella* sp., *Yersinia* sp., enteropathogenic *Escherichia coli* (EPEC), *Shigella* sp., *Chlamydia* sp., and *Erwinia carotovora* (22, 56). The injected effector proteins have diverse effects on the host cell, including alteration of host-cell functions and membrane cytoskeletons to promote invasion, survival, and growth of the bacterium, or the facilitation of symbiosis.

Electron micrographs of the injectisome and the flagellum reveal remarkable structural similarities (Figure 6): i) a basal, cylindrical structure that spans the inner and outer membrane and contains the type III secretion apparatus; ii) an extracellular, hollow tubular structure, the so-called needle (32, 185). These extracellular appendages have different structures and lengths, depending on the family of injectisomes; for example, a stiff needle with an approximate length of 58 nm in *Yersinia enterocolitica*, a filament with a length up to 600 nm in enteropathogenic *Escherichia coli*, or a Hrp pilus with a length of several µm in *Pseudomonas syringae* (32). The main differences between the structures of the flagellum and injectisome are the diameter of the cytoplasmic ring, which is significantly wider in the flagellar basal body (approximately 40 nm (115)) compared to the ring of the injectisomes (approximately 20 nm (68, 124)), and the lack of a C-ring-like structure in case of the injectisome.

Similar to the assembly process of the flagellum, the injectisome complex also assembles in a sequential manner (193). The basal body of the injectisome includes a specific type III secretion system that exports extra-cytoplasmic components of the injectisome structure and effector proteins. In addition to structural resemblance, many of the constituent proteins are conserved in both systems (Table 1). In *Salmonella*, the inner ring proteins PrgH and PrgK are homologous to the flagellar MS-ring protein FliF (90, 100). The flagellar C-ring (FliGMN) attaches to the MS-ring on the cytoplasmic face and while an attached C-ring-like structure is missing in EM images of the injectisome complex, the YscQ family shares significant similarity to FliN and FliM (32).

A protruding rod structure assembles on top of the MS-ring in the flagellar basal body, and it has been suggested that the inner rod of the *Salmonella* injectisome is composed of PrgJ (100, 124). As it is the case in the flagellar system, a pair of rings formed by proteins of the YscC family are associated with the peptidoglycan layer and the outer membrane in the injectisome (96, 100). Most components of the type III secretion apparatus are also conserved in sequence or function in both systems (22, 32, 98, 117). The integral membrane proteins YscR, YscS, YscT, YscU, and YscV are located within the inner membrane ring of the injectisome and share high sequence homology to the inner membrane proteins FliP, FliQ, FliR, FlhA and FlhB of the flagellar type III secretion apparatus (Table 1). Protein export in both the injectisome and flagellar

TABLE 1

Comparison of structurally and/or functionally related components of the flagellum and injectisome.

The table lists structurally and/or functionally related components of the flagellum and injectisome systems of *Salmonella enterica*, *Yersinia* ssp., *Shigella* ssp., and enteropathogenic *Escherichia coli*. T3S, type III secretion component. Table adapted from (45).

Flagellum (*S. enterica*)	**Injectisome** (*S. enterica* SPI-1)	**Injectisome** (*Yersinia* ssp. Ysc)	**Injectisome** (*Shigella* ssp.)	**Injectisome** enteropathogenic *E. coli* EPEC	**Structure/ Function**
FliF	PrgH/PrgK	YscJ	MxiJ	MxiJ	inner-membrane ring - MS-ring
FliI	InvC	YscN	Spa47	EscN	ATPase
FliJ		YscO			T3S chaperone
FliGMN	PrgJ/SpaO	YscQ	Spa33		cytoplasmic ring - C-ring (HrcQ in *Pseudomonas*)
FliP	SpaP	YscR	Spa24		T3S apparatus inner-membrane protein
FliQ	SpaQ	YscS	Spa33		T3S apparatus inner-membrane protein
FliR	SpaR	YscT	Spa29		T3S apparatus inner-membrane protein
FlhA	InvA	YscV	MxiA		T3S apparatus inner-membrane protein
FlhB	SpaS	YscU	Spa40		T3S apparatus inner-membrane protein
N/A	InvG	YscC	MxiD		outer-membrane ring
FlgE?	PrgI	YscF	MxiH	EscF	extracellular needle
N/A	SipBC	YopBD	IpaBC	EsoBD	translocation pore
FliC?	SseB	LcrV	IpaD	EspA	needle extension
FliH?		YscL	MxiN		ATPase regulator
FliK	InvJ	YscP	Spa32		hook/needle length regulator

secretion systems depends on the proton motive force (140, 158, 200). At the base of the injectisome complex, the hexameric ATPase of the YscN family shares striking similarity to the flagellar ATPase FliI (76, 211). The *Salmonella* homolog InvC energizes the secretion substrate release from its cognate cytoplasmic chaperone (9), suggesting a function of the type III secretion ATPase that is independent from the actual transport process.

Based on the fact that flagellar type III secretion systems are present in both Gram-positive and Gram-negative bacteria, it has been proposed that type III secretion required for Gram-negative pathogenesis evolved from flagellar-specific type III secretion (72, 117). Recent phylogenetic studies, however, indicate that both flagellar and injectisome type III secretion systems share a common ancestor (62).

Analogous to the flagellar hook and filament structure, the extracellular components of the *Yersinia* injectisome are exported by the membrane-embedded export apparatus. Three extracellular structures can be distiguished: i) a straight needle; ii) a needle-extension forming the tip complex; and iii) the translocation pore that presumably forms a channel in the eukaryotic host cell membrane. The injectisome needle polymerizes into a filamentous structure and consists of approximately 100 - 150 molecules of the YscF protein (32, 100). The molecular ruler YscP controls length of the needle structure to about 58 $\pm$ 10 nm in *Yersinia* (78). At the distal end of the needle, LcrV forms the tip complex (36, 148). It has been suggested that the tip complex forms a scaffold for the assembly of the translocator pore consisting of YopB and YopD, which inserts into the membrane of host cells (32).

Models for determination of hook length in *Salmonella*

When the flagellar hook reaches 55 nm length (67), an interaction between FliK and the FlhB component of the flagellar type III secretion apparatus induces a switch in secretion specificity from early to late substrate secretion (48, 104, 130, 137, 201). This flip in secretion specificity results in export of the anti-σ^{28} factor FlgM, freeing σ^{28} to turn on Class III gene expression as discussed above (73).

Without control of length, hook polymerization continues beyond the physiological length of 55 nm, resulting in a wide length distribution of hooks, called polyhooks. The uncontrolled hook growth coincides with a failure of the export apparatus to flip the secretion specificity switch. Thus, the length of the external hook determines when FliK induces the switch in secretion substrate specificity.

As mentioned, the switch in secretion specificity requires an interaction between FliK and the FlhB component of the export apparatus. Control of hook length is lost in mutant strains defective for the *fliK* gene (157). In addition, the FlhB component has to autocleave its C-terminal cytoplasmic domain between amino acid residues N269 and P270 in order for the substrate specificity switch to occur (48, 137). Mutations of N269 and P270 in FlhB are defective in cleavage of the C-terminal domain (53).

The fundamental question was how the length of the external hook is sensed and signaled back to the secretion apparatus in the inner membrane. Several models of how

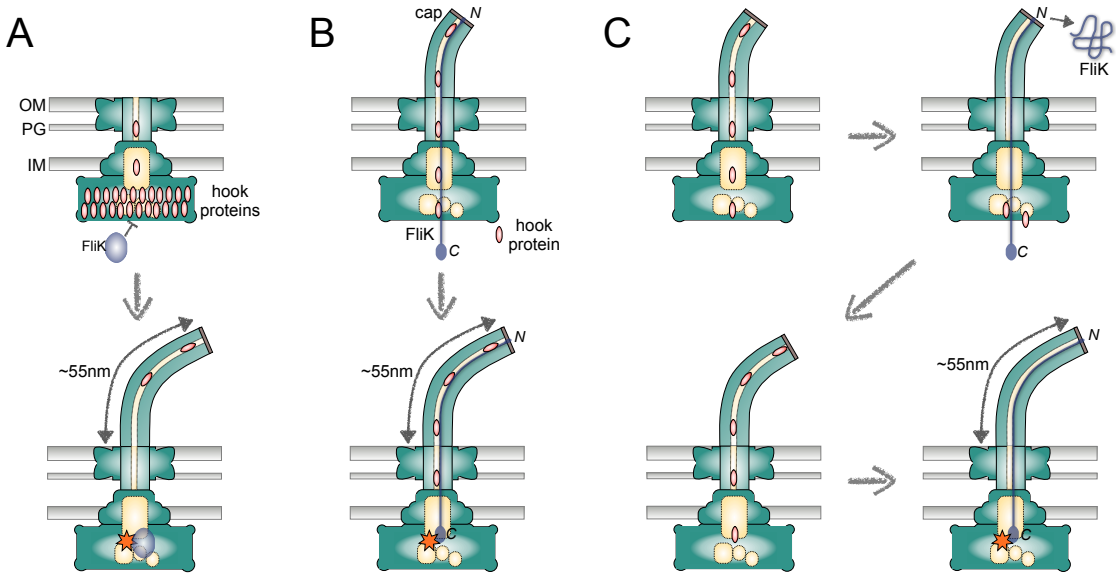

FIGURE 7

Models for control mechanisms of flagellar hook length. (A) The 'Measuring Cup' model. The C-ring functions as a measuring cup that is filled with the appropriate number of hook subunits necessary to build a hook of physiological length and thereby prevents a premature FliK interaction with the secretion apparatus. (B) The 'Static Ruler' model. FliK acts as a molecular ruler that statically measures hook length while being attached to the tip of the growing hook structure. FliK remains in the channel during hook polymerization. (C) The 'Infrequent Ruler' model. The molecular ruler, FliK, and hook subunits are intermittently secreted during hook polymerization. During a FliK measurement of hook length, export of hook subunits temporarily halts and FliK is subsequently released into the supernatant. The speed of FliK secretion is inversely correlated to hook length, such as FliK secretion is initially fast e.g. due to lacking interactions with polymerized hook subunits. In hooks polymerized to the physiological length or longer, FliK secretion slows down and the C-terminus is provided with enough time for a productive interaction with the FlhB component of the secretion apparatus that flips the secretion specificity switch.

hook length is controlled has been proposed and are discussed below (Figure 7).

FliK is secreted as a rod-hook-type substrate (131) and has an elongated structure in solution (142). The N-terminus of FliK interacts strongly with the hook cap FlgD and with less affinity to hook subunits FlgE (139, 145). An interaction of the type III secretion substrate specificity switch (T3S4) domain at the C-terminus of FliK with the cytoplasmic domain of FlhB is believed to trigger the switch in substrate specificity (130, 142). However, most intramolecular deletions of the FliK protein result in uncontrolled hook length as mentioned above and therefore initially a possible molecular ruler mechanism of hook-length determination by FliK was not considered likely (84).

An alternative model was based on the observation that certain mutations in the rotor-switch complex proteins FliG, FliM and FliN resulted in shorter hook structures. Here, it was proposed that the C-ring at the base of the flagellum acts as a measuring cup that fills up with an appropriate number of hook subunits necessary for the assembly of a hook of physiological length (120). Upon emptying of the cup-full of hook subunits, FliK would be able to interact with the FlhB component of the export apparatus and induce the flip in substrate specificity (Figure 7A). However, the capacity of the C-ring cup suggests that it can at most contain 50 of the 120 required hook subunits, without taking the space requirement of possible chaperones or the cargo-delivery complex FliHIJ into account (27). In addition, the measuring cup model has been recently refuted by the observation that hook length is partially controlled in the absence of the C-ring under conditions where the ATPase FliI is overexpressed or flagellar genes expression is generally enhanced (43, 94).

In the homologous type III injectisome system of *Yersinia enterocolitica*, length of the needle is controlled by the FliK homologue, YscP. Similar to FliK, YscP needs to be secreted to control length of the needle structure (4). Loss of YscP abolished length control and insertions or deletions in YscP resulted in longer and shorter needle structures, respectively, suggesting a molecular ruler mechanism for needle length control (78). The mechanism of needle length determination by YscP resembles the length control of bacteriophage λ tails by a molecular ruler (82, 83). Similar to the results of the needle system, insertions and deletions of FliK resulted in longer and shorter hooks that directly correlated to the length of the FliK molecule. However, some deletion mutants retained the ability to control hook length without apparent secretion. This led to the proposition that FliK would somehow measure hook length in the cytoplasm as an internal molecular ruler (172). Recently, it has been demonstrated that these deletion variants of FliK that retain hook length control are unstable but are secreted and can be detected in the external medium using a more sensitive detection method (43).

In case of YscP, the proposed model suggested a static ruler, where needle length is determined by a single ruler residing within the secretion channel during needle polymerization (Figure 7B). Here, the ruler molecule gradually stretches as the needle growths and flips substrate specificity when the needle has reached the correct length and the C-terminal domain of the ruler is in correct position to interact with the export apparatus (78, 195). A prerequisite of this model is the attachment of the ruler N-terminus to the growing tip of the structure. In case of the flagellar system, an interaction between the hook cap FlgD and FliK has been demonstrated (145). Thus far, no capping

protein has been identified at the end of the growing needle. Since a static ruler would remain within the secretion channel during needle/hook polymerization, subunits of the growing structure would need to pass by. However, a simultaneous accommodation of an α-helical ruler and structural subunits is physically improbable in both the *Yersinia* needle and flagellar hook length control systems because the inner diameter of the hook is smaller than 2.0 nm (171).

Recently, a new model has been proposed that accounts for all published data on hook length control by FliK (43, 86). As discussed in more detail in Chapter 5, FliK acts as a molecular ruler that takes infrequent (temporal) length measurements during the assembly of the hook structure. In this model, FliK is intermittently secreted with hook subunits. The frequency of ruler molecule secretion during hook polymerization defines the ultimate length of the hook. During a measurement of hook length by FliK, hook subunit export would temporarily halt and resume after secretion of FliK if proper hook length had not been achieved. In hooks of physiological or longer length, interaction of the N-terminus of FliK with the hook cap and assembled hook subunits could retard FliK secretion and provide sufficient time for a productive interaction of the FliK C-terminus with the FlhB component of the export system in order to flip the specificity switch (Figure 7C). This model is also consistent with the effects of over/underexpression of FlgE or over/underexpression of FliK on hook length (131, 149, 150). Longer hooks are observed under conditions where FlgE is overexpressed or FliK is underexpressed and shorter hooks are observed when FlgE is expressed less or FliK is expressed more (149, 150). In all cases, the ratio of secreted ruler molecules to secreted hook subunits has been changed in a way where FliK measures hook length more or less frequently resulting in shorter or longer hook structures, respectively.

Additionally, it appears that the secretion specificity switch is further regulated to prevent a premature switching event. Secretion of FliK is normally required for a productive interaction of FliK and FlhB that results in the substrate specificity switch. However, overexpression of a FliK mutant that lacks the secretion signal and is therefore not secreted, partially complemented a *fliK* null mutant to restore motility. Hook length was also only partially controlled, but shorter than the average polyhook phenotype independent on the size of the non-secreted FliK variants (66). This observation suggests that a mechanism exists that prevents non-secreted, cytoplasmic FliK from a premature interaction with FlhB. Evidence has accumulated that suggests that the Fluke (RflH) protein prevents cytoplasmic FliK from interacting with FlhB, either as a physical barrier forming a cork-like structure at the base of the flagellum or by interacting with the C-terminus of FliK during its secretion until the ruler is secreted beyond a point where this interaction can occur (65, 139).

1

Energy Source of Flagellar Type III Secretion

Koushik Paul[1, †], **Marc Erhardt**[1, †], Takanori Hirano[1], David F. Blair[1, *], Kelly T. Hughes[1, *]

Nature (2008) vol. 451 (7177) pp. 489-92

[1]Department of Biology, University of Utah, Salt Lake City, UT 84112, USA
[†]These authors contributed equally to this work
[*]Co-corresponding authors; Kelly T. Hughes and David F. Blair; Mailing address: Department of Biology, University of Utah, 257 South 1400 East, Salt Lake City, UT, 84112; Tel: +801-587-3367; Fax: +801-585-9735; E-mail: blair@bioscience.utah.edu. hughes@biology.utah.edu

1.1 Abstract

Bacterial flagella contain a specialized secretion apparatus that functions to deliver the protein subunits that form the filament and other structures to outside the membrane (115). This apparatus is related to the injectisome used by many gram-negative pathogens and symbionts to transfer effector proteins into host cells; in both systems this export mechanism is termed 'type III' secretion (22, 32). The flagellar secretion apparatus comprises a membrane-embedded complex of about five proteins, and soluble factors, which include export-dedicated chaperones and an ATPase, FliI, that was thought to provide the energy for export (47, 115). Here we show that flagellar secretion in *Salmonella enterica* requires the proton motive force (PMF) and does not require ATP hydrolysis by FliI. The export of several flagellar export substrates was prevented by treatment with the protonophore CCCP, with no accompanying decrease in cellular ATP levels. Weak swarming motility and rare flagella were observed in a mutant deleted for FliI and for the non-flagellar type-III secretion ATPases InvJ and SsaN. These findings show that the flagellar secretion apparatus functions as a proton-driven protein exporter and that ATP hydrolysis is not essential for type III secretion.

1.2 Results and Discussion

Flagellar assembly begins with structures in the cytoplasmic membrane and proceeds through steps that add the exterior structures in a proximal-to-distal sequence (Figure 1.1) (115). Assembly of the rod, hook and filament requires the action of the secretion apparatus, which transports the needed subunits into a central channel through the structure that conducts them to their site of incorporation at the tip (Figure 1.1). Flagellar export is notably fast: in the early stages of filament growth flagellin is delivered at a rate of several 55 kDa subunits per second (75).

ATP hydrolysis by FliI was thought to provide the energy for export because mutations that delete or reduce the activity of FliI block flagellar synthesis at the stage of rod assembly (47, 115, 192) (Figure 1.1). Homologues of FliI also occur in the type III secretion apparatus of injectisomes and are usually assumed to energize export in those systems as well. Some evidence for a different view has also been reported: it was observed that type III secretion in *Yersinia enterocolitica* was prevented by the protonophore CCCP (200), and it was shown that the secretion ATPase InvC of *Salmonella* functions to dissociate export substrate from the chaperone (9), a role distinct from transport itself. The energy source for type III secretion thus remains uncertain.

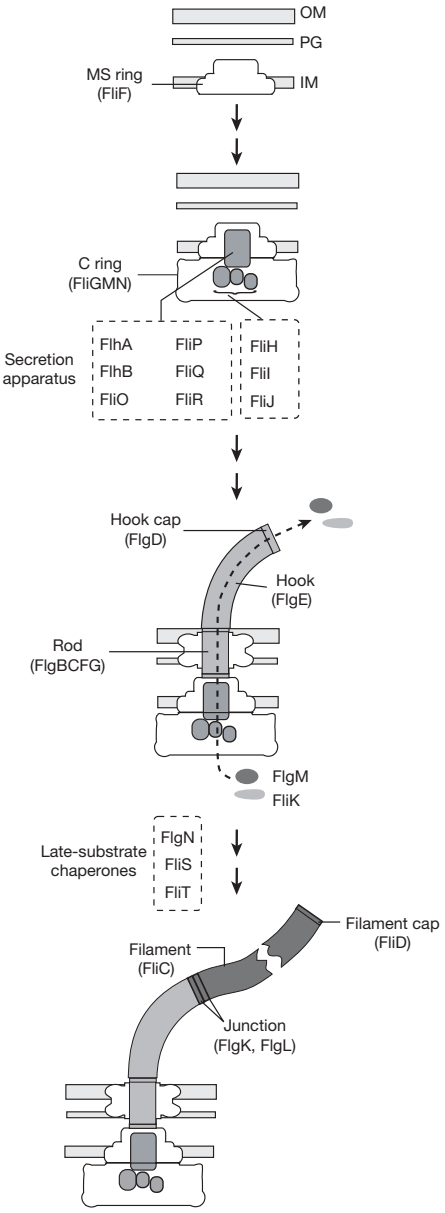

FIGURE 1.1

Steps in flagellar assembly. Dashed boxes indicate the proteins that function in flagellar secretion, either in the membrane-bound part of the apparatus or in delivery of substrate. Flagellar components that depend on export are indicated in light- (early substrates) or dark- (late substrates) grey; these include the structural proteins that form the rod, hook and filament, the transcriptional regulator FlgM, and the hook-length regulator FliK. OM, outer membrane; PG, peptidoglycan; CM, cytoplasmic membrane.

To address the energy requirements for type III secretion, we first measured the effect of the uncoupler CCCP on flagellar export in *S. enterica*, assayed by accumulation of the export substrate FlgM in the medium. FlgM export was prevented by 10 µM or more CCCP (Figure 1.2a). Overall cellular energy levels seemed unaffected, because cells grew normally in 10 µM CCCP (growth data not shown) and ATP levels were unchanged (Figure 1.4a). The effect was reversible: FlgM export was largely restored following a 30 minutes washout of the 10 µM CCCP (Figure 1.2b). FlgM inhibits transcription of its own gene, and so reduced FlgM export might partially reflect decreased cellular levels of the protein (59). To circumvent this auto-inhibitory effect the experiment was repeated with a strain in which *flgM* was placed under control of a non-native (P_{araB}) promoter. In this strain, the cytoplasmic level of FlgM remained nearly constant, whereas FlgM secretion was again prevented by 10 µM or more CCCP (Figure 1.2c).

The maintenance of normal ATP levels in the presence of CCCP was noted previously in experiments with *Y. enterocolitica* (200) and is thought to be due to a regulatory mechanism that inhibits the hydrolytic activity of the ATP synthase when the membrane is de-energized (182). Because this protective mechanism may not act instantaneously, cellular ATP levels might undergo a transient drop following CCCP treatment that would escape detection in our measurements. To rule out such an effect, we measured FlgM export in a Δ*atpA* strain that lacks a major subunit of the ATP synthase. FlgM secretion was again prevented by 10 µM or higher CCCP, and ATP levels were unaffected (Figure 1.2d, e).

The flagellum exports more than a dozen substrates, which are classified as early or late according to whether they are secreted during assembly of the hook/basal-body or the filament (115) (Figure 1.1). To test the generality of the PMF requirement we examined the effect of CCCP on secretion of additional substrates, assayed by their accumulation in the culture medium (93). We observed the early substrate FliK and the late-export substrates FlgK, FlgL and FliC in culture supernatants of LB-grown cells. Accumulation of all four substrates was prevented by treatment with 20 µM CCCP (Figure 1.2f). The band between FliC and FlgK does not correspond to the size of a known flagellar protein and is likely to be a stable protein secreted in (relatively) low amounts.

CCCP functions as a proton carrier to discharge both the electric potential ($\Delta\Psi$) and concentration (ΔpH) components of the PMF. To examine the contribution of the $\Delta\Psi$ component separately, we measured FlgM secretion in cells treated with the K^+-ionophore valinomycin. In medium containing 150 mM KCl, FlgM secretion was inhibited by 10 µM valinomycin (Figure 1.3a). Thus, the electrical potential component seems essential for export under the conditions of this experiment (extracellular pH = 7.3). Next, the ΔpH component of the gradient was discharged by the weak acid acetate (34 mM), which crosses the membrane in neutral (protonated) form and releases protons inside the cell. At an external pH of 7, FlgM secretion was not affected by treatment with acetate (Figure 1.3b), indicating that flagellar export can be supported by $\Delta\Psi$ alone. At an external pH of 5, acetate prevented secretion (Figure 1.3b), presumably owing to acidification of the cytoplasm and the resulting protonation of one or more functionally important acidic groups. A similar effect was reported with the flagellar motor, which ceased rotating when the cytosolic pH was lowered to 5 (135).

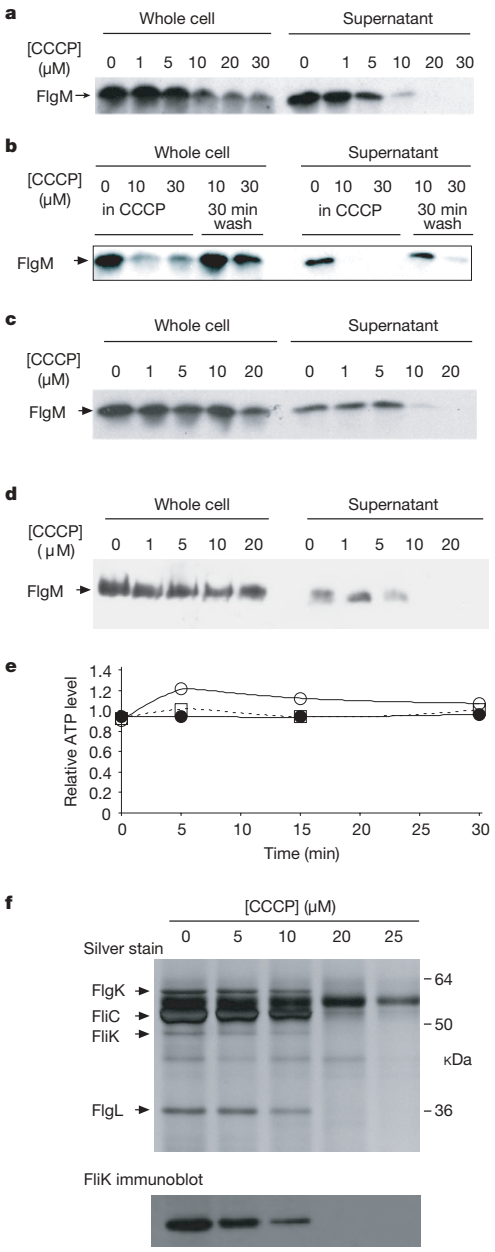

FIGURE 1.2

Inhibition of FlgM secretion by CCCP. (a) Secretion in *Salmonella* strain TH3730 (Tet-inducible *flhDC*). (b) Partial restoration of export following a 30-min wash into CCCP-free buffer. (c) Secretion in strain TH10874 (arabinose-inducible *flgM*). (d) Inhibition of FlgM secretion by CCCP in an ATP-synthase defective (Δ*atpA*) strain (TH11802). (e) ATP levels in the Δ*atpA* mutant at various times following treatment with CCCP. Open circles, no treatment; open square, 10 μM CCCP; and filled circles, 30 μM CCCP. (f) Inhibition of secretion of other flagellar substrates (FlgK, FlgL, FliC and FliK) by CCCP.

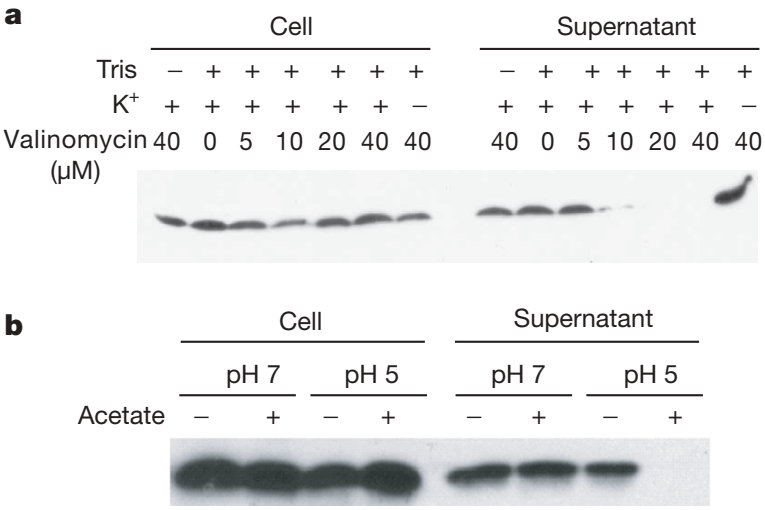

FIGURE 1.3

Effect of ΔΨ and ΔpH on FlgM export. (a) Inhibition of FlgM secretion by valinomycin and K^+. Where indicated, cells were pretreated with Tris (120 mM) to permeabilize the outer membrane to valinomycin. (b) Inhibition of FlgM secretion by acetate (34 mM) at pH 5.

We characterized export requirements further using an assay based on secretion of a FlgE-Bla (hook/β-lactamase) fusion protein. Cells were deleted for the rod proteins FlgB and FlgC (Figure 1.1) to direct the fusion protein into the periplasm, allowing export to be quantified by the MIC (minimum inhibitory concentration) for ampicillin (108). The MIC value was reduced by uncoupler, from a value of 25 μg/ml in the untreated control to about 4 μg/ml in 30 μM CCCP (Table 1.1, and Supplementary Information Figure 1.4).

If energy for flagellar transport comes from the proton gradient, then ATP hydrolysis by FliI may be less important than has been supposed. To examine the FliI requirement more closely we measured FlgE-Bla export in a strain deleted for *fliI* and the flanking genes *fliH* and *fliJ*. FliH is a regulator of FliI (138) and FliJ interacts with the FliHI complex and with other export components (46, 52). The MIC measured for the Δ*fliHIJ* strain was 12 μg/ml, reproducibly larger than that of a negative-control strain lacking the MS-ring gene *fliF* (< 3 μg/ml) or a strain with all the flagellar genes repressed by downregulation of the master regulators *flhDC* (< 3 μg/ml) (Table 1.1). Furthermore, the MIC value of the Δ*fliHIJ* strain was greatly increased (to 800 μg/ml) by overexpression of FliR, a membrane-associated part of the export apparatus (Table 1.1, and Supplementary Information Figure 1.4). Prompted by this evidence of export in the absence of FliI, we examined motility of Δ*fliHIJ* cells. The Δ*fliHIJ* cells migrated in soft agar at about one-tenth the wild-type rate (Figure 1.5a), and a fraction of the cells were observed to swim in liquid media. Cells isolated from the centre, edges or intermediate positions in the swarm showed the same phenotype when purified and re-tested (not shown), and so the slow motility is a property of the population and is not due to suppressing mutations. Staining showed flagella on a small fraction (< 1%) of the cells

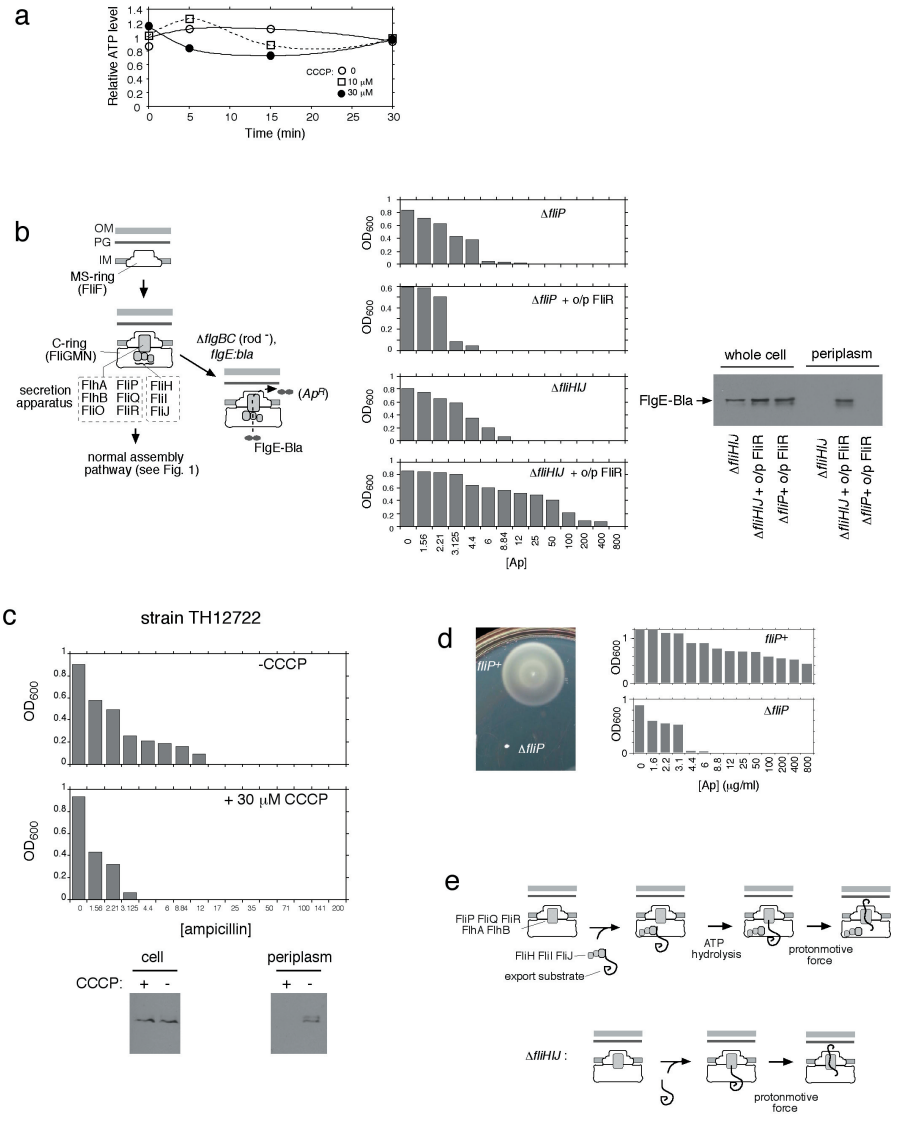

FIGURE 1.4

Supplementary Information. (a) ATP levels in strain TH10874 (Δ*flgM* P_{ara}-*flgM*$^+$) at various times after addition of CCCP. (b) Additional evidence of export in the Δ*fliHIJ* strain. In a strain deleted for the rod components FlgB and FlgC, the FlgE:Bla fusion protein enters the periplasm where it confers ampicillin resistance. OD_{600} data is shown from the MIC (Minimum Inhibitory Concentration for Amp) assays with the Δ*fliP* and Δ*fliHIJ* mutants under FlgE:Bla inducing conditions, in the presence and absence of a FliR expressing plasmid. Moderately overexpressed FliR can rescue secretion of FlgE:Bla into the periplasm in the Δ*fliHIJ* strain, but not in the Δ*fliP* strain. The rescue of FlgE:Bla export in the periplasm in the Δ*fliHIJ* strain by FliR was confirmed by anti-Bla immunoblot. (c) The effect of CCCP on FlgE:Bla export. Decreased Amp resistance of strain TH12722 (Δ*flgBC* P_{ara}-*flgE*(aa1-50)::*bla*) in the presence of arabinose was observed after CCCP treatment. The reduction of FlgE:Bla export in the periplasm was confirmed by anti-Bla immunoblot. (d) Effects of *fliP* deletion on swarming motility and ampicillin resistance in the FlgE:Bla assay. (e) Hypothesis for the roles of PMF and ATP hydrolysis in flagellar type-III secretion. The FliHIJ complex, which utilizes ATP, functions to deliver the substrate in an export-competent form. Transport of the substrate across the membrane is energized by PMF.

TABLE 1.1

Effects of CCCP and mutation on flagellar export.

MIC, minimum inhibitory concentration of ampicillin required in cells with rod-gene (*flgBC*) deletions to direct the hook-β-lactamase (FlgE-Bla) fusion protein into the periplasm (108).

Genotype (treatment)	MIC (μg/ml)
Δ*flgBC flgE*::*bla*	25
Δ*flgBC flgE*::*bla* (30 μM CCCP)	<3
Δ*flgBC flgE*::*bla* Tet-inducible *flhDC* (no Tet)	<3
Δ*flgBC flgE*::*bla* Tet-inducible *flhDC* (15 μg/ml Tet)	50
Δ*flgBC flgE*::*bla* Tet-inducible *flhDC*, Δ*fliF* (15 μg/ml Tet)	<3
Δ*flgBC flgE*::*bla* Δ*fliHIJ*	12
Δ*flgBC flgE*::*bla* Δ*fliHIJ*, *fliR* expressed from plasmid	800
Δ*flgBC flgE*::*bla* Δ*fliI*	6
Δ*flgBC flgE*::*bla* Δ*fliP*	4.4
Δ*flgBC flgE*::*bla* Δ*fliP*, *fliR* on plasmid	4.4
Δ*flgBC flgE*::*bla* Δ*fliP*, *fliP* on plasmid	800

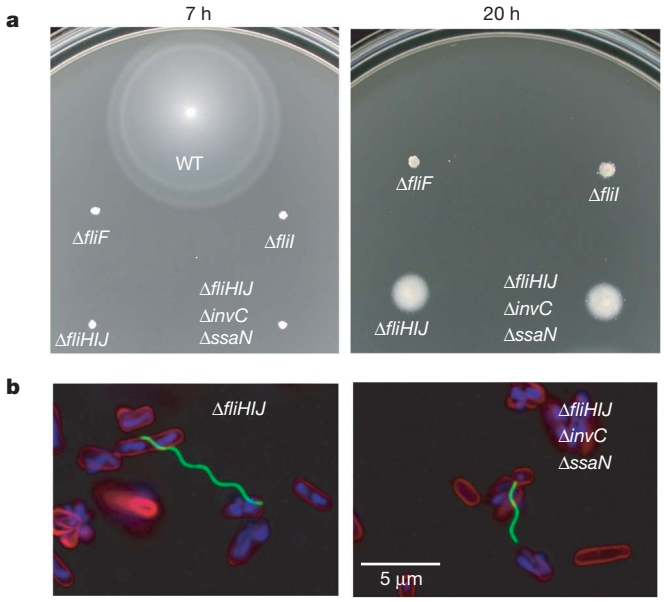

FIGURE 1.5

FliI is non-essential for flagellar assembly and function. (a) Swarming of the Δ*fliHIJ* deletion strain and a Δ*fliHIJ* Δ*invC* Δ*ssaN* strain with all type-III secretion ATPases deleted. The Δ*fliF* strain, blocked in the earliest step of flagellar assembly (Figure 1.1), is included as a negative control. Plates were incubated at 32 ℃. (b) Flagella on cells of the Δ*fliHIJ* mutant (left panel) and the Δ*fliHIJ* Δ*invC* Δ*ssaN* triple-deletion (right panel). Flagella were visualized with FITC-conjugated anti-FliC antibody (green) (161). DNA was stained with DAPI (blue), and membranes by FM64 (red).

(Figure 1.5b, left panel). A Δ*fliI* mutant swarmed more slowly than the Δ*fliHIJ* strain (Figure 1.5a) and also showed reduced export in the MIC assay (Table 1.1), consistent with the more severe motility defect reported previously for a Δ*fliI* mutant (41, 47).

In addition to the flagella apparatus, members of *Salmonella spp.* contain two non-flagellar (injectisome) type III secretion systems, with associated ATPases InvC and SsaN (9, 63). To rule out any involvement of InvC or SsaN in the secretion observed in Δ*fliHIJ* cells, we repeated the experiments in a Δ*invC* Δ*ssaN* Δ*fliHIJ* strain. The triple-deletion mutant swarmed equally as well as the Δ*fliHIJ* strain in soft agar (Figure 1.5a), and flagella were again seen on a few cells (Figure 1.5b, right). Thus, none of the secretion ATPases is required for flagellar export, assembly or function.

Our conclusions are consistent with previous observations of a PMF requirement for flagellar growth from more than 25 years ago (57), and extend the earlier findings in showing that export can be energized by PMF alone in the absence of any type III secretion ATPase (200). Use of the proton gradient is perhaps not surprising given the speed of type III secretion and the likely advantage of tapping a proximal energy source. Rapid subunit export presumably requires a rapid supply of energy, which might be more easily delivered by a proton current than by ATP hydrolysis. Given that type III secretion is energized by PMF, future studies should focus on the molecular mechanism of proton movement through the apparatus and its coupling to movement of substrate.

1.3 Methods

General methods

Media, growth conditions, methods for phage-mediated transduction and motility assays were performed as described previously (35, 58, 59). Carbonylcyanide *m*-chlorophenylhydrozone (CCCP) and valinomycin were from Sigma (analytical grade). Potassium acetate was from J. T. Baker, growth media from Difco, and buffers from Sigma. Swarming motility was assayed in plates containing tryptone broth and 0.28% bacto-agar. Plates were incubated at 32 ℃.

FlgM-secretion assay

FlgM secreted into the culture medium was measured as described previously (81), with the following modifications. Strain TH3730 (Tc-induced flagellar synthesis) was cultured overnight at 37 ℃ in LB media, then diluted 100-fold into 3 ml of fresh LB and cultured to an $OD_{600} = 0.5$. Tetraycline (15 µg/ml) was added to induce transcription of the flagellar regulatory genes *flhDC* and growth was continued for one hour at 37 ℃ before cells were harvested. Strain LT2 was cultured in the same way except without tetracycline induction and harvested at an $OD_{600} = 0.8$. Cells were collected by centrifugation and washed twice with 3 ml LB containing appropriate concentrations of the PMF-discharging agents (CCCP or valinomycin), introduced from freshly prepared stocks in DMSO. Controls received only DMSO. Following resuspension the cells were incubated at 37 ℃ for the times indicated in the figures (typically 30 min), then kept on ice until

further processing. Strains TH10874 and TH11802 were treated in a similar way, except media included 0.2% L-arabinose to induce transcription of *flgM*.

To quantify FlgM in the culture medium, cells of a 2 ml sample were pelleted in a tabletop centrifuge and 1.8 ml of the supernatant was passed through a 0.45 µm cellulose acetate filter (Nalgene) to remove any remaining cells. Filtrate (1.6 ml) was filtered through a prewetted 0.45 µm pore-size BA85 nitrocellulose filter (Schleicher & Schuell) for protein binding. Proteins were eluted by addition of 40 µl of 2x SDS sample buffer (105) and heating to 65 ℃ for 30 min. For quantification of intracellular FlgM, the pelleted cells were resuspended in 50 µl 1x SDS sample buffer and boiled for 10 min. Pellet and supernatant fractions were adjusted to equal volumes (corresponding to 20 OD_{600} units for the cells), 10 µl samples were loaded onto SDS-PAGE gels and FlgM was detected by immunoblotting, essentially as described (73).

ATP measurement

ATP was measured using the firefly luciferase assay (time-stable ATP determination kit, Biaffin) and the sample-processing procedures of Bakker and Mangerich (14). Following resuspension in the media with or without CCCP, cells were incubated at 37 ℃ for the times indicated, then 2 ml samples were withdrawn and mixed with 2 ml of ice-cold 6% $HClO_4$, 2.5 mM Na_2HPO_4, 1 mM KCl. Samples were left on ice for 30 min then centrifuged in the cold to remove denatured proteins. Supernatants were brought to pH 7.0 with 2 M KOH, 0.3 M MOPS, then frozen at -20 ℃, quickly thawed, and immediately centrifuged at 4 ℃ to remove crystals of $KClO_4$. Samples were kept on ice and used for ATP determination within 2 h. For ATP measurements, 50 µl of supernatant was mixed with an equal volume of luciferase reagents in a 96-well plate and the luminescence was measured at 560 nm using a TopCount NXT Microplate scintillation and luminescence counter (Packard).

FlgE/β-lactamase activity

FlgE/β-lactamase assays were performed essentially as described in reference (108), with minor modifications. Briefly, 1 ml cultures in LB were grown overnight at 37 ℃. Cultures were diluted 100-fold into 3 ml LB and grown at 37 ℃ to a OD_{600} = 0.5-0.7, then diluted 50-fold into fresh LB media containing ampicillin in a series of dilutions ranging from 800 µg/ml to 1.56 µg/ml. The OD_{600} of each sample was measured after 4.5 h of further growth at 37 ℃, and the minimum inhibitory concentration (MIC) was taken as the lowest ampicillin concentration giving $OD_{600} < 0.05$. For the experiment that measured the effect of CCCP, the *flgE-bla* gene was expressed from the *ara* promoter, induced with arabinose 30 min before addition of CCCP, to minimize FlgE/Bla accumulation in the periplasm before the addition of the uncoupler.

Staining

Flagellar immunostaining was performed as described in reference (161).

Measurement of FlgE-Bla in periplasm

Spheroplast preparation, periplasmic fractionation and immunoblot detection of FlgE-Bla in the cellular and periplasmic fractions was performed as described in reference (10).

1.4 Acknowledgements

We thank S. Williams for his help and permission for using the luminometer, F. Chevance for advice and assistance with strain constructions, M. Sarkar for assistance with MIC assays, and V. Clougherty for flagellar-staining experiments. M. Erhardt gratefully acknowledges scholarship support of the Studienstiftung des deutschen Volkes. This work was supported by Public Service grants (K.T.H. and D.F.B.) from the National Institutes of Health.

2

C-ring Requirement in Flagellar Type III Secretion is Bypassed by FlhDC Upregulation

Marc Erhardt[1,*] and Kelly T. Hughes[1]

Molecular Microbiology (2010) vol. 75 (2) pp. 376-393

[1]Department of Biology, University of Utah, Salt Lake City, UT 84112, USA
[*]Corresponding author; Marc Erhardt; Mailing address: Department of Biology, University of Utah, 257 South 1400 East, Salt Lake City, UT, 84112; Tel: +801-585-6950; Fax: +801-585-9735; E-mail: marc.erhardt@utah.edu

2.1 Abstract

The cytoplasmic C-ring of the flagellum consists of FliG, FliM and FliN and acts as an affinity cup to localize secretion substrates for protein translocation via the flagellar-specific type III secretion system. Random T-POP transposon mutagenesis was employed to screen for insertion mutants that allowed flagellar type III secretion in the absence of the C-ring using the flagellar type III secretion system-specific hook-β-lactamase reporter (108). Any condition resulting in at least a twofold increase in *flhDC* expression was sufficient to overcome the requirement for the C-ring and the ATPase complex FliHIJ in flagellar type III secretion. Insertions in known and unknown flagellar regulatory loci were isolated as well as chromosomal duplications of the *flhDC* region. The twofold increased *flhDC* mRNA level coincided in a twofold increase in the number of hook-basal bodies per cell as analysed by fluorescent microscopy. These results indicate that the C-ring functions as a nonessential affinity cup-like structure during flagellar type III secretion to enhance the specificity and efficiency of the secretion process.

2.2 Introduction

Many bacteria propel themselves in their environments by rotation of one or more propeller-like appendages called flagella (18). The flagellum consists of mainly three structural parts: (i) a basal body that spans the inner and outer membranes and is composed of a ion-powered (proton or sodium) rotary motor, which incorporates a specific type III protein secretion system, (ii) an external, flexible hook that acts as a universal joint between the rigid drive shaft (rod) of the basal motor and (iii) the rigid, external filament (17, 27, 115) (Figure 2.1A).

The flagellar-specific type III secretion (T3S) apparatus is believed to assemble at the base of the flagellar basal body within the MS-ring (consisting of FliF) in the inner membrane. The core T3S proteins include six integral membrane proteins (FlhA, FlhB, FliO, FliP, FliQ, FliR) and three cytoplasmic proteins (FliH, FliI, FliJ) (136). Recently, it was discovered that translocation of substrates across the inner membrane was dependent on the proton motive force (140, 158), and is presumably coupled to ATP-dependent substrate release and unfolding (9). The ATPase complex $FliH_2IJ$ seems to function in cargo delivery to the C-ring and unfolding of the polypeptide prior to secretion. The FliH dimer has been shown to interact with the C-ring protein FliN (60), thereby presumably targeting substrates to the secretion system.

Beneath the MS-ring in the inner membrane, the cytoplasmic C-ring forms, which con-

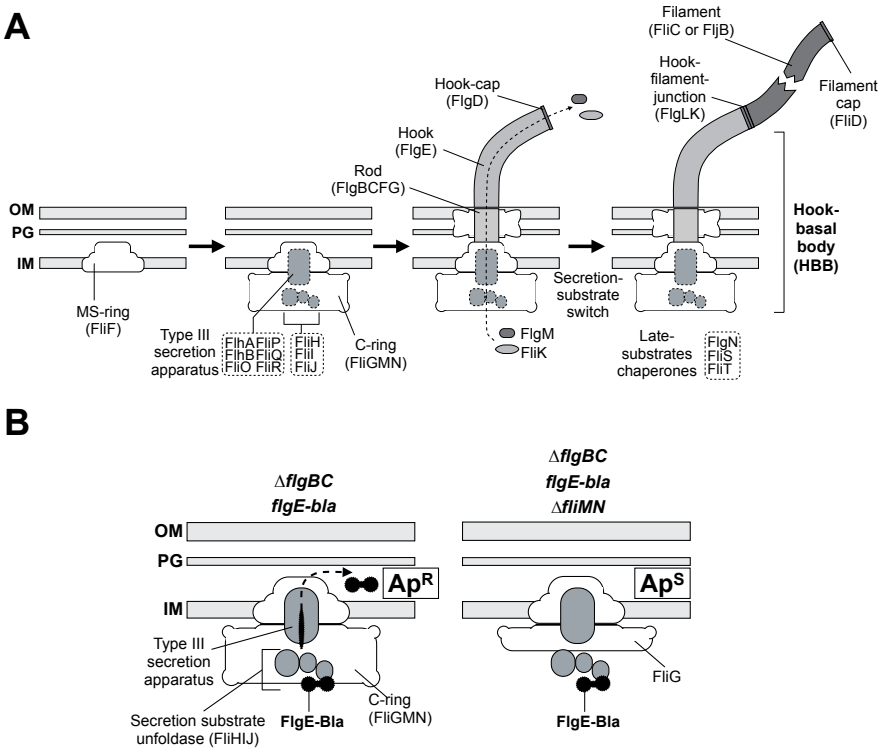

FIGURE 2.1

Steps in the assembly of the bacterial flagellum and Hook-β-lactamase reporter system. (A) Steps in the assembly of the bacterial flagellum. The self-assembly process of the flagellum initiates with formation of the MS-ring (FliF) in the cytoplasmic membrane. Afterwards, a flagellar-specific T3S apparatus assembles within a central pore of the MS-ring and the C-ring is attached to the cytoplasmic face of the MS-ring. At this point, flagellar secretion substrates are now selectively secreted coupled to the proton motive force via the T3S apparatus (158). The hook polymerizes to an approximate length of 55 nm that is determined by the molecular ruler FliK and this triggers a secretion specificity switch from rod-hook-type substrates to late-substrates secretion. Upon completion of the HBB complex, the negative regulator of late-substrates gene expression, the anti-σ^{28} factor FlgM, is secreted thereby freeing σ^{28} to initiate transcription of late-substrate genes, like *fliC* or the genes of the chemosensory system. (B) Hook-β-lactamase reporter system. Left panel: in a strain deleted for the proximal rod subunit genes, *flgBC*, rod-hook-type substrates are secreted via the flagellar-specific T3S apparatus into the periplasm and subsequently degraded. β-Lactamase (Bla) fused C-terminally to the hook protein FlgE is not degraded and confers resistance against lactam antibiotics, like ampicillin when secreted into the periplasm (Ap^R). Right panel: in a strain additionally deleted for two-thirds of the cytoplasmic C-ring (Δ*fliMN*), flagellar T3S is severely impaired and thus FlgE-Bla is not secreted into the periplasm and the strain is sensitive against ampicillin (Ap^S).

sists of FliG, FliM and FliN and is also referred to as the switch complex as this structure forms the rotor of the flagellar motor and controls the clockwise/counterclockwise rotation of the flagellum. The C-ring serves dual roles as the rotor of the flagellar motor and cup-like structure that possibly facilitates docking and secretion of flagellar substrates (60). Flagellar assembly is blocked at an early stage in strains deleted for *fliG*, *fliM* or *fliN* (99, 136). Recently, it has been shown that filament assembly in C-ring mutants is possible in a small fraction of the population upon overexpression of the T3S-specific ATPase FliI (94).

The assembly of the flagellum is a highly regulated process. In *Salmonella enterica* and *Escherichia coli*, the flagellar regulon is controlled by a transcriptional hierarchy of three promoter classes for the expression of more than 30 structural and assembly related proteins (Figure 2.1A) (27). At the top of the transcriptional hierarchy stands the Class I promoter for transcription of the flagellar master operon, *flhDC*. Many different signals influence expression of the Class I promoter to ultimately determine the level of flagellar gene expression. In *S. enterica*, six transcriptional start sites have been mapped within the *flhDC* promoter region (207). The *flhDC* operon encodes the $FlhD_4C_2$ activator complex (111, 197), which directs σ^{70}-bound RNA polymerase to initiate transcription from Class II promoters.

Class II gene products are required for the structure and assembly of the hook-basal body (HBB), which includes the T3S apparatus. Class II promoters also direct transcription of regulatory proteins such as the flagellum-specific σ factor, σ^{28} (153) and its cognate anti-σ factor, FlgM (73). Upon completion of the HBB, substrate specificity of the flagellar-specific T3S system is switched from rod hook substrate specificity to the secretion of late substrates like the filament subunits and the anti-σ factor FlgM. FlgM secretion after HBB completion releases σ^{28} to interact with RNA polymerase and activate transcription from Class III promoters. Class III promoters control expression of late flagellar substrates like the filament subunits, the motor force generators (MotA and MotB) and the chemosensory system, but only in coordination with HBB completion (27).

As mentioned above, many environmental signals are integrated on the level of the *flhDC* Class I promoter to control the initiation or cessation of flagellar synthesis in *S. enterica*. Binding of the cyclic AMP-catabolite gene activator protein complex to the *flhDC* promoter is required to activate transcription of *flhDC* (92, 103, 176). The iron-regulatory protein Fur, Fis and H-NS also activate *flhDC* transcription. Fis in *S. enterica* and Fur/H-NS in *E. coli* were shown to bind directly to the *flhDC* promoter (87, 176, 179). Another transcriptional regulator, SlyA that is required for virulence in *Salmonella* (110), has been shown to enhance flagellin expression (178).

Expression of *flhDC* is negatively regulated at both transcriptional and post-transcriptional levels by many other regulatory proteins. The RcsB regulator binds to the RcsAB box located within the *flhDC* promoter to inhibit motility (196). The RcsCDB system senses several external signals, like high osmolarity, desiccation and low temperature with high zinc concentrations (119). FimZ, a response regulator that activates type 1 fimbrial genes, inhibits motility by affecting Class I gene expression (31). Similarly, the PefI/SrgD complex, which activates the fimbrial genes encoded on the *S. enter-*

ica virulence plasmid, inhibits *flhDC* transcription in *Salmonella* (203). In *E. coli*, the LysR-type DNA-binding protein LrhA has been identified as another negative regulator of *flhDC* transcription that directly binds to the *flhD* promoter and thereby inhibits transcription (109). The binding of RtsB, another pathogenesis-related DNA-binding protein, also inhibits transcription of the Class I *flhDC* promoter (42). EcnR, an uncharacterized regulatory protein, was also identified as a novel negative regulator of Class I transcription in *S. enterica* (203). Finally, deficiencies of guanosine tetraphosphate and guanosine pentaphosphate [ppGpp(p)] and the RNA-polymerase binding protein DksA, respectively, have divergent effects on flagellar gene expression and motility (1).

Following transcription, the RNA-binding protein CsrA, which is also involved in carbon storage regulation, stabilizes the *flhDC* transcript (199). The c-di-GMP-related protein YdiV negatively regulates $FlhD_4C_2$ activity on Class II promoters at a post-transcriptional level (203). The $FlhD_4C_2$ complex is also degraded by the ClpXP protease (190) and the formation of active $FlhD_4C_2$ complex is promoted by the Hsp70 chaperone DnaK (184).

In this work we sought mutants that allowed secretion of the flagellar hook protein fused to a β-lactamase reporter (deleted for its N-terminal Sec-dependent secretion signal) (FlgE-Bla) in strains defective in C-ring formation (Δ*fliMN*). We have shown previously that in strains deleted for flagellar rod genes (Δ*flgBC*), FlgE-Bla is efficiently secreted into the periplasm by the flagellar T3S system where it confers ampicillin resistance (Ap^R) (108, 158). Here we show that a Δ*flgBC*Δ*fliMN* double mutant will not secrete FlgE-Bla and the cells are Ap^S. Mutants able to secrete FlgE-Bla in the Δ*flgBC*Δ*fliMN* double mutant background (Ap^R) resulted in increased *flhDC* expression and HBB production supporting a role of the C-ring as an affinity cup that enhances the efficiency and specificity of flagellar T3S.

2.3 Results

2.3.1 Duplications of the *flhDC* operon overcome inhibition of FlgE-Bla secretion in a Δ*fliMN* C-ring mutant strain

For selective and quantitative measurement of flagellar T3S, we developed a reporter system consisting of the flagellar T3S-specific substrate FlgE (hook protein) fused to β-lactamase lacking its own Sec-dependent secretion signal (FlgE-Bla) (108, 158). In a mutant strain lacking the proximal rod subunits FlgB and FlgC, the hook-β-lactamase fusion protein is secreted into the periplasm conferring resistance to β-lactam antibiotics, like ampicillin (Figure 2.1B). As the FlgE-Bla fusion protein is selectively secreted via the flagellar-specific T3S system, this powerful model system enables us to positively select for mutants with enhanced T3S by growth on otherwise inhibitory ampicillin concentrations. As mentioned earlier, the components of the cytoplasmic C-ring, FliG, FliM and FliN are needed for efficient T3S under wild-type conditions. In order to isolate mutants that allowed for secretion in the absence of the C-ring, overnight cultures of strain TH12470 (Δ*flgBC* Δ*fliMN* *flgE-bla*) were plated onto MacConkey ampicillin (15

µg/ml) selective medium. Ampicillin-resistant (Ap^R) revertants arose at a frequency of $\sim10^{-5}$. This high frequency of reversion suggested that loss-of-function mutations in one or more genes would allow FlgE-Bla secretion in the Δ*fliMN* mutant strain.

We performed T-POP transposon mutagenesis in an attempt to isolate insertions that resulted in FlgE-Bla secretion in a rod-defective (Δ*flgBC*), C-ring-defective (Δ*fliMN*) strain by screening insertion mutants for those that resulted in an Ap^R phenotype. T-POP transposons are derivatives of the mini-Tn*10* transposon Tn*10d*Tc that encodes tetracycline resistance (Tc^R) (107, 160). The T-POP transposon used, Tn*10d*Tc[Δ25], is a Tn*10d*Tc derivative that lacks Tn*10* transposase and is deleted for the transcriptional terminator of the tetracycline resistance gene, *tetA*, within the transposon (the [Δ25] deletion). The divergently transcribed *tetA* and *tetR* genes encode an inner membrane efflux pump (TetA) and the TetR repressor of *tetA* and *tetR* transcription. When tetracycline (Tc) is present, it will bind to TetR and prevent DNA binding resulting in de-repression of the *tetA* and *tetR* genes. Some of the *tetA* and *tetR* transcripts will continue into adjacent chromosomal DNA flanking a Tn*10d*Tc insertion. When Tc is added to strains that carry the Tn*10d*Tc[Δ25] T-POP insertion, a substantial amount of transcription from the *tetA* promoter will continue into adjacent chromosomal DNA flanking the site of T-POP insertion (160).

The T-POP transposon was introduced into strain TH14953 (pNK2880Km/Δ*flgBC* Δ*fliMN flgE-bla*), which constitutively expresses a mutant Tn*10* transposase from plasmid pNK2880Km. The mutant Tn*10* transposase has lost target specificity and catalyses random transposition into the chromosome by P22 transduction selecting for Tc^R and screening for Ap^R in the presence and absence of Tc. Of 24 000 Tc^R insertions, 91 were isolated that showed an Ap^R phenotype: 32 were Ap^R with or without added Tc, 23 were Ap^R only with added Tc and 36 were Ap^S when Tc was added to the medium. This is an unusually high mutation rate. The *S. enterica* chromosome has about 5 000 genes. Assuming to the first approximation that the T-POP transposon inserts with an equal frequency in any given gene, 91/24 000 suggests a target of 18 genes that, when mutated, result in an Ap^R phenotype. During the handling of the Ap^R T-POP insertions, nine of the mutants segregated Tc^S Ap^S colonies at a high frequency (> 10% from an overnight culture) when Tc and Ap were absent from the medium. As duplication of a region of the *Salmonella* chromosome was reported to occur at a frequency of $\sim10^{-4}$ (12), these observations led us to conclude that Ap^R was occurring at a high frequency, independent of transposon mutagenesis by chromosomal duplications.

In order to test whether chromosomal duplications were giving rise to Ap^R in the Δ*flgBC* Δ*fliMN flgE-bla* background, Mu*d*J transposon mutagenesis was performed on strain TH12470 (Δ*flgBC* Δ*fliMN flgE-bla*) to isolate insertions in duplicated regions that result in Ap^R. These would have the phenotype of losing the Mu*d*J transposon at a high frequency when selection for maintaining the duplication is removed by growing these strains without added Ap to the medium. Mu*d*J transposon mutagenesis was performed on strain TH12470 selecting for kanamycin resistance (Km^R) in the presence of bromo-chloro-indolyl-galactopyranoside (XGal). The Mu*d*J is a *lac* operon fusion vector. When Mu*d*J inserts into a gene in the correct orientation the promoter of the inserted gene will transcribe promoterless *lac* operon within Mu*d*J. We screened for

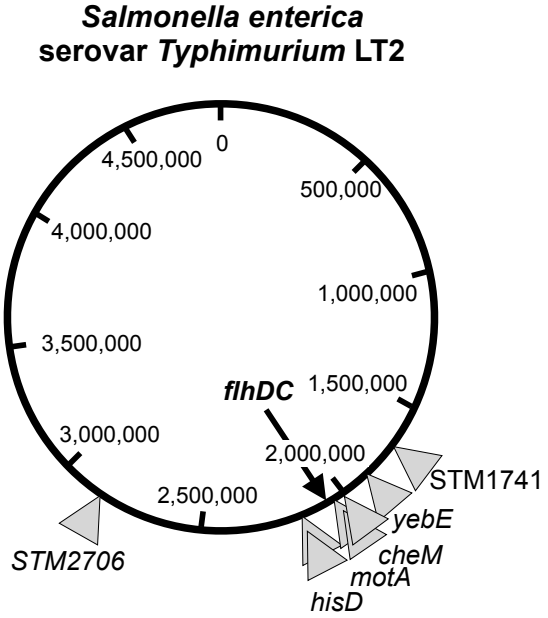

FIGURE 2.2

Locations of unstable Mu*d* insertions in the *Salmonella* chromosome in strains duplicated for the *flhDC* region that conferred ampicillin resistance in the absence of the C-ring. The positions of eight Ap^R Mu*d* insertions in the *Salmonella* chromosome were determined by DNA sequence analysis. Individual Mu*d* insertions are indicated by a grey triangle and additionally the chromosomal loci of the insertions. These unstable Ap^R Mu*d* insertions resulted from transposition into duplications of the *flhDC* region of the chromosome thus conferring ampicillin resistance in the absence of the C-ring by increased *flhDC* expression. The precise insertion points are given in Table 2.1.

Ap^R Mu*d*J insertion mutants that showed an initial Lac^+ phenotype in the presence of XGal (= blue colony), but upon restreaking on XGal medium lacking both Ap and Km segregated Lac^- (white on XGal) colonies. This indicated that the Mu*d*J had inserted within a duplicated region. A number of the unstable (duplication-held) Ap^R Mu*d*J insertions were analysed by DNA sequencing. As shown in Figure 2.2 and Table 2.1, these Mu*d*J insertions were in a number of unrelated genes, yet they localized to a region of the chromosome that includes the *flhDC* operon, suggesting that duplication of the region of the chromosome that includes *flhDC* resulted in the Ap^R phenotype.

TABLE 2.1

Mu*d* insertions and spontaneous mutations resulting in FlgE-Bla secretion in the absence of the C-ring.

Summary of isolated Mu*d* insertions that transposed into duplicated *flhDC* regions of the chromosome and conferred ampicillin resistance in the C-ring deletion resulting from increased *flhDC* expression. Additionally shown are spontaneous mutations isolated in *fliA* and *flhD* promoter region that also allowed for FlgE-Bla secretion in the absence of the C-ring.

Mu*d* insertion / Allele	**Location of insertion / point mutation**
mud2	161 bp downstream of *yebE* stop, 39 bp upstream of *ptrB* start
mud4	204 bp downstream of *hisD* start
mud10	204 bp downstream of *hisD* start
mud13	439 bp downstream of STM2706 start
mud19	1308 bp downstream of *cheM* start
mud26	1323 bp downstream of *cheM* start
mud32	404 bp downstream of STM1741 start
mud36	703 bp downstream of *motA* start
fliA7463	Q106:STOP (TH14683)
fliA7464	Q106:STOP (TH14684)
$P_{flhD7460}$	*-38G:A* from *AUG* (TH14680)
$P_{flhD7461}$	*-152C:T* from *AUG* (TH14681)

To verify this possibility, C-ring deletions strains (Δ*fliMN*, Δ*fliG* and Δ*fliGMN*), as well as deletions of the MS-ring (Δ*fliF*) and the ATPase complex (Δ*fliHIJ*), were constructed with an extra copy of the *flhDC* operon expressed from the arabinose promoter. Expression of *flhDC* from the arabinose promoter will provide about 60-fold more copies of *flhDC* mRNA than *flhDC* expressed from its native promoter (Figure 2.3B); however, it has been shown previously that duplications tend to amplify to many more copies as well (102).

In the strain expressing *flhDC* from the arabinose promoter, the C-ring deletion strains were Ap^R in the presence of arabinose and Ap^S without added arabinose, confirming that

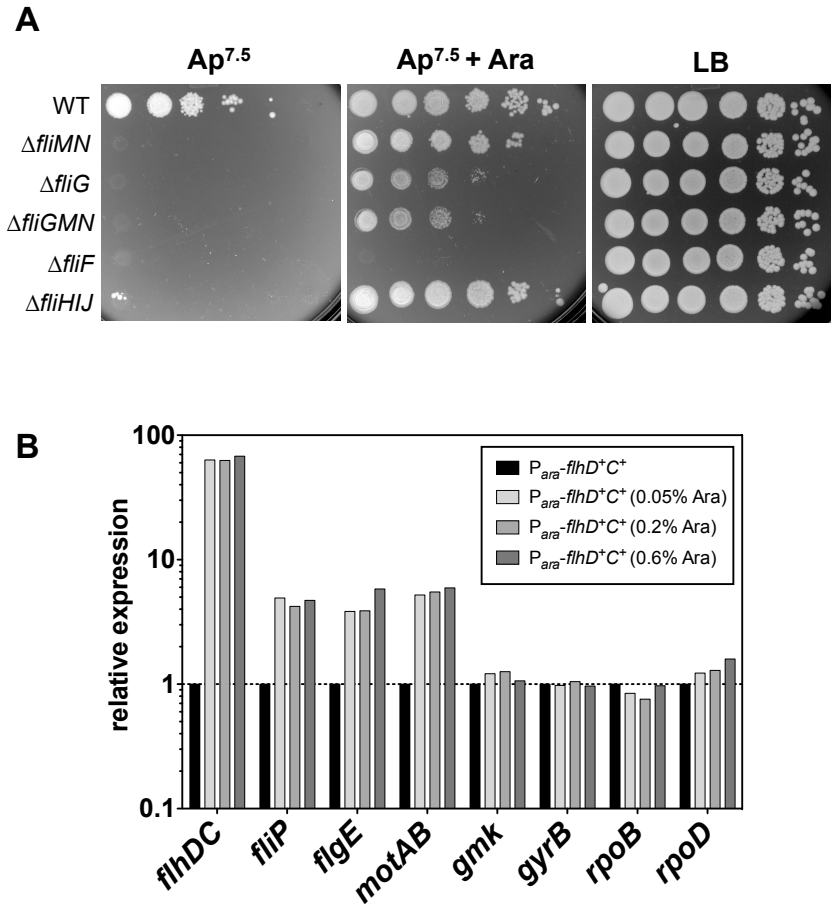

FIGURE 2.3

Overexpression of *flhDC* in deletion mutants of the C-ring and ATPase complex and effects of excess FlhDC on flagellar gene expression. (A) Overexpression of *flhDC* from the arabinose promoter confers ampicillin resistance in deletion mutants of the C-ring and ATPase complex. Strains harboring an additional, functional copy of *flhDC* under the control of the arabinose promoter were grown overnight in the absence of arabinose. Equal volumes of 10-fold serial dilutions were spotted on LB plates and PPBS $Ap^{7.5}$ plates in the presence or absence of 0.2% arabinose. Mutant strains missing two-thirds (Δ*fliMN*) or the complete C-ring (Δ*fliG* and Δ*fliGMN*), as well as a strain deleted for the ATPase complex FliHIJ, but not a mutant strain missing the MS-ring (Δ*fliF*) are able grow in the presence of excess FlhDC. WT = TH14902; Δ*fliMN* = TH15498; Δ*fliG* = TH15497; Δ*fliGMN* = TH14906; Δ*fliF* = TH14903; Δ*fliHIJ* = TH14905. (B) Effects of excess FlhDC on flagellar gene expression. Strain TH14156 (P_{araBAD}::$flhD^+C^+$) was grown for 2.5 h in LB media containing different concentrations of arabinose (0%, 0.05%, 0.2% and 0.6%) and total RNA was isolated of the pooled cultures of three biological replicates. Class I (*flhDC*), Class II (*fliP* and *flgE*), Class III (*motAB*) and *rpoD* transcript levels were analysed by real-time qPCR as described in Experimental procedures. Relative gene expression was determined using the $2^{-\Delta\Delta CT}$ method (112) and individual mRNA levels were normalized against multiple reference genes (*rpoB*, *gyrB* and *gmk*) and presented as fold change relative against the 0% arabinose control (black bars) (191).

an at least twofold excess *flhDC* was sufficient to allow FlgE-Bla secretion in the C-ring defective strain (Figure 2.3A). The strain deleted for the ATPase complex FliHIJ was also Ap^R in the presence of arabinose, confirming previous results that the ATPase function is not necessary for flagellar T3S (140, 158). While efficient secretion is possible under excess FlhDC in both the absence of the C-ring or ATPase complex, the deletion of the MS-ring prevented secretion. This indicates that the MS-ring has an essential function as a scaffold harboring the secretion apparatus, but the requirement of the C-ring and the ATPase complex can be overcome by excess substrate concentrations and increased number of potential secretion systems (see below).

It is important to note that the expression of *flhDC* from the arabinose promoter resulted in an about 60-fold upregulation of *flhDC* transcript levels if compared with wild-type *flhDC* expression (Figure 2.3B). However, different arabinose concentrations (0%, 0.05%, 0.2% and 0.6%) neither changed *flhDC* mRNA levels, nor upregulated Class II gene expression further than four- to fivefold. As shown below, consensus -10 box mutations of the *flhD* promoter result in only twofold upregulation of *flhDC*, as well as Class II gene expression (Figure 2.7C). However, this change is sufficient to allow for efficient T3S in the absence of the C-ring. This indicates that activation of Class II gene expression by the $FlhD_4C_2$ complex is saturated early by only a small increase in *flhDC* levels and cannot be increased further. Importantly, this result explains why already a small increase in *flhDC* expression (e.g. a P_{flhD} promoter up mutation or duplication of the *flhDC* operon) is sufficient to bypass the C-ring deletion.

2.3.2 Characterization of T-POP insertions that allow hook-β-lactamase (FlgE-Bla) secretion in the absence of the C-ring

DNA sequence analysis was performed on 42 independent Ap^R T-POP insertions in the Δ*flgBC* Δ*fliMN* *flgE-bla* background that did not appear to contain a duplication (they did not segregate Ap^S Tc^S segregants in the absence of selection) (Figure 2.4 and Table 2.2). Most T-POP transposon insertions resulted in an increase in FlhDC activity, by either downregulation of known transcriptional and post-transcriptional inhibitors of FlhDC (e.g. FliT, LrhA, ClpP) or upregulation of the *flhDC* operon itself (e.g. insertions in the *flhDC* promoter that increase *flhDC* expression).

Initially, the Ap^R T-POP mutants fell into three phenotypic classes (Table 2.2). (i) The first class of mutants was Ap^R solely by the T-POP insertion, indicating that the insertion knocked out a gene whose product negatively influenced flagellar T3S in the absence of the C-ring (Ap^R::T-POP). (ii) The Ap^R phenotype of the second class of mutants was dependent on addition of tetracycline, indicating that the transcriptional readthrough from the *tetA* promoter induces expression of an adjacent gene that positively influences flagellar T3S in the absence of the C-ring (Tc-Ap^R). Alternatively, the transcriptional readthrough from the *tetA* promoter could produce anti-sense RNA that would impair expression of adjacent genes. (iii) The last class of Ap^R mutants displayed an Ap^S phenotype in the presence of tetracycline (Tc-Ap^S). In this case the induction of *tetA* by addition of tetracycline presumably induces the expression of genes that negatively influence flagellar T3S in the absence of the C-ring.

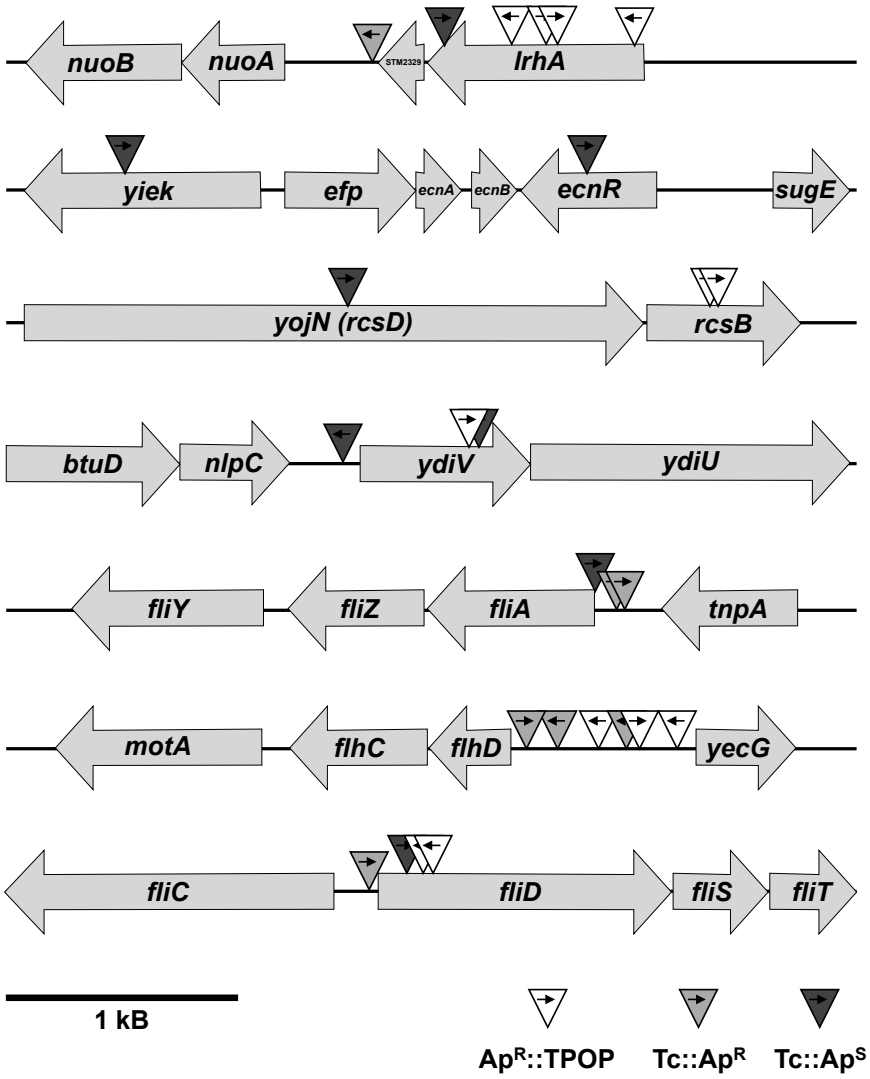

FIGURE 2.4

Schematic overview of T-POP insertions at seven different chromosomal loci that conferred ampicillin resistance in a C-ring deletion mutant. Individual T-POP insertions are shown by a triangle with an arrow indicating the direction of the *tetA* transcript. A summary of the precise insertion point of every T-POP insertion and the effect of the *tetA* transcript reading in adjacent chromosomal genes is given in Table 2.2.

TABLE 2.2

T-POP transposon insertions that allow for FlgE-Bla secretion in the absence of the C-ring.

Summary of isolated T-POP transposon insertions in the C-ring deletion strain TH12470. The *tetA* gene of the T-POP transposon lacks a terminator sequence and therefore genes upstream of *tetA* can be induced by *tetA* expression. If the addition of tetracycline conferred ampicillin resistance, the Tc effect is indicated as Tc-Ap^R and if the addition of tetracycline resulted in an ampicillin sensitive phenotype, the Tc effect is indicated as Tc-Ap^S. In all other cases, the T-POP insertion conferred ampicillin resistance on its own and the addition of tetracycline showed no effect (Ap^R::TPOP).

Allele	Insertion	Tc effect
lrhA1	*lrhA* coding region, 9 bp downstream of *ATG*	Ap^R::TPOP
lrhA2	*lrhA* coding region, 607 bp downstream of *ATG*	Ap^R::TPOP
lrhA3	*lrhA* coding region, 536 bp downstream of *ATG*	Ap^R::TPOP
lrhA4	*lrhA* coding region, 936 bp downstream of *ATG*	Tc-Ap^S
lrhA5	STM2329 terminator, 9 bp downstream of stop	Tc-Ap^R
ecnR6	*ecnR* coding region, 157 bp downstream of *ATG*	Tc-Ap^S
ecnR7	*yjek* coding region, 859 bp downstream of *ATG*	Tc-Ap^S
slyA1	*slyA* coding region, 170 bp downstream of *ATG*	Ap^R::TPOP
rcsB131	*rcsB* coding region, 332 bp downstream of *ATG*	Ap^R::TPOP
rcsB132	*rcsB* coding region, 332 bp downstream of *ATG*	Ap^R::TPOP
yojN253	*yojN* coding region, 1211 bp downstream of *ATG*	Tc-Ap^S
ydiV254	*ydiV* coding region, 634 bp downstream of *ATG*	Ap^R::TPOP
ydiV255	*ydiV* coding region, 640 bp downstream of *ATG*	Tc-Ap^S
ydiV256	*ydiV* promoter, 68 bp upstream of *ATG*	Tc-Ap^S
clpP71	*clpP* coding region, 579 bp downstream of *ATG*	Tc-Ap^S
fliA7876	*fliA* promoter, 30 bp upstream of *ATG*	Tc-Ap^R
fliA7877	*fliA* promoter, 11 bp upstream of *ATG*	Tc-Ap^R
fliA7878	*fliA* promoter, 1 bp upstream of *ATG*	Tc-Ap^S
flhDC7872	*flhD* promoter, 426 bp upstream of *ATG*	Ap^R::TPOP
flhDC7873	*flhD* promoter, 625 bp upstream of *ATG*	Ap^R::TPOP
flhDC7874	*flhD* promoter, 799 bp upstream of *ATG*	Ap^R::TPOP
flhDC7875	*flhD* promoter, 615 bp upstream of *ATG*	Tc-Ap^R
flhDC5	*flhD* promoter, 178 bp upstream of *ATG*	Tc-Ap^RR
flhDC6	*flhD* promoter, 22 bp upstream of *ATG*	Tc-Ap^R
flgM1	*flgM* coding region, 152 bp downstream of *ATG*	Ap^R::TPOP
flgM2	*flgA* promoter, 85 bp upstream of *ATG*	Ap^R::TPOP
fliD7879	*fliD* coding region, 93 bp downstream of *ATG*	Ap^R::TPOP
fliD7880	*fliD* coding region, 95 bp downstream of *ATG*	Ap^R::TPOP
fliD7881	*fliD* promoter, 30 bp upstream of *ATG*	Tc-Ap^R
fliD7882	*fliD* coding region, 85 bp downstream of *ATG*	Tc-Ap^S
fliR1	*fliR* coding region, 608 bp downstream of *ATG*	Ap^R::TPOP
STM1856-1	STM1854 coding region, 5 bp downstream of *ATG*	Ap^R::TPOP
STM1856-2	STM1856 promoter, 465 bp upstream of *ATG*	Tc-Ap^S
STM2011-1	*amn* coding region, 5 bp downstream of *ATG*	Tc-Ap^R
STM2011-2	STM2011 promoter, 272 bp upstream of *ATG*	Tc-Ap^R
rfbP1	*rfbP* coding region, 1300 bp downstream of *ATG*	Tc-Ap^S
pgtE1	*pgtE* coding region, 444 bp downstream of *ATG*	Tc-Ap^R

Allele	Insertion	Tc effect
ddg/yfdZ1	*ddg/yfdZ* terminator, 8 bp downstream of ddg stop	Ap^R::TPOP
pykF1	*pykF* terminator, 264 bp downstream of pykF stop	Tc-Ap^R
garL1	*garL* coding region, 74 bp downstream of *ATG*	Ap^R::TPOP
yieP1	*yieP* coding region, 398 bp downstream of *ATG*	Tc-Ap^R
hpaX1	*hpaX* coding region, 196 bp downstream of *ATG*	Tc-Ap^R

In summary, we isolated three Ap^R::T-POP insertions in the promoter region of *flhDC* that potentially disrupt binding sites of negative regulators of *flhDC* transcription. Three more T-POP insertions in the *flhDC* promoter displayed a Tc-dependent Ap^R phenotype (Tc-Ap^R), indicating an overexpression of *flhDC* upon Tc addition (Figure 2.4). Two Ap^R::T-POP, one Tc-Ap^R and one Tc-Ap^S T-POP transposon insertion were in the coding region or promoter of *fliD* respectively (Figure 2.4). The transposon insertions in *fliD* presumably resulted in a polar effect on the expression of *fliT*, an anti-$FlhD_4C_2$ factor that prevents binding of the activator complex to Class II promoters (206). This was verified by the introduction of a *fliT* deletion allele into strain TH12470 (Δ*flgBC* Δ*fliMN flgE-bla*), which resulted in an Ap^R phenotype. Additionally, we isolated T-POP insertions in known negative regulators of *flhDC* transcription or *flhDC* levels, like *lrhA*, *ecnR*, *rcsB*, *ydiV* and *clpP*. Null alleles of these inhibitor loci presumably resulted in increased *flhDC* expression or increased stability of the $FlhD_4C_2$ activator complex.

Accordingly, we isolated five T-POP insertions in the coding region or vicinity of *lrhA*, a LysR-type DNA-binding protein that was previously characterized as a regulator of *flhDC* transcription in *E. coli* (109) (Figure 2.4). One Tc-Ap^S T-POP insertion was found in the coding region of *ecnR*, a recently characterized regulator of flagellar gene expression (203). Another Tc-Ap^S T-POP insertion had been inserted in *yjek*, downstream of *ecnR*, thereby presumably negatively influencing the expression of *ecnR* (Figure 2.4). One Ap^R::T-POP transposon had inserted in the coding region of *slyA*, a DNA-binding protein that has been previously shown to enhance expression of filament subunits (178). Two Ap^R::T-POP transposons were isolated in the coding region of *rcsB* and one Tc-Ap^S transposon had inserted in *rcsD* (*jojN*), upstream of *rcsB* (Figure 2.4). RcsB is another negative regulator of *flhDC* expression and has been shown to directly bind the *flhD* promoter (196). We isolated one Tc-Ap^S T-POP insertion in the promoter region and two T-POP insertions (one Ap^R::T-POP and one Tc-Ap^S T-POP) in the coding region of the c-di-GMP-related protein YdiV (Figure 2.4). YdiV negatively regulates $FlhD_4C_2$ activity at a post-transcriptional level (203). One Tc-Ap^S T-POP transposon had inserted in the coding region of *clpP*. It has been previously shown that the $FlhD_4C_2$ complex is degraded by the ClpXP protease (190).

T-POP insertions isolated in the promoter region of the *fliAZ* operon showed opposite effects: two were Tc-Ap^R and one was Tc-Ap^S (Figure 2.4). The *fliZ* gene encodes an activator of *flhDC* (164) and the SpiI virulence system. The *fliA* gene encodes σ^{28}, which inhibits *flhDC* transcription (see below). Thus, these insertions could affect *fliA*, *fliZ* or both. We also isolated two Ap^R::T-POP transposon insertions in the coding

region of *flgM* and promoter region of *flgA*, upstream of *flgM*, respectively. Insertions in *flgA* are polar on *flgM* transcription. Kutsukake (103) showed that the *flhDC* operon is autogenously repressed in the presence of both σ^{28} and its cognate anti-σ factor FlgM. However, *flhDC* expression is activated in the presence of σ^{28} and the absence of FlgM. As shown in Figure 2.5D, the overproduction of *fliA* from the arabinose promoter results in inhibition of *flhC* transcription in a strain harboring a functional copy of the *flgM* gene. This unknown mechanism of *flhDC* regulation would explain the effects on *flhDC* expression by our T-POP insertions in both *flgM* and the promoter region of the *fliAZ* operon.

Additionally, we isolated 12 T-POP transposon insertions in genes that are not obviously related to *flhDC* regulation. One Ap^R::T-POP insertion was located after bp 608 of the 795 bp *fliR* gene. Two T-POP had inserted into the vicinity of *sopE2*, a type III-secreted effector protein. Two more Tc-Ap^R T-POP insertions were located to the coding region or vicinity of STM2011, a protein of unknown function. Seven more single T-POP insertions were found to be in *rfbP* (undecaprenol-phosphate galactosephosphotransferase/O-antigen transferase), *pgtE* (outer membrane protease), *ddg/yfdZ* (lipid A biosynthesis palmitoleoyl-acyltransferase and aminotransferase), *pykF* (pyruvate kinase), *garL* (α-dehydro-β-deoxy-D-glucarate aldolase), *yieP* (putative regulatory protein) and *hpaX* (4-hydroxyphenylacetate permease) respectively. Each will require further characterization to determine how they result in Ap^R.

2.3.3 Effects of T-POP insertions on flagellar gene transcription

T-POP insertions in *fliD* presumably have a polar effect on *fliT*, a negative regulator of *flhDC*. Accordingly, we analysed Class II transcription in various T-POP insertions that resulted in an Ap^R phenotype in the absence of the C-ring components FliM and FliN (Figure 2.5A). We found that the T-POP insertions in *fliD*, *fliD7879* and *fliD7881*, respectively, increased Class II transcription about 20-30%. T-POP insertions in the coding region of *lrhA*, *slyA* and *ecnR* had the most pronounced effect on Class II transcription. The loss-of-function T-POP insertion in *lrhA2* increased Class II transcription about 1.7-fold, whereas the T-POP insertions in *slyA* and *ecnR* allowed for 1.3- to 1.4-fold enhanced Class II transcription.

Several other analysed T-POP insertion had no apparent effect on Class II transcription, although the insertions resulted in an Ap^R phenotype in the C-ring deletion mutant. Surprisingly, the induction of down- and upstream genes of the respective T-POP insertions by induction with tetracycline resulted in 10-30% decreased Class II transcription in the cases of *ecnR7* (insertion in *yjek*, upstream of *ecnR*), STM1856, *ddg/yfdZ1* and STM2011 (Figure 2.5A). We therefore asked the question whether the Tc-Ap^S phenotype of the *ecnR7*::T-POP (insertion in *yjek*, upstream of *ecnR*) was due to Tc-dependent induction of *ecnR*. Accordingly, we analysed *ecnR* transcription using an *ecnR*::Mu*d*J (*lac* transcriptional fusion) insertion described previously (203). As shown in Figure 2.5B, the T-POP insertion in *yiek* (*ecnR7*) displayed no apparent defect in *ecnR* transcription in the presence or absence of tetracycline.

Also, the effects of other T-POP insertions in less characterized genes or in intergenic

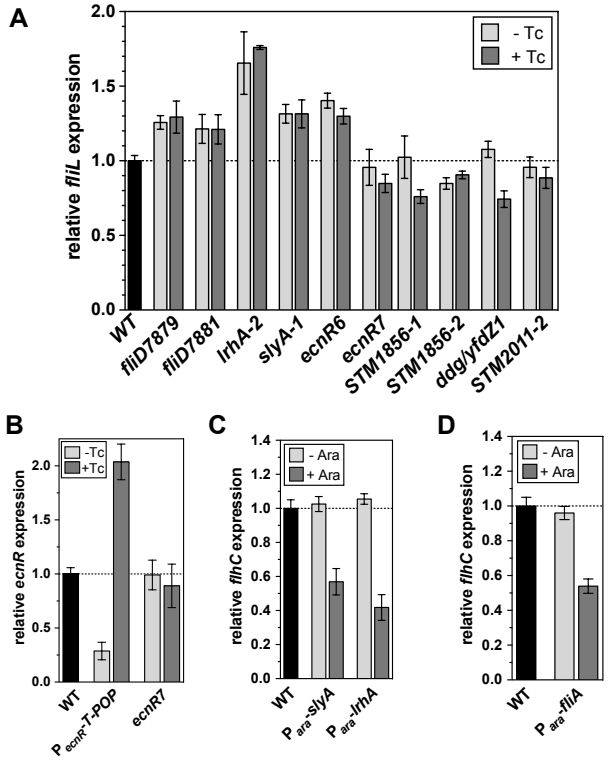

FIGURE 2.5

Flagellar Class I and Class II expression levels of various T-POP insertion mutants. (A) Relative flagellar Class II transcription levels of selected, ampicillin-resistance conferring, T-POP insertions. Relative Class II transcription from the *fliL*::Mu*dJ* transcriptional reporter was measured by β-galactosidase assays as described in Experimental procedures. Class II transcription was measured in the presence or absence of tetracycline and normalized against the wild-type control. Addition of tetracycline induces transcription from the *tetA* promoter, which proceeds into chromosomal DNA adjacent to the T-POP insertion. The data shown are the mean ± SD of at least three independent, biological replicates. (B) Relative *ecnR* transcription in a strain with a T-POP insertion in *yiek* near *ecnR*. Relative *ecnR* transcription from the *ecnR*::Mu*dJ* transcriptional reporter was measured by β-galactosidase assays as described in Experimental procedures in strains harboring a T-POP insertion upstream of *ecnR* (P_{ecnR}::T-POP) or in *yiek* near *ecnR* (*ecnR7*). *ecnR* transcription was measured in the presence or absence of tetracycline and normalized against the wild-type control. The data shown are the mean ± SD of at least three independent, biological replicates. (C) Relative flagellar Class I transcription in strains overexpressing the transcriptional regulators SlyA and LrhA. Relative Class I transcription from the *flhC*::Mu*dJ* transcriptional reporter was measured by β-galactosidase assays as described in Experimental procedures in strains harboring *slyA* or *lrhA* under control of the arabinose promoter. Class I transcription was measured in the presence or absence of 0.2% arabinose respectively, and normalized against the wild-type control. The data shown are the mean ± SD of at least three independent, biological replicates. (D) Relative flagellar Class I transcription in a strain overexpressing the flagellar-specific σ factor σ^{28}. Relative Class I transcription from the *flhC*::Mu*dJ* transcriptional reporter was measured by β-galactosidase assays as described in Experimental procedures in a strain harboring *fliA*, the gene encoding for the flagellar-specific σ factor σ^{28}, under control of the arabinose promoter. Class I transcription was measured in the presence or absence of 0.2% arabinose respectively, and normalized against the wild-type control. The data shown are the mean ± SD of at least three independent, biological replicates.

regions remain elusive so far. Those T-POP insertions might confer Ap^R in the C-ring deletion mutant by the means of other mechanisms unrelated to regulation of *flhDC*. Possible reasons that would allow for elevated FlgE-Bla secretion include an increased proton motive force gradient, less competition between secretion substrates or effects on localization of T3S substrates.

In conclusion, most of the analysed T-POP insertions directly affect negative regulators of *flhDC*, thus resulting in increased Class II transcription and accordingly in enhanced secretion substrate levels. If the C-ring functions as an affinity cup that increases the efficiency of the secretion process, then elevated levels of substrates, like the hook-β-lactamase protein, would still allow for sufficient secretion to confer Ap^R.

2.3.4 LrhA and SlyA negatively regulate *flhDC* transcription in *S. enterica*

In our screen for mutants that allowed flagellar T3S in the absence of the C-ring, we isolated several T-POP insertions in two previously uncharacterized regulatory loci of *flhDC* expression in *S. enterica*, *lrhA* and *slyA* (Table 2.2). The LysR-type regulator LrhA has been previously shown to negatively regulate transcription of *flhDC* in *E. coli* (109). Conversely, the lack of the DNA-binding protein SlyA has been associated with increased flagellin expression (178). To analyse the effects of LrhA and SlyA in *Salmonella*, we cloned both putative regulators under the control of the arabinose promoter. As shown in Figure 2.5C, the expression of LrhA and SlyA, respectively, from the arabinose promoter decreases *flhDC* transcription 40-60%. Therefore, we conclude that both LrhA and SlyA act as negative regulators of *flhDC* transcription in *S. enterica*.

2.3.5 Null alleles in *fliA* and *flhDC* promoter mutants result in FlgE-Bla secretion in the absence of the C-ring

We attempted to isolate amino acid substitutions in flagellar genes that resulted in FlgE-Bla secretion in strains missing parts (Δ*fliMN*) or all (Δ*fliG*) of the C-ring. Using the FlgE-Bla reporter construct in the rod-minus mutant background described above, we used transposons linked to the *flh* and *fli* flagellar regions to separate *flh*- and *fli*-linked Ap^R mutants from mixed pools of spontaneous Ap^R colonies. Spontaneous Ap^R mutants arose in strain TH12470 (Δ*flgBC flgE-bla* Δ*fliMN*) at a frequency of 10^{-5} and in strain TH12466 (Δ*flgBC flgE-bla* Δ*fliG*) at a frequency of 10^{-8}. A *mutS*::*Km* insertion was introduced into strain TH12466 and the frequency of spontaneous Ap^R mutants rose to 10^{-6}. In the Δ*fliG* strain the complete C-ring is missing as FliG acts as a scaffold for FliMN assembly, whereas in the Δ*fliMN* strain two-thirds of the C-ring are not assembled. The lower frequency of mutation in the Δ*fliG* strain compared with the Δ*fliMN* strain can be explained by the following: (i) the physical C-ring structure may have importance in providing affinity sites for substrates or excluding non-substrates or (ii) FliG in addition to FliMN provides additional interaction sites for secretion substrates. Accordingly, if the whole structure is missing (Δ*fliG*), one would expect a more pronounced effect than if two-thirds are missing (Δ*fliMN*). Additionally, we showed above that Δ*fliMN* displays increased FlgE-Bla secretion under excess FlhDC conditions com-

pared with both Δ*fliG* and Δ*fliGMN*, where the complete C-ring is missing (Figure 2.3A). These results provide important evidence for our model of the C-ring acting as an affinity cup-like structure that locally increases secretion substrate concentration prior to secretion or excludes non-substrate interactions as discussed below.

Individual mutants that were linked to the *flhDC* operon were isolated in the Δ*fliMN* and Δ*fliG* backgrounds. DNA sequence analysis showed them to be single-base pair changes in the *flhD* promoter region: *-368G::A* (relative to *AUG* start codon) in the Δ*fliG* background and *-152C::T* in the Δ*fliMN* background). The *-368G::A* allele changed the -10 sequence for the P4 promoter towards the consensus -10 σ^{70} binding site from TGGAAT to TAGAAT and the *-152C::T* allele change was outside any known promoter region, but presumably allowing for increased *flhDC* expression by affecting the binding site of a negative regulator of *flhDC* expression (Table 2.2). Two mutations that mapped to the *fliAZY* operon were both single-base pair changes resulting in nonsense mutations of the *fliA* gene (Q106::STOP, Table 2.2). This suggested that loss of σ^{28}-dependent transcription increased FlhDC activity. We tested for the effect of increased *fliA* gene expression on an *flhC*::Mu*d*J reporter construct by overexpression of a second copy of *fliA* from the arabinose promoter. If the loss of σ^{28}-dependent transcription would increase FlhDC activation of Class II promoters, then increased *fliA* expression should have a negative effect on *flhDC* expression. As shown in Figure 2.5D, the addition of arabinose resulted in the inhibition of *flhDC* transcription. This result is an apparent contradiction to our earlier results that showed increased *flhDC* activity, as measured by FlgE-Bla secretion in the Δ*flgBC* Δ*fliMN* background in strains with reduced FlgM levels. One would expect that reduced FlgM levels result in increased σ^{28} activity, which in turn should negatively influence *flhDC* expression as described above. However, these results are consistent with previous results from Kutsukake (103) who showed that the *flhDC* operon was autogenously repressed, except under the condition where *flgM* was inactivated in a *fliA*$^+$ background. In the *flgM*-defective *fliA*$^+$ background the *flhDC* operon was autogenously activated (103). These apparent conflicting results of σ^{28}-dependent inhibition of *flhDC*, and FlgM (anti-σ^{28})-dependent inhibition of *flhDC* warrant further study. It is possible that the FlgM/σ^{28} complex acts directly or indirectly to inhibit *flhDC* transcription.

2.3.6 Effects of *flhDC* perfect -10 box promoter mutants on swimming motility and HBB number

Based on the discovery that single-base pair changes in the *flhD* promoter are sufficient to allow for flagellar T3S in the absence of the C-ring, we further characterized the effects of *flhD* promoter mutants. The *flhDC* operon is transcribed from at least six different promoters and we constructed mutations in the known P1, P2, P3, P5 and P6 *flhD* promoter sequences to have a consensus -10 box (TATAAT) (Figure 2.6). As shown in Figure 2.7A, the perfect -10 box mutations of the P3, P5 and P6 promoters had no apparent effect on swimming motility. However, the mutation of the P1 promoter resulted in an apparent 1.7-fold increased migration rate in the swim plate compared with the wild type (Figure 2.7A and B).

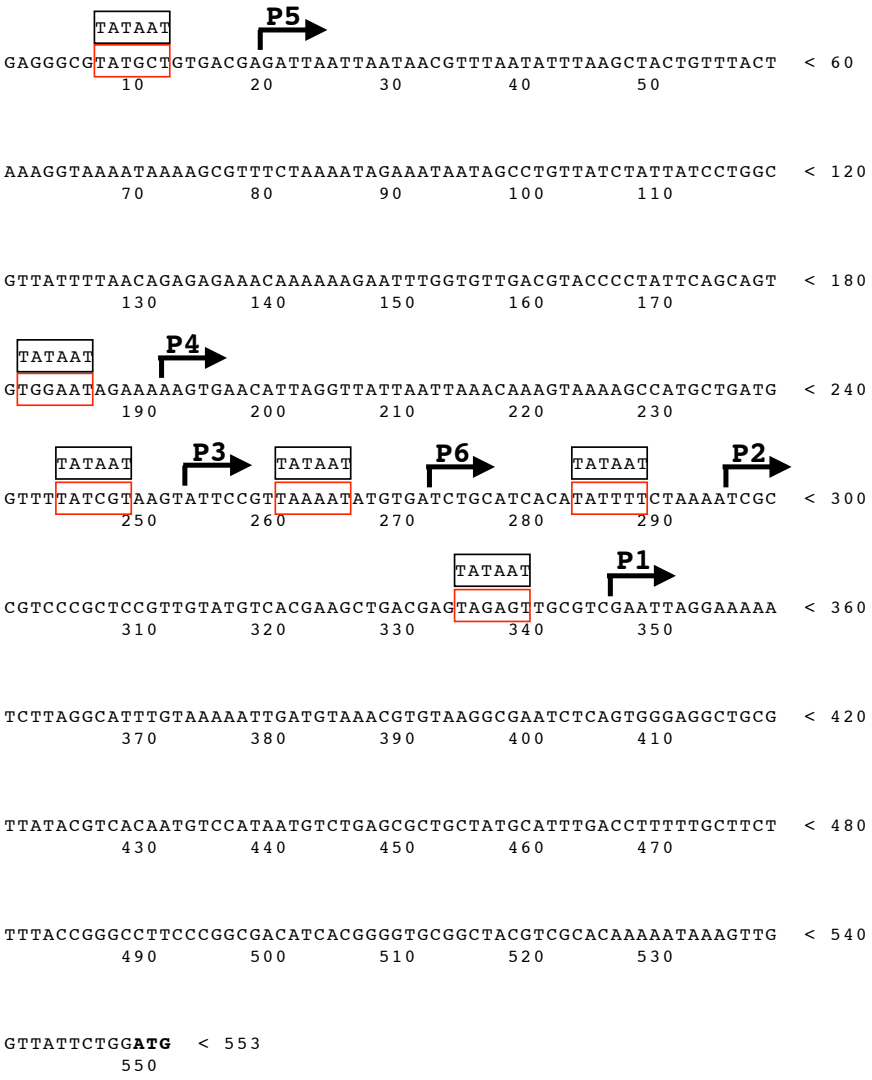

FIGURE 2.6

Schematic of the *flhD* promoter region. The DNA sequence of the *flhD* promoter region of *S. enterica* and the six described transcriptional start sites (207) of the *flhD* promoter are displayed. A red box annotates the wildtype -10 box sequence, whereas the black box annotates the respective consensus -10 box mutation. A black arrow displays the transcriptional start site (+1) of the respective promoter.

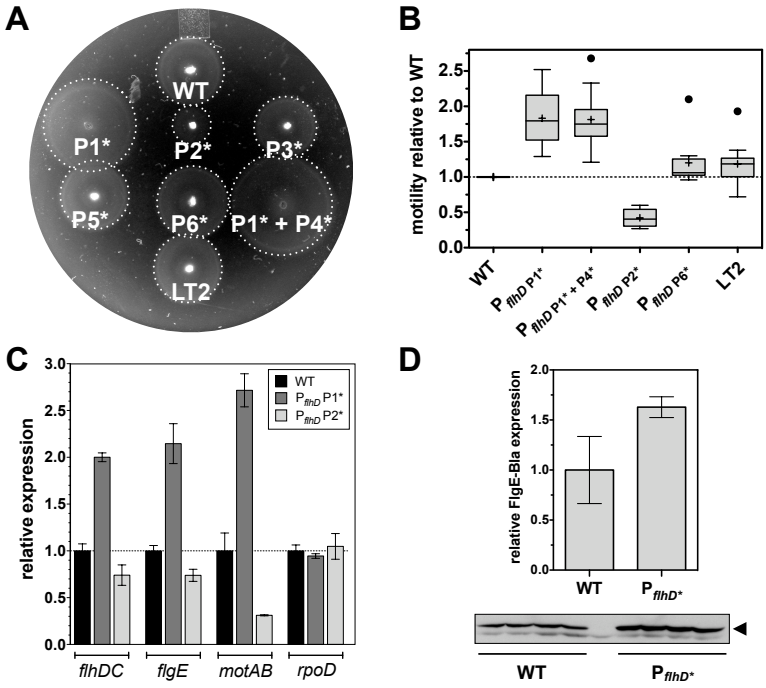

FIGURE 2.7

Motility, flagellar gene transcription and FlgE-Bla protein levels of P_{flhD} promoter mutants. (A) Motility of P_{flhD} promoter mutants. A representative image shows the motility of different P_{flhD} promoter mutants after 4 h of incubation at 37 ℃. A dotted white line indicates the radius of the swarming circle. Consensus -10 box mutants of the P3, P5 and P6 *flhD* promoter display motility comparable to wild type. The consensus -10 box mutant of the P1 *flhD* promoter and the combination of the consensus -10 box mutations of both the P1 and P4 *flhD* promoter showed increased swimming behaviour, whereas the consensus -10 box mutation of the P2 *flhD* promoter displayed a decreased motility. The P_{flhD} promoter mutants were constructed in a strain harboring a functional *fliM-gfp* mutation (denoted here as WT). Motility was compared with *S. enterica* LT2 to show that the *fliM-gfp* mutation did not affect flagellar assembly or motility. (B) Quantitative motility assay of P_{flhD} promoter mutants. The motility of different mutant strains was measured by determining the motility diameter after 4 h incubation at 37℃. For each strain the diameter of 10 independent biological replicates was measured and normalized to the motility diameter of the wild-type control (*fliM-gfp*) on the same motility plate. Motility was compared with *S. enterica* LT2 to show that the *fliM-gfp* mutation did not affect flagellar assembly or motility. The data are presented as box diagrams with whiskers according to the Tukey method. A horizontal line indicates the median and a black cross the mean. Outliners are represented by a black dot. (C) Relative Class I, Class II and Class III mRNA levels as quantified by real-time qPCR. Class I (*flhDC*), Class II (*flgE*), Class III (*motAB*) and *rpoD* mRNA levels were analysed by real-time qPCR as described in Experimental procedures. Relative gene expression was determined using the $2^{-\Delta\Delta CT}$ method (112). Individual mRNA levels were normalized against *rpoA*, *gyrB* and *gmk* transcript levels and presented as fold change relative against the wild-type control (191). The data shown represent the mean of three independent, biological samples ± SD. (D) Relative FlgE-Bla protein levels analysed by quantitative Western blotting. Whole-cell lysates were prepared of four independent biological replicates of wild-type or P1 + P4 consensus -10 box *flhD* promoter mutant cells respectively. The experiment was performed in a Δ*fliP* background in order to analyse total protein levels. The reporter protein FlgE-Bla was expressed from its native promoter and FlgE-Bla was detected using FlgE-specific antibodies and quantified as described in Experimental procedures. Data shown are the mean of four replicates ± SD.

The combination of P_{flhDC} P1 and P4 -10 box mutations did not further increase motility, whereas the perfect -10 box mutation of the P2 promoter decreased motility to about 50% of wild-type motility (Figure 2.7A+B). In order to further characterize the effects of the P_{flhDC} promoter mutations on flagellar gene expression, we performed real-time quantitative PCR analysis of cDNA reversely transcribed from strains harboring the P_{flhDC} P1 or the P_{flhDC} P2 perfect -10 box mutation. As displayed in Figure 2.7C, the P1 mutation resulted in an about twofold upregulation of *flhDC* mRNA, whereas the P2 mutation resulted in a slight downregulation of *flhDC* mRNA levels. We additionally confirmed this finding using an *flhC-lac* fusion construct (data not shown). On the level of Class II and Class III flagellar genes expression, the P1 and P2 -10 box mutations also resulted in an up- or downregulation respectively (Figure 2.7C). In case of the P1 mutation, *flgE* expression is enhanced about twofold, whereas *flgE* expression in the P2 mutant is slightly decreased. Similarly, the mRNA levels of the motor force generator proteins MotAB are upregulated more than twofold in the P1 mutant and downregulated in the P2 mutant background (Figure 2.7C). Taken together, the increase in *flhDC* expression results in an about two- to fourfold increase in flagellar Class II and Class III gene expression that explains the differences in motility described above. To confirm the twofold upregulation of HBB-type secretion substrates on a protein level, we examined expression of the hook-β-lactamase fusion construct in the P_{flhDC} P1 perfect -10 box mutation background by quantitative Western blot analysis. As shown in Figure 2.7D, FlgE-Bla is upregulated about 1.6-fold in the P1 promoter mutant.

Accordingly, every mutation that resulted in an increase in $FlhD_4C_2$ levels resulted in an about twofold upregulation of both structural components of the HBB complex, as well as HBB-type secretion substrates.

Based on the upregulation of HBB-type substrates we next investigated whether the number of hook-basal bodies per cell is also increased. For this we utilized an FlgE variant harboring a haemagglutinin epitope tag for specific and sensitive immunodetection of completed HBB structures. We additionally used GFP fusions to components of the C-ring, FliM and FliG, respectively, to analyse assembled C-rings by fluorescent microscopy. As shown in Figure 2.8A, the number of completed hook-basal bodies per cell under wild-type *flhDC* levels peaks at about two HBB per µm cell length. Accordingly, wild-type *S. enterica* produces about four to six HBB structures per cell. We next investigated the effects of both the P_{flhDC} P1 perfect -10 box mutation and the combination of the P1 + P4 perfect -10 box mutation on the number of HBB structures per cell. As displayed in Figure 2.8B and C, the number of HBBs doubles to about four HBBs per µm cell length in either the P1 or the P1 + P4 combination mutant. The P_{flhDC} P1 perfect -10 box mutant therefore effectively doubles the number of available secretion systems (= HBBs) per cell, which is consistent with the gene expression data mentioned earlier. The number of completed HBBs in the P_{flhDC} P2 perfect -10 box mutant, however, is greatly reduced (Figure 2.8D). The majority of the cells do not complete a HBB, which might provide an explanation for the severe reduction in motility as shown in Figure 2.7A and B.

We additionally confirmed the twofold upregulation of flagellar basal body structures using FliG-GFP and FliM-GFP protein fusions mentioned above (Figure 2.9A and B). By

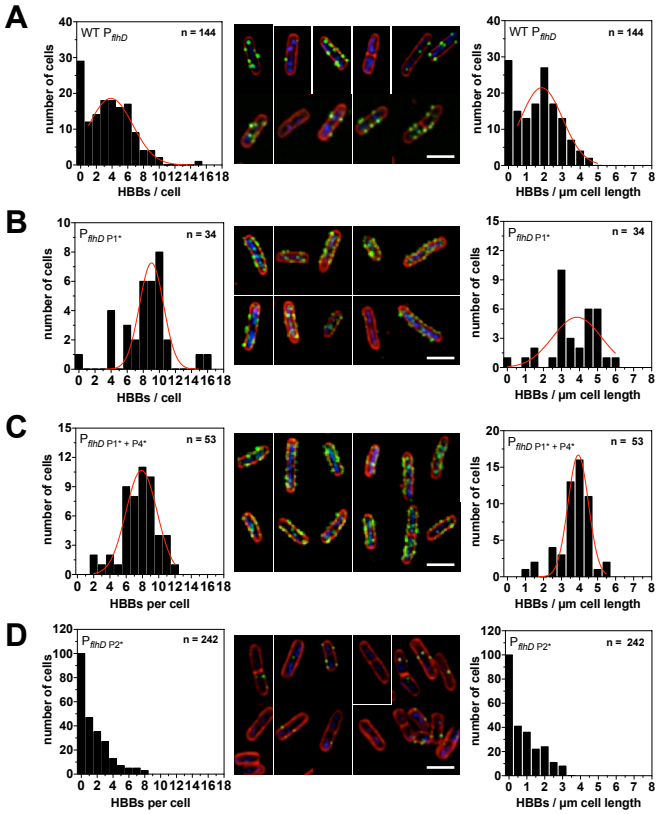

FIGURE 2.8

Number of assembled HBB complexes as analysed by hook immunostaining. (A) Number of HBB complexes of the wild-type control. Left panel: distribution of HBBs per cell. Non-linear fitting of the Gaussian distribution was employed (red line) and the average HBB number per cell is 3.8 ± 2.8 (n = 144). Middle panel: hook immunostaining of exemplary cells expressing wild-type levels of *flhDC*. Right panel: distribution of HBBs per µm cell length. Cell length was measured based on the FM-64 membrane staining. Non-linear fitting of the Gaussian distribution was employed (red line) and the average HBB number per µm is 1.9 ± 1.2 (n = 144). (B) Number of HBB complexes of the P_{flhD} P1 consensus -10 box mutant. Left panel: distribution of HBBs per cell. Non-linear fitting of the Gaussian distribution was employed (red line) and the average HBB number per cell is 9.0 ± 1.5 (n = 34). Middle panel: hook immunostaining of exemplary P_{flhD} P1 consensus -10 box mutant cells with increased *flhDC* expression levels. Right panel: distribution of HBBs per µm cell length. Cell length was measured based on the FM-64 membrane staining. Non-linear fitting of the Gaussian distribution was employed (red line) and the average HBB number per µm is 3.9 ± 1.4 (n = 34). (C) Number of HBB complexes of the P_{flhD} P1 + P4 consensus -10 box mutant. Left panel: distribution of HBBs per cell. Non-linear fitting of the Gaussian distribution was employed (red line) and the average HBB number per cell is 7.9 ± 1.9 (n = 53). Middle panel: hook immunostaining of exemplary P_{flhD} P1 + P4 consensus -10 box mutant cells with increased *flhDC* expression levels. Right panel: distribution of HBBs per µm cell length. Cell length was measured based on the FM-64 membrane staining. Non-linear fitting of the Gaussian distribution was employed (red line) and the average HBB number per µm is 3.9 ± 0.6 (n = 53). (D) Number of HBB complexes of the P_{flhD} P2 consensus -10 box mutant. Left panel: distribution of HBBs per cell. Middle panel: hook immunostaining of exemplary P_{flhD} P2 consensus -10 box mutant cells with decreased *flhDC* expression levels. Right panel: distribution of HBBs per µm cell length. Cell length was measured based on the FM-64 membrane staining.
Green: HBB complexes (FlgE::3xHA tag) labelled with anti-haemagglutinin antibodies coupled to Alexa Fluor^{488}. Red: cell membrane stained with FM-64. Blue: DNA stained with Hoechst. Scale bar is 2 µm.

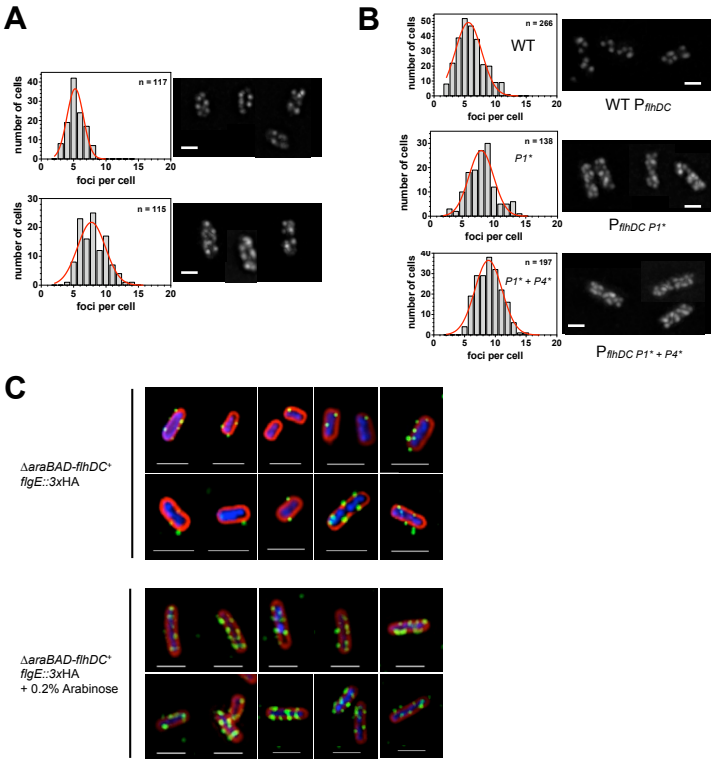

FIGURE 2.9

Number of hook-basal-body (HBB) complexes as analyzed by C-ring-GFP microscopy and hook immunostaining. (A) Number of C-ring complexes as analyzed by FliG-GFP microscopy. A strain harboring a functional FliG-GFP fusion as well as the *flhDC* operon under arabinose control was grown in the presence or absence of arabinose and analyzed by fluorescence microscopy. Upper panel: distribution of C-rings per cell and exemplary images of cells expressing FliG-GFP in the absence of arabinose (wildtype *flhDC* levels). Non-linear fitting of the Gaussian distribution was employed (red line) and the average number of C-rings per cell is 5.2 ± 1.3 (n = 117). Lower panel: distribution of C-rings per cell and exemplary images of cells expressing FliG-GFP in the presence of arabinose (increased *flhDC* levels). Non-linear fitting of the Gaussian distribution was employed (red line) and the average number of C-rings per cell is 7.8 ± 2.2 (n = 115). Scale bar is 2 µm. (B) Number of C-ring complexes as analyzed by FliM-GFP microscopy. A strain harboring a functional FliM-GFP fusion as well as several *flhD* promoter mutations was analyzed by fluorescence microscopy. Upper panel: distribution of C-rings per cell and exemplary images of a strain expressing FliM-GFP with a wildtype *flhD* promoter. Non-linear fitting of the Gaussian distribution was employed (red line) and the average number of C-rings per cell is 5.6 ± 2.2 (n = 266). Middle panel: distribution of C-rings per cell and exemplary images of a strain expressing FliM-GFP with a perfect -10 box of the P1 *flhD* promoter. Non-linear fitting of the Gaussian distribution was employed (red line) and the average number of C-rings per cell is 8.0 ± 2.0 (n = 138). Lower panel: distribution of C-rings per cell and exemplary images of a strain expressing FliM-GFP with a perfect -10 box of the P1 + P4 *flhD* promoter. Non-linear fitting of the Gaussian distribution was employed (red line) and the average number of C-rings per cell is 8.9 ± 2.2 (n = 197). Scale bar is 2 µm. (C) Number of assembled hook-basal-body (HBB) complexes as analyzed by hook immunostaining. A strain harboring a functional FlgE::3xHA mutation as well as *flhDC* under arabinose control was grown in the presence or absence of arabinose and analyzed by fluorescence microscopy. Upper panel: exemplary images of cells with immunostained hooks in the absence of arabinose (wildtype *flhDC* levels). Lower panel: exemplary images of cells with immunostained hooks in the presence of arabinose (increased *flhDC* levels). Green: HBB complexes (FlgE::3xHA tag) labeled with anti-hemagglutinin antibodies coupled to Alexa Fluor^{488}. Red: cell membrane stained with FM-64. Blue: DNA stained with Hoechst. Scale bar is 2 µm.

overexpressing functional *flhDC* from the inducible arabinose promoter (P_{araB}-*flhD*$^+$ *C*$^+$) we could furthermore confirm that elevated $FlhD_4C_2$ levels and thus increased expression of Class II genes produces about twofold more HBB structures per cell compared with wild-type *flhDC* levels (Figure 2.9C).

In summary, these data demonstrate that the upregulation of *flhDC* expression increases both the availability of secretion substrates and the number of export systems *per se* and taken together, these effects account for flagellar T3S even in the absence of the C-ring.

2.4 Discussion

In this work we employed a random screen for enhanced flagellar type III-specific protein secretion in a secretion deficient C-ring deletion mutant using the T-POP transposon. We utilized a hook-β-lactamase (FlgE-Bla) fusion construct in a strain deleted for the rod proteins FlgB and FlgC to positively select for flagellar T3S. The hook-β-lactamase reporter protein is selectively secreted via the flagellar T3S apparatus located at the base of the HBB and confers ampicillin resistance if secreted into the periplasm in a strain missing the proximal rod subunits FlgB and FlgC (108). In a strain deleted for two-thirds of the cytoplasmic C-ring (Δ*fliMN*), flagellar T3S is severely impaired and the FlgE-Bla reporter remains in the cytoplasm. Using a random T-POP transposon mutagenesis approach, we positively selected for T-POP transposon insertions that allowed for FlgE-Bla secretion even in the absence of the C-ring.

We isolated and analysed by DNA sequencing 42 independent T-POP insertions that we grouped into three different classes. The first class of T-POP insertions conferred ampicillin resistance without induction of down- or upstream genes using tetracycline (Ap^R::T-POP). The second class of mutants conferred ampicillin resistance after induction of down- or upstream genes using tetracycline (Tc-Ap^R). The mutants where induction with tetracycline resulted in an ampicillin sensitive phenotype were grouped into the third class of T-POP insertions (Tc-Ap^S). In summary, we obtained Ap^R::T-POP insertions in the coding region of several negative regulators of *flhDC*, e.g. *lrhA*, *slyA*, *ydiV*, *rcsB*, *ecnR* and *clpP*. Those proteins have been previously shown to regulate *flhDC* expression or $FlhD_4C_2$ protein stability in *E. coli* or *S. enterica*. We additionally isolated several T-POP insertion in *fliD*, upstream of *fliT*, another negative regulator of *flhDC*. In a complimentary approach, we selected Mu*d* insertions in the *Salmonella* chromosome that conferred ampicillin resistance in the absence of the C-ring by duplication of the *flhDC* operon. We confirmed this finding by expressing a second copy of *flhDC* from the arabinose promoter. Mutant strains (Δ*flgBC flgE-bla* P_{ara}-*flhD*$^+$ *C*$^+$) missing two-thirds (Δ*fliMN*) or the complete C-ring (Δ*fliG* and Δ*fliGMN*) were found to be Ap^R in the presence of arabinose, but not without. Importantly, excess FlhDC also allows for efficient secretion in a Δ*fliHIJ* deletion mutant, confirming the previous finding that the ATPase complex FliHIJ is not needed for flagellar T3S *per se* (140, 158). Additionally, we obtained several spontaneous mutants of the *flhD* promoter region that conferred ampicillin resistance, as well as nonsense mutations in *fliA*. The σ-factor σ^{28} has been

shown to repress *flhDC* transcription in the presence of its cognate anti-σ factor FlgM (103). Additionally, σ^{28} activates the expression of negative regulators of *flhDC*, like FliT. Accordingly, the nonsense mutation of *fliA* allows for increased *flhDC* expression, which in turn confers ampicillin resistance using the same mechanism proposed below.

We analysed several T-POP insertions for their effects on Class II gene expression and found an increased Class II expression by the T-POP insertions in *lrhA*, *slyA* and *fliD*. We additionally demonstrated that both LrhA and SlyA act as negative regulators of *flhDC* expression in *S. enterica*. LrhA (109) and SlyA (178) have been previously shown to act as regulators of *flhDC* and *fliC*, respectively, in *E. coli*.

In summary, we identified by our T-POP mutagenesis approach several known regulatory loci of flagellar Class I gene expression in *S. enterica*, like *ecnR* (203), *ydiV* and *rcsB* (196). We showed that both LrhA and SlyA act as negative regulators of *flhDC* expression also in *S. enterica*. We additionally identified several putative regulators of Class II transcription like STM1856 and STM2401/STM2402. A summary of the regulatory network influencing Class I gene expression is given in Figure 2.10A. Taken together, we conclude that the upregulation of *flhDC* expression by impairing the function of the above-mentioned negative regulators of *flhDC* expression is sufficient to answer the selective pressure of our FlgE-Bla secretion assay in the absence of the C-ring.

To further analyse the effects of *flhDC* upregulation, we designed several *flhD* -10 box promoter mutants (Figure 2.6). Using those mutants we demonstrate that single-base pair changes in the P1 *flhD* promoter result in a significant upregulation of *flhDC* gene expression. The increased expression of *flhDC* results in two to fourfold increase in Class II and Class III gene expression and additionally in an about twofold increased migration rate as analysed using motility plates. The enhanced Class II gene expression also translates in an almost twofold increase in protein levels of the reporter protein FlgE-Bla as analysed by quantitative Western blotting. Interestingly, *Salmonella* cells harbouring the perfect -10 box mutation of the P1 *flhD* promoter produce about twofold more HBB per cell if compared with cells expressing wild-type *flhDC* levels. A perfect -10 box mutation of the P2 *flhD* promoter, however, resulted in a decrease of Class I, Class II and Class III gene expression, as well as in significantly reduced number of HBB per cell as analysed by fluorescent microscopy. It was surprising to find that just a twofold increase in the level of *flhDC* mRNA can circumvent the impaired secretion activity caused by the absence of the C-ring. It suggests that the role of the C-ring as the rotor of the flagellar motor is its primary function and the C-ring plays only a minor role in the secretion process as an affinity site for substrate localization.

In summary, we propose the following mechanism for flagellar T3S in the absence of the C-ring by upregulation of *flhDC*: every mutation that results in an increased level of functional $FlhD_4C_2$, like T-POP insertions in negative regulators of *flhDC* or mutations in the P1 promoter of *flhD*, will allow for FlgE-Bla secretion even in the absence of the C-ring by a combination of: (i) more available substrates (FlgE-Bla) and (ii) more potential secretion systems (more HBB complexes). Under conditions where the function of the C-ring is missing or impaired, flagellar T3S might still occur, although more inefficient, if the concentration of secretion substrates is increased. This is the case in our isolated T-POP mutants that increase *flhDC* expression by impairing the function of negative

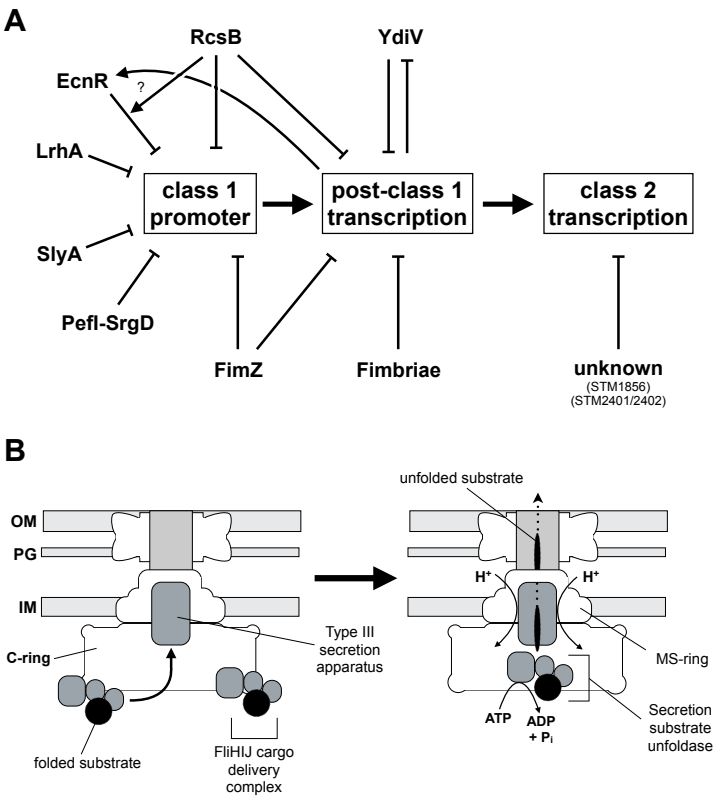

FIGURE 2.10

Regulatory network of flagellar Class I gene expression and model for flagellar T3S. (A) Schematic representation of the regulatory network of flagellar Class I gene expression of *Salmonella enterica*. Arrows represent interactions between different regulators of flagellar Class I transcription or post Class I transcription. LrhA (109) and SlyA (178) have been previously identified as regulators of *flhDC* and FliC, respectively, in *Escherichia coli*. Our T-POP mutagenesis identified LrhA and SlyA as negative regulators of *flhDC* expression in *S. enterica*, as well as several known regulators like EcnR (203) or RcsB (196). We also identified several putative regulators of Class II transcription like STM1856 and STM2401/STM2402. (B) Model of the role of the C-ring affinity cup in flagellar T3S. Folded secretion substrates in complex with the cargo delivery complex FliHIJ dock to affinity sites of the C-ring awaiting secretion. Before proton motive force-dependent secretion, the secretion substrates are presumably unfolded using ATP-hydrolysis of the ATPase FliI thereby increasing the efficiency of the secretion process. The C-ring presumably acts as an affinity cup to enhance the specificity and efficiency of the flagellar T3S process under wild-type conditions by recruiting secretion substrates bound to the FliHIJ cargo delivery complex. Flagellar T3S is possible in the absence of the C-ring and ATPase complex if $FlhD_4C_2$ levels are increased. Increased $FlhD_4C_2$ levels result in elevated level of Class II secretion substrates and additionally in more potential secretion systems by doubling the number of available basal bodies. Accordingly, increased substrate levels and more potential secretion systems overcome the requirement for both the C-ring and the ATPase complex in flagellar T3S.

regulators of *flhDC*, as well as in our *flhDC* promoter mutants that directly increase *flhDC* gene expression.

Accordingly, we propose that the C-ring acts under physiological conditions as an affinity cup that locally increases the secretion substrate concentration prior to T3S by either: (i) transiently binding secretion substrates or (ii) excluding non-secretion substrate interactions with the secretion apparatus (Figure 2.10B). Folded secretion substrates are bound by the cargo delivery complex FliHIJ and recruited to the C-ring affinity cup, thereby locally increasing the substrate concentration prior to secretion. Importantly, the function of the C-ring as an affinity cup in T3S seems to be highly conserved. Recently, it has been shown that in case of the *Chlamydia* injectisome T3S system a multiple cargo secretion chaperone (Mcsc) bound to secretion substrates is recruited to the putative C-ring homologue CdsQ, thereby presumably allowing for a more efficient secretion process (177).

2.5 Experimental procedures

Bacterial strains, plasmids and media

All bacterial strains used in this study are listed in Table 2.3. Cells were cultured in either LB or peptone/protease-peptone/bile-salts (PPBS) (17 g/l peptone, 3 g/l protease peptone, 1.5 g/l bile salts #3, 5 g/l sodium chloride, 10.8 g/l agar). A concentration of 5 µg/ml ampicillin and 15 µg/ml tetracycline was used in PPBS plates. Growth of strain TH12470 harboring the hook-β-lactamase reporter protein and missing two-thirds of the C-ring (Δ*fliMN*) was inhibited on PPBS plates containing 5 µg/ml ampicillin. Motility agar plates were prepared as described before (58, 203). The generalized transducing phage of *Salmonella typhimurium* P22 *HT105/1 int-201* was used in all transductional crosses (168).

TABLE 2.3
***Salmonella enterica* serovar *typhimurium* strains used and constructed in this study.**
Strains for which no source or reference is given were constructed for this study.

Strains	Relevant characteristics	Source/ reference
TH437	LT2 Wild-type for motility and chemotaxis	J. Roth
TH7420	*fliM5978*::*GFPmut2*	lab stock
TH9857	*ecnR*::T-POP *ecnR3*::Mu*dJ*	C. E. Wozniak
TH9949	*flgE6554*::*bla* Δ*flgBC6557*	(108)
TH10068	*ecnR3*::Mu*dJ*	(203)
TH12470	*flgE6569*::*bla* Δ*flgBC6557* Δ*fliMN7392*	
TH12731	Δ*flgBC6557 flgE6569*::*bla* Δ*fliP7457*	
TH14156	Δ*araBAD1007*::*flhD*$^+$ *C*$^+$	

Strains	Relevant characteristics	Source/ reference
TH14525	*flgE7742*::3xHA (HA-tag after aa241)	F. F. V. Chevance
TH14680	Δ*flgBC6557 flgE6569*::*bla* P_{flhD}*7460* (*-38G:A* from *AUG*) STM1911::Tn*10d*Tc Δ*fliG7388*	
TH14681	Δ*flgBC6557 flgE6569*::*bla* P_{flhD}*7461* (*-152C:T* from *AUG*) STM1911::Tn*10d*Tc Δ*fliMN7392*	
TH14683	Δ*flgBC6557 flgE6569*::*bla zec-3521*::Tn*10d*Cm Δ*fliMN7392 fliA7463* ($Ap5^R$)	
TH14684	Δ*flgBC6557 flgE6569*::*bla zec-3521*::Tn*10d*Cm Δ*fliMN7392 fliA7464*	
TH14781	P_{flhD}*7776* (P1 -10 TATAAT promoter) *fliM5978*::*GFPmut2*	C. E. Wozniak
TH14782	P_{flhD}*7777* (P5 -10 TATAAT promoter) *fliM5978*::*GFPmut2*	C. E. Wozniak
TH14815	P_{flhD}*7790* (P3 -10 TATAAT) *fliM5978*::*GFPmut2*	C. E. Wozniak
TH14902	Δ*araBAD1007*::*flhD*$^+$ *C*$^+$ Δ*flgBC6557 flgE6569*::*bla*	
TH14903	Δ*araBAD1007*::*flhD*$^+$ *C*$^+$ Δ*flgBC6557 flgE6569*::*bla* Δ*fliF7387*	
TH14905	Δ*araBAD1007*::*flhD*$^+$ *C*$^+$ Δ*flgBC6557 flgE6569*::*bla* Δ*fliHIJ7398*	
TH14906	Δ*araBAD1007*::*flhD*$^+$ *C*$^+$ Δ*flgBC6557 flgE6569*::*bla* Δ*fliG7402* Δ*fliMN7392*	
TH14909	Δ*araBAD1007*::*flhD*$^+$ *C*$^+$ Δ*flgBC6557 flgE6569*::*bla* Δ*fliMN7392 fliG7780*::*GFPmut2*	
TH14924	P_{flhD}*7793* (P1 + P4 -10 TATAAT) *fliM5978*::*GFPmut2*	
TH14980	P_{flhD}*7797* (P2 -10 TATAAT) *fliM5978*::*GFPmut2*	C. E. Wozniak
TH14981	P_{flhD}*7798* (P6 -10 TATAAT) *fliM5978*::*GFPmut2*	C. E. Wozniak
TH15184	*flgE7742*::3xHA Δ*araBAD1007*::*flhD*$^+$ *C*$^+$	
TH15413	P_{flhD}*7776* (P1 -10 TATAAT) *flhC5213*::Mu*d*J *fliM5978*::*GFPmut2*	
TH15414	P_{flhD}*7793* (P1 + P4 -10 TATAAT *flhC5213*::Mu*d*J *fliM5978*::*GFPmut2*	
TH15415	P_{flhD}*7797* (P2 -10 TATAAT) *flhC5213*::Mu*d*J *fliM5978*::*GFPmut2*	
TH15434	P_{flhD}*7793* (P1 + P4 -10 TATAAT) Δ*flgBC6557 flgE6569*::*bla* Δ*fliP7457*	
TH15461	*fliL5100*::Mu*d*J *fliD7879*::TPOP	
TH15462	*fliL5100*::Mu*d*J *lrhA2*::TPOP	
TH15463	*fliL5100*::Mu*d*J STM1856-1::TPOP	
TH15464	*fliL5100*::Mu*d*J *slyA1*::TPOP	
TH15466	*fliL5100*::Mu*d*J *ddg/yfdZ1*::TPOP	
TH15467	*fliL5100*::Mu*d*J STM2011-2::TPOP	
TH15468	*fliL5100*::Mu*d*J *fliD7881*::TPOP	
TH15469	*fliL5100*::Mu*d*J *ecnR6*::TPOP	

Strains	Relevant characteristics	Source/ reference
TH15470	*fliL5100*::MudJ STM1856-2::TPOP	
TH15471	*fliL5100*::MudJ *ecnR7*::TPOP	
TH15496	*ecnR3*::MudJ *ecnR7*::TPOP	
TH15497	Δ*araBAD1007*::*flhD*$^+$*C*$^+$ *flgE6569*::*bla* Δ*flgBC6557* Δ*fliG7388*	
TH15498	Δ*araBAD1007*::*flhD*$^+$*C*$^+$ *flgE6569*::*bla* Δ*flgBC6557* Δ*fliMN7392*	
TH15567	*flgE7742*::3xHA P_{flhD}*7776*	
TH15568	*flgE7742*::3xHA P_{flhD}*7793*	
TH15569	*flgE7742*::3xHA P_{flhD}*7797*	
TH15589	*flgE6569*::*bla* Δ*flgBC6557* Δ*fliMN7392* *lrhA1*	
TH15590	*flgE6569*::*bla* Δ*flgBC6557* Δ*fliMN7392* *lrhA2*	
TH15591	*flgE6569*::*bla* Δ*flgBC6557* Δ*fliMN7392* *lrhA3*	
TH15592	*flgE6569*::*bla* Δ*flgBC6557* Δ*fliMN7392* *lrhA4*	
TH15593	*flgE6569*::*bla* Δ*flgBC6557* Δ*fliMN7392* *lrhA5*	
TH15594	*flgE6569*::*bla* Δ*flgBC6557* Δ*fliMN7392* *ecnR6*	
TH15595	*flgE6569*::*bla* Δ*flgBC6557* Δ*fliMN7392* *ecnR7*	
TH15596	*flgE6569*::*bla* Δ*flgBC6557* Δ*fliMN7392* *slyA1*	
TH15597	*flgE6569*::*bla* Δ*flgBC6557* Δ*fliMN7392* *rcsB131*	
TH15598	*flgE6569*::*bla* Δ*flgBC6557* Δ*fliMN7392* *rcsB132*	
TH15599	*flgE6569*::*bla* Δ*flgBC6557* Δ*fliMN7392* *yojN253*	
TH15600	*flgE6569*::*bla* Δ*flgBC6557* Δ*fliMN7392* *clpP71*	
TH15601	*flgE6569*::*bla* Δ*flgBC6557* Δ*fliMN7392* *ydiV254*	
TH15602	*flgE6569*::*bla* Δ*flgBC6557* Δ*fliMN7392* *ydiV255*	
TH15603	*flgE6569*::*bla* Δ*flgBC6557* Δ*fliMN7392* *ydiV256*	
TH15604	*flgE6569*::*bla* Δ*flgBC6557* Δ*fliMN7392* STM1856-1	
TH15605	*flgE6569*::*bla* Δ*flgBC6557* Δ*fliMN7392* STM1856-2	
TH15606	*flgE6569*::*bla* Δ*flgBC6557* Δ*fliMN7392* STM2011-1	
TH15607	*flgE6569*::*bla* Δ*flgBC6557* Δ*fliMN7392* STM2011-2	
TH15608	*flgE6569*::*bla* Δ*flgBC6557* Δ*fliMN7392* *rfbP1*	
TH15609	*flgE6569*::*bla* Δ*flgBC6557* Δ*fliMN7392* *pgtE1*	
TH15610	*flgE6569*::*bla* Δ*flgBC6557* Δ*fliMN7392* *ddg/yfdZ1*	
TH15611	*flgE6569*::*bla* Δ*flgBC6557* Δ*fliMN7392* *pykF1*	
TH15612	*flgE6569*::*bla* Δ*flgBC6557* Δ*fliMN7392* *garL1*	
TH15613	*flgE6569*::*bla* Δ*flgBC6557* Δ*fliMN7392* *yieP1*	
TH15614	*flgE6569*::*bla* Δ*flgBC6557* Δ*fliMN7392* *hpaX1*	
TH15615	*flgE6569*::*bla* Δ*flgBC6557* Δ*fliMN7392* *flhDC7872*	
TH15616	*flgE6569*::*bla* Δ*flgBC6557* Δ*fliMN7392* *flhDC7873*	
TH15617	*flgE6569*::*bla* Δ*flgBC6557* Δ*fliMN7392* *flhDC7874*	
TH15618	*flgE6569*::*bla* Δ*flgBC6557* Δ*fliMN7392* *flhDC7875*	
TH15619	*flgE6569*::*bla* Δ*flgBC6557* Δ*fliMN7392* *fliA7876*	
TH15620	*flgE6569*::*bla* Δ*flgBC6557* Δ*fliMN7392* *fliA7877*	
TH15621	*flgE6569*::*bla* Δ*flgBC6557* Δ*fliMN7392* *fliA7878*	
TH15622	*flgE6569*::*bla* Δ*flgBC6557* Δ*fliMN7392* *fliD7879*	
TH15623	*flgE6569*::*bla* Δ*flgBC6557* Δ*fliMN7392* *fliD7880*	
TH15624	*flgE6569*::*bla* Δ*flgBC6557* Δ*fliMN7392* *fliD7881*	
TH15625	*flgE6569*::*bla* Δ*flgBC6557* Δ*fliMN7392* *fliD7882*	

Strains	Relevant characteristics	Source/ reference
TH15756	*flgE6569*::*bla* Δ*flgBC6557* Δ*fliMN7392* Δ*fliT5758*::FCF	
TH15885	*flhC5213*::MudJ Δ*araBAD1049*::*slyA*$^+$ (D97E and A98P compared to the published *S.t.* LT2 genome sequence)	
TH15886	*flhC5213*::MudJ Δ*araBAD1050*::*lrhA*$^+$	
TH15939	Δ*araBAD956*::*fliA*$^+$ Δ*flgM5628*::FRT Δ*fliA5647*::FRT *flhC5213*::MudJ	

SDS-PAGE and Western blotting

Whole-cell lysates of Salmonella were subjected to SDS-PAGE and analysed by immunoblotting using anti-FlgE antibodies (rabbit) for detection of FlgE-β-lactamase. Specific protein detection of horseradish peroxidase-conjugated secondary antibodies (Bio-Rad) was performed using ECL plus Western blotting detection reagents (Amersham Biosciences). Densitometric measurements of FlgE-β-lactamase bands were performed using ImageJ 1.42m for Mac OS X (2).

Isolation of random T-POP insertions and spontaneous Ap^R mutants that allow hook-β-lactamase secretion in the absence of the C-ring

The screen for random Tn*10d*Tc[Δ25] transposon insertions allowing type III-specific secretion in the C-ring deletion mutant was essentially performed as described in Lee et al. (107) and Wozniak et al. (203) using strain TH12470 as the recipient on PPBS plates containing 5 µg/ml ampicillin.

Spontaneous mutations that conferred FlgE-Bla secretion in a C-ring deletion strain that were linked to either the *flh* or *fli* regions were isolated using transposons STM1911::Tn*10d*Tc and *zec-3521*::Tn*10d*Cm that are linked to the *flh* and *fli* regions, respectively. Ap^R mutants were pooled, a phage P22 transducing lysate was grown on the pooled cells and used to transduce either a Δ*flgBC flgE-bla* Δ*fliG* (TH12466) or Δ*flgBC flgE-bla* Δ*fliMN* (TH12470) recipient to either Tc^R or Cm^R. Tc^R transductants that also inherited Ap^R resulted from cotransduction of the Ap^R allele with *flh*-linked STM1911::Tn*10d*Tc. Cm^R transductants that also inherited Ap^R resulted from cotransduction of the Ap^R allele with *fli*-linked *zec-3521*::Tn*10d*Cm. Linked Ap^R mutants were characterized further using three-factor crosses and the mutations were determined using DNA sequencing analysis.

β-Galactosidase assays

β-Galactosidase assays were performed based on the protocol of (212) with minor modifications. Briefly, logarithmic growing cells were permeabilized using 100 mM Na_2HPO_4, 20 mM KCl, 2 mM $MgSO_4$, 0.08% CTAB (hexadecyl-trimethylammonium bromide), 0.04% sodium deoxycholate and 5.4 µl/ml β-mercaptoethanol. Afterwards, the reaction was started by addition of 60 mM Na_2HPO_4, 40 mM NaH_2PO_4, 1 mg/ml *o*-nitrophenyl-β-D-Galactoside and 2.7 µl/ml β-mercaptoethanol. The reaction was stopped using 1 M sodium carbonate (Na_2CO_3) and Miller units were calculated as described (128). For each strain, the assay was performed using three independent, biological replicates.

RNA isolation and quantitative real-time PCR

RNA was prepared from three independent, biological replicates essentially as described (174) using the SV Total RNA Isolation System (Promega) and on-column DNase I treatment. Alternatively, cultures of three independent, biological replicates were mixed equally and used for the subsequent purification of total RNA as described above. For complete removal of genomic DNA, purified RNA samples were treated a second time with DNase I for 30 minutes at 37 °C (ZymoResearch). Afterwards, RNA samples were reverse-transcribed using the RETROscript kit and random decamers (Ambion). qPCR reactions were performed using the EvaGreen qPCR master mix (Bio-Rad) and primers 5'-GTAG-GCAG-CTTT-GCGT-GTAG + 5'-TCCA-GCAG-TTGT-GGAA-TAAT-ATCG (*flhDC*), 5'-GAAC-ACGT-TCGC-GCAG-TG + 5'-TAGG-CAAT-TTTC-CAGG-AACC-G (*motAB*), 5'-GATG-GCGG-CGAA-ATCG + 5'-AGGG-TCCG-TTG A-GTTC-AGGT-T (*flgE*), 5'-GGCC-AAAG-CTGG-TCAT-TATC-C + 5'-TCGC-CGG C-AGAA-ACGT (*fliP*), 5'-CGCC-CTGT-TGAC-GATC-TGG + 5'-TTTA-CCCA-AGT T-AGGC-GTCT-TAAG (*rpoA*), 5'-CAAC-CTGT-TCGT-ACGT-ATCG-AC + 5'-CAG C-TCCA-TCTG-CAGT-TTGT-TG (*rpoB*), 5'-CAAC-AGTA-TGCG-CGTG-ATGA-T + 5'-CGAC-GCAG-AGCT-TCAT-GATC (*rpoD*), 5'-CTGC-TCAA-AGAG-CTGG-TG TA-TCA + 5'-AGCG-CGTT-ACAG-TCTG-CTCA-T (*gyrB*) and 5'-TTGC-AGAA-AT GA-GCCA-TTAC-GCCG + 5'-GACG-TTCA-GCGC-GAAT-GATG-GTTT (*gmk*) on a CFX96 real-time PCR instrument (Bio-Rad). Relative changes in mRNA levels were determined using the $2^{-\Delta\Delta CT}$ method described previously (112) by simultaneous normalization against transcript levels of multiple reference genes (*rpoA*, *gyrB* and *gmk*) (191).

Fluorescent microscopy

For fluorescent microscopy analysis, cells were grown to mid-log phase and fixed by addition of final 5% formaldehyde. Hooks were stained using monoclonal anti-haemagglutinin antibodies coupled to Alexa Fluor^{488} (Invitrogen). Fixed cells were immobilized using poly L-lysine treated coverslips. DNA and membrane stainings were performed using Hoechst (Invitrogen) and FM-64 (0.5 µg/ml, Invitrogen). Images were collected using an Applied Precision optical sectioning microscope with optical Z sections every 100 nm and deconvolved using softWoRx v.3.4.2 (Applied Precision). The pixel data of individual Z sections of the deconvolved images were projected on a single plane using the Quick Projection tool (settings: maximal intensity) of softWoRx Explorer v1.3 (Applied Precision) and used for quantitative scoring of the number of HBB complexes per cell.

2.6 Acknowledgements

This work was supported by PHS Grant GM056141 from the National Institutes of Health. We thank Christopher E. Wozniak for helpful comments on how to quantify the number of HBB complexes and Fabienne F.V. Chevance and Christopher E. Wozniak for strain construction. We also thank Yichi Su and Anoush Emrazian for technical assistance and the Hughes lab for useful discussions of the manuscript. M.E. gratefully acknowledges scholarship support of the Boehringer Ingelheim Fonds.

3

Genetic Dissection of the Bacterial Type III Secretion Apparatus Reveals Minimal Components Essential for Export

Marc Erhardt[1, 2, †], Mayukh K. Sarkar[1, †], Koushik Paul[1], Takanori Hirano[1], Kelly T. Hughes[1, 2, *], David F. Blair[1, *]

in preparation

[1]Department of Biology, University of Utah, 257 South 1400 East, Salt Lake City, UT 84112, USA
[2]present address: Département de Médecine, Université de Fribourg, CH-1700 Fribourg, Switzerland
[†]These authors contributed equally to this work
[*]Co-corresponding authors; Kelly T. Hughes and David F. Blair; Mailing address: Department of Biology, University of Utah, 257 South 1400 East, Salt Lake City, UT, 84112; Tel: +801-587-3367; Fax: +801-585-9735; E-mail: blair@bioscience.utah.edu. kelly.hughes@unifr.ch

3.1 Abstract

Type III secretion is a type of protein export important for flagellar assembly and the virulence of many gram-negative pathogens. Type III secretion involves about a dozen proteins and is energized by both ATP and the proton gradient. Here, a battery of export-apparatus mutants, and assays of export function are used to dissect the functional roles of the components in the flagellar type III secretion apparatus. Several cytosolic components associated with the apparatus were found dispensable for export. In an assay based on export of a flagellar-hook/β-lactamase fusion protein into the periplasm, which is independent of assembly of flagellar structures, most membrane components were also dispensable, including the FliF protein that has been regarded as the housing for the apparatus. The membrane protein FliP was both necessary and sufficient for substrate translocation. Implications for the organization, mechanism, and evolution of the type III secretion apparatus are discussed.

3.2 Author summary

Bacteria swim through liquid environments using propulsion of a rotating, propeller-like appendage, the flagellum. Pathogenic bacteria also employ an related needle-like complex to inject virulence factors into eukaryotic host cells. The bacterial flagellum and the needle complex of pathogenic bacteria are highly sophisticated nanomachines that share a unique, multicomponent transport system constructed from more than a dozen proteins, the so-called type III secretion apparatus. In *Salmonella enterica* the flagellar type III secretion apparatus consists of six membrane-associated proteins FliO, FliP, FliQ, FliR, FlhA, and FlhB and three cytoplasmic proteins, FliH, FliI, and FliJ. In this study we dissect the flagellar type III secretion apparatus using a battery of export-apparatus mutants and *in vivo* reporter protein assays to probe the export function. We demonstrate that most components including the housing of the apparatus, FliF, are dispensable and one membrane protein, FliP, was sufficient to catalyze significant translocation of a reporter substrate. These findings have important implications for the evolution of the flagellum, and we present the first molecular-level hypothesis for the organization and mechanism of the type III secretion apparatus.

3.3 Introduction

Many species of bacteria swim using rotating organelles called flagella, which are energized by the membrane ion gradient and under control of the chemotaxis signaling pathway (18, 106, 173). The flagellum consists of i) a basal body spanning the inner and outer membranes, which includes a specialized secretion apparatus for exporting protein subunits that form the exterior structures; ii) a flexible hook that acts as universal joint; and iii) a relatively rigid helical filament that is the propeller (Figure 3.1) (17, 20, 167). These structures are formed from about 20 different proteins, in copy numbers ranging from a few to several thousand. Many additional proteins are required for assembly and operation of the flagellum; the entire flagellar regulon consists of more than 60 genes, organized in a three-level regulatory hierarchy. At the top are *flhD* and *flhC*, which encode a master transcriptional regulator and are themselves under the control of numerous environmental factors (6, 23, 27, 111, 115). The FlhD/FlhC complex stimulates transcription of level-II genes, which encode structural proteins of the basal body, hook, and secretion apparatus, as well as regulatory proteins including the hook-length controller FliK (67), the flagellum-specific transcription factor σ^{28}, and its cognate anti-σ factor, FlgM (73). Upon completion of the basal body and hook, the flagellar secretion apparatus undergoes a change in substrate specificity that switches it from exporting rod and hook proteins to export of filament-associated components. The anti-σ^{28} factor FlgM is an export substrate of the filament (late-substrate) class, and removal of FlgM from the cell releases σ^{28} to activate expression of the late genes. These encode the proteins that form the filament, drive motor rotation, and enable chemotaxis (27).

The bacterial flagellum is structurally and functionally related to the 'injectisome' apparatus used by many pathogens to inject virulence factors into host cells (32, 72, 114). Electron microscopic images of the injectisome and the flagellum show clear structural correspondences, as well as differences that must reflect their divergent functions: injectisomes have somewhat smaller basal structures and a straight, relatively short 'needle' in place of the filament (32, 98, 124). Like the flagellum, the injectisome contains an apparatus for rapid protein secretion, which functions in this case to export virulence factors into host cells. Several (about 10) protein components of the flagellum and injectisome show clear homoloogy. Most of these shared components function in the export process, which in both systems has been termed type III secretion, or T3S (Figure 3.1) (22, 32, 117). T3S systems are notable for both their speed and selectivity: the flagellar apparatus can secrete several 55-kDa flagellin subunits per second in the early stages of filament assembly (75), yet selects only a few proteins for export from among the many hundreds in the cell. Substrates of the flagellar export apparatus have amino-terminal regions that are structurally disordered prior to their assembly into the structure (8). Specialized secretion chaperones function to stabilize these partially unfolded substrates and target them to the export apparatus (11, 156).

The membrane-associated part of the flagellar export apparatus is presumed to lie inside the basal-body MS-ring (Figure 3.1B) and to contain the proteins FliO, FliP, FliQ, FliR, FlhA, and FlhB. Cytoplasmic proteins implicated in export are FliH, FliI, and FliJ, which form a complex that binds substrate (136). FliI is an ATPase (47, 192)

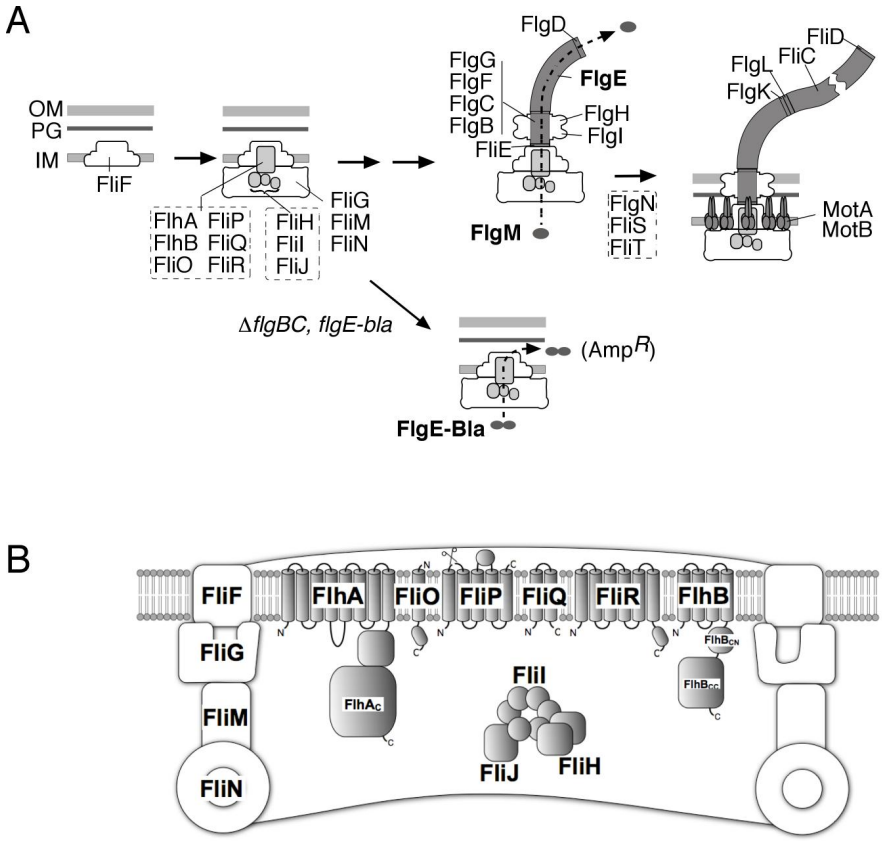

FIGURE 3.1

Flagellar assembly sequence and components of the secretion apparatus. (A) Sequence of events in flagellar assembly. Components involved in export are in dashed boxes; FlgN, FliS, and FliT function as chaperones for the late-export substrates and are not considered in detail here. The alternative process shown below the main pathway is the basis of an export assay in which a flagellar hook/β-lactamase fusion protein is directed into the periplasm where it confers ampicillin resistance. (B) Schematic view of the components in the flagellar secretion apparatus. Membrane components are shown, with the most probable number and topology of TM segments indicated.

whose state of association is modulated by ATP binding and hydrolysis (30, 85). FliH regulates the ATPase activity of FliI (138) and also binds to the rotor protein FliN, a component of the flagellar direction switch (60, 159, 169). FliJ is thought to function as a general secretion chaperone for the early substrates (129) and to orchestrate cycling of the other chaperones (46). While the role of ATP hydrolysis has not been precisely defined, it presumably provides energy to accelerate one or more steps in substrate delivery, such as disassembly of cargo-delivery complexes or the release of substrate from the delivery complex into the transport apparatus.

The FliN protein, together with FliM and FliG, forms a large feature at the bottom of the basal body called the C-ring (50, 51, 88, 89). Mutations in the C-ring proteins can disrupt flagellar assembly, rotation, and direction control, and the FliG/M/N complex is usually termed the 'switch complex' (204, 205). As noted, FliN binds to FliH (60, 159) and so the role of the C-ring in assembly might be to localize FliH/I/J/substrate complexes to the basal body and position them for efficient delivery of the cargo into the membrane apparatus. All of the proteins just described (FliO/P/Q/R/FlhA/B in the membrane; FliH/I/J of the substrate-delivery complex; FliG/M/N of the switch complex) have been classified as essential for export, because null mutants were reportedly nonflagellate (117, 136). Recent results indicate, though, that flagella can occasionally assemble even in the absence of the substrate-delivery proteins (140, 158) or the switch-complex proteins (43, 94). Additionally, it has recently been shown that mutations in FliP can bypass the non-motile phenotype of in a *fliO* deletion strain. Overexpression of the cytoplasmic domain of FliO enhanced the motility further and overexpression of full-length FliO increased FliP protein levels, indicating that FliO stabilizes FliP through interactions of the transmembrane domains (15).

While substrate delivery is energized by ATP hydrolysis, substrate translocation across the membrane appears to be energized by the proton gradient (140, 158, 200). The core of the secretion apparatus is thus a proton-fueled protein transporter. The molecular mechanism of this transporter is unknown. Important mechanistic questions concern which component(s) form the conduit for translocating substrate, which component(s) harness the proton gradient to energize translocation, and how the substrates are engaged and driven through the apparatus. Here, we have undertaken a systematic study of the proteins implicated in flagellar type III secretion, with the aim of identifying those most critical for export. Measurements of export function included an assay based on the export of a flagellar-hook/β-lactamase fusion protein into the periplasm, where it confers quantifiable ampicillin (Amp) resistance. Unlike previous assays based on filament assembly or motility, these measurements report on the export process *per se* and do not rely on assembly of the rod or any other overt flagellar structures. The results confirm that neither the substrate-delivery proteins FliH/I/J nor the switch-complex proteins FliG/M/N are essential for substrate translocation across the membrane. FliO was found to be dispensable for both flagellar assembly and function, provided some other components were over-expressed. Surprisingly, the measurements show that substantial export occurs in the absence of the MS-ring protein FliF, and also in the absence of the highly conserved membrane components FliQ, FliR, FlhA, or FlhB. FliP alone was found to be essential and sufficient for subunit translocation. We propose that FliP is

at the core of the apparatus where it forms the conduit for substrate. The probable disposition and functions of the other components are discussed.

3.4 Results

3.4.1 FliO is not essential for flagellar assembly or function.

Unlike the other components of the flagellar secretion apparatus, FliO has no ortholog in most injectisome systems and might be expected to play a relatively minor role in export. A *fliO* null mutant was found to be nonflagellate (181), presumably owing to a defect in flagellar export (121, 152). Here, we observed that a *Salmonella* Δ*fliO* strain retained slight function in a soft-agar motility assay, migrating at a few percent of the wild-type rate (Figure 3.2A), and exhibited low, but measurable, export activity in an assay of FliC secretion (Figure 3.2E). Motility of the *fliO*-null cells was substantially improved in a strain with the master-regulatory *flhDC* genes overexpressed and the negative regulator FlgM deleted (Figure 3.2B). In this strain, slightly more than half of the cells produced at least one flagellum (Figure 3.2C). Thus, the requirement for FliO can be bypassed to a large extent by overexpression of one or more flagellar genes. To identify the component(s) contributing to the motility improvement we examined motility of the *fliO*-null strain with individual membrane components of the export apparatus overexpressed. Motility was restored to the wild-type level by overexpression of FliP (Figure 3.2D). Overexpression of FliQ, FliR, FlhA, or FlhB gave no measurable improvement (data not shown).

These results are consistent with the recent findings of Barker et al. (15) who demonstrated that point mutations in FliP were able to bypass a *fliO* deletion. The authors also showed that overexpression of full-length FliO enhanced expression levels of FliP.

3.4.2 Dispensability of the FliG/M/N complex and FliH/I/J complex.

Recent findings indicate that the switch-complex proteins FliG, FliM, and FliN, once regarded as essential for flagellar assembly, are not required for assembly when the ATPase FliI is overexpressed (94) or when flagellar gene expression is globally up-regulated (43, 44, 94). In a previous study we reported the occurrence of flagella on cells of a Δ*fliG* strain (43, 94); as a further test of the dispensability of the switch complex, we examined flagellation of Δ*fliN* cells in which flagellar gene expression was increased by a *flhD* promoter-up mutation together with deletion of *flgM*. About one-fourth of the cells produced flagella, of approximately normal length (Figure 3.3). The cells remained immotile, as expected given the involvement of the C-ring in motor rotation. Flagellar formation in this strain was further increased by deletion of the α-subunit of the F_OF_1 ATP synthase (Figure 3.3), which increases the proton motive force (77) and thus the energy available to drive substrate translocation (140, 158).

As noted above, the switch complex might facilitate export by localizing FliH/I/J/cargo complexes to the basal body, via the interaction between FliN and FliH (60, 159). The assembly of numerous flagella in a Δ*fliN* strain implies that this localization process

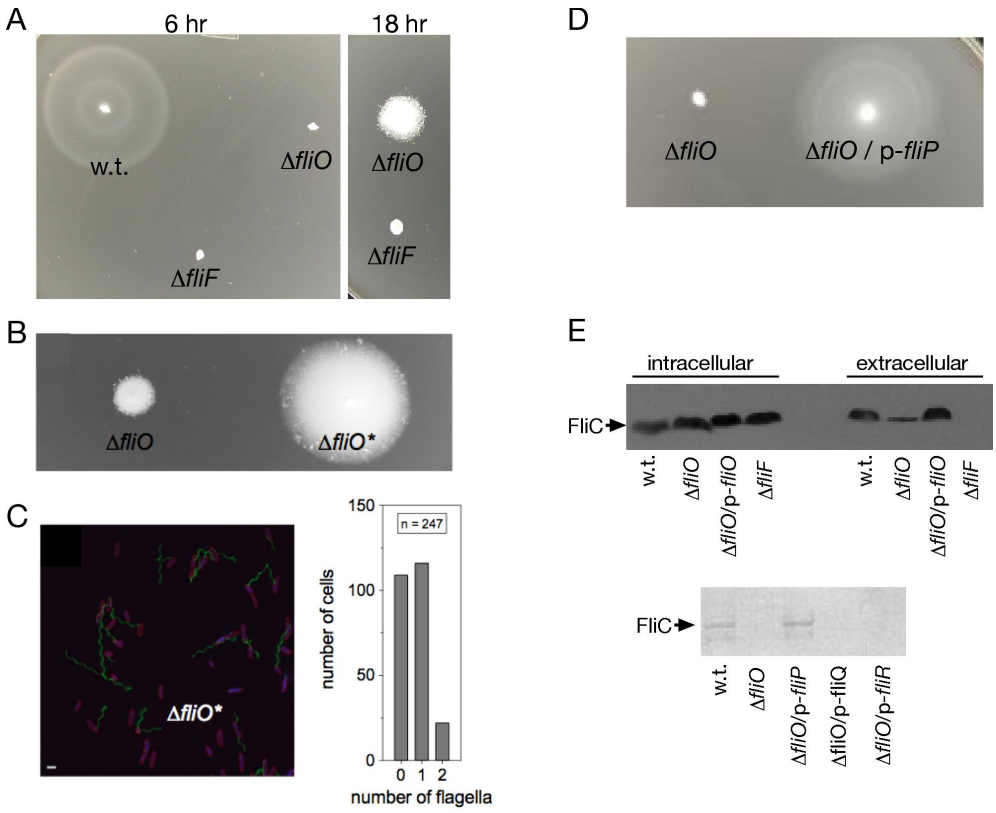

FIGURE 3.2

Dispensability of FliO for flagellar assembly and function. (A) Soft-agar motility phenotypes of Δ*fliO* and Δ*fliF* strains. (B) Enhanced motility of a Δ*fliO* strain (termed Δ*fliO**) that is deleted of the negative-regulator FlgM and that has a promoter-up mutation giving increased expression of the *flhDC* master regulator genes. (C) Flagellation of the Δ*fliO** strain. (D) Enhanced motility of the Δ*fliO* strain upon overexpression of FliP. (E) Retention of some FliC (flagellin) export activity in the Δ*fliO* strain (top), and enhanced export upon overexpression of FliP (bottom).

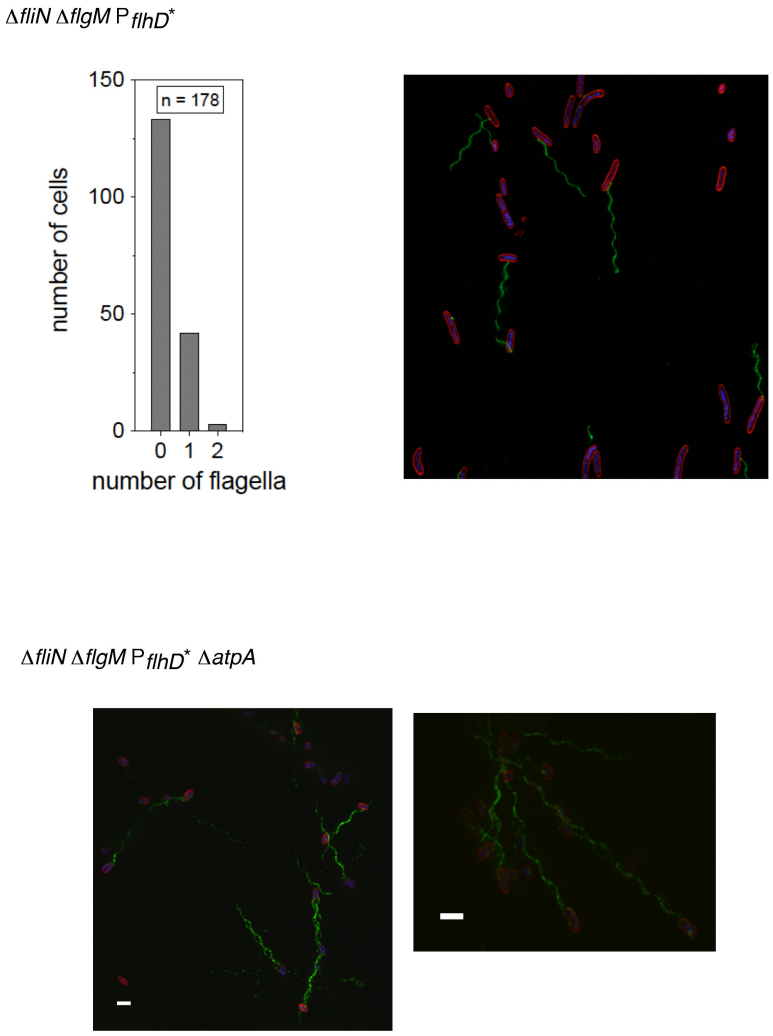

FIGURE 3.3

Flagellation of Δ*fliN* strains. The strains contained other deletions, as indicated, either to enhance expression of flagellar genes or to increase the proton motive force by disruption of the ATP synthase.

is not strictly required for export. Further, we found previously that a Δ*fliHIJ* strain produced a few flagella and could migrate slowly in soft-agar plates (140, 158). To examine more systematically the contributions of the FliG/M/N and FliH/I/J proteins, we used an assay based on export of a FlgE-Bla (Hook subunit/β-lactamase) fusion protein, described previously (108). This assay uses cells in which the basal-body rod is disrupted by mutation, and measures transport of the fusion protein into the periplasm where it confers Amp resistance. Importantly, the assay does not rely on assembly of the rod, hook, or any flagellar structure besides the export apparatus itself. Export is quantified as the Minimal Inhibitory Concentration, or MIC-value, of ampicillin (see Methods).

The FlgE-Bla assay was applied to a battery of deletion-mutant strains including Δ*fliG*, Δ*fliMN*, Δ*fliGMN*, Δ*fliI*, Δ*fliHIJ*, Δ*fliGMNHIJ*, Δ*fliO*, Δ*fliP*, Δ*flhA*, and Δ*flhB*, initially using a 96-well format. Experiments were carried out in a background expressing the flagellar genes at their normal levels and also in a *flhD* promoter-up background (denoted $flhDC^{++}$) that expresses the flagellar master-regulatory genes at about twice the normal level (44). Representative data are shown in Figure 3.4A and MIC values are summarized in Figure 3.4B.

The Δ*fliP* strain gave relatively low MIC values in all of the experiments and can accordingly be used as a reference for comparison to the other strains. When flagellar genes were expressed at normal levels (i.e., in cells with the wild-type *flhD* promoter), most of the deletion strains had low MIC values similar to the Δ*fliP* strain (5-10 µg/ml, as compared to about 800 µg/ml in positive controls.). The Δ*fliMN*, Δ*fliI*, and Δ*fliHIJ* strains were exceptions, having MIC values about twice as large as the others. In the $flhDC^{++}$ background, export was enhanced in several of the deletion mutants. MIC values of the Δ*fliO*, Δ*fliG*, Δ*fliGMN*, Δ*fliHIJGMN*, and Δ*fliI* strains were all significantly (2- to 5-fold) above that of the Δ*fliP* strain, while the MIC values of the Δ*fliMN* and Δ*fliHIJ* strains increased to about 10 times the Δ*fliP* reference (Figure 3.4B).

To determine whether the export observed in the Δ*fliG*MNHIJ strain could be improved further by mutation, we carried out a random T-POP transposon mutagenesis (43). Parent strains lacked the switch complex, the substrate-delivery complex, and also the injectisome ATPases (Δ*fliHIJGMN*Δ*ssaN*Δ*invC*), and either expressed flagellar genes at normal levels or had the *flhD* promoter-up mutation to boost expression. Mutants showing enhanced ampicillin resistance were isolated, then transposons were transferred back into the parent strain and the insertion point determined by DNA sequencing analysis. A summary of the characterized T-POP insertions is given in Table 3.1. The majority of mutants had insertions in positions that are known or believed to affect the expression of *flhDC*. These included insertions in *fliD*, likely to effect expression of the downstream gene *fliT* that encodes a negative regulator of *flhDC* (206); near *encR*, a repressor of *flhDC* (203); or in *lrhA*, another negative regulator of *flhDC* (44). Up-regulation of flhDC therefore appears to be the major avenue for increasing export in this deletion background.

The MS-ring of the basal body, formed from the FliF protein, is often presumed to form the housing for the export apparatus, and the Δ*fliF* strain exhibited a low MIC value comparable to that of the Δ*fliP* strain (Figure 3.4). As a further test of whether

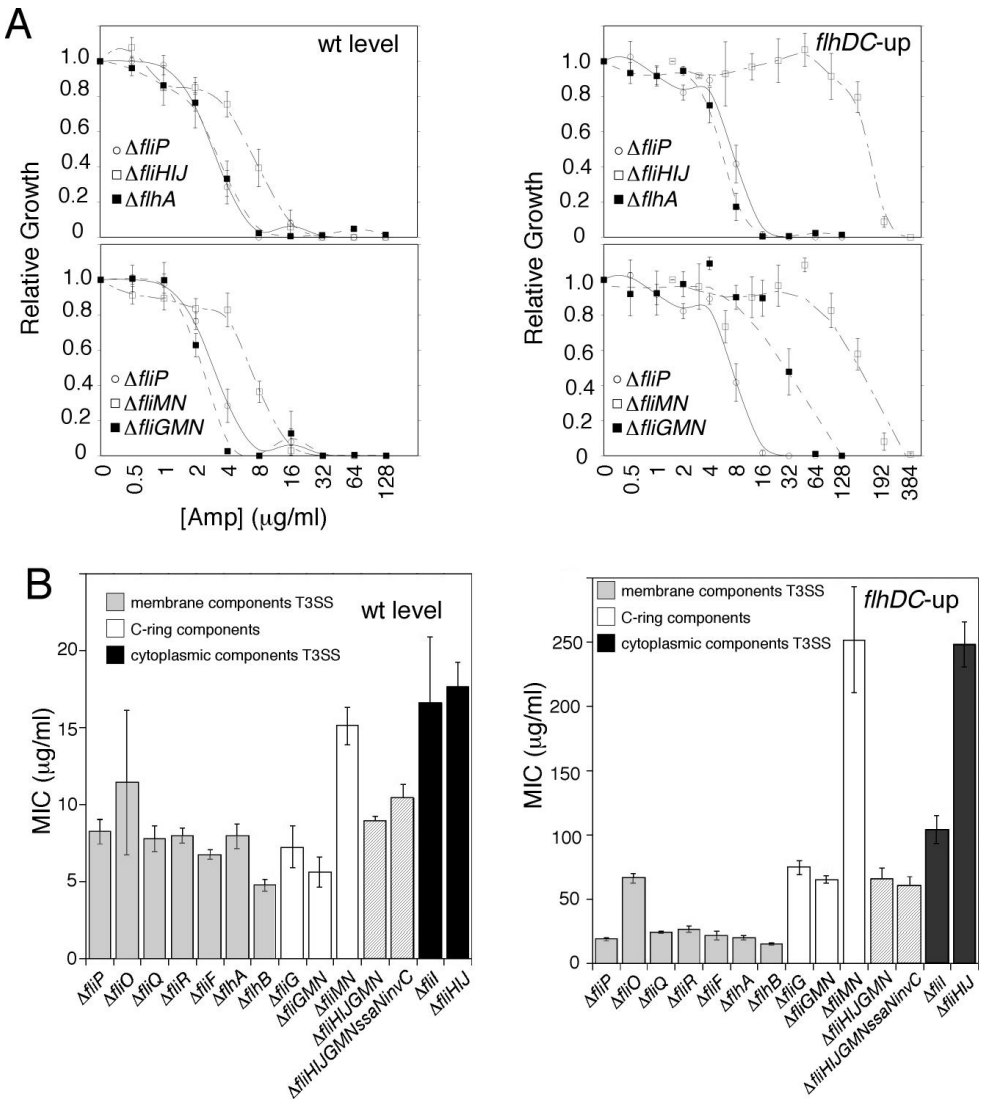

FIGURE 3.4

Assays of FlgE-Bla export in strains deleted of cytoplasmic components of the export apparatus. (A) Culture growth as a function of ampicillin concentration, in representative deletion strains. Flagellar genes were expressed at normal levels in the left-hand panels, and at elevated levels in the right-hand panels (owing to a *flhD* promoter-up mutation). (B) Summary of MIC (Minimal Inhibitory Concentration) values for the various cytoplasmic component deletion strains, with flagellar genes expressed at normal levels (left) or at elevated levels (right).

TABLE 3.1
Isolated T-POP transposon insertions that allowed FlgE-Bla secretion in TH15033 and TH16034.
List of T-POP transposon insertions that allowed FlgE-Bla secretion in strain TH15033 (Δ*flgBC flgE-bla* Δ*fliGMN* Δ*fliHIJ* Δ*ssaN* Δ*invC*) and strain TH16034 (Δ*flgBC flgE-bla* Δ*fliGMN* P_{flhD^*} Δ*fliHIJ* Δ*ssaN* Δ*invC*). Tc-Ap^R, T-POP insertions were ampicillin resistant (Ap^R) in the presence of tetracycline.

T-POP TH16034	locus	position of insertion	notes
1	*fliD*	85 bp after *ATG*	Tc-Ap^R
2	*fliD*	94 bp after *ATG*	
3	*fliD*	93 bp after *ATG*	
4	*yieK*/*ecnR*	858 bp after *ATG*	upstream of *ecnR*
5	*fliD*	116 bp upstream of *fliD ATG*	Tc-Ap^R
6	*fliD*	37 bp upstream of *fliD ATG*	
7	*fliD*	94 bp after *ATG*	
8	*fliD*	93 bp after *ATG*	
9	*fkpA*	429 bp after *ATG*[a]	
10	*fliD*	85 bp after *ATG*	
11	*fliD*	85 bp after *ATG*	
12	*fliD*	85 bp after *ATG*	
13	*fliD*	85 bp after *ATG*	
14	*fliD*	29 bp upstream of *fliD ATG*	Tc-Ap^R
15	*fliD*	85 bp after *ATG*	Tc-Ap^R
16	*hisQ*	153 bp after *ATG*	transport protein; Tc-Ap^R
17	*wcaK*	60 bp after *ATG*[b]	Tc-Ap^R
18	*mgtC*[c]/ *yicL*[d]	237 bp upstream of *mgtC ATG*; 271 bp upstream of *yicL ATG*	Tc-Ap^R

T-POP TH15033	locus	position of insertion	notes
1	*lrhA*	536 bp after *ATG*	Tc-Ap^R
2	*mutL*[e]	120 bp after *ATG*	
3	*lrhA*	712 bp after *ATG*	
4	*ssaV*[f]	1012 bp after *ATG*	

[a] downstream of regulatory protein YheO
[b] downstream of WzxC = colanic acid transporter
[c] MgtC = Mg^{2+} transport protein
[d] YicL = putative permease
[e] MutL = DNA mismatch repair protein
[f] SsaV = Spi-2 FlhA ortholog

export can occur in the absence of the MS-ring, we carried out a transposon mutagenesis in the Δ*fliF* strain. Ampicillin resistance in the Δ*fliF* strain was enhanced by mutations in diverse genes (summarized in Table 3.2). Representative mutants were characterized further using the MIC assay and showed an approximately 5-fold increase relative to the Δ*fliP* strain and the Δ*fliF* parents (data not shown). A few of the insertions were in the *marAB* (multiple antibiotics resistance) locus and probably confer Amp resistance by a mechanism unrelated to flagellar secretion, but most were in genes that function in one way or another as negative regulators of *flhDC* expression, which suggests that export through the flagellar secretion apparatus can occur even in the absence of the MS-ring.

TABLE 3.2

T-POP transposon insertions that allowed FlgE-Bla secretion in a strain lacking the MS-ring (TH12465 Δ*flgBC flgE-bla* Δ*fliF*).

Out of 65 isolated Ap^R colonies, in 18 colonies the precise transposon insertion point was determined by DNA sequencing (summarized in the table). Genetic mapping revealed six more T-POP insertion near the *flg* operon and five more T-POP insertion mapped to *ydiV*. Tc-Ap^R indicates a Tc-dependent ampicillin-resistant phenotype, presumably the result of transcriptional read-through of the T-POP transposon into adjacent chromosomal genes.

T-POP number	locus	position of insertion	notes
3	*clpXP*	51 bp after *lon STOP*	near *clpXP*
4	*ydiV*	678 bp after *ydiV ATG*	
6	*rcsB*	227 bp after *rcsB ATG*	
9	*rcsB*	341 bp after *rcsB ATG*	
11	*rcsB*	333 bp after *rcsB ATG*	
13	*rcsB*	219 bp after *rcsB ATG*	
16	*STM0580*	294 bp after STM0580 *ATG*	putative AcrR-like protein[a]
23	*marR*	388 bp after *marR ATG*	repressor MarR[b], Tc-Ap^R
31	*clpXP*	33 bp after *lon STOP*	near *clpXP*
33	*lrhA*	613 bp after *lrhA ATG*	
35	*lrhA*	859 bp after *lrhA ATG*	
38	*rcsB*	2603 bp after *yojN ATG*	near *rcsBC*
44	*marR*	260 bp after *marR ATG*	Tc-Ap^R
62	*flgD*	678 bp after *flgD ATG*	before *flgE-bla*, Tc-Ap^R
63	*ydiV*	678 bp after *ydiV ATG*	
65	P_{flhD}	609 bp before *ATG* of *flhD*	
66	*lrhA*	312 bp after *lrhA ATG*	
69	*clpX*	65 bp after *ATG*	

[a] AcrR-like protein involved in AcrAB multidrug resistance

[b] DNA-binding transcriptional repressor of the multiple antibiotic resistance (*mar*) locus that is involved in resistance to different antibiotics

Export was increased in several deletion backgrounds by global up-regulation of the flagellar genes. To identify the components responsible, we tested the effects of over-expressing each membrane protein of the export apparatus, in selected deletion backgrounds. Experiments were carried out as described above except using cuvette-based

measurements of cell density instead of 96-well plates. MIC values are summarized in Table 3.3 and representative data are shown in Figure 3.5. The Δ*fliHIJ*, Δ*fliGMN*, and Δ*fliGMNHIJ* strains were generally similar, each showing increased MIC values upon overexpression of FliP, FliQ, or FliR. The FliHIJ strain was somewhat more rescuable, responding also to FlhA and FlhB overexpression and showing particularly strong stimulation by FliR. Overall, the results are consistent with the proposal that the FliG/M/N and FliH/I/J proteins function together to localize substrate to the basal body. The substantially elevated MIC values in the overexpressing strains indicates that substantial export can occur in the absence of this C-ring-based mechanism of substrate delivery.

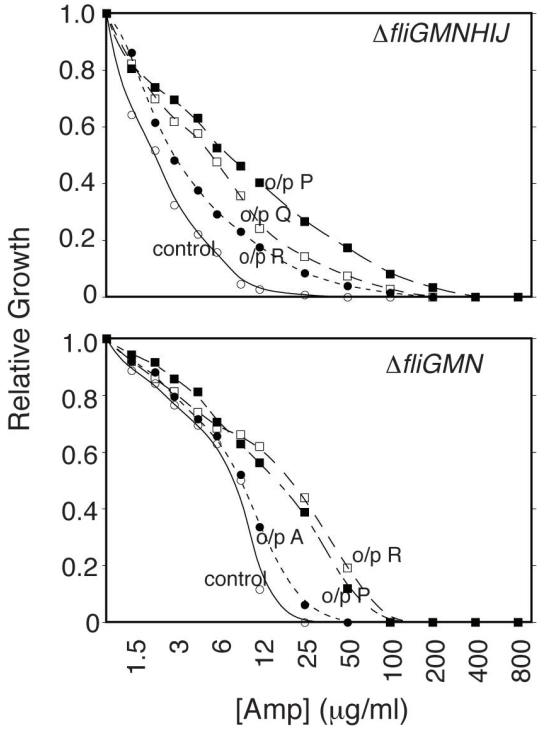

FIGURE 3.5

Examples of the export enhancement accompanying membrane-component overexpression in the Δ*fliGMNHIJ* and Δ*fliGMN* backgrounds. Experiments were carried out using cuvette-based measurements of cell density as described in the text. o/p, overexpression; P, FliP; Q, FliQ; R, FliR; A, FlhA.

FliP was most effective in enhancing export in the Δ*fliHIJGMN* background, increasing the MIC value by about 10-fold relative to the normal-expression controls. To test whether the export in this strain is due to the action of the export apparatus (rather than, for example, membrane leakiness induced by protein overexpression), we used a dominant-negative variant of FliP (D197N; described more fully below) in place of the wild-type protein. In contrast to the wild-type protein, the dominant-negative FliP caused a decrease in the MIC value of the Δ*fliHIJGMN* strain (Table 3.3).

TABLE 3.3

Summary of FlgE-Bla export in flagellar deletion strains.

Given is the minimal inhibitory concentration (MIC) value for ampicillin in µg/ml; (s.d.); (s.d.), standard deviation; (n.m.), not measured. The MIC value for the wildtype strain is 800 µg/ml.

Deleted Components	Overexpressed Component						
	none	FliP	FliP^{D197N}	FliQ	FliR	FlhA	FlhB
Δ*fliHIJGMN*	3 (1)	104 (46)	5 (1)	78 (31)	42 (8)	24 (4)	22 (11)
Δ*fliHIJ*	9 (3)	75 (17)	n.m.	46 (7)	600 (160)	91 (12)	88 (16)
Δ*fliGMN*	16 (1)	69 (1)	n.m.	74 (3)	94 (59)	28 (1)	37 (1)
Δ*fliF*	3 (1)	92 (6)	5 (1)	34 (15)	9 (1)	21 (3)	11 (2)
Δ*fliP*	7 (1)	800 (220)	n.m.	8 (1)	4 (1)	10 (2)	5 (1)
Δ*fliQ*	15 (2)	13 (1)	n.m.	610 (4)	11 (1)	8 (1)	7 (1)
Δ*fliR*	9 (1)	37 (4)	7 (1)	36 (1)	410 (19)	9 (1)	11 (1)
Δ*flhA*	3 (1)	6 (1)	1.7 (0.4)	7 (1)	4 (1)	360 (120)	15 (2)
Δ*flhB*	3 (1)	34 (7)	9 (1)	36 (4)	36 (8)	26 (5)	380 (120)
all (strain TH16980)	1 (0.1)	8 (1.2)	1 (0.1)	3 (0.1)	2 (0.1)	4 (1)	2 (0.1)
all (strain TH16980)[a]	1 (0.1)	10 (0.5)	n.m.	3 (0.3)	2 (0.1)	5 (0.1)	3 (0.3)
all (strain TH16988)	1 (0.1)	6 (0.2)	n.m.	2 (0.2)	2 (0.2)	3 (0.2)	2 (0.1)

[a] expression induced at higher level (10 µM salicylate)

3.4.3 Dispensability of FliF.

The T-POP mutagenesis results suggest that export can occur even in the absence of the MS-ring, provided some other components are over-expressed. To identify the factors enabling export in the absence of the MS-ring, we measured MIC values in the Δ*fliF* strain with each of the membrane components of the apparatus overexpressed. The MIC value of the Δ*fliF* strain was increased greatly by overexpression of FliP, and was also significantly increased by overexpression of FliQ or FlhA (Table 3.3). Homologs of FliF are found in all known flagellar and injectisome systems, and so the observation of export in a Δ*fliF* strain was unexpected. As a test of whether this export utilizes the normal pathway, we used the dominant-negative FliP variant. In contrast to the wild-type protein, the $FliP^{D197N}$ protein gave a barely measurable increase in the MIC value of the Δ*fliF* strain (Table 3.3 and Figure 3.6).

3.4.4 Other membrane components.

Next, the FlgE-Bla assay was used to measure export in strains deleted for single membrane components of the apparatus, and to examine the effects of overexpressing the other components. Strains lacking the various membrane components fell into different categories according to which other components, if any, could increase the MIC value when overexpressed (Table 3.3). Cells lacking FliP or FliQ showed export defects that were rescued only by complementation with the corresponding gene. The Δ*fliR* strain also exhibited a severe defect (MIC value ∼10 µg/ml) but in this case the MIC value could be increased to greater than 30 µg/ml by overexpression of either FliP or FliQ. The MIC value of the Δ*flhB* strain was quite low (∼3 µg/ml) but was increased by about 10-fold upon overexpression of any of the other proteins in the set, while export in the Δ*flhA* strain, also low initially, was increased about two-fold upon overexpression of FliP and about 5-fold on overexpression of FlhB (Table 3.3 and Figure 3.6).

The several instances where export in a membrane-component deletion strain was enhanced by overexpression of another component are consistent with the proposal that these proteins function together in a complex. The results further indicate that the membrane components FliR, FlhA, and FlhB, in spite of occurring universally in type III secretion systems, are not essential for the translocation of substrate across the membrane: MIC values of the Δ*fliR*, Δ*flhA*, and Δ*flhB* strains were significantly increased upon overexpression of some other component(s). Because export in all three strains was enhanced by overexpression of FliP, the dominant-negative FliP variant was again used to establish a connection with the normal protein function. In all cases, the $FliP^{D197N}$ protein was less effective than wild-type FliP in enhancing export (Table 3.3 and Figure 3.6).

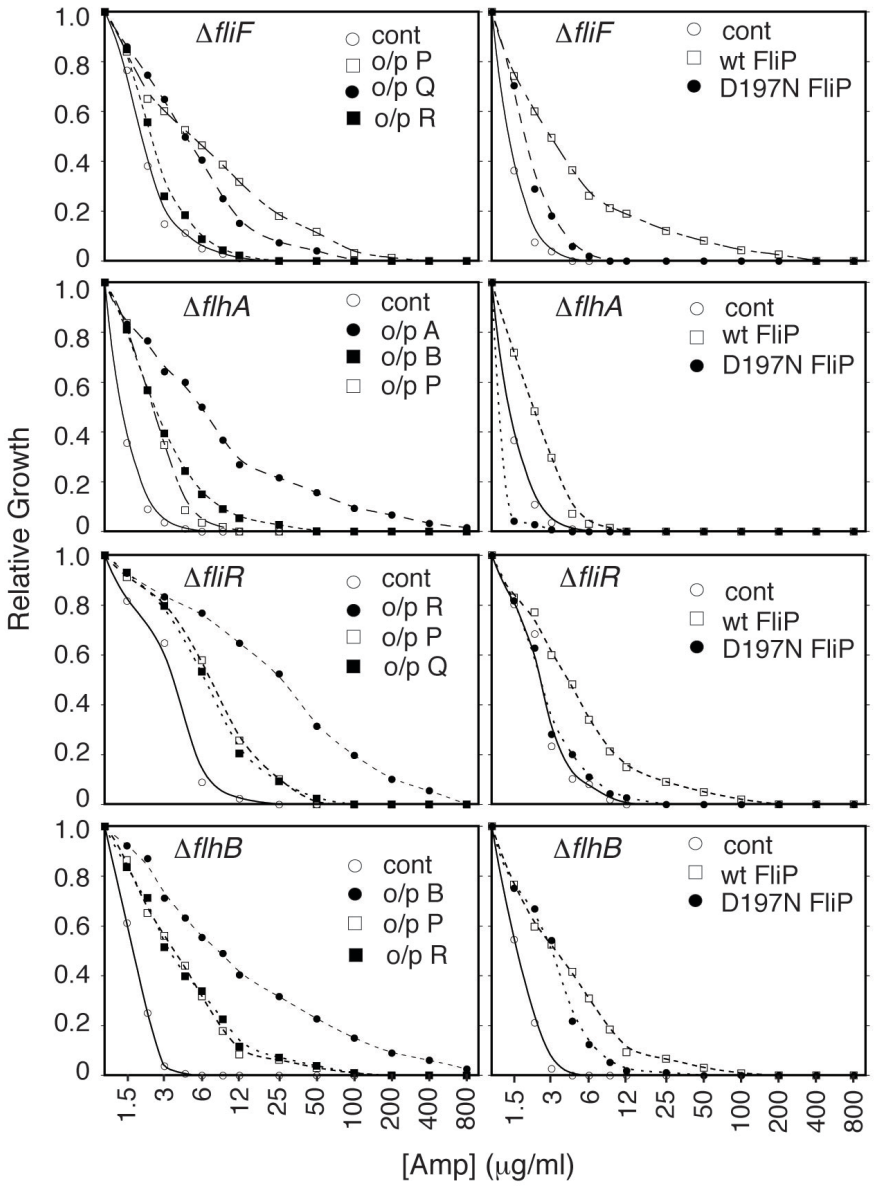

FIGURE 3.6

Assays of FlgE-Bla export in strains deleted of membrane components of the export apparatus, and effects of overexpressing other membrane components. The plots show culture growth as a function of ampicillin concentration. The components deleted, and components overexpressed, are indicated in each panel. D197N is a dominant, non-functional variant of FliP, as described in the text. o/p, overexpression of indicated membrane component (P, FliP; Q, FliQ; R, FliR; A, FlhA and B, FlhB); cont., empty vector control.

3.4.5 Translocation in the absence of all components but FliP.

The foregoing results show that export can occur when any single component besides FliP or FliQ is removed, but do not establish whether FliP and/or FliQ are, by themselves, sufficient for secretion. To address this we constructed a strain deleted of all flagellar genes. The gene encoding the FlgE-Bla fusion protein was retained in the chromosome under control of the arabinose-inducible promoter, and genes encoding the various membrane components of the secretion apparatus were introduced on salicylate-inducible plasmids. Export of the FlgE-Bla fusion was assayed as before by measuring MIC values for ampicillin. Representative data are shown in Figure 3.7 and the findings are summarized in Table 3.3.

The 'super-deletion' strain containing no flagellar genes exhibited a MIC value of about 1 µg/ml, lower than any of the partial-deletion strains. The MIC-value was increased about 10-fold when FliP was expressed in the cells. FlhB and FliR produced only modest increases in the MIC-value (to about 2 µg/ml), and FlhA gave an intermediate effect, increasing the MIC to about 4 µg/ml (Table 3.3). FliP and FliQ together were about as effective as FliP alone (data not shown). The dominant-negative FliP variant was once again used to establish a connection with the normal protein function. When $FliP^{D197N}$ was expressed in the fully deleted strain the MIC value was slightly decreased, to about 0.9 µg/ml (Figure 3.7A). To establish the importance of the FlgE (hook-protein) portion of the fusion construct, which marks it as a substrate for flagellar secretion, we measured the MIC value of the full-deletion strain expressing β-lactamase deleted of its signal sequence (and not fused to any flagellar gene). The MIC value in the control cells was again very low (1 µg/ml), and in this case was not significantly increased by the introduction of FliP and FliQ on a plasmid (Figure 3.7C). Finally, to confirm that these results do not reflect any involvement of the Spi-1 or Spi-2 injectisome systems, the FliP-expression experiment was done in a strain deleted of all *spi-1* and *spi-2* genes as well as all chromosomal flagellar genes. The MIC value in the negative control was again very low (1.2-1.3 µg/ml), and was increased to 9 µg/ml upon overexpression of wild-type FliP but not the D197N FliP variant (Figure 3.7B).

3.4.6 Mutations identify critical residues in TM3 and TM4 of FliP.

The results indicate that FliP is both necessary and sufficient for translocation of FlgE-Bla across the membrane. FliP is among the best-conserved components of the T3S system and contains four clearly predicted transmembrane segments, as well as an N-terminal signal sequence that is cleaved from the mature protein (121, 152). Sequence alignments show that the TM3 and TM4 segments are especially well conserved (Figure 3.10). As an initial step in probing structure-function relations in the FliP membrane segments, we made single Trp replacements at four consecutive positions in each segment (positions 56-59, 94-97, 196-199, and 222-225 in the *Salmonella* protein) and measured the effects on function in a soft-agar motility assay. Results are shown in Figure 3.8. Trp replacements were tolerated at all positions in TM1 and TM2 and at most positions in TM3 and TM4. Motility was eliminated by the replacements at position 197 in TM3 and

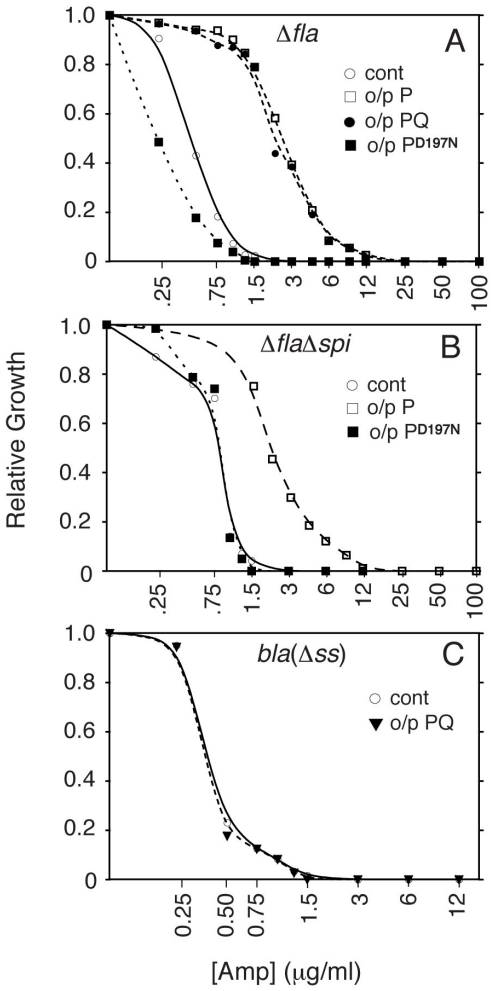

FIGURE 3.7

Assays of FlgE-Bla export in strains lacking all but one export-apparatus component. The cells were deleted of all chromosomal flagellar genes and contained a single copy of *flgE-bla*. (A) FlgE-Bla export activity in a strain deleted for all flagellar genes, and expressing only FliP, or FliP and FliQ together. Export is not supported by the dominant-negative $FliP^{D197N}$ protein. (B) Similar to panel A, except using a strain additionally deleted for the *spi-1* and *spi-2* genes. (C) Requirement for the FlgE portion of the FlgE-Bla substrate. Instead of the FlgE-Bla reporter protein, β-lactamase deleted for its Sec-signal peptide (*bla*(Δ*ss*)) was expressed from the same P_{araBAD} promoter. o/p, overexpression of indicated membrane component (P, FliP; PQ, FliPQ; P^{D197N}, dominant, non-functional variant of FliP); cont., empty vector control.

position 222 in TM4, which are invariant Asp and Lys residues, respectively, in the wild-type protein. Additional replacements were made to probe the functional requirements at these positions. Ala replacement of Lys 222 gave a milder effect than Trp, retaining 20% function in the motility assay. At position 197, function was eliminated by replacements with Ala, Asn, Gly, or Pro. When cells of the D197A mutant were incubated on soft-agar plates, motile pseudo-revertants appeared and were found to have Glu in place of the wild-type Asp at position 197. To test the dominance of the Asp 197 and Lys 222 replacements, plasmids expressing the mutant proteins were expressed in wild-type cells and swarming rates were measured. In most cases the motility of the wild type was not affected, indicating either that the mutant proteins are not incorporated efficiently into the export apparatus or are incorporated but are functionally rescued by association with the wild-type protein. An exception was the D197N replacement, which exerted a strong dominant-negative effect (Figure 3.8). As described above, the D197N variant was useful for establishing a connection between FliP-induced MIC enhancements and the normal protein function. The strong dominance of the D197N mutation indicates that the protein is stable and capable of replacing the wild-type protein in the apparatus.

3.5 Discussion

3.5.1 Secondary importance of the cytoplasmic components.

Previous studies gave evidence that the switch-complex proteins FliG/M/N, and the cargo-escort proteins FliH/I/J, are not strictly required for substrate translocation through the flagellum (44, 94, 140, 158). The present results solidify and extend this conclusion. Substantial export was observed in a Δ*fliHIJGMN* strain lacking both the switch complex and the cargo-escort complex. Even while bypassing the cytoplasmic components, export in the Δ*fliHIJGMN* strain evidently uses the normal trans-membrane secretion pathway because it was enhanced by overexpression of the membrane components, especially FliP, FliQ, and FliR. Most notably, the MIC value of the Δ*fliHIJGMN* strain was increased ten-fold upon overexpression of wild-type FliP but was decreased by about 3-fold on overexpression of the dominant-negative $FliP^{D197N}$ variant (Table 3.3). These findings are consistent with the idea that the C-ring and FliH/I/J complexes are not involved directly in the membrane-translocation step but function to deliver the substrate and position it near the entrance to the export channel (60, 159). While such ushering of the substrate may be needed for very rapid export, the present results show that substrate can arrive at a substantial rate in the absence of this targeting mechanism.

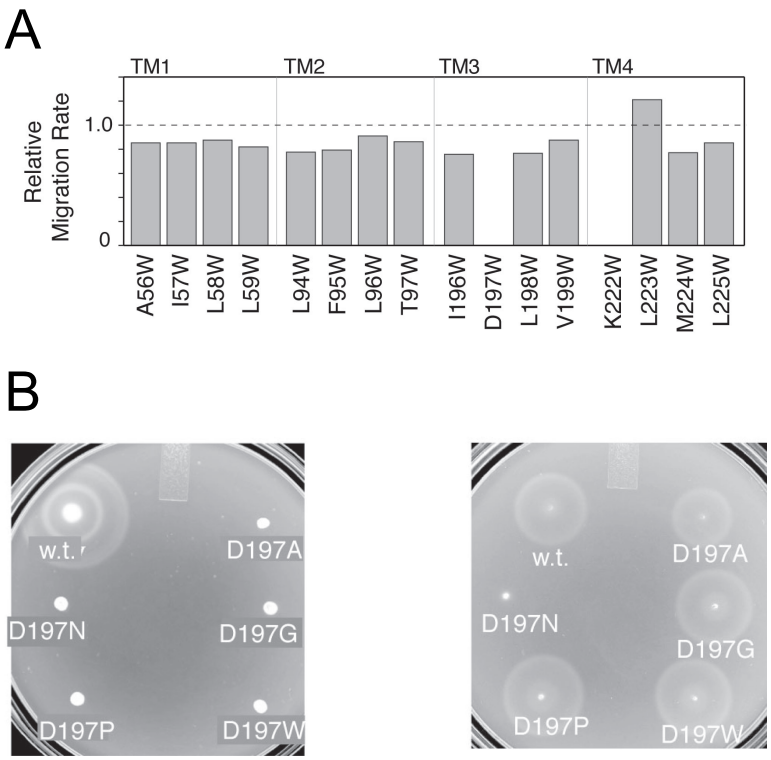

FIGURE 3.8

Effects of Tryptophan substitutions in FliP and motility of FliP mutants. (A) Effects of Trp substitutions near the middles of the four TM segments of FliP. Bars indicate rates of movement on soft-agar plates, relative to a wild-type control. Values are the average of two measurements, which differed by less than 10%. (B) Function in a soft-agar motility assay (left) and dominance (right) of FliP proteins with mutations in residue Asp 197. Mutant proteins were expressed in a Δ*fliP* deletion strain (A) or in the wildtype strain (B).

3.5.2 Dispensability of most membrane components.

A surprising new finding is that the MS-ring, often presumed to be the housing for the flagellar export apparatus, is not essential for substrate secretion. Export in the Δ*fliF* strain was stimulated by overexpression of the other membrane components, especially FliP (Table 3.3). This implies that FliP (and to a lesser extent FliQ), when present at a high enough level, can nucleate assembly of functional export complexes independently of the MS-ring. The hypothesized export complexes could be fairly large (containing multiple copies of the P/Q/R/A/B proteins), but as they lack a rod or rings to identify them as flagellar precursors they would not have been noted in previous studies. FliP was also most effective in restoring flagella to the Δ*fliO* strain (Figure 3.2), further indicating its involvement at a critical nexus in assembly. A simple interpretation is that FliP is at the center of the complex, probably in multiple copies, where it forms a core structure onto which the other components can assemble. Other results, discussed below, also point to a central location of FliP.

Results with the other membrane-component deletions similarly indicate the central importance of FliP, followed closely by FliQ. Strains deleted for *fliP* or *fliQ* could be complemented by the corresponding gene but were not significantly helped by overexpression of any of the other membrane components. By contrast, the MIC-values of the Δ*fliR*, Δ*flhA*, and Δ*flhB* strains were significantly increased by overexpression of some other membrane component(s). While export in the Δ*fliR*, Δ*flhA*, and Δ*flhB* strains is slower than that occurring during flagellar assembly, it nevertheless appears to use the normal pathway because it was enhanced by overexpression of wild-type FliP but was not helped and in some cases was inhibited by overexpression of the dominant-negative $FliP^{D197N}$ variant. Finally, experiments in the 'super-deletion' strain lacking all flagellar components show that FliP, by itself, is sufficient to catalyze substrate translocation (Table 3.3). We conclude that FliP can form a transmembrane conduit for substrate.

3.5.3 Hypothesis for the secretion mechanism.

In its mature form, FliP has four membrane segments. Segments TM3 and TM4 are highly conserved (Figure 3.10) and the present mutational analysis identified two functionally critical charged residues, Asp 197 and Lys 222, near the middles of these segments. TM1 and TM2 are less stringently conserved and more tolerant of mutation, and on this basis appear less likely to contribute directly to the channel (though they are likely to be important for the structure and stability of the protein). Model building with hypothetical helical segments indicates that a channel of sufficient (several Å) size could be formed from the TM3 and TM4 segments of three FliP subunits (Figure 3.9). If the TM3 and TM4 segments are oriented with the Asp-197 and Lys-222 side-chains pointing inward, some other conserved residues are predicted also to lie inside the channel. These include large hydrophobic residues (most often Phe but occasionally Tyr) at positions 190, 193, and 226, which could form a substrate-enfolding gasket similar to the 'phenylalanine-clamp' inside the anthrax-toxin channel (97), and two small residues near the cytoplasmic end of TM3 (residues 201 and 208, conserved as Ala or Ser) that

could make the channel wider near its mouth (Figure 3.9).

While FliP alone can catalyze some substrate translocation, FliQ, FliR, FlhA, and FlhB occur universally in type III secretion systems and are evidently needed for normal rates of export. FlhB has a medium-sized (∼150-residues) cytoplasmic domain that interacts with the FliH/I/J cargo-delivery complexes (215) and that is believed to control the switch in specificity from early (rod/hook) to late (filament) substrate types (67, 137, 201). Such a function in substrate acquisition and identification accords with our conclusion that FlhB is not essential for the substrate translocation step. FlhB has four strongly predicted TM segments, but these are relatively poorly conserved (Figure 3.14), and accordingly less likely to contribute directly to either a substrate conduit or proton channel.

There are few clues to the function of FliR. It is the least conserved membrane protein in the apparatus, and the most hydrophobic, consisting about half of TM segments (Figure 3.11). FliR can function in the context of a FliR-FlhB fusion protein (13) and so is believed to be near FlhB in the complex, probably in a 1:1 association. Given the poor conservation of the FliR TM segments (of which there are probably six; see Figure 3.11) and the non-essentiality of FliR in the FlgE-Bla export assay (Table 3.3), we suggest that FliR does not contribute directly to the substrate- or proton-channel but might serve a mainly structural role, interacting with the other components in the membrane to organize and stabilize the complex.

FlhA has a quite large (∼350 residues) cytoplasmic domain and, like FlhB, has been implicated in the substrate-input stage of export (143, 163, 215). Unlike FlhB, however, FlhA displays very strong sequence conservation in several of its membrane segments, and so is likely to carry out an important membrane-related function. Because it is not essential for substrate translocation (Table 3.3; Figures 3.6 and 3.7), yet has strongly conserved TM segments and is required for transport to be rapid, we propose that FlhA is the energy-transducing element that harnesses the proton gradient to energize substrate translocation. Sequence alignments show that FlhA has several invariant acidic and basic residues that could function in proton binding and conduction, including some in or near the TM segments (Figure 3.12 and Figure 3.13).

An hypothesis for export-apparatus organization and function that incorporates the present findings is presented in Figure 3.9. Multiple copies of FliP (three are shown but more are possible) are positioned at the center of the complex, where they form the conduit for substrate. FliQ and FliR are near FliP, stabilizing the substrate channel but not contributing directly to it. FlhA and FlhB are arranged around the pore with their cytoplasmic domains positioned to capture substrate, and with the cytoplasmic domain of FlhA poised to engage the substrate and drive its movement through the channel. The protons that energize export are proposed to act through FlhA, binding to one or more conserved titratable groups to drive cyclic conformational changes. A crystal structure of the FlhA cytoplasmic domain shows that it is formed from several sub-domains connected by linkers that could confer conformational flexibility (162). Key features of the model remain to be tested; questions to address will include the occurrence and identities of functionally important proton-binding residues in FlhA or the other proteins, the number of FliP (and other component) subunits present in the complex, and the occurrence and nature of conformational changes that drive substrate movement.

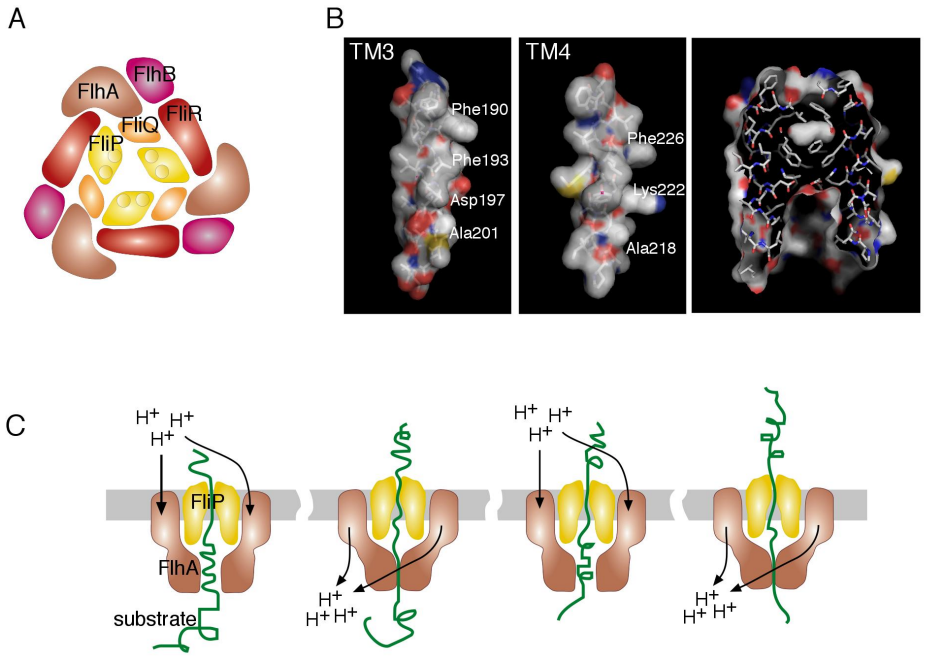

FIGURE 3.9

Model for the organization and function of the flagellar export apparatus. (A) Proposed arrangement of the membrane-associated components of the flagellar secretion apparatus. The view is from a direction perpendicular to the membrane. Key features of the model are the central location of FliP, the nearby location for FliQ, and the presence of multiple copies of all of the proteins. TM3 and TM4 of FliP are proposed to be most directly involved in forming the substrate channel. (B) Left: Conserved features of the TM3 and TM4 segments of FliP. The segments are modeled as α helices and are oriented with the invariant, functionally important charged residues (Asp 197 and Lys 222) pointing to the right. Conserved bulky residues occur above the charged groups, and conserved small residues below. Right: cut-away view of a hypothetical substrate channel formed from the TM3 and TM4 segments of multiple (in this case, three) FliP subunits. The model assumes that the invariant charged residues point into the the channel, and illustrates the structural asymmetry that may be expected to result from the presence of bulky residues above the charged groups and small residues below; the channel is relatively open toward the cytoplasmic end but largely filled by Phe side-chains near the periplasmic end. The Phe-residue cluster bears resemblance to the 'phenylalanine gasket' found in the anthrax-toxin channel (97). (C) Proposed mechanism of flagellar type III secretion. FliP forms the central channel and protons flow through FlhA. The proton flow energizes cyclic conformational changes in the large cytoplasmic domain of FlhA that drive the substrate through the channel.

3.5.4 Implications for evolution of the flagellum.

The complexity of the flagellum has prompted questions regarding its evolution; specifically, it has been suggested that the manifestation of a useful flagellar function would have required co-evolution of numerous components, and would accordingly have been highly improbable (16). The present results show, however, that the single flagellar protein FliP can catalyze translocation of a substrate from cytosol to periplasm. An ancestral FliP channel, however rudimentary, might have provided a useful transport activity on which selection could act to enable the stepwise addition and refinement of other components. Thus, the early steps in flagellar evolution might have been roughly the reverse of the deconstruction undertaken in the present experiments, with an initially weak transport activity of FliP being augmented first by the addition of FliQ, FliR, FlhA and FlhB, then by the cytoplasmic substrate-delivery machinery. At some point, the structure must have become specialized for the production of an external appendage (though not necessarily a rotating one). The axial structures of the present-day flagellum - the rod, hook, and filament - are formed from several different components, but these are all related structurally and appear to have descended from a single ancestral substrate (71).

3.6 Materials and Methods

Bacterial strains, plasmids and media

Bacterial strains and plasmids used in this study are listed in Table 3.4 and Table 3.5. Cells were grown in either LB medium (per liter: 10 g tryptone, 5 g peptone, 5 g NaCl) or PPBS plates (per liter: peptone/protease-peptone/bile-salts (PPBS) (17 g peptone, 3 g protease-peptone, 1.5 g bile salts #3, 5 g sodium chloride, 10.8 g bacto-agar). As needed, plates contained ampicillin at 7.5-25 µg/ml and tetracycline at 15 µg/ml. Liquid media used ampicillin at 100 µg/ml, tetracycline at 15 µg/ml, and chloramplhenicol at 12.5 µg/ml. Crosses used the generalized transducing phage P22 *HT105/1 int-201* (168). Chromosomal deletions were generated using λ-RED mediated recombination (34) and tetracycline-sensitive selection as described (122, 202). The *fliO*, *fliP*, *fliQ*, *fliR* and *flhA* genes were subcloned in vector pKG116 using NdeI and KpnI sites. The mutant variants of the proteins were obtained by site-directed mutagenesis (Altered-Sites procedure, Promega or QuikChange mutagenesis, Qiagen). The function of the mutant FliP, FliQ, FliR, or FlhA proteins was tested by complementation assays using corresponding null tester strains (K.T. Hughes) and measuring rates of swarming in soft agar.

TABLE 3.4
Strains used in this study.
All strains were constructed for this study if not noted otherwise.

Strain number	Genotype	Reference
TH437	*Salmonella enterica* serovar *Typhimurium* LT2	J. Roth
TH9949	Δ*flgBC6557 flgE6569*::*bla*	
TH10548	Δ*fliO6708*	lab collection
TH12465	Δ*flgBC6557 flgE6569*::*bla* Δ*fliF7387*	
TH12466	Δ*flgBC6557 flgE6569*::*bla* Δ*fliG7388*	
TH12468	Δ*flgBC6557 flgE6569*::*bla* Δ*fliM7390*	
TH12469	Δ*flgBC6557 flgE6569*::*bla* Δ*fliN7391*	
TH12470	Δ*flgBC6557 flgE6569*::*bla* Δ*fliMN7392*	
TH12473	Δ*flgBC6557 flgE6569*::*bla* Δ*fliI7395*	
TH12476	Δ*flgBC6557 flgE6569*::*bla* Δ*fliHIJ7398*	
TH12480	Δ*flgBC6557 flgE6569*::*bla* Δ*fliMN7392* Δ*fliG7402*	
TH12640	Δ*flgBC6557 flgE6569*::*bla* Δ*fliMN7392* Δ*fliG7402* Δ*fliHIJ7451*	
TH12643	Δ*flgBC6557 flgE6569*::*bla* Δ*flhA7453*	
TH12662	Δ*flgBC6557 flgE6569*::*bla* Δ*fliHIJ7398* Δ*invC* Δ*ssaN111*	
TH12667	Δ*flgBC6557 flgE6569*::*bla* Δ*flhB7456*	
TH12731	Δ*flgBC6557 flgE6569*::*bla* Δ*fliP7457*	
TH14255	Δ*flgBC6557 flgE6569*::*bla* Δ*fliO6708*	
TH15033	Δ*flgBC6557 flgE6569*::*bla* Δ*fliG7402* Δ*fliMN7392* Δ*fliHIJ7451* Δ*ssaN109* Δ*invC*	
TH15426	Δ*flgBC6557 flgE6569*::*bla* $P_{flhDC7793}$(P1&P4 -10 TATAAT)	
TH15427	Δ*flgBC6557 flgE6569*::*bla* Δ*fliF7387* $P_{flhDC7793}$	
TH15428	Δ*flgBC6557 flgE6569*::*bla* Δ*fliG7388* $P_{flhDC7793}$	
TH15429	Δ*flgBC6557 flgE6569*::*bla* Δ*fliMN7392* $P_{flhDC7793}$	
TH15431	Δ*flgBC6557 flgE6569*::*bla* Δ*fliHIJ7398* $P_{flhDC7793}$	
TH15432	Δ*flgBC6557 flgE6569*::*bla* Δ*fliMN7392* Δ*fliG7402* $P_{flhDC7793}$	
TH15433	Δ*flgBC6557 flgE6569*::*bla* Δ*flhB7456* $P_{flhDC7793}$	
TH15434	Δ*flgBC6557 flgE6569*::*bla* Δ*fliP7457* $P_{flhDC7793}$	
TH15435	Δ*flgBC6557 flgE6569*::*bla* Δ*fliO6708* $P_{flhDC7793}$	
TH15924	Δ*flgBC6557 flgE6569*::*bla* Δ*flhA7453* $P_{flhDC7793}$	
TH15930	Δ*flgBC6557 flgE6569*::*bla* Δ*fliQ6710*	
TH15931	Δ*flgBC6557 flgE6569*::*bla* Δ*fliR6711*	
TH15957	Δ*flgBC6557 flgE6569*::*bla* $P_{flhDC7793}$ Δ*fliQ6710*	
TH15958	Δ*flgBC6557 flgE6569*::*bla* $P_{flhDC7793}$ Δ*fliR6711*	
TH16033	Δ*flgBC6557 flgE6569*::*bla* $P_{flhDC7793}$ Δ*fliG7402* Δ*fliHIJ7451* Δ*fliMN7392*	
TH16034	Δ*flgBC6557 flgE6569*::*bla* $P_{flhDC7793}$ Δ*fliG7402* Δ*fliHIJ7451* Δ*fliMN7392* Δ*ssaN109* Δ*invC*	
TH16048	Δ*flgM5628*::FRT $P_{flhD7460}$(*-38G:A* from *AUG*) Δ*fliO6708*	
TH16049	Δ*flgM5628*::FRT $P_{flhD7460}$(*-38G:A* from *AUG*) Δ*fliN7359*	

Strain number	Genotype	Reference
TH16062	Δ*atpA*::*tetRA* Δ*flgM5628*::FRT $P_{flhD7460}$(*-38G:A* from *AUG*) Δ*fliO6708*	
TH16063	Δ*atpA*::*tetRA* Δ*flgM5628*::FRT $P_{flhD7460}$(*-38G:A* from *AUG*) Δ*fliN7359*	
TH16161	Δ*flgBC6557 flgE6569*::*bla* Δ*invH-sprB*::FKF	
TH16162	Δ*flgBC6557 flgE6569*::*bla* Δ*fliMN7392* Δ*invH-sprB*::FKF	
TH16163	Δ*flgBC6557 flgE6569*::*bla* Δ*fliG7402* Δ*fliMN7392* Δ*invH-sprB*::FKF	
TH16164	Δ*flgBC6557 flgE6569*::*bla* Δ*fliG7402* Δ*fliHIJ7451* Δ*fliMN7392* Δ*invH-sprB*::FKF	
TH16165	Δ*flgBC6557 flgE6569*::*bla* Δ*fliP7457* Δ*invH-sprB*::FKF	
TH16166	Δ*flgBC6557 flgE6569*::*bla* Δ*fliO6708* Δ*invH-sprB*::FKF	
TH16211	Δ*flgBC6557 flgE6569*::*bla* Δ*invH-sprB*::FKF Δ*sseA-ssaU*::FCF	
TH16212	Δ*flgBC6557 flgE6569*::*bla* Δ*fliMN7392* Δ*invH-sprB*::FKF Δ*sseA-ssaU*::FCF	
TH16213	Δ*flgBC6557 flgE6569*::*bla* Δ*fliG7402* Δ*fliMN7392* Δ*invH-sprB*::FKF Δ*sseA-ssaU*::FCF	
TH16214	Δ*flgBC6557 flgE6569*::*bla* Δ*fliG7402* Δ*fliHIJ7451* Δ*fliMN7392* Δ*invH-sprB*::FKF Δ*sseA-ssaU*::FCF	
TH16215	Δ*flgBC6557 flgE6569*::*bla* Δ*fliP7457* Δ*invH-sprB*::FKF Δ*sseA-ssaU*::FCF	
TH16216	Δ*flgBC6557 flgE6569*::*bla* Δ*fliO6708* Δ*invH-sprB*::FKF Δ*sseA-ssaU*::FCF	
TH16217	Δ*flgBC6557 flgE6569*::*bla* Δ*fliG7402* Δ*fliHIJ7451* ΔfliMNO7897 Δ*invH-sprB*::FKF Δ*sseA-ssaU*::FCF	
TH16218	Δ*flgBC6557 flgE6569*::*bla* $P_{flhDC7793}$ Δ*invH-sprB*::FKF Δ*sseA-ssaU*::FCF	
TH16219	Δ*flgBC6557 flgE6569*::*bla* $P_{flhDC7793}$ Δ*fliMN7392* Δ*invH-sprB*::FKF Δ*sseA-ssaU*::FCF	
TH16220	Δ*flgBC6557 flgE6569*::*bla* $P_{flhDC7793}$ Δ*fliG7402* Δ*fliMN7392* Δ*invH-sprB*::FKF Δ*sseA-ssaU*::FCF	
TH16221	Δ*flgBC6557 flgE6569*::*bla* $P_{flhDC7793}$ Δ*fliP7457* Δ*invH-sprB*::FKF Δ*sseA-ssaU*::FCF	
TH16222	Δ*flgBC6557 flgE6569*::*bla* $P_{flhDC7793}$ Δ*fliO6708* Δ*invH-sprB*::FKF Δ*sseA-ssaU*::FCF	
TH16223	Δ*flgBC6557 flgE6569*::*bla* $P_{flhDC7793}$ Δ*fliG7402* Δ*fliHIJ7451* Δ*fliMN7392* Δ*invH-sprB*::FKF Δ*sseA-ssaU*::FCF	
TH16224	Δ*flgBC6557 flgE6569*::*bla* $P_{flhDC7793}$ Δ*fliG7402* Δ*fliHIJ7451* ΔfliMNO7897 Δ*invH-sprB*::FKF Δ*sseA-ssaU*::FCF	
TH16254	Δ*flgBC6557 flgE6569*::*bla* Δ*fliG7402* Δ*fliHIJ7451* Δ*fliMN7392* Δ*ssaN109* Δ*invC lhrA*::T-POP	
TH16255	Δ*flgBC6557 flgE6569*::*bla* Δ*fliG7402* Δ*fliHIJ7451* Δ*fliMN7392* Δ*ssaN109* Δ*invC mutL*::T-POP	
TH16256	Δ*flgBC6557 flgE6569*::*bla* Δ*fliG7402* Δ*fliHIJ7451* Δ*fliMN7392* Δ*ssaN109* Δ*invC ssaV*::T-POP	
TH16257	Δ*flgBC6557 flgE6569*::*bla* $P_{flhDC7793}$ Δ*fliG7402* Δ*fliHIJ7451* Δ*fliMN7392* Δ*ssaN109* Δ*invC fliD7910*::T-POP	

Strain number	Genotype	Reference
TH16258	Δ*flgBC6557 flgE6569*::*bla* P$_{flhDC7793}$ Δ*fliG7402* Δ*fliHIJ7451* Δ*fliMN7392* Δ*ssaN109* Δ*invC yieK*::T-POP	
TH16259	Δ*flgBC6557 flgE6569*::*bla* P$_{flhDC7793}$ Δ*fliG7402* Δ*fliHIJ7451* Δ*fliMN7392* Δ*ssaN109* Δ*invC fkpA*::T-POP	
TH16260	Δ*flgBC6557 flgE6569*::*bla* P$_{flhDC7793}$ Δ*fliG7402* Δ*fliHIJ7451* Δ*fliMN7392* Δ*ssaN109* Δ*invC fliD7911*::T-POP	
TH16261	Δ*flgBC6557 flgE6569*::*bla* P$_{flhDC7793}$ Δ*fliG7402* Δ*fliHIJ7451* Δ*fliMN7392* Δ*ssaN109* Δ*invC hisQ*::T-POP	
TH16262	Δ*flgBC6557 flgE6569*::*bla* P$_{flhDC7793}$ Δ*fliG7402* Δ*fliHIJ7451* Δ*fliMN7392* Δ*ssaN109* Δ*invC wcaK*::T-POP	
TH16263	Δ*flgBC6557 flgE6569*::*bla* P$_{flhDC7793}$ Δ*fliG7402* Δ*fliHIJ7451* Δ*fliMN7392* Δ*ssaN109* Δ*invC mgtC/yicL*::T-POP	
TH16316	Δ*flgBC6557 flgE6569*::*bla* Δ*fliF7387* Δ*invH-sprB*::FKF	
TH16316	Δ*flgBC6557 flgE6569*::*bla* Δ*fliF7387* Δ*invH-sprB*::FKF	
TH16317	Δ*flgBC6557 flgE6569*::*bla* Δ*fliHIJ7398* Δ*invH-sprB*::FKF	
TH16317	Δ*flgBC6557 flgE6569*::*bla* Δ*fliHIJ7398* Δ*invH-sprB*::FKF	
TH16318	Δ*flgBC6557 flgE6569*::*bla* Δ*flhA7453* Δ*invH-sprB*::FKF	
TH16318	Δ*flgBC6557 flgE6569*::*bla* Δ*flhA7453* Δ*invH-sprB*::FKF	
TH16324	Δ*flgBC6557 flgE6569*::*bla* Δ*fliF7387* Δ*invH-sprB*::FKF Δ*sseA-ssaU*::FCF	
TH16325	Δ*flgBC6557 flgE6569*::*bla* Δ*fliHIJ7398* Δ*invH-sprB*::FKF Δ*sseA-ssaU*::FCF	
TH16326	Δ*flgBC6557 flgE6569*::*bla* Δ*flhA7453* Δ*invH-sprB*::FKF Δ*sseA-ssaU*::FCF	
TH16327	Δ*flgBC6557 flgE6569*::*bla* P$_{flhDC7793}$ Δ*fliF7387* Δ*invH-sprB*::FKF Δ*sseA-ssaU*::FCF	
TH16328	Δ*flgBC6557 flgE6569*::*bla* P$_{flhDC7793}$ Δ*fliHIJ7398* Δ*invH-sprB*::FKF Δ*sseA-ssaU*::FCF	
TH16329	Δ*flgBC6557 flgE6569*::*bla* P$_{flhDC7793}$ Δ*flhA7453* Δ*invH-sprB*::FKF Δ*sseA-ssaU*::FCF	
TH16615	Δ*flgBC6557 flgE6569*::*bla* Δ*flhA7453* Δ*fliE-R7838* P$_{flhDC7793}$	
TH16616	Δ*flgBC6557 flgE6569*::*bla* Δ*flhA7453* Δ*fliE-R7838*	
TH16617	Δ*flgBC6557 flgE6569*::*bla* Δ*flhA7453* Δ*fliHIJ7367*	
TH16625	Δ*flgBC6557 flgE6569*::*bla* Δ*fliF7387 hupB*::T-POP	
TH16626	Δ*flgBC6557 flgE6569*::*bla* Δ*fliF7387 ydiV*::T-POP	
TH16627	Δ*flgBC6557 flgE6569*::*bla* Δ*fliF7387 rcsB*::T-POP	
TH16628	Δ*flgBC6557 flgE6569*::*bla* Δ*fliF7387 rcsB*::T-POP	
TH16629	Δ*flgBC6557 flgE6569*::*bla* Δ*fliF7387 rcsB*::T-POP	
TH16630	Δ*flgBC6557 flgE6569*::*bla* Δ*fliF7387 rcsB*::T-POP	
TH16631	Δ*flgBC6557 flgE6569*::*bla* Δ*fliF7387* STM0580::T-POP	
TH16632	Δ*flgBC6557 flgE6569*::*bla* Δ*fliF7387 marA*::T-POP	
TH16633	Δ*flgBC6557 flgE6569*::*bla* Δ*fliF7387 lrhA*::T-POP	
TH16634	Δ*flgBC6557 flgE6569*::*bla* Δ*fliF7387 lrhA*::T-POP	
TH16636	Δ*flgBC6557 flgE6569*::*bla* Δ*fliF7387 marA*::T-POP	
TH16637	Δ*flgBC6557 flgE6569*::*bla* Δ*fliF7387 ydiV*::T-POP	
TH16640	Δ*flgBC6557 flgE6569*::*bla* Δ*fliF7387 lrhA*::T-POP	

Strain number	Genotype	Reference
TH16643	Δ*flgBC6557 flgE6569*::*bla* Δ*fliF7387 clpX*::T-POP	
TH16647	Δ*flgBC6557 flgE6569*::*bla* Δ*flhA7453* ΔfliE-R7838 Δ*sseA-ssaU*::FKF	
TH16649	Δ*flgBC6557 flgE6569*::*bla* Δ*flhA7453* ΔfliE-R7838 Δ*invH-sprB*::FKF	
TH16980	DEL1103 (Δ*tct-fljB*) DEL1131 (Δ*fliA-fliR*) DEL1133 (Δ*flhB-flhD*) DEL1137 (Δ*flgN-flgL*) Δ*araBAD1014*::*flgE-bla*	
TH16988	DEL1103 (Δ*tct-fljB*) DEL1131 (Δ*fliA-fliR*) DEL1133 (Δ*flhB-flhD*) DEL1137 (Δ*flgN-flgL*) Δ*araBAD1077*::*flgDE-bla*	

FliC secretion assay

FliC secretion assays were performed essentially as described previously (158). Briefly, 1 ml cultures in LB were grown overnight at 37 ℃. Cultures were diluted 100-fold into 5 ml LB and grown at 37 ℃ to an OD_{600} between 0.5 and 0.7, for 6.5 hours. The cells were removed at 18,500 x g for 15 min. Supernatant (1 ml) was removed into an Eppendorf tube, mixed with prechilled 25% Tricloroacetic acid (TCA) (final concentration 6%), chilled on ice for 15 min and centrifuged at 10,000 g for 10 min. The pellets were suspended with 0.3 ml of acetone, and the suspension was quickly dissolved and centrifuged at 10,000 g for 5 min. Acetone washing was repeated twice to remove TCA from the precipitates completely. The pellets were dissolved in SDS sample buffer and analyzed by SDS-PAGE. The proteins bands were visualized by Coomassie brilliant blue (CBB) staining.

Fluorescence microscopy

For fluorescence microscopy analysis of ΔfliO and ΔfliN deletion strains, overnight cultures were diluted 1:100 in fresh LB media grown to mid-log phase grown at 30 ℃. A well of approximately 25 µl volume was formed by putting one layer of sticky tape between a glass slide and the coverslip. Cells were applied to the well and immobilized on the poly-L-lysine treated coverslips. For immunofluorescence, cells were fixed by addition of final 2% formaldehyde + 0.2% gluteraldehyde. Filaments were labeled using a mix of polyclonal anti-FliC and anti-FljB antibodies (rabbit) and stained using secondary anti-rabbit antibodies coupled to Alexa Fluor-488 (Invitrogen). DNA and membrane staining was performed using Hoechst (10 µg/ml, Invitrogen) and FM-64 (5 µg/ml, Invitrogen). An Applied Precision optical sectioning microscope based on a Olympus IX71 inverted microscope equipped with an UPlanSApo 1003 objective and a coolSNAP HQ (Photometrics) CCD camera was used to collect images. The images were acquired with optical Z sections every 200 nm and deconvolved using softWoRx v.3.4.2 (Applied Precision). The pixel data of individual Z sections of the deconvolved images were projected on a single plane using the Quick Projection tool (settings: maximal intensity) of softWoRx

Explorer v1.3 (Applied Precision) and the contrast of the images was adjusted using ImageJ 1.43q (U. S. National Institutes of Health (2)).

TABLE 3.5
Plasmids used in this study.
All plasmids were constructed for this study if not noted otherwise.

plasmid number	Relevant characteristics	Reference
pKG116	vector for Salicylate-inducible expression; Cm^R	J.S. Parkinson
pMS9	*fliO* in pKG116	
pMS10	*fliP* in pKG116	
pMS11	*fliQ* in pKG116	
pMS12	*fliR* in pKG116	
pMS122	*flhA* in pKG116	
pMS123	*flhB* in pKG116	

Hook-β-lactamase secretion assay

The hook-β-lactamase secretion assay was essentially performed as described in Lee et al. (108) with minor modifications to adapt for a 96-well microtiter plate format. Briefly, cultures were grown overnight in LB at 34 ℃ in 96-well microtiter plates. The cells were then diluted 100-fold into fresh LB medium and grown to mid-log phase for about 2 hours at 34 ℃. Afterwards, the cells were again diluted 100-fold in fresh LB medium containing appropriate concentrations of ampicillin and incubated at 34 ℃ for 4.5 hours. Afterwards, the optical density at 595 nm of each sample was measured using the absorbance protocol of a PolarStar Optima (BMG Labtech). On every microtiter plate, a wildtype control (TH9949 in case of WT *flhDC* and TH15426 in case of P_{flhD^*}), as well as a reference control strain (the respective wildtype control strain background with an additional deletion of *fliP*) was included. The relative growth of each strain (measured OD_{595} values normalized to the value at zero ampicillin) were plotted against ampicillin concentration, and fitted to a smooth curve (a Stineman interpolation). The MIC for ampicillin was defined as the Amp concentration at which the curve crossed 0.05; i.e., the concentration that reduced growth to 5% of the zero-Amp value of the respective strain. Assays in culture tubes were done similarly, except using a growth temperature of 37 ℃. Cultures were diluted 100-fold into 3 ml LB and grown to an OD_{600} between 0.5 and 0.7, then diluted 50-fold into fresh LB media containing ampicillin at the concentrations indicated in the figures (typically ranging from 800 µg/ml to 1.56 µg/ml). The OD_{600} of each sample was measured after 4.5 hours of further growth at 37 ℃, and the minimum inhibitory concentration was determined as described above. Reported MIC values are the averages of at least three independent determinations.

Isolation of random T-POP transposon insertion mutants

The screen for random Tn*10*dTc[Δ25] transposon (T-POP) insertions that allowed for flagellar type III-specific secretion of the hook-β-lactamase reporter protein in the Δ*fliHIJGMN* or Δ*fliF* deletion background was essentially performed as described in (44, 107, 202). The screening for enhanced hook-β-lactamase secretion in those deletion backgrounds was performed using PPBS plates containing otherwise inhibitory ampicillin concentrations (7.5 µg/ml and 25 µg/ml ampicillin, respectively).

3.7 Acknowledgements

Supported by PHS grants GM056141 and GM087260Z from the National Institutes of Health. We thank members of the Blair and Hughes labs for discussions. M.E. gratefully acknowledges scholarship support of the Boehringer Ingelheim Fonds. We thank Joshua Gowans, Eun A Kim, and Yang Zhang for assistance with MIC assays.

3.8 Sequence alignments

The following figures display sequence alignments for the flagellar export apparatus components FliP, FliQ, FliR, FlhA, and FlhB.

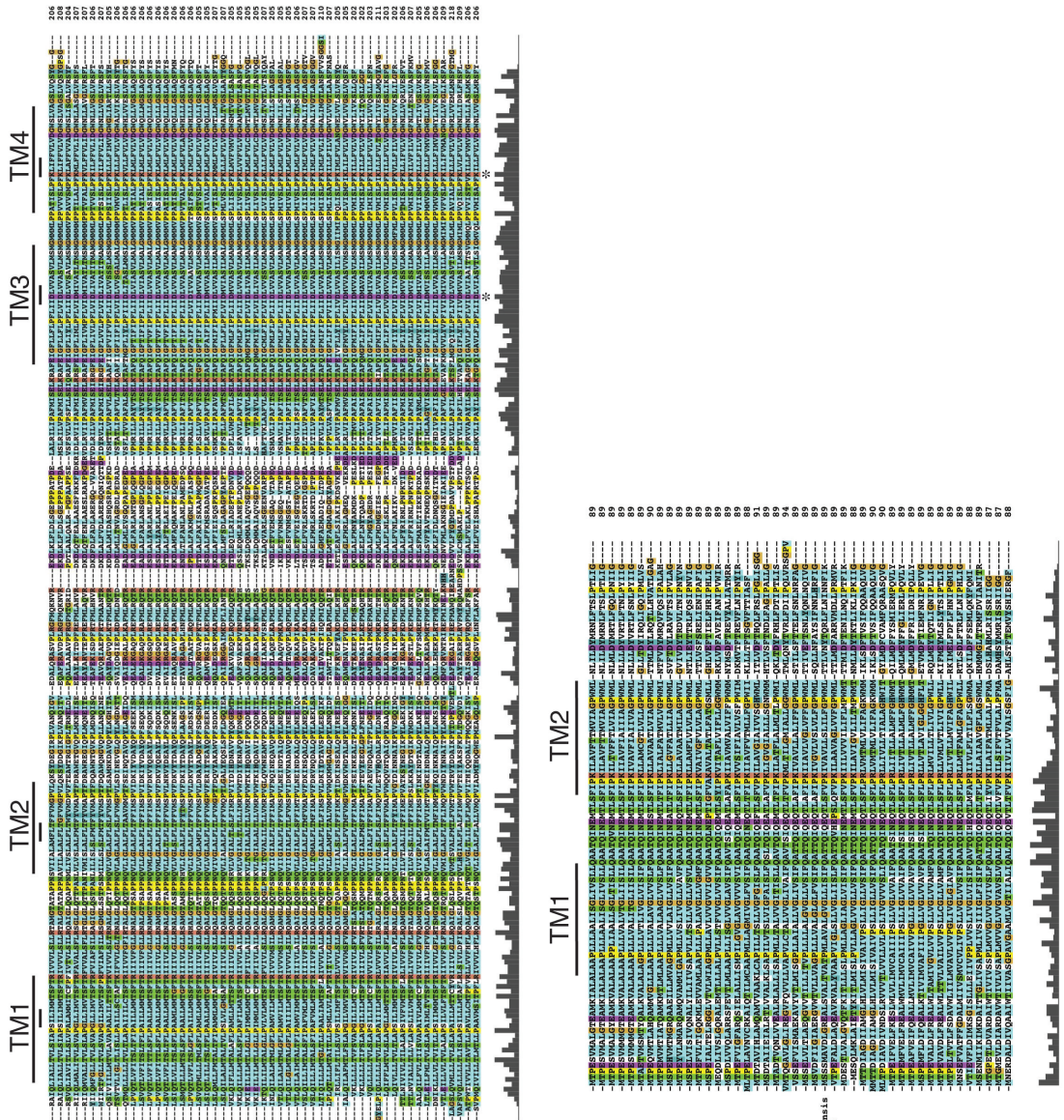

FIGURE 3.10

Sequence alignments for the flagellar export apparatus components FliP and FliQ. Predicted TM segments are indicated by lines at the top of the alignments. Conservation scores are shown below. The invariant charged residues of FliP, found important in the present mutational analysis, are indicated by asterisks.

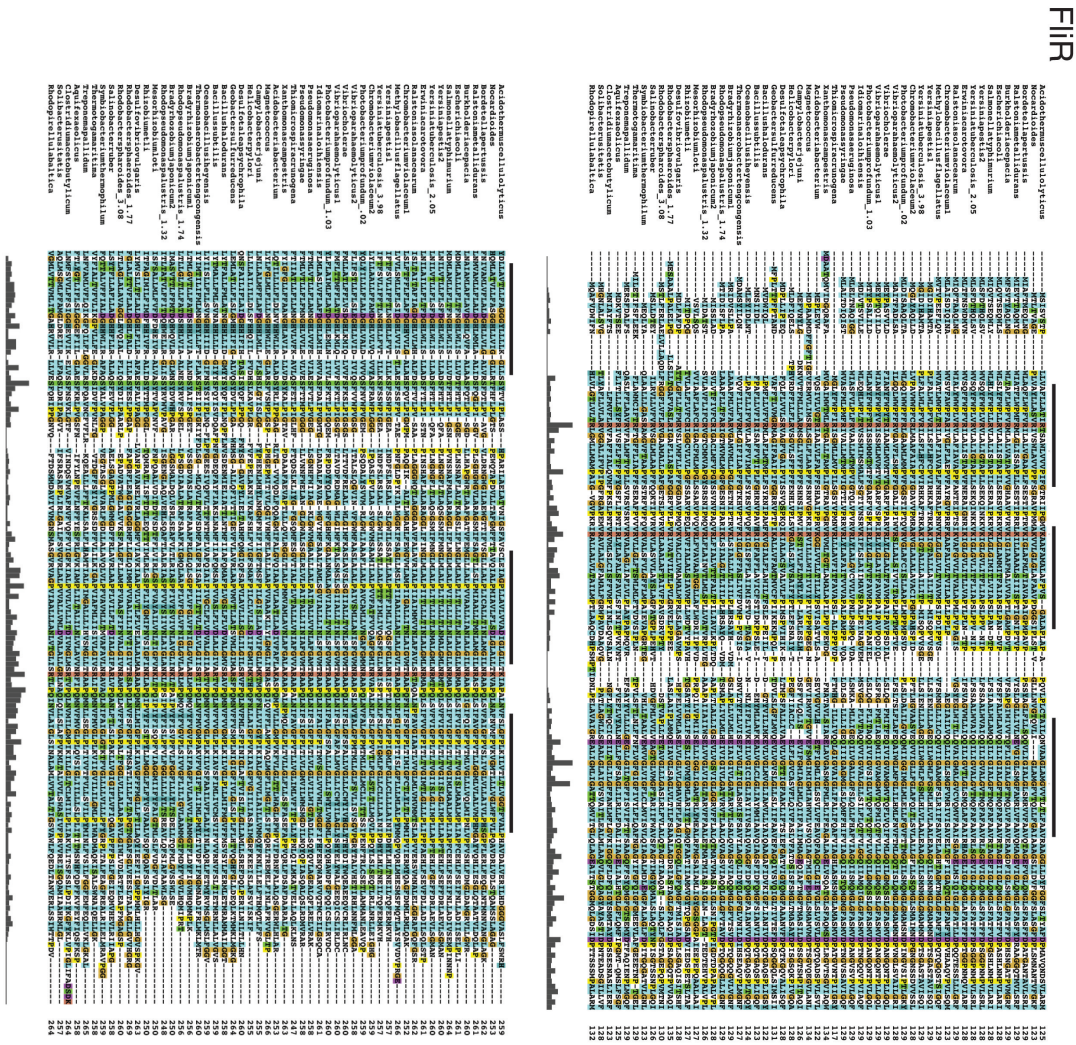

FIGURE 3.11

Sequence alignment for the flagellar export apparatus component FliR. Predicted TM segments are indicated by lines at the top of the alignments. Conservation scores are shown below.

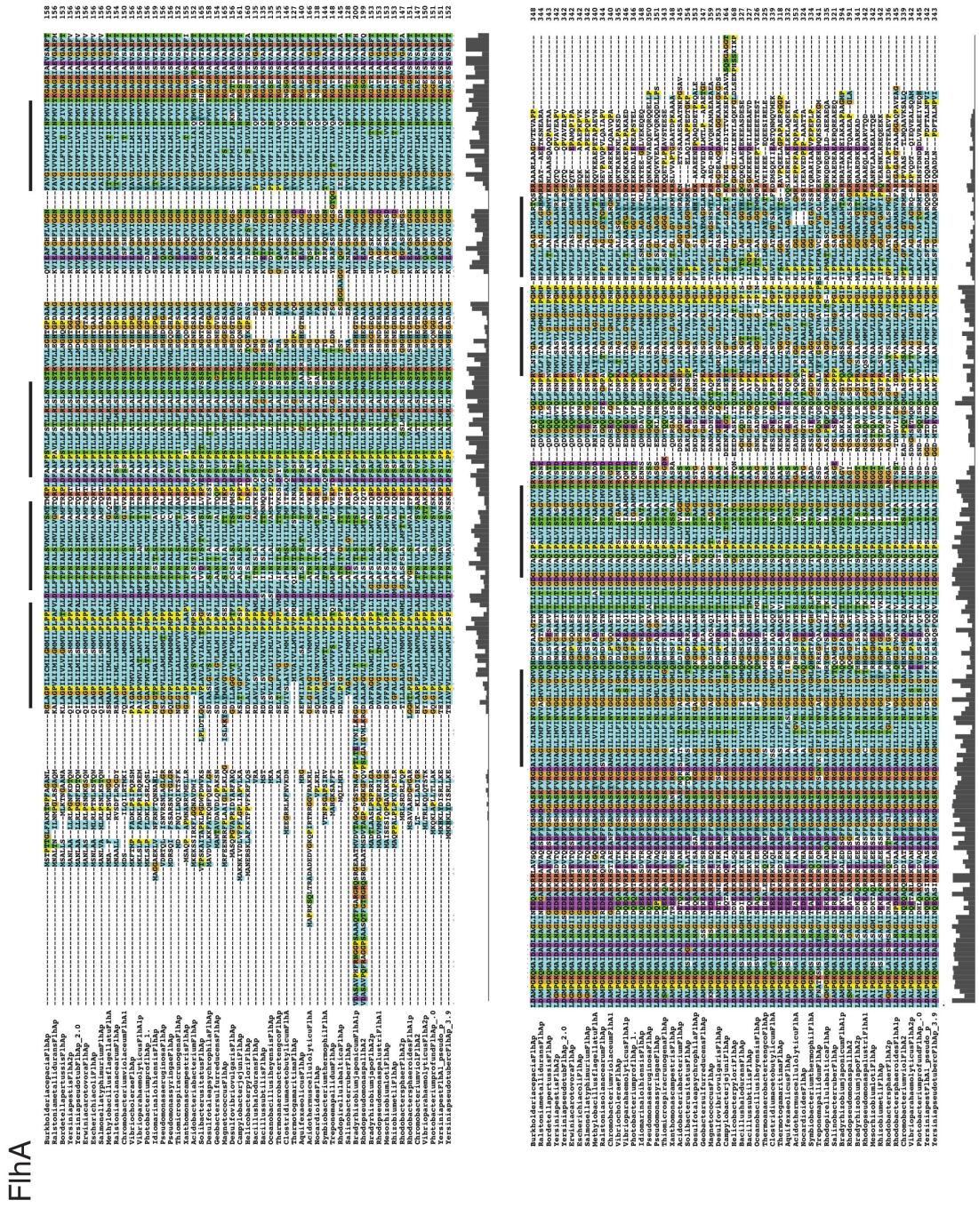

FIGURE 3.12

Sequence alignment for the flagellar export apparatus component FlhA - part 1. Predicted TM segments are indicated by lines at the top of the alignments. Conservation scores are shown below.

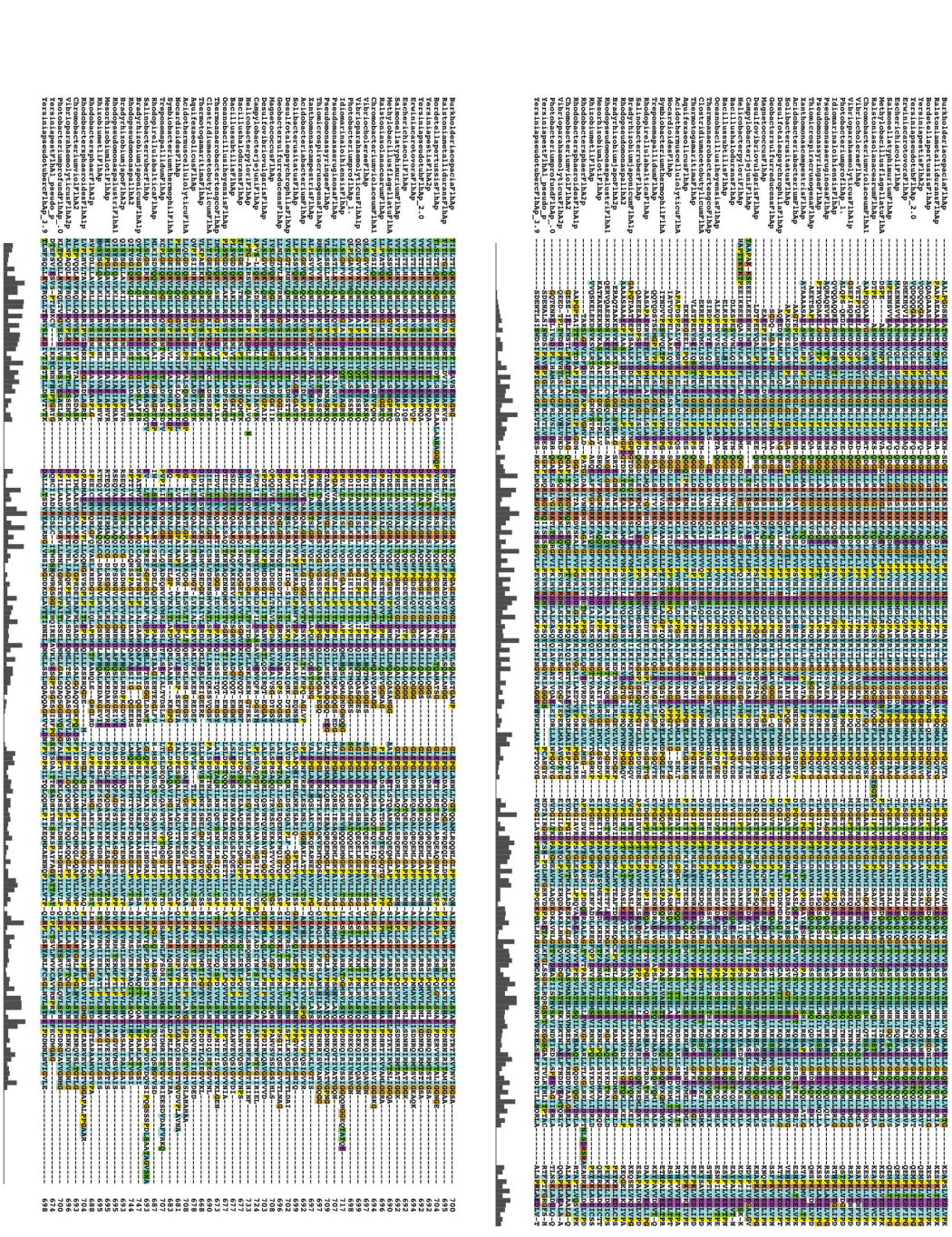

FIGURE 3.13

Sequence alignment for the flagellar export apparatus component FlhA - part 2. Predicted TM segments are indicated by lines at the top of the alignments. Conservation scores are shown below.

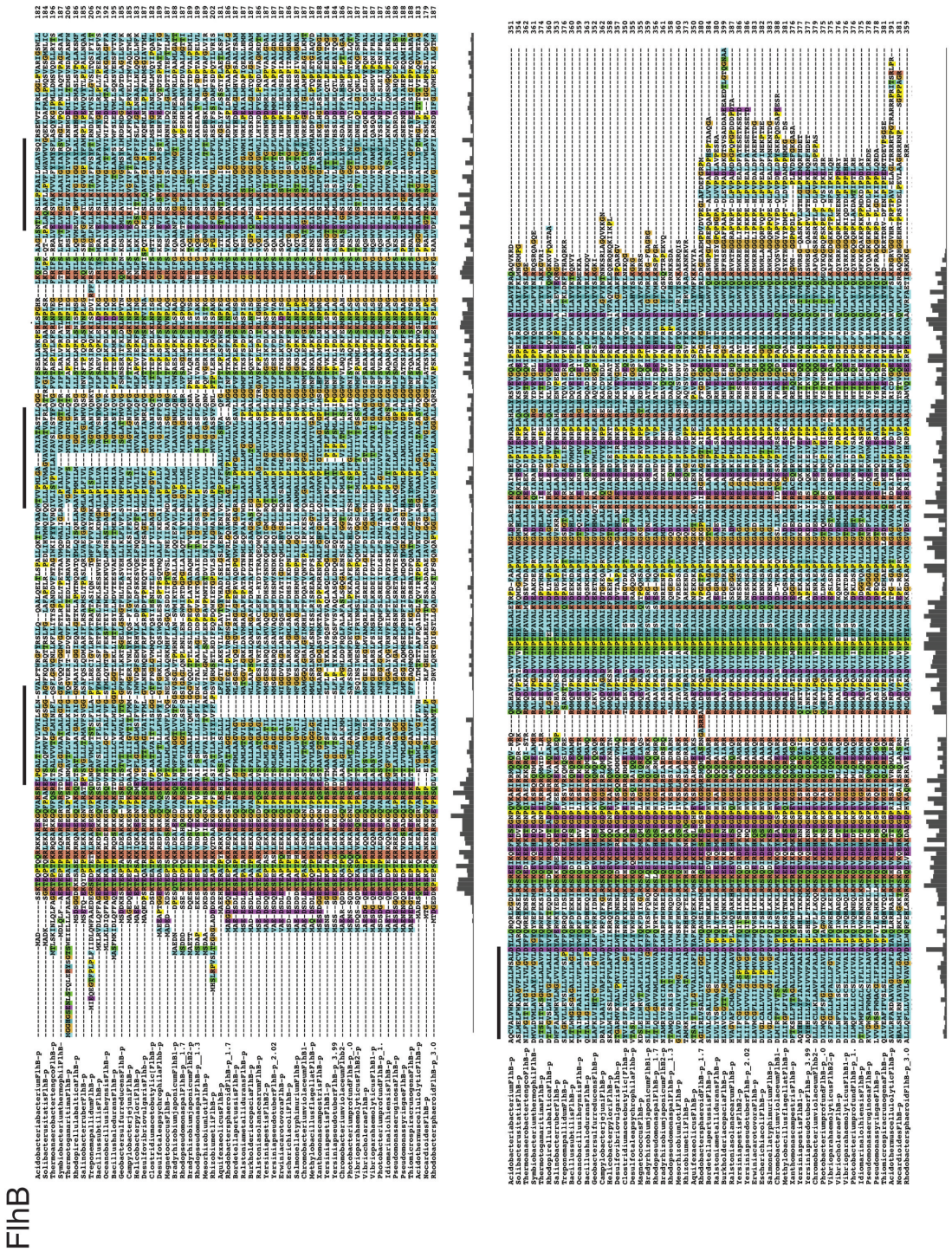

FIGURE 3.14

Sequence alignment for the flagellar export apparatus component FlhB. Predicted TM segments are indicated by lines at the top of the alignments. Conservation scores are shown below.

4

The Role of the FliK Molecular Ruler in Hook-length Control in *Salmonella enterica*

Marc Erhardt[1, †], Takanori Hirano[1, †], Yichu Su[1], Koushik Paul[1], Daniel H. Wee[1], Shino Mizuno[2], Shin-Ichi Aizawa[2], Kelly T. Hughes[1, *]

Molecular Microbiology (2010) vol. 75 (5) pp. 1272-1284

[1]Department of Biology, University of Utah, Salt Lake City, UT 84112, USA
[†]These authors contributed equally to this work
[2]Department of Life Sciences, Prefectural University of Hiroshima, 562 Nanatsuka, Shobara, Hiroshima 727-0023, Japan
[*]Corresponding author; Kelly T. Hughes; Mailing address: Department of Biology, University of Utah, 257 South 1400 East, Salt Lake City, UT, 84112; Tel: +801-587-3367; Fax: +801-585-9735; E-mail: hughes@biology.utah.edu

4.1 Abstract

A molecular ruler, FliK, controls the length of the flagellar hook. FliK measures hook length and catalyzes the secretion-substrate specificity switch from rod-hook substrate specificity to late substrate secretion, which includes the filament subunits. Here, we show normal hook-length control and filament assembly in the complete absence of the C-ring thus refuting the previous 'cup' model for hook-length control. Mutants of C-ring components, which are reported to produce short hooks, show a reduced rate of hook-basal-body assembly thereby allowing for a premature secretion-substrate specificity switch. Unlike *fliK* null mutants, hook-length control in an autocleavage-defective mutant of *flhB*, the protein responsible for the switch to late-substrate secretion, is completely abolished. FliK deletion variants that retain the ability to measure hook length are secreted thus demonstrating that FliK directly measures rod-hook length during the secretion process. Finally, we present a unifying model accounting for all published data on hook-length control in which FliK acts as a molecular ruler that takes measurements of rod-hook length while being intermittently secreted during the assembly process of the hook-basal-body complex.

4.2 Introduction

In order to propel themselves in their living environments towards nutrients, bacteria, such as *Escherichia coli* and *Salmonella enterica*, have developed a sophisticated ion-powered rotary machine called the flagellum (91). The bacterial flagellum extends from the cytoplasm to the cell exterior and is made from about 25 different proteins each in multiple copies from a few to many thousands (115). The flagellum is a motor organelle that includes a protein secretion apparatus, which is a member of the type III family of bacterial secretion systems (117).

Typically, the bacterial flagellum is composed of three main structures: an engine, a propeller and a universal joint that connects them (Figure 4.1) (18). The engine, or basal body, includes a rotor and stator embedded in the cytoplasmic membrane, a rod that acts as a drive-shaft and extends from the rotor through the peptidoglycan to the outer membrane; a bushing-like complex that assembles around the distal rod forming a pore in the outer membrane (116). The propeller is a long helical filament composed of up to 20,000 subunits of a single protein capped by a scaffold that permits the folding and polymerization of secreted filament subunits as they reach the tip of the structure following secretion (209). The universal joint, also known as the hook, allows for the transmission of torque energy generated at the cytoplasmic rotor to rotational energy of the external filament (166).

The three structures that comprise the axial component of the flagellum, the rod, the hook and the filament, are all capable of continuous polymerization. However, each is under a different length control mechanism (27). The rod extends from the cytoplasmic membrane through the outer membrane, a distance of about 22 nm, the hook extends from the surface of the cell 55 nm and the filament extends about 10 microns from the hook or about 10 times the length of the cell. Filament growth decreases exponentially with length suggesting that terminal filament length is determined by hindered diffusion, so after about 10 microns in length subunits are no longer able to diffuse out to the filament tip. Recent evidence suggests that terminal rod length occurs by a stacking mechanism that allows distal rod subunits to polymerize onto identical protein subunits only once (28). Hook-length has been reported to rely on multiple factors including molecular cups, clocks and rulers (48, 120, 141, 145, 172).

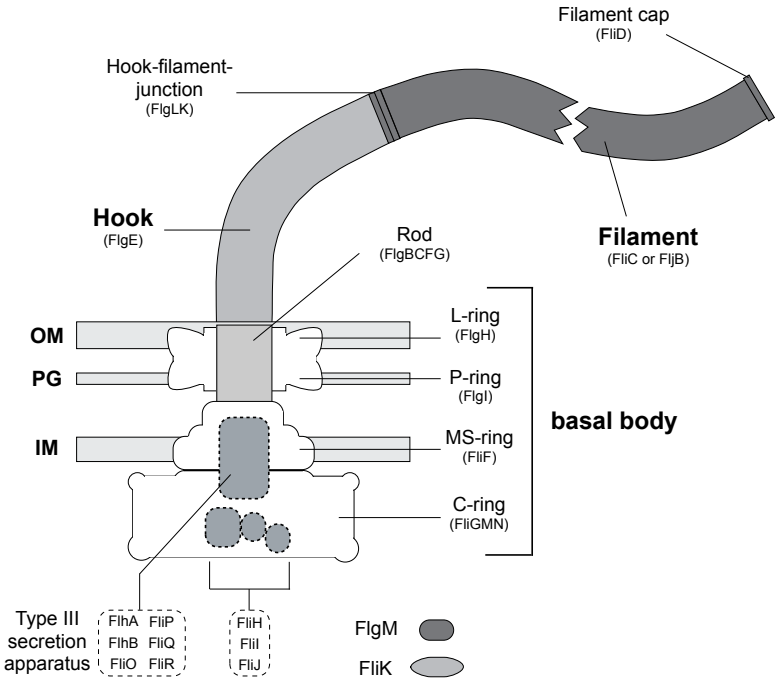

FIGURE 4.1

Schematic overview of the bacterial flagellum. The structure of the flagellum can be divided in three parts: 1) a basal body consisting of the MS-ring in the inner membrane (IM), the cytoplasmic C-ring, the P-ring in the peptidoglycan layer (PG), the L-ring in the outer membrane (OM), the rod spanning the periplasmic space and the type III secretion apparatus assembled within the MS-ring in the inner membrane; 2) a flexible hook with hook-associated proteins; 3) the rigid filament and the filament cap. Dashed boxes indicate proteins that function in flagellar type III secretion, either in the membrane-bound part of the secretion apparatus or in delivery and unfolding of the secretion substrate. Flagellar components that depend on export are indicated in light gray (early substrates) or dark gray (late substrates). Export-dependent components are structural proteins that form the rod, hook, and filament, the negative regulator of late substrate gene expression, FlgM, and the hook-length regulator FliK.

Loss of hook-length control was first observed in strains defective in the *fliK* gene (157). The absence of a functional FliK protein produces hooks with a wide length distribution up to about a micron in length, called polyhooks. A measurement of the distribution of hook-lengths in the polyhook mutant showed that the population of lengths peaked at near wild-type length followed by a tail of increasing size and decreasing numbers (95). This hook-length distribution study suggested that a mechanism is in place, in the absence of FliK, to ensure that most hooks are of the wildtype length and that inclusion of FliK added another layer of regulation to control hook length by preventing the polyhook structures from forming.

Ultimately, hook length is controlled at the level of substrate secretion. Upon formation of the flagellar type III secretion (T3S) apparatus at the cytoplasmic base of the basal structure, secretion is specific for rod and hook subunits. The hook-basal-body (HBB) is complete when the hook reaches 55 nm (67). At this point in the assembly process, an interaction between FliK and an integral membrane component of the flagellar T3S system, FlhB, results in a change in secretion substrate specificity from rod-hook subunits to late secretion substrates (48, 104, 130, 137, 201). Late secretion substrates include the hook-filament junction proteins and the filament cap, historically referred to as hook-associated proteins (HAPs), the filament proteins, FliC or FljB, and a transcriptional inhibitor FlgM.

In addition to interaction with FliK, FlhB also undergoes an autocleavage event with a 5 minutes half-life *in vitro* (137). The 383 amino acid protein FlhB is composed of a 211 amino acid, membrane-embedded N-terminal domain followed by a 172 amino acid cytoplasmic C-terminal domain (132). Cleavage of the C-terminal cytoplasmic domain of FlhB between amino acid residues N269 and P270 in addition to interaction with FliK is required for the secretion-specificity switch to occur. Mutants of amino acid residues N269 and P270 thus remain in rod-hook-type secretion mode. In the *fliK* null background, hook growth is fast, starting at 40 nm/min slowing until wild-type hook length of 55 nm is achieved and followed by a steady growth rate of 8 nm/min (95).

The fundamental problem has been to determine how FliK measures a hook length of 55 nm beyond the cell surface and then interact with FlhB in the inner, cytoplasmic membrane to flip the secretion specificity switch. Initially, the possibility that FliK acted as a molecular ruler was argued against because deletions of the FliK protein resulted in long, polyhook structures rather than shorter hook structures (84). Later, a cup model was proposed suggesting that the components that make up the flagellar rotor, FliG, FliM and FliN act as a measuring cup (120). Electron micrograph pictures show that these proteins make a cup-like structure, called the C-ring at the base of the flagellum (188). It was proposed that the C-ring fills with a cup-full of hook subunits, which upon emptying the cup results in hooks of proper size and exposure of the cytoplasmic component of FlhB to interact with FliK. This model was based on the observation that mutants in *fliG*, *fliM*, and *fliN* produce shorter hook structures (120). However, the dimension of the C-ring suggests that it has the capacity to contain at most 50 of the 130 hook subunits required (27).

Evidence has now accumulated to support a molecular ruler model that was originally discarded. The FliK ruler model was revised based on findings in the *Yersinia enterocol-*

itica virulence-associated type III system (78). Virulence-associated T3S systems utilize needle-like structures, which resemble flagellar hook-basal-bodies, to secrete virulence determinants into host cells (32, 56). A FliK functional homolog, YscP, functions to control needle length. Secretion of YscP through the needle structure is necessary for its function (4). Loss of YscP resulted in needles of uncontrolled growth and insertions and deletions of YscP resulted in needle lengths that directly corresponded to the length of YscP. Recently, a study by Wagner et al. (194) further supports the ruler model by modeling the structure of YscP. The authors showed that functional YscP likely has a helical structure. Based on the results with YscP, insertions and deletions in FliK were constructed and resulted in longer and shorter hooks, respectively, that directly corresponded to the increase or decrease in FliK length (172).

FliK is secreted through the flagellar basal structure as a rod-hook substrate even though it is not incorporated into the flagellar structure (131). Recently, it has been shown that an interaction between FliK and the hook proteins are needed for an efficient secretion specificity switch. It has been suggested that a temporary interaction of FliK with the hook subunits, within the secretion channel during FliK secretion, resulted in a pause in FliK secretion. That pause would allow for interaction of the C-terminal domain of FliK with FlhB thereby catalyzing the secretion specificity switch (139). In addition, a strong interaction was reported between the N-terminus of FliK and the hook capping protein FlgD. It was proposed that after FliK was secreted, the N-terminus would interact with the hook cap pulling FliK into the secretion channel as the hook elongated until the C-terminus of FliK was in vicinity of FlhB at the base to catalyze the secretion-specificity switch (141). However, the secretion channel is too narrow to allow secreted hook subunits to pass by a FliK molecule that is maintained within the channel. The average width of an α-helix is about 1 nm and the inner diameter of the filament has been shown to be 2.0 nm (209), whereas the inner diameter of the hook channel is even smaller (171). In the *Yersinia* needle case, the YscP ruler is estimated to have a maximum width of 1.3 nm (194). Thus, the retention of a ruler while subunits pass by would be physically improbable in both the *Yersinia* needle-length and flagellar hook-length control systems.

In this work, we present data that FliK is a molecular ruler that directly measures hook length in a temporal manner. We present a model proposing that intermittent FliK secretion during hook polymerization results in temporal measurements of hook length to produce the wild-type spectrum of hooks that range from 35 - 75 nm peaking at 55 nm (67).

4.3 Results

4.3.1 Hook-filament assembly in the absence of the C-ring

Here, we address the assembly of hook-filament structures *in vivo* in the complete absence of the C-ring. In order to facilitate type III-dependent secretion and maximize late substrate concentrations, we combined an F_OF_1 ATP synthase mutant to increase the proton-motive force as described previously (158), and additionally *flgM* null as well as *flhD** promoter-up mutations. The removal of the negative regulator of late substrate gene expression, FlgM, and the promoter-up mutation of *flhD* promoter both increase availability of flagellar secretion substrates (M. Erhardt, T. Hirano, K.T. Hughes, unpublished results).

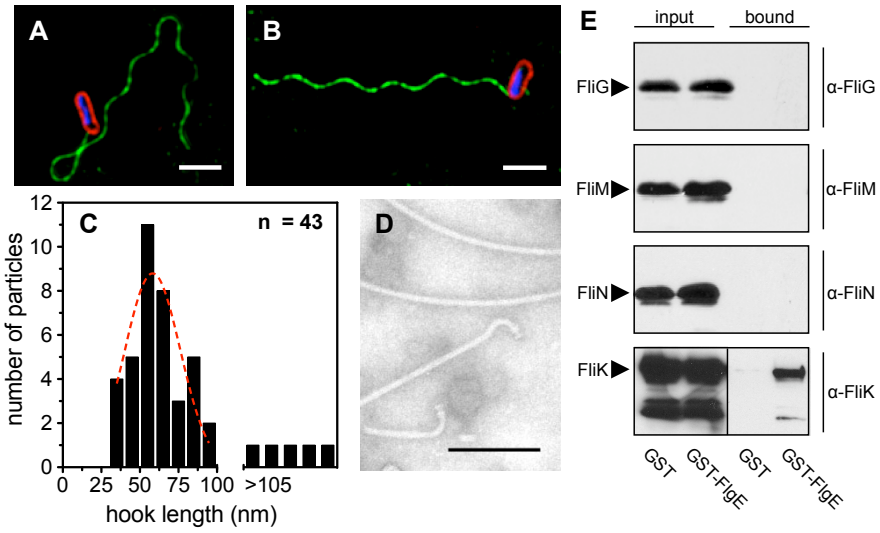

FIGURE 4.2

Filament assembly and hook length in the absence of the C-ring. Interaction of C-ring subunits with the hook. (A + B) Fluorescent microscopy of C-ring null mutants (Δ*fliG*) that assemble one, unusual long flagellum under excess secretion substrate conditions (Δ*flgM*, P_{flhD^*}) and increased proton motive force (Δ*atpA*). Filament was detected by anti-FliC polyclonal antibodies (rabbit) and stained using anti-rabbit Alexa Fluor^{488} (green), membranes were stained using FM-64 (red) and DNA was stained using DAPI (blue). Scale bar = 2 µm. Staining of wild type cells is shown in Figure 4.3. (C) Hook-length peaks around 58 nm in the absence of the C-ring. Hook-length distribution in the C-ring null mutant that assembles filaments (Δ*fliG* Δ*flgM*, P_{flhD} Δ*atpA*) as measured by electron microscopy. Overall hook length is not completely controlled (71 ± 26 nm, n = 43), but peaks around wildtype 55 nm hook length. Non-linear fitting of the Gaussian distribution was employed for hook-lengths below 100 nm (dashed red line) and the mean hook-length of the majority of hooks is 58 ±18 nm (n = 38) compared to 55 ± 6 nm of the wildtype (67). (D) Electron-microscopic images of hooks and filaments isolated from the C-ring null mutant (Δ*fliG* Δ*flgM*, P_{flhD^*} Δ*atpA*). Scale bar = 200 nm. (E) C-ring subunits do not interact with the hook. The interaction of the C-ring with the hook subunit FlgE was assayed using GST-pulldown assay and immunoblotting using specific antibodies against the C-ring subunits FliG, FliM and FliN, as well as FliK respectively. As a control, the previously reported interaction of FlgE with FliK was tested (145).

We analyzed those mutants lacking components of the C-ring (Δ*fliG* or Δ*fliGMN*) by fluorescent microscopy and found that in the absence of the ATP synthase a significant fraction of the analyzed cells assemble flagella (Figure 4.2A+B). It is of interest that almost all analyzed mutant cells possessed only one, unusually long flagellum despite the probable presence of multiple hook-basal-body structures within each cell. This would indicate a possible mechanism of preferentially localized secretion of flagellar components. However, due to the preparation and staining procedures involved in visualizing flagella for fluorescent microscopy, we are unable to quantify the exact fraction of cells producing flagella. The flagella are sheared easily during the slide preparation and therefore most of the flagella are not attached to cells anymore. It also seems possible that the long flagella on the mutant cells are more sensitive to shearing than those on wild-type cells.

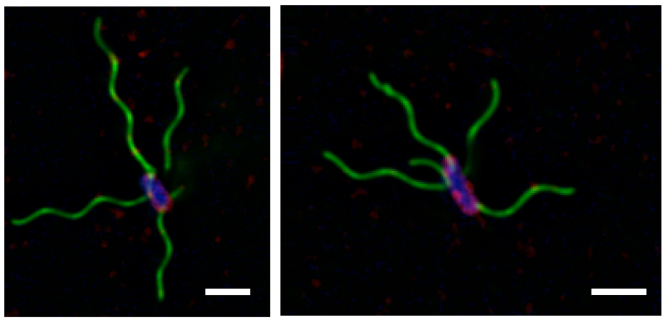

FIGURE 4.3
Fluorescent microscopy of flagellar filaments of wildtype *Salmonella enterica* LT2. Filament was detected by anti-FliC polyclonal antibodies (rabbit) and stained using anti-rabbit Alexa Fluor^{488} (green), membranes were stained using FM-64 (red) and DNA was stained using DAPI (blue). Scale bar = 2 µm.

Additionally, we measured the hook-length in mutants lacking the C-ring and found a hook-length distribution with a mean of about 71 ± 26 nm and a peak at the wild-type length of 55 nm (Figure 4.2C+D). We employed non-linear fitting of the Gaussian distribution for hooks of lengths below 100 nm corresponding to 88% of the total analyzed hooks (Figure 4.2C, dashed red line). Accordingly, the average hook-length of the majority of hooks in the C-ring deletion mutant is 58 ± 18 nm, closely following the average hook-length of 55 ± 6 nm of the wildtype (67).

By utilizing the combination of Δ*atpA*, Δ*flgM* and P_{flhD^*}, the capability of the cell for type III secretion is increased substantially by both excess substrates and energy. This is consistent with our recent finding where we screened for transposon insertions that allowed for type III secretion in the complete absence of the C-ring. We found that any condition that increased levels of the flagellar master regulatory proteins, FlhDC, bypassed the C-ring requirement in flagellar type III secretion (44). Accordingly, we conclude that the C-ring is not essential for flagellar type III secretion under excess secretion substrate conditions. This conclusion is also supported by the fact that we primarily observed unusually long filaments (Figure 4.2A+B), which indicates that the

secretion process *per se* is not impaired. Hook-length, however, seems to be only partially controlled in the C-ring null mutant. If the C-ring acts under wildtype conditions as an affinity cup-like structure for secreted substrates, then we would presume that in the C-ring deletion mutant, targeting of secreted proteins is impaired. Thus, secretion of proteins is now only dependent on their concentration and an increase in the ratio of FlgE to FliK subunits secreted during hook growth would account for the longer hook structures observed in the absence of the C-ring. Less secreted FliK molecules during hook elongation will result in longer hooks because of fewer measurements.

4.3.2 C-ring subunits do not interact with the hook subunit FlgE.

A prediction of the C-ring cup model is that the FliG, FliM and FliN subunits that make up the C-ring structure interact with FlgE subunits. We tested for possible interactions between purified GST-FlgE and purified FliG, FliM and FliN proteins using standard pull-down assays. Importantly, the FliG, FliM and FliN constructs used here are able to fully complement respective *fliG*, *fliM* and *fliN* deletion strains (Figure 4.4). As a positive control, FliK, which was previously shown to interact with FlgE *in vitro* (145), was also tested. As shown in Figure 4.2E, GST-FlgE did interact with FliK, but not with FliG, FliM or FliN. Thus, if FlgE interacts with the C-ring proteins *in vivo*, then it is likely to interact only after these proteins are assembled into the C-ring. Alternatively, these results suggest an alternative model in which the *fliG*, *fliM*, and *fliN* mutants produce short hooks by a mechanism distinct from the measuring cup model.

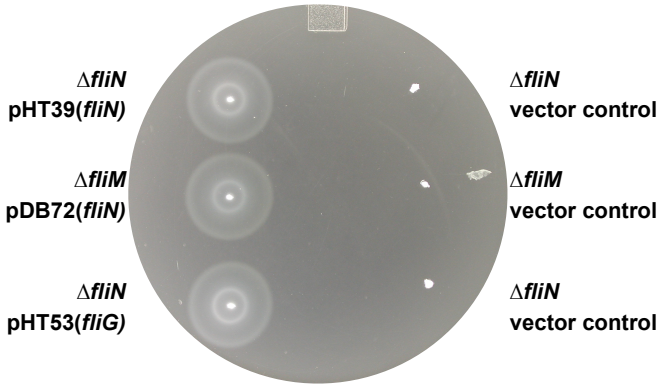

FIGURE 4.4
Complementation assay of a Δ*fliG*, Δ*fliM* and Δ*fliN* deletion strains. Strains were complemented with IPTG-inductible plasmids expressing *fliG*, *fliM* and *fliN* used for the GST-pulldown experiments. The complementation was performed in the presence of 40 µM IPTG and the plate was incubated at 32 ℃ for 7 hours.

These results are consistent with recently published data showing that the formation of filaments in mutants partially deleted for the C-ring occurred under conditions where the flagellar type III secretion system-specific ATPase FliI was overproduced (94). Recently, the C-ring was shown to act as an affinity cup-like structure that is not essential to

the secretion process, but does facilitate secretion. The C-ring appears to increase the efficiency of the secretion process by locally increasing secretion substrate concentrations prior to secretion or preventing non-substrates interactions with the type III secretion apparatus (44). Together, these results refute the measuring cup model and support a temporal, molecular ruler model of hook-length determination as described below.

4.3.3 C-ring mutants producing short hooks are defective in HBB assembly.

A clue to explain how mutants in the C-ring structural genes *fliG*, *fliM*, and *fliN*, could affect hook length came with the discovery of a polymerization-defective hook mutant that also produced shorter hook structures (145). This led to the idea that once hook formation was initiated, a molecular clock prevented or slowed hook elongation after a given amount of time. The molecular clock may result from the FlhB autocleavage event (48, 137). The FlhB protein was shown to undergo autocleavage with a 5 min half-life. A FlhB mutant protein that is defective in autocleavage stays in the rod-hook secretion mode. Thus, the cleavage of FlhB is required to switch to the late secretion mode. It is therefore possible that FlhB autocleavage might result in an inability or reduced ability to secrete hook subunits as proposed by Moriya et al. (145).

Thus, we decided to assay whether C-ring mutants in the *fliG*, *fliM* or *fliN* genes are slow to assemble HBB structures because they are defective in HBB assembly. We analyzed i) temporal secretion deficiencies of the C-ring mutants by determining the necessary time for induction of the *motA* promoter, which indicates completion of the HBB complex, and ii) additionally deficiencies in cumulative secretion by determining ampicillin resistance conferred by secreted FlgE-Bla fusion protein. Previously, we have shown that we could synchronize the flagellar assembly pathway by placing the flagellar master control operon under a tetracycline-inducible promoter (80). Upon HBB completion, an inhibitor of late flagellin gene expression, FlgM, which is also a flagellar late secretion substrate, is secreted from the cell. Secretion of FlgM, releases a transcription factor (σ^{28}) that is specific for transcription of the flagellin genes, *fliC* or *fljB*, the genes encoding the motor force generators (flagellar stator complex), *motA* and *motB*, and the genes of the chemosensory response system.

To monitor the time for completion of HBB structures upon induction of the flagellar master operon, we used a fusion of the *motA* promoter to the luciferase operon, *luxCDABE* of *Photorhabdus luminescens* (61) in a strain with the flagellar master operon under tetracycline (Tc) control (80). As shown in Figure 4.5, we determined a half-maximal induction time of 82 $\pm$ 3.5 minutes for the *motA* promoter by non-linear regression analysis, which was consistent with half-maximal P_{motA} induction times reported in an earlier study (24). Importantly, in a previously described hook polymerization-defective mutant the half-maximal P_{motA} induction time was greatly increased to 106 $\pm$ 3.0 minutes (Figure 4.5D). Thus, variation in the time it takes for HBB completion is readily observed in our assay system.

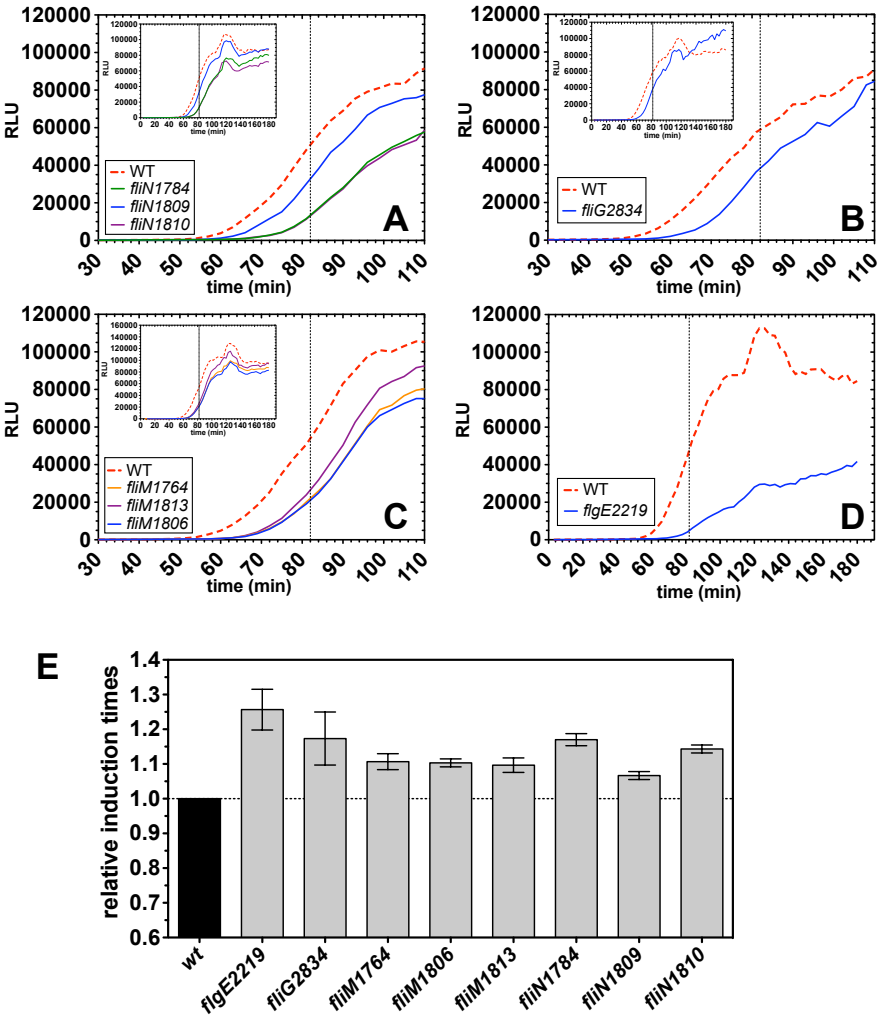

FIGURE 4.5

Time for hook-basal-body completion is prolonged in short-hook mutants. (A-D) Dynamic comparison of *motA* promoter induction times in (A) *fliN1784*, *fliN1809*, *fliN1810*, (B) *fliG2834*, (C) *fliM1764*, *fliM1806*, *fliM1813* and (D) *flgE2219*$_{\text{T149N}}$ short-hooks producing mutants. *flgE2219*$_{\text{T149N}}$ is defective in hook-polymerization (145). Completion of hook-basal bodies (= corresponds to induction of the *motA* promoter) was monitored over time following the induction of flagellar gene expression as described in Experimental procedures. The dashed line at 82 min indicates the calculated half-maximal *motA* induction time of the wildtype control. Dashed red line = wildtype control, RLU = relative light units. Data shown are the average of at least three independent, biological replicates. (E) Relative *motA* half-maximal promoter induction times of the first class of short-hooks producing mutants. Half-maximal *motA* promoter induction times were calculated using the incomplete γ function as described in Experimental procedures and normalized against the wildtype control. Data shown are mean ± SD.

TABLE 4.1

Class I C-ring mutants producing short hooks.

Summary of the properties of the first class of C-ring mutants *fliG2834*, *fliM1764*, *fliM1806*, *fliM1813*, *fliN1784*, *fliN1809*, *fliN1810* and the polymerization-deficient mutant *flgE2219*(T149N). Mutation sites of the mutants were confirmed by sequencing and hook lengths were taken from (67) or (120). The ability of the mutants to secrete FlgE-Bla was assayed as described in Experimental procedures and is reported as the minimal-inhibitory concentration of ampicillin (µg/ml). Half-maximal induction times ± SD of the *motA* promoter indicate hook-basal-body completion and were compared to the wildtype (82 ± 3.5 min) as described below. The half-maximal P_{motA} induction times of the analyzed C-ring mutants were significantly different compared to the wildtype control (P value < 0.01). One-step ANOVA with Dunett's post test was employed to compare statistical significances to the wildtype control. SD = standard deviation.

gene	**allele**	**mutation**	**reported hook length (nm)**	**MIC (amp µg/ml)**	Half-maximal P_{motA} induction time (min)
WT	-	-	55 ± 6	>400	82 ± 3.5
fliG	*fliG2834*	R160H	44 ± 7	400	90 ± 2.5
fliM	*fliM1764*	F131L	46 ± 4	200	92 ± 1.3
	fliM1806	G133D	45 ± 5	200	92 ± 0.5
	fliM1813	H106P	42 ± 7	200	91 ± 1.4
fliN	*fliN1784*	G103V	47 ± 7	400	96 ± 1.2
	fliN1809	L78Q	44 ± 6	400	88 ± 0.8
	fliN1810	N24(Δ1bp)	46 ± 5	200	94 ± 1.6
flgE	*flgE2219*	T149N	45 ± 10	n.d.	106 ± 3.0

We analyzed the half-maximal P_{motA} induction times for various C-ring mutants (120) and found two different classes of mutants based on the time for HBB completion, hook length, and secretion of FlgE-Bla, respectively (Table 4.1). The first class of C-ring mutants displayed significantly longer half-maximal P_{motA} induction times compared to the wildtype. Similarly to the hook polymerization-defective mutant $FlgE^{T149N}$, the hook-length of the class I C-ring mutants has previously been measured by Makishima et al. (120) to be only slightly shorter than the wildtype (45 nm compared to 55 nm). We additionally determined if the class I C-ring mutants have impaired secretion by analyzing secretion of an FlgE-Bla fusion protein. The β-lactamase protein (Bla) must be secreted into the periplasm to confer resistance to ampicillin (Ap^R). In a strain deleted for the flagellar proximal rod genes *flgB* and *flgC*, the FlgE-Bla fusion is secreted into the periplasm and the cells are Ap^R (108). By measuring the minimal inhibitory concentration (MIC) to ampicillin, one can determine the amount of FlgE-Bla secretion into the periplasm for the short-hook, C-ring mutants as compared to a wild-type C-ring

strain (Table 4.1 and Table 4.2). Compared to the wildtype (MIC >400 µg/ml) we found that four of seven of the first class of C-ring mutants indeed showed severely impaired secretion as judged by a low MIC of 200 µg/ml, whereas the remaining three mutants displayed a lower MIC of 400 µg/ml (Table 4.1).

The second class of C-ring mutants displayed no significant difference in P_{motA} induction times and additionally no significantly impaired FlgE-Bla secretion (Table 4.2). However, this class of C-ring mutants is reported to have very short hooks with an average length of 25 nm (120). Importantly, a re-examination of the hook-length of several of the class II C-ring mutants revealed no significant difference in hook length compared to wildtype (N. Moriya, T. Minamino and K. Namba, unpublished results). As shown in Figure 4.6, we analyzed hook length of the *fliM1813* allele (Class I mutant based on P_{motA} induction time; reported hook length 42 ± 7 nm (120)) and the *fliM2309* allele (Class II mutant based on P_{motA} induction time; reported hook length 26 ± 6 nm (120)) and found a hook length of 45 ± 9 nm in case of *fliM1813* and 51 ± 5 nm in case of *fliM2309*. Accordingly, we presume that the originally described short-hooks, class II C-ring mutants are unstable and accumulated secondary mutations that restored normal hook-length control.

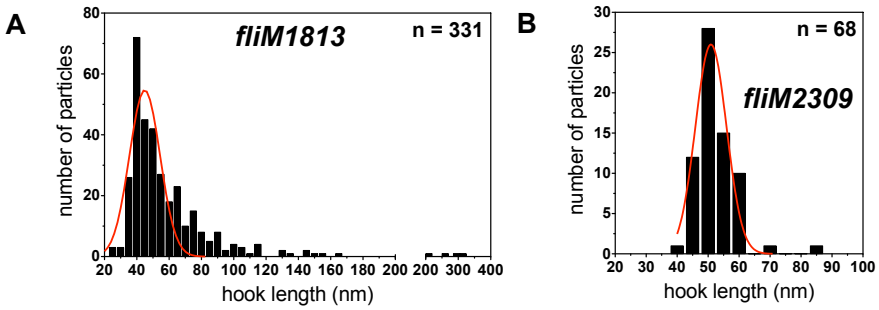

FIGURE 4.6

Re-examination of hook lengths of C-ring mutants. (A) Hook-length distribution of the *fliM1813* allele. Non-linear regression of the Gaussian distribution revealed an average hook-length of 45 ± 9 nm. The hook length of the *fliM1813* mutation was reported to be 42 ± 7 nm (120). (B) Hook-length distribution of the *fliM2309* allele. Non-linear regression of the Gaussian distribution revealed an average hook-length of 51 ± 5 nm. The hook length of the *fliM2309* mutation was reported to be 26 ± 6 nm (120).

TABLE 4.2

Class II of short-hooks producing mutants.

Summary of properties of the second class of C-ring mutants *fliG2323*, *fliG2325*, *fliG2332*, *fliG2826*, *fliM1804*, *fliM1814*, *fliM2293*, *fliM2299*, *fliM2308*, *fliM2309*, *fliM2310*, *fliM2311*, *fliM2312*, *fliN1765* and *fliN2287*. Mutation sites of the mutants were confirmed by sequencing and hook-lengths are taken from (67) and (120). The ability of the mutants to secrete FlgE-Bla was assayed as described in Experimental procedures and is reported as the minimal-inhibitory concentration of ampicillin (µg/ml). Half-maximal induction times of the *motA* promoter indicate hook-basal-body completion and are compared to the wildtype (82 ± 3.5 min). One-step ANOVA with Dunett's post test was employed to compare statistical significances to the wildtype control. SD = standard deviation.

gene	**allele**	**mutation**	**reported hook length (nm)**	**MIC (amp µg/ml)**	Half-maximal P_{motA} induction time (min)	P value of P_{motA} induction times compared to WT
WT	-	-	55	>400	82 ±3.5	-
fliG	*fliG2323*	V135L	26.4	400	83 ± 7.1	$P > 0.05$
	fliG2325	V135F	26.8	400	79 ± 4.8	$P > 0.05$
	fliG2332	G185D	43.1	400	78 ± 2.8	$P > 0.05$
	fliG2826	Δaa282-287	28.5	400	81 ± 0.3	$P > 0.05$
fliM	*fliM1804*	L250P	26.5	400	88 ± 0.7	$P < 0.05$
	fliM1814	T147I	28.1	400	94 ± 2.5	$P < 0.01$
	fliM2293	G143C	23.3	400	80 ± 1.6	$P > 0.05$
	fliM2299	R60C	24.7	400	88 ± 2.6	$P < 0.05$
	fliM2308	E59K	24.1	400	88 ± 1.5	$P < 0.05$
	fliM2309	R63C	25.9	400	85 ± 0.6	$P > 0.05$
	fliM2310	R181L	27.1	400	87 ± 1.2	$P > 0.05$
	fliM2311	R181S	26.8	400	88 ± 3.1	$P < 0.05$
	fliM2312	R181C	24.6	400	84 ± 1.0	$P > 0.05$
fliN	*fliN1765*	L105Q	27.1	400	88 ± 1.8	$P < 0.01$
	fliN2287	G94C	23.4	400	81 ± 2.8	$P > 0.05$

In summary, the class I C-ring mutants took longer to build the HBB and produced shorter hooks because the mutants displayed a defect in the secretion process. We hypothesized that the incorporation of FlhB into a functional secretion apparatus started a countdown for the FlhB autocleavage event that ultimately resulted in cessation or slow-down of hook-polymerization. Accordingly, the secretion-impaired class I C-ring mutants produced shorter hooks because of inefficient secretion, therefore allowing a premature FlhB autocleavage event. As discussed below, independent from FlhB autocleavage, a change in the ratio of secreted FlgE/FliK molecules would result in shorter hooks. This would be the case e.g. if secretion of hook subunits, but not FliK ruler

molecules, was impaired in the class I C-ring mutants. To test if FlhB autocleavage indeed was responsible for the termination of hook subunits secretion, we next analyzed the hook-length distribution in an autocleavage-defective FlhB mutant.

4.3.4 Hook-length distribution in a *flhB* mutant that is unable to undergo autocleavage.

FliK is generally referred to as the hook-length control protein. Loss of FliK results in polyhook structures (157). However, a hook-length distribution analysis in a *fliK* null strain demonstrated that hook length still peaks at the wild type hook length (95). Furthermore, hook growth was shown to be initially fast followed by an exponential reduction in growth rate up to 55 nm in length after which the hook grows at a constant rate. This result suggests a hook-length control mechanism that controls hook growth up to 55 nm followed by a FliK-dependent inhibition of further hook elongation to prevent the 'long monotonic tail' of extended polyhook structures, which extend up to 1.7 µm on cells missing FliK.

A mechanism to explain the biphasic hook growth rates is based on the autocleavage of FlhB. The secretion specificity switch from rod-hook-type to late-substrates requires a cleavage of the C-terminal cytoplasmic domain of FlhB ($FlhB_{CC}$) and the interaction of this domain with the C-terminus of FliK (130). As with FlhB, the EscU and SpaS homologs of virulence-associated type III secretion systems undergo autocleavage (210). These systems are different in that FlhB undergoes autocleavage with a 5 min half-life after folding, while EscU and SpaS undergo autocleavage immediately after folding. However, in all three systems failure to autocleave prevents the secretion-specificity switch. All systems require both autocleavage followed by a conformational change in their cleaved C-terminal domains to switch to late secretion mode. In the flagellar system, this conformational change in $FlhB_{CC}$ can occur spontaneously at a low frequency, and at higher frequencies in mutant strains, but is believed to be catalyzed efficiently through an interaction between $FlhB_{CC}$ and $FliK_C$.

If the 55 nm peak of hook-length observed in the *fliK* null mutant were due to FlhB autocleavage, then we would not expect the same hook-length distribution in the *flhB* autocleavage mutant. Accordingly, hook length distribution was measured in the *flhB* autocleavage mutant. Figure 4.7A shows the measurements of hook structures in a strain harboring the N269A autocleavage-defective FlhB mutant. This mutant does not show a peak at 55 nm as was shown for the *fliK* null strain and instead gives a broad length distribution of hook structures. Importantly, a Δ*fliK* $flhB_{N269A}$ double mutant also shows no hook length control at wildtype 55 nm, demonstrating that the autocleavage-defective FlhB mutant is dominant over the *fliK* deletion and that hook length control is completely abolished in the absence of FlhB autocleavage (Figure 4.7B). We conclude that upon initiation of HBB assembly, hook secretion stops or is substantially slowed after a certain time. FlhB autocleavage could control hook-length in the absence of FliK, if cleaved FlhB is unable or has a reduced ability to secrete FlgE.

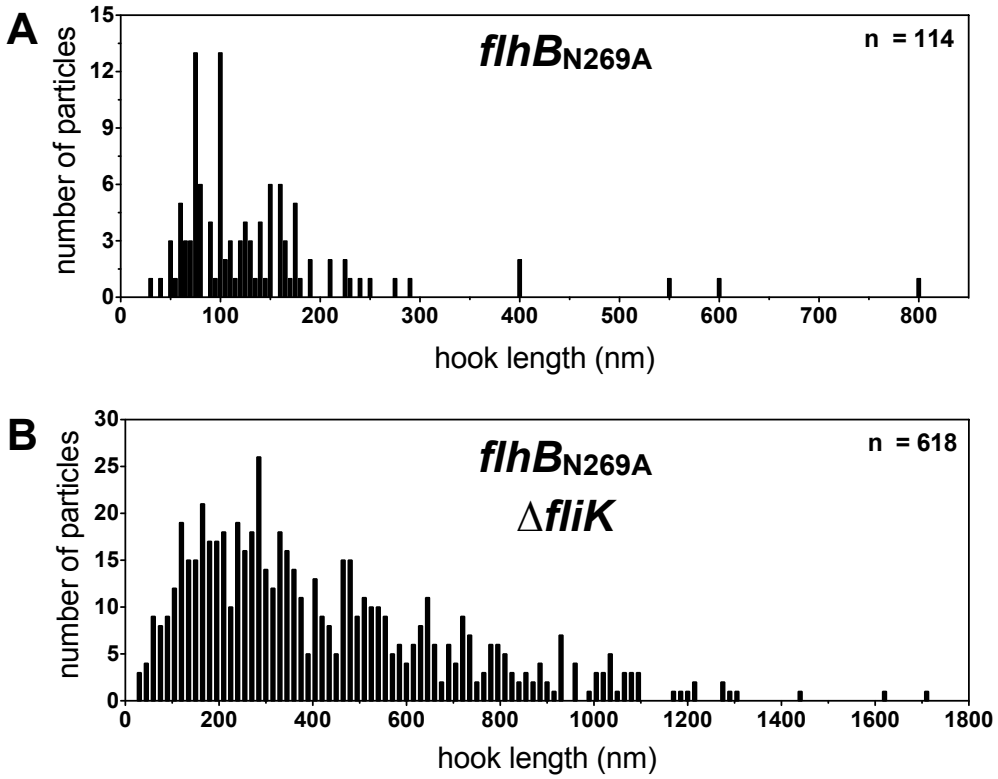

FIGURE 4.7

Hook length is not controlled in an *flhB* mutant defective in autocleavage. (A) Hook-length distribution of the $flhB_{N269A}$ autocleaveage-defective mutant. Hook-length control is completely abolished and does not peak at the wildtype length of 55 nm. (B) Hook-length distribution of the Δ*fliK* $flhB_{N269A}$ double mutant. Hook-length control is completely abolished in the combination mutant and does not peak at the wildtype length of 55 nm compared to the Δ*fliK* deletion mutant (95).

4.3.5 FliK deletion variants that retain hook-length control are secreted.

The *Y. enterocolitica* YscP protein was proposed to act as a molecular ruler that physically measured the distance from the tip of the needle to the cytoplasmic base of the secretion apparatus (78). The *S. enterica* FliK protein was proposed to act as a ruler that could somehow measure the final hook length in the cytoplasm, presumably prior to hook secretion (172). This conclusion was based on the finding that some of the FliK deletion variants retained the ability to measure hook length, but were not found in the external medium. A problem with this interpretation is the fact that the FliK deletions, which were not in the secreted fraction, were also absent in the cellular fraction. This suggests that these variants were simply unstable and not present in sufficient quantities to be readily detected in the external medium. We repeated the secretion experiments using anti-FliK antibodies that are more sensitive than those used in the previous study.

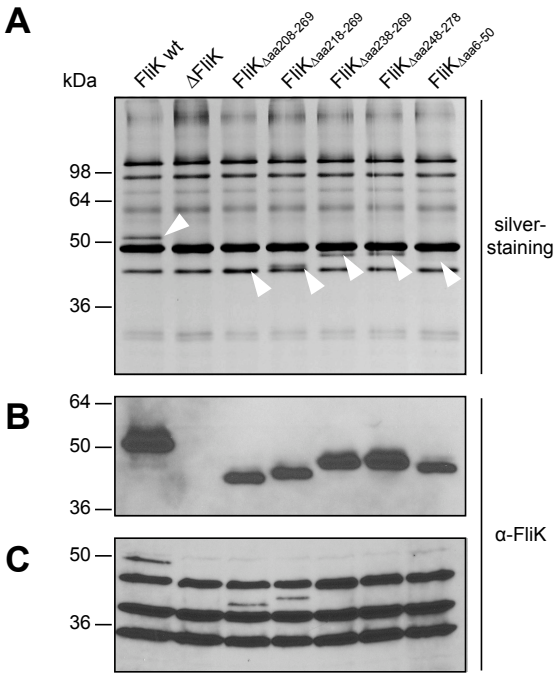

FIGURE 4.8

FliK deletion variants are secreted. FliK truncation mutants that were previously reported to produce short hooks (172) are secreted outside of the cell. A Δ*flgE* deletion mutation was introduced to facilitate FliK secretion. (A) Silver-staining of supernatant fractions. Proteins secreted into the culture supernatant were precipitated by 10% TCA. White arrowheads indicate positions of FliK variants. (B) Anti-FliK immunoblotting of the same culture supernatant fractions as in (A). (C) Anti-FliK immunoblotting of cellular fractions. Non-specific bands are only visible in the cellular fraction and can be used to compare equal loading. Whole cell fractions were disrupted by sonication and mixed with 5x SDS-sample buffer.

As shown in Figure 4.8, the FliK deletion variants were less stable in the cytosolic fraction than wildtype FliK, but in all cases, the FliK deletion variants were secreted

from the cell. Thus, the instability of the FliK deletion variants resulted in reduced amount of protein in the cytoplasm and even less in the secreted fraction, such that they were not detected in the secreted fractions in the previous study. With the improved detection method that includes a more sensitive anti-FliK antibody preparation we were able to detect the FliK truncated proteins, which retained hook-length control, in the secreted fraction. These results refute the internal (cytoplasmic) ruler model.

4.4 Discussion

Previously, several alternative models have been proposed for the mechanism of flagellar hook-length control: i) the measuring tape model (Figure 4.9A), where FliK constantly measures hook length during hook subunit secretion while being attached to the hook cap FlgD (141); ii) the internal ruler model, where FliK somehow measures the final hook length in the cytoplasm (172); iii) the measuring cup model (Figure 4.9B), where the C-ring is filled with FlgE subunits thereby preventing a FliK-FlhB interaction (120); or iv) the molecular clock model (Figure 4.9C), where autocleavage of FlhB is the timing device that switches secretion specificity after a certain time (145). Importantly, all previously proposed models of flagellar hook-length control conflict with published data of hook lengths under conditions where the ratio of secreted FliK to FlgE molecules is changed and thus those models cannot explain the mechanism of flagellar hook-length control sufficiently (see below).

We refute previous models for hook-length control (Figure 4.9A-C) and hereby propose a unifying, new model that accounts for all published data on hook-length control where FliK acts as a molecular ruler taking temporal measurements of rod-hook length throughout the assembly of the external axial component of the HBB (Figure 4.9D), thus providing experimental evidence for a similar model previously proposed for the YscP needle-length control (32). We propose that the ratio of FliK rulers secreted per hook monomers secreted would determine the average hook length. Thus, any situation that results in an increase in FliK measurements per time it takes to complete the HBB will produce shorter hooks and the converse, any situation that results in a decrease in FliK measurements per time it takes to complete the HBB will produce longer hooks.

In this temporal ruler model, FliK acts as a molecular ruler that takes measurements of rod-hook length while being intermittently secreted throughout the assembly process of the HBB complex and the number of secreted FliK ruler molecules per time it takes to complete the HBB defines the ultimate length of the flagellar hook (Figure 4.9D).

Here, we show that this temporal ruler model in conjunction with FlhB autocleavage accounts for the short-hook mutants in *fliG*, *fliM* and *fliN*, the structural genes for the C-ring complex (120), as well as for the polymerization-defective hook mutants (145). Similar to the hook polymerization-defective mutants, we found that one class of the short-hook mutants in *fliG*, *fliM* and *fliN* take longer to build the HBB structure and switch to late secretion specificity. In both the hook polymerization-defective and C-ring mutants, the more frequent FliK measurements per time it takes to complete the HBB result in shorter hooks.

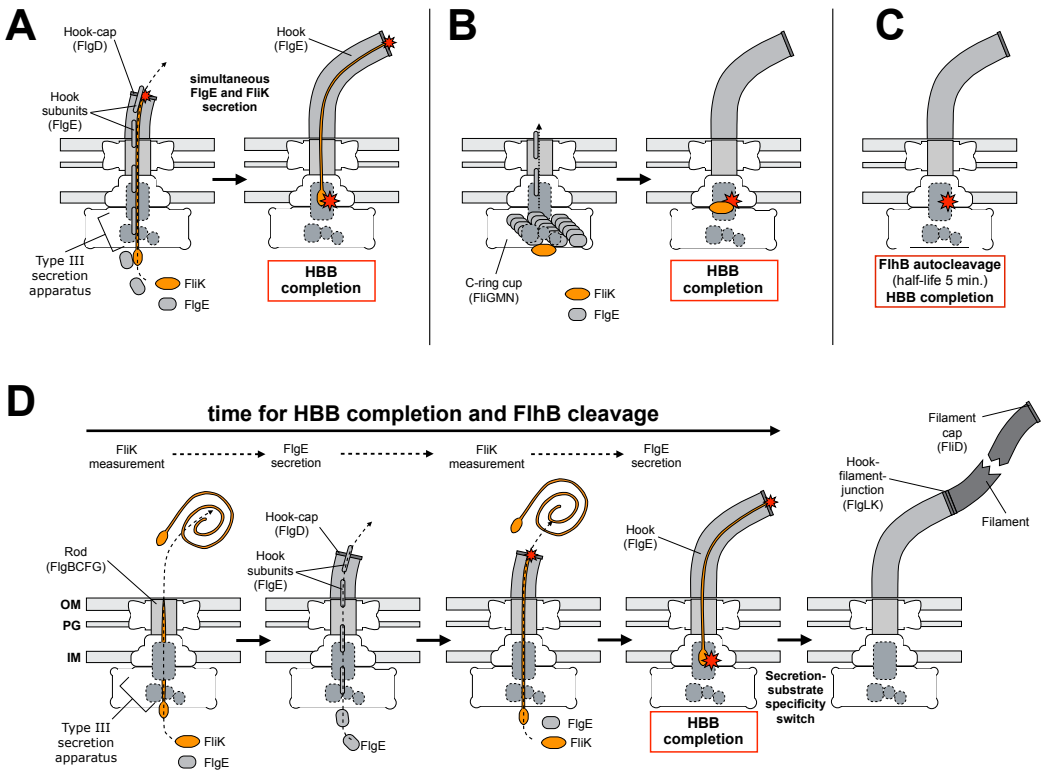

FIGURE 4.9

Comparison of flagellar hook-length control models. (A-C) Previously suggested models for flagellar hook-length control. (A) FliK acts as a measuring tape that constantly measures hook-length during hook subunit secretion while being attached to the hook cap FlgD (141). (B) The C-ring acts as a measuring cup filled with hook subunits that prevent FliK-FlhB interaction prior to hook completion (120). (C) FlhB autocleavage as a molecular clock controlling hook-length in a temporal manner (145). (D) Temporal, molecular ruler model. The molecular ruler FliK and hook subunits FlgE are intermittently secreted during the hook-basal-body assembly process. Accordingly, FliK takes several, independent measurements of rod-hook length in a temporal manner. Interaction of the FliK N-terminus with the hook subunits FlgE and the hook cap FlgD at the end of the growing hook structure results in a pause that enables the C-terminus of FliK to interact with FlhB and thereby catalyzing the secretion specificity switch if the hook has reached the proper length. The red star at the N-terminus of FliK signifies a potential interaction with the hook cap as the N-terminus reaches the exit portal and the red star at the C-terminus of FliK a potential interaction with FlhB that stimulates the secretion-substrate specificity switch. Exported flagellar components are indicated in light gray (early substrates) or dark gray (late substrates). Dashed boxes represent components of the type III secretion apparatus. The hook-length regulator FliK is highlighted in orange. OM = outer membrane; PG = peptidoglycan; IM = inner membrane.

In summary, our model of FliK taking temporal measurements of hook lengths is consistent not only with the FlgE polymerization-defective mutants (145), but also previous findings of effects of over/under-expression of FlgE or over/under-expression of FliK on flagellar hook length (131, 149, 150). It has been reported that over-expression of FlgE or under-expression of FliK resulted in longer hooks (149, 150). These results can be explained with fewer FliK measurements per time it takes to assemble the HBB because of the changed ratio of secreted FliK to secreted FlgE molecules, therefore resulting in longer hooks. On the contrary, under-expression of FlgE or over-expression of FliK produced shorter hooks (149, 150). As it is the case for C-ring mutants or the hook polymerization-defective mutants (145), the under-expression of FlgE or over-expression of FliK changes the ratio of secreted FliK to FlgE molecules in a way that FliK measures hook length more frequently in the time it takes for HBB completion. This produces shorter hooks. Consistently, over-expression of the hook polymerization-defective mutants rescued the short-hook phenotype and resulted in hooks of wildtype length (145). This can be explained with the changed ratio of secreted FliK rulers to over-expressed FlgE mutant subunits. Because the FlgE mutants are defective in polymerization, in this case the over-expression of mutant FlgE produces wildtype hooks because of fewer FliK measurements per time it takes for HBB completion.

4.5 Experimental procedures

Bacterial strains, plasmids and media.

All bacterial strains and plasmids used in this study are listed in Table 4.3. Cells were grown in either lysogeny broth (LB) or TB broth (1% Tryptone and 0.5% NaCl) and, when necessary, supplemented by chloramphenicol (12.5 µg/ml) or tetracycline (15 µg/ml). The generalized transducing phage of *S. typhimurium* P22 HT105/1 *int-201* was used in all transductional crosses (168).

SDS-PAGE and Western blotting.

Whole cell fractions and culture supernatant fractions were prepared by described methods (66). Silver staining of the gel was performed as described (147). Anti-FliK antibodies were kindly provided by Keiichi Namba. Specific protein detection was performed using ECL plus Western blotting detection reagents (Amersham Biosciences).

Minimum Inhibitory Concentration (MIC) assays.

MIC assays to ampicillin were performed as described (108) with a minor modification. Overnight cell cultures were inoculated by a 1/100 dilution into 3 ml of LB and the cells were incubated at 37 ℃ for one hour. To induce P_{fhDC}::T-POP, tetracycline was added at the final concentration of 15 µg/ml and the culture was incubated for an additional hour. The cells were then inoculated 1/50 into 3 ml LB containing different concentrations of ampicillin and the culture was incubated for 4.5 hours. The minimum inhibitory concentration (MIC) was taken as the lowest ampicillin concentration giving an $OD_{595} < 0.05$.

TABLE 4.3
Strains and plasmids used in this study.
All strains and plasmid were constructed for this study if not noted otherwise. n.d., not determined.

Strains/ plasmids	Relevant characteristics	Source/ reference
E. coli		
RP3098	Δ*flhDC* protein expression host for GST pull-down	J.S. Parkinson
Salmonella		
TH437	LT2 Wild-type for motility and chemotaxis	J. Roth
TH5633	pRG19/ *flhDC5451*::TPOP	lab collection
TH8434	Δ*fliK6145*(Δaa6-50)	lab collection
TH9933	Δ*flgD6541*(Δaa2-224)	(108)
TH10333	Δ*fliK6617*(Δaa208-269)	(172)
TH10334	Δ*fliK6618*(Δaa218-269)	(172)
TH10335	Δ*fliK6619*(Δaa238-269)	(172)
TH10338	Δ*fliK6622*(Δaa248-278)	(172)
TH13452	Δ*fliK6140*(Δaa6-405)	
TH13470	Δ*flgE7599*(Δaa6-398)	(65)
TH13763	*flhB7152*(N269A) *fljBenx vh2*	
TH13776	*flhB7152*(N269A) Δ*hin-5717*::FRT Δ*fliK6140*	
TH13927	*fliK*$^+$ Δ*flgE7659*(Δaa6-398)	
TH14117	pRG19/ *flhDC5451*::TPOP *flgE2219*	
TH14118	pRG19/ *flhDC5451*::TPOP *flgE2219* Δ*flK5627*::FCF	
TH14200	Δ*fliK6140*(Δaa6-409) Δ*flgE7659*	
TH14201	Δ*fliK6617*(Δaa208-269) Δ*flgE7659*	
TH14202	Δ*fliK6618*(Δaa218-269) Δ*flgE7659*	
TH14203	Δ*fliK6619*(Δaa238-269) Δ*flgE7659*	
TH14204	Δ*fliK6622*(Δaa248-278) Δ*flgE7659*	
TH14205	Δ*fliK6145*(Δaa6-50) Δ*flgE7659*	
TH14350	*flhDC5451*::TPOP *flgE6569*::*bla* Δ*flgBC6557 fliG2325*	
TH14351	*flhDC5451*::TPOP *flgE6569*::*bla* Δ*flgBC6557 fliG2323*	

Strains/ plasmids	Relevant characteristics	Source/ reference
TH14352	*flhDC5451*::TPOP *flgE6569*::*bla* Δ*flgBC6557 fliN1809*	
TH14353	*flhDC5451*::TPOP *flgE6569*::*bla* Δ*flgBC6557 fliN2287*	
TH14354	*flhDC5451*::TPOP *flgE6569*::*bla* Δ*flgBC6557 fliM1814* Δ*hin-5717::FRT*	
TH14355	*flhDC5451*::TPOP *flgE6569*::*bla* Δ*flgBC6557 fliM2299* Δ*hin-5717::FRT*	
TH14356	*flhDC5451*::TPOP *flgE6569*::*bla* Δ*flgBC6557*	
TH14357	*flhDC5451*::TPOP Δ*flgBC6557*	
TH14406	*flhDC5451*::TPOP *flgE6569*::*bla* Δ*flgBC6557 fliG2332*	
TH14407	*flhDC5451*::TPOP *flgE6569*::*bla* Δ*flgBC6557 fliG2826*	
TH14408	*flhDC5451*::TPOP *flgE6569*::*bla* Δ*flgBC6557 fliG2834*	
TH14409	*flhDC5451*::TPOP *flgE6569*::*bla* Δ*flgBC6557 fliM1764*	
TH14410	*flhDC5451*::TPOP *flgE6569*::*bla* Δ*flgBC6557 fliM1804*	
TH14411	*flhDC5451*::TPOP *flgE6569*::*bla* Δ*flgBC6557 fliM1806*	
TH14412	*flhDC5451*::TPOP *flgE6569*::*bla* Δ*flgBC6557 fliM1813*	
TH14413	*flhDC5451*::TPOP *flgE6569*::*bla* Δ*flgBC6557 fliM2293*	
TH14414	*flhDC5451*::TPOP *flgE6569*::*bla* Δ*flgBC6557 fliM2308*	
TH14415	*flhDC5451*::TPOP *flgE6569*::*bla* Δ*flgBC6557 fliM2309*	
TH14416	*flhDC5451*::TPOP *flgE6569*::*bla* Δ*flgBC6557 fliM2310*	
TH14417	*flhDC5451*::TPOP *flgE6569*::*bla* Δ*flgBC6557 fliM2311*	
TH14418	*flhDC5451*::TPOP *flgE6569*::*bla* Δ*flgBC6557 fliM2322*	
TH14419	*flhDC5451*::TPOP *flgE6569*::*bla* Δ*flgBC6557 fliN1765*	
TH14420	*flhDC5451*::TPOP *flgE6569*::*bla* Δ*flgBC6557 fliN1784*	
TH14421	*flhDC5451*::TPOP *flgE6569*::*bla* Δ*flgBC6557 fliN1810*	
TH14439	Δ*flgD6541 flgE6569*::*bla*	
TH14471	Δ*flgD6541 flgE6569*::*bla fliG2323*(V135F)	
TH14472	Δ*flgD6541 flgE6569*::*bla fliG2325*(V135L)	
TH14473	Δ*flgD6541 flgE6569*::*bla fliG2332*(G185D)	
TH14474	Δ*flgD6541 flgE6569*::*bla fliG2826*(Δaa282 to 287)	
TH14475	Δ*flgD6541 flgE6569*::*bla fliG2834*(R160H)	
TH14476	Δ*flgD6541 flgE6569*::*bla fliM1764*(F131L)	
TH14477	Δ*flgD6541 flgE6569*::*bla fliM1804*(L250P)	
TH14478	Δ*flgD6541 flgE6569*::*bla fliM1806*(G133D)	
TH14479	Δ*flgD6541 flgE6569*::*bla fliM1813*(H106P)	
TH14480	Δ*flgD6541 flgE6569*::*bla fliM1814*(T147I) Δ*hin-5717*::FRT	
TH14481	Δ*flgD6541 flgE6569*::*bla fliM2293*(G143C)	
TH14482	Δ*flgD6541 flgE6569*::*bla fliM2299*(R60C) Δ*hin-5717*::FRT	
TH14483	Δ*flgD6541 flgE6569*::*bla fliM2308*(E59K)	
TH14484	Δ*flgD6541 flgE6569*::*bla fliM2309*(R63C)	
TH14485	Δ*flgD6541 flgE6569*::*bla fliM2310*(R181L)	
TH14486	Δ*flgD6541 flgE6569*::*bla fliM2311*(R181S)	
TH14487	Δ*flgD6541 flgE6569*::*bla fliM2312*(R181C)	
TH14488	Δ*flgD6541 flgE6569*::*bla fliN1765*(L105Q)	
TH14489	Δ*flgD6541 flgE6569*::*bla fliN1784*(G103V)	
TH14490	Δ*flgD6541 flgE6569*::*bla fliN1809*(L78Q)	
TH14491	Δ*flgD6541 flgE6569*::*bla fliN1810*(n.d.)	

Strains/ plasmids	**Relevant characteristics**	**Source/ reference**
TH14492	Δ*flgD6541 flgE6569*::*bla fliN2287*(G94S)	
TH14630	pRG19/ *flhDC5451*::TPOP *fliG2332*	
TH14631	pRG19/ *flhDC5451*::TPOP *fliG2826*	
TH14632	pRG19/ *flhDC5451*::TPOP *fliG2834*	
TH14633	pRG19/ *flhDC5451*::TPOP *fliM1764*	
TH14634	pRG19/ *flhDC5451*::TPOP *fliM1804*	
TH14635	pRG19/ *flhDC5451*::TPOP *fliM1806*	
TH14636	pRG19/ *flhDC5451*::TPOP *fliM1813*	
TH14637	pRG19/ *flhDC5451*::TPOP *fliM2293*	
TH14638	pRG19/ *flhDC5451*::TPOP *fliM2308*	
TH14639	pRG19/ *flhDC5451*::TPOP *fliM2309*	
TH14640	pRG19/ *flhDC5451*::TPOP *fliM2310*	
TH14641	pRG19/ *flhDC5451*::TPOP *fliM2311*	
TH14642	pRG19/ *flhDC5451*::TPOP *fliM2312*	
TH14643	pRG19/ *flhDC5451*::TPOP *fliN1765*	
TH14644	pRG19/ *flhDC5451*::TPOP *fliN1784*	
TH14645	pRG19/ *flhDC5451*::TPOP *fliN1810*	
TH14646	pRG19/ *flhDC5451*::TPOP *fliG2323*	
TH14647	pRG19/ *flhDC5451*::TPOP *fliG2325*	
TH14648	pRG19/ *flhDC5451*::TPOP *fliM1814* Δ*hin-5717*::FRT	
TH14649	pRG19/ *flhDC5451*::TPOP *fliM2299* Δ*hin-5717*::FRT	
TH14650	pRG19/ *flhDC5451*::TPOP *fliN1809*	
TH14651	pRG19/ *flhDC5451*::TPOP *fliN2287*	
TH15292	Δ*flgM5628*::FRT $P_{flhD7460}$ Δ*fliG7356* Δ*atpA*::*tetRA*	
plasmids		
pTMB30	P_{trc} expression vector; Ap^R	J.S. Parkinson
pHT100	GST expression vector, Km^R	(125)
pKP20	*E. coli* wild-type *fliK* in pTMB30	
pKP48	*E. coli* wild-type *flgE* in pHT100	
pHT39	*E. coli* wild-type *fliN* in pTMB30	(159)
pDB72	*E. coli* wild-type *fliM* in pTMB30	(125)
pHT53	*E. coli* wild-type *fliG* in pTMB30	(113)
pRG19	*S. enterica* serovar *Typhimurium motA*::*luxCDABE*	(61)

Binding assays.

In this experiments we used two cell protocols, one expressing GST-FlgE from plasmid pHT100 and another expressing *fliN*, *fliM*, *fliG* and *fliK* from plasmid pTMB30 (125, 186). Control experiments used GST only, expressed from plasmid pHT100 (186). The protein expression host strain used for this experiment was RP3098 (Δ*flhDC*; expresses no chromosomal flagellar genes, J.S. Parkinson). Cells were cultured overnight at 32 ℃ in 40 ml of TB containing the appropriate antibiotics and 400 µM IPTG. Cells were harvested and resuspended in lysozyme containing buffer as described (125). Following one-hour incubation on ice, the cells were further disrupted by sonication (Branson model 450 Sonifier; power of 3, duty cycle of 50%, 180 s). Debris were pelleted (16,000 g, 40 min, 4℃), and 50 µl of the supernatant was saved for use in estimating the amount of FliN, FliM, FliG and FliK present before addition of affinity beads (pre beads). The remaining supernatant (∼1 ml) was transferred to a clean tube, mixed with 150 µl of a 50% slurry of glutathione-Sepharose 4B (Pharmacia) prepared according to the manufacturer's directions, and incubated for one hour at room temperature with gentle rotation to allow binding. The Sepharose beads were then pelleted by a 1 min microcentrifuge spin, washed twice with 1 ml of phosphate-buffered saline containing 1% BSA and 0.1% Triton X-100, and pelleted again by a brief spin. The beads were then incubated with 50 µl of elution buffer (50 mM reduced glutathione in 50 mM Tris-HCl, pH 8.0) for 10 min at room temperature with gentle rotation to release the GST-FlgE and associated proteins. Beads were then pelleted, and the supernatant was collected for analysis by SDS-PAGE gel electrophoresis and immunoblotted using anti-FliN/ anti-FliM/ anti-FliG or anti-FliK antibody (159, 186).

Luciferase assays.

Plasmid pRG19 harboring *Salmonella enterica* serovar *Typhimurium motA*::*luxCDABE* was used for monitoring flagellar Class III gene expression (61). The flagellar master operon was induced using a *tetA* promoter placed upstream of *flhDC* (P_{flhDC}::T-POP (80)), and the cultures were grown in 96-well microtiter plates (Greiner Scientific) at 30 ℃. OD_{595} and luciferase light production was measured over time using a PolarStar Optima microplate reader (BMG labtech). After background correction, the relative light units (RLU) were calculated as follows: $RLU = light \cdot \left(\frac{OD_{595} \cdot t=0}{OD_{595} \cdot t=n}\right)$. Half-maximal induction times $\left(\frac{t_{max}}{2}\right)$ of each mutant strain were determined from at least three independent, biological samples and normalized to the wildtype control of the same microtiter plate. The incomplete γ function $f_{\left(\frac{t}{a,b}\right)} = \frac{1}{\Gamma_{(a)}} \int_0^{t/b} x^{a-1} e^x dx$ was used for parameterizing the individual gene expression trajectories as described previously (24). Non-linear curve fitting was performed using the *nlinfit* function of the Optimization Toolbox of Matlab 7.4 (Mathworks). Subsequently, the half-maximal induction time was calculated using $\left(\frac{t_{max}}{2}\right) = a \cdot (b-1)$ with given estimates for a and b. One-way ANOVA with Dunnett's post test was employed to compare statistical significances between half-maximal induction times of the C-ring mutants relative to the respective wildtype control. All statistical analysis were performed using GraphPad Prism 5.0b for Macintosh (GraphPad

Software, San Diego California USA, www.graphpad.com).

Hook-length measurement.

For hook-length measurements, flagellar structures were isolated and the hook-basal bodies were prepared as described (67).

Fluorescent microscopy.

For fluorescent microscopy analysis, cells were grown to mid-log phase and immobilized with poly-L-lysine treated coverslips. Cells were fixed by addition of formaldehyde (5% final). DNA and membrane staining was performed using DAPI and FM-64 (0.5 µg/ml). Flagella were stained using polyclonal anti-FliC antibodies (rabbit) and anti-rabbit Alexa Fluor^{488} secondary antibodies (Invitrogen). Images were collected using an Applied Precision optical sectioning microscope and deconvolved using softWoRx v.3.4.2 (Applied Precision).

4.6 Acknowledgements

This work was supported by PHS grant GM056141 from the National Institutes of Health. We thank Christopher Rao for help with the statistical analysis and Manabu Konishi and Yoshika Nosaka for technical assistance. We are grateful to Nao Moriya and Tohru Minamino for providing the more sensitive FliK antibody. We thank N. Moriya and T. Minamino and the Hughes lab for useful comments and discussions of the manuscript, and in particular we thank the Molecular Microbiology reviewers, which led to a significant improvement of this manuscript. M.E. gratefully acknowledges scholarship support of the Boehringer Ingelheim Fonds.

5

An Infrequent Molecular Ruler Controls Flagellar Hook Length in *Salmonella enterica*

Marc Erhardt[1], Hanna M. Singer[1, †], Daniel H. Wee[1, †], James P. Keener[2, *], Kelly T. Hughes[1, *]

in preparation

[1]Département de Médecine, Université de Fribourg, CH-1700 Fribourg, Switzerland
[†]These authors contributed equally to this work
[2]Department of Mathematics, University of Utah, Salt Lake City, UT 84112, USA
[*]Co-corresponding authors; K. T. Hughes: Mailing address: Département de Biologie, Chemin du Musée 10, Université de Fribourg, CH-1700 Fribourg, Switzerland; Tel: +41 26 300 9436; E-mail: kelly.hughes@unifr.ch; J. P. Keener: Mailing address: Department of Mathematics, University of Utah, Salt Lake City, UT 84112, USA; Tel: +801-581-6089; E-mail: keener@math.utah.edu

5.1 Abstract

The bacterial flagellum consists of a long external filament connected to a membrane-embedded basal-body at the cell surface by a short curved structure, called the hook. In *Salmonella enterica* the hook extends 55 nm from the cell surface. The FliK molecular ruler controls hook length. Upon hook completion, FliK induces a secretion-specificity switch to filament-type substrate secretion. Here, we demonstrate that an Infrequent Ruler mechanism determines flagellar hook length. FliK is intermittently secreted during hook polymerization. The probability of the specificity switch is an increasing function of hook length. By uncoupling hook polymerization from FliK expression, we illustrate that FliK secretion immediately triggers the specificity switch in hooks greater than the physiological length. The experimental hook length data display excellent agreement with a mathematical model of the Infrequent Ruler hypothesis. Finally, we present evidence that the speed of FliK secretion determines the probability of FliK interaction with the secretion apparatus thus providing a possible mechanism for the induction of the specificity switch at the physiological hook length.

5.2 Introduction

Bacteria propel themselves through liquid environments by rotating helical flagellar filaments (Figure 5.1A) (18). The bacterial flagellum is a motor organelle that is composed of three main structural parts: i) a basal body that includes rotor and stator structures embedded in the cytoplasmic membrane, a rod traversing the periplasmic space and a flagellar-specific protein export system; ii) the hook, a flexible coupling structure that functions as a universal joint between the basal body and iii) the rigid filament serving as a propeller that extends several µm from the cell (27, 115). This sophisticated nanomachine is evolutionary and structurally related to the virulence-associated injectisome or needle complex of pathogenic bacteria (32, 72). Common features of both the flagellum and the injectisome systems are a type III protein export machine at the base of the structures (22, 32) and an intrinsic control mechanism for length control of the flagellar hook or injectisome needle, respectively (78, 172). For the flagellum, rod-hook-type substrates are exported via the flagellar type III protein export system until the hook is of appropriate length (55 ± 6 nm) (67) and then the type III secretion system switches substrate specificity and starts exporting filament-type substrates (201). For the injectisome needle system of *Yersinia enterocolitica*, the needle polymerizes to a length of 58 ± 10 nm (78) before substrate specificity is switched towards export of effector proteins (175).

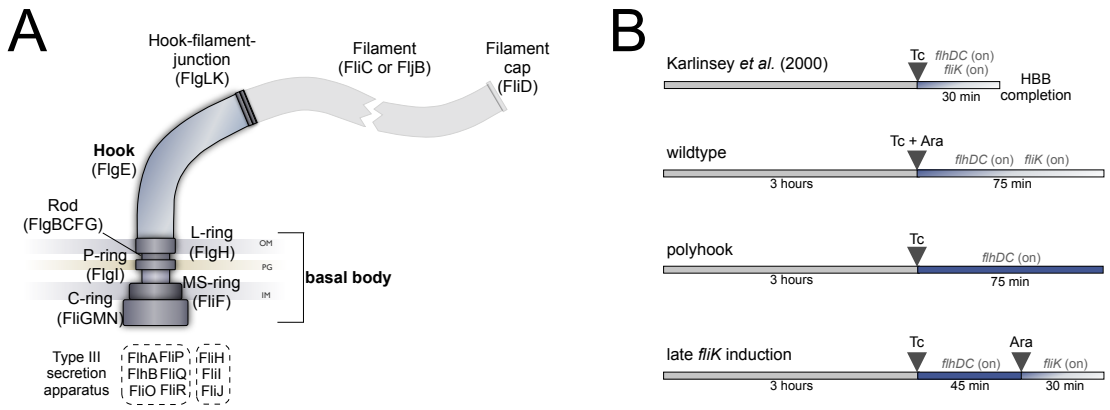

FIGURE 5.1

Schematic of axial components of the bacterial flagellum and experimental outline. (A) Schematic of axial components of the bacterial flagellum. The structure of the bacterial flagellum can be divided in three parts: (i) the basal body structure that harbors the flagellar-specific type III secretion apparatus at the base; (ii) the hook that functions as a flexible coupling structure between the basal body and (III) the rigid filament. Stator elements (Mot proteins) that span the inner membrane and apply torque to the C-ring in response to transmembrane proton flow are not shown. Rod-hook-length is determined by a molecular ruler, FliK that in turn induces a switch in secretion specificity from rod-hook-type to filament-type substrates upon hook completion, presumably by interaction with FlhB, an component of the type III secretion apparatus at the base of the structure. (B) Schematic of experimental outline. An overnight culture of a strain expressing the flagellar master operon *flhDC* from a tetracycline (Tc)-inducible P_{tetA} promoter is diluted into fresh LB and grown for 3 hours. After 3 hours growth, flagellar gene expression is induced by addition of Tc and 30 minutes after induction transcription of Class III promoters is observed which indicates HBB completion (80). Here, we uncoupled FliK expression from flagellar genes expression to analyze the effects of late FliK induction on switching from HBB-type secretion to filament-type secretion in a strain deleted for its native *fliK* gene and expressing *fliK* from the inducible P_{araBAD} promoter (P_{tetA}-*flhD*$^+$*C*$^+$ P_{araBAD}-*fliK*$^+$ Δ*fliK*). In the first sample ('wildtype'), flagellar genes expression and *fliK* expression are induced simultaneously by addition of Tc to induce the flagellar master regulator *flhDC* (P_{tetA}-*flhD*$^+$*C*$^+$) and Arabinose (Ara) to induce *fliK* expression (P_{araBAD}-*fliK*$^+$) resulting in hooks of wild-type length. In the second sample ('polyhook'), only Tc is added to induce flagellar gene expression, giving rise to polyhooks because FliK is not induced. In the third sample ('late FliK induction'), flagellar gene expression is induced for 45 minutes without FliK expression. This allows for hook growth beyond the physiological length. Afterwards, FliK is induced by addition of Arabinose and the culture grown for an additional 30 minutes to allow for induction of the secretion specificity switch and filament assembly.

In *Salmonella enterica* the secretion specificity switch is thought to occur by an interaction between secreted FliK and the substrate specificity determining component of the flagellar secretion apparatus, FlhB (130). Null mutants of *fliK* and dominant-negative alleles of *flhB* fail to switch the secretion specificity to filament-type substrates and continue uncontrolled hook polymerization (53, 67, 131, 157). Homologous proteins of FliK and FlhB in the *Yersinia* ssp. injectisome system are YscP and YscU (78, 118). The C-terminal domains of FliK and YscP are thought to be responsible for induction of the specificity switch within the type III secretion apparatus, presumably by interaction with FlhB or YscU, respectively (67, 130, 175). Export of FliK and YscP is required for hook and needle length control, respectively (4, 131). Deletions and insertions in FliK (YscP) revealed a linear correlation between length of the hook (needle) structure and the length of FliK (YscP), illustrating that these proteins determine hook (needle) length as a molecular ruler that directly measures the length of the structure (78, 172).

Several models for the mechanism of how FliK (YscP) regulates hook (needle) length have been proposed. The fundamental problem is how, during the process of being secreted, the ruler molecule is able to transmit hook (needle)-length information beyond the cell surface back to the type III export apparatus in the inner membrane in order to flip the switch. Initially, a molecular ruler model was not considered for the flagellar system because all *fliK* mutants isolated resulted in longer, not shorter hooks (84). However, mutants in the C-ring components *fliG*, *fliM* or *fliN* were identified that resulted in short hooks (120). Thus, it was proposed that the cytoplasmic rotor of the flagellum functions as a measuring cup. This C-ring cup would fill-up with hook subunits that would correspond to the required number of hook molecules for the assembly of a hook of appropriate length. Upon emptying of the cup, FliK would be able to access and interact with FlhB (120). Recent results show, however, that controlled hook lengths are observed in mutants missing parts or all of the C-ring (43, 94). Later, a static ruler model has been proposed where a single ruler molecule remains in the secretion channel and is attached to the growing tip of the needle (hook) structure (78). In this model, needle (hook) subunits must be able to pass by the retained ruler inside a secretion channel as narrow as 1.5 nm. Finally, an alternative model was proposed where FliK is intermittently secreted throughout hook growth and the length signal is determined via a stochastic process where the probability of hook growth termination is an increasing function of hook length (43, 86). In this work, we present experimental evidence in favor of this infrequent molecular ruler model and provide for the first time a mechanism for flagellar hook length determination by FliK in which the speed of FliK secretion dictates the probability of a productive interaction with the secretion apparatus for the specificity switch to occur.

5.3 Results

5.3.1 Experimental approach and motility of the model strains.

The Infrequent Ruler model for hook length regulation predicts that the ruler, FliK, can be intermittently secreted with hook (FlgE) subunits at any time during hook polymerization. During secretion, FliK takes temporal measurements of hook length. The probability of a productive interaction of the FliK C-terminus with the type III secretion apparatus, which is a prerequisite for the switch in secretion specificity, increases with hook length. Termination of hook polymerization would be unlikely for short hooks, but highly probable at longer hook lengths. A possible mechanism is that the speed of FliK secretion is facilitated while the hook is shorter than its physiological length. This would prevent a productive interaction of the FliK C-terminus with the FlhB component of the secretion system. In hooks of or greater than the physiological length the rate of FliK secretion is slow enough to allow for enough time for the C-terminus of FliK to interact with FlhB and flip the specificity switch to late-substrates.

One prediction of the Infrequent Ruler hypothesis is that FliK triggers the secretion specificity switch every time FliK is secreted through a hook of physiological length or greater. To this end, we envisaged a *Salmonella enterica* model strain in which FliK induction (and hence secretion) is uncoupled and independently controlled from hook-basal-body (HBB) assembly. Flagellar gene expression, and accordingly HBB assembly, is under control of a tetracycline-inducible promoter. In this strain induction of flagellar gene expression is controlled by a tetracycline (Tc)-inducible promoter (80), thereby enabling us to control and synchronize expression of the flagellar master regulator *flhDC* (P_{tetA}-*flhD*$^+$ *C*$^+$). It has been previously reported that approximately 30 minutes after induction of the *flhDC* operon, the secretion-specificity switch has occurred, which corresponds to HBB completion (80). In a strain that is deleted for its chromosomal *fliK* gene, induction of the flagellar master regulon will result in HBB assembly. However in the absence of FliK, the secretion apparatus will fail to flip the secretion specificity switch and hook growth will continue beyond physiological lengths, resulting in a polyhook phenotype. To control expression of FliK, the *fliK* gene was placed under arabinose induction (P_{araBAD}-*fliK*$^+$). This model strain (P_{tetA}-*flhD*$^+$ *C*$^+$ P_{araBAD}-*fliK*$^+$ Δ*fliK*) allows for induction of FliK at times after hook-length has reached its physiological length. As shown in Figure 5.2, the model strain displayed motility compared to wildtype on soft agar plates containing tetracycline and arabinose as inducers of both FliK and flagellar gene expression.

To probe the proposed Infrequent Ruler model for hook length determination, the model strain was grown under three different conditions (Figure 5.1B). For the 'wild-type' control, flagellar genes (P_{tetA}-*flhD*$^+$ *C*$^+$) and *fliK* expression (P_{araBAD}-*fliK*) were induced simultaneously by addition of both inducers for 75 minutes. In case of the polyhook control, flagellar gene expression in the absence of *fliK* expression was induced by addition of only Tc for 75 minutes. To assess the effects of late FliK secretion in a population where the majority of the hooks have polymerized beyond the physiological length, expression of the flagellar master regulator was induced with Tc for 45 minutes followed by induction of *fliK* expression with arabinose for an additional 30 minutes.

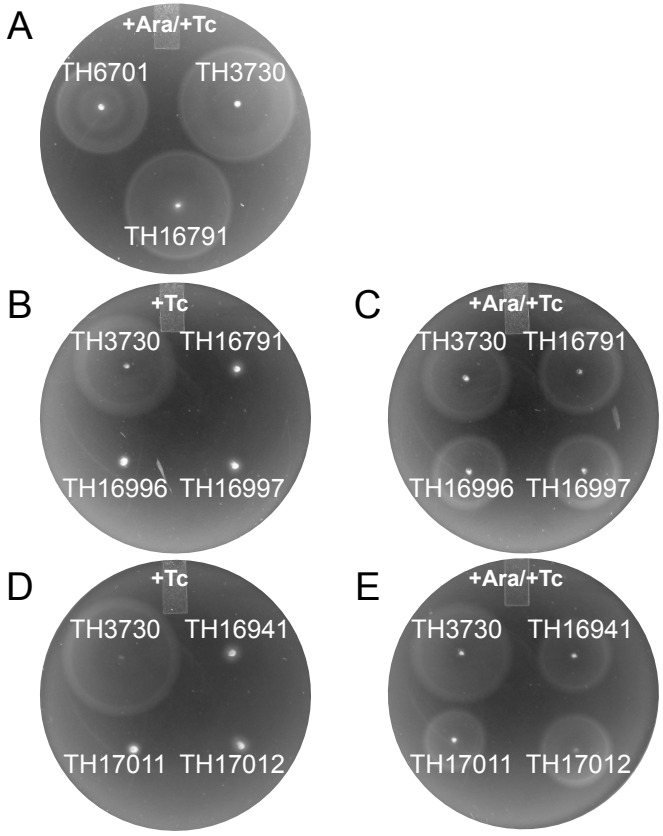

FIGURE 5.2

Motility of model strains. Overnight cultures were grown in LB and poked into motility agar containing 15 µg/ml tetracycline and/or 0.2% arabinose, respectively and incubated for 5 hours at 37 ℃. (A) Motility of the model strain TH16791 (P_{tetA}-*flhD*$^+$ *C*$^+$ P_{araBAD}-*fliK*$^+$ Δ*fliK*) in the presence of 15 µg/ml tetracycline and 0.2% arabinose. TH6701 (Δ*araBAD*::*tetRA*), TH3730 (P_{tetA}-*flhD*$^+$ *C*$^+$), TH16791 (P_{tetA}-*flhD*$^+$ *C*$^+$ P_{araBAD}-*fliK*$^+$ Δ*fliK*). (B) Motility of strains TH3730, TH16791, TH16996 (P_{tetA}-*flhD*$^+$ *C*$^+$ P_{araBAD}-*fliK*-*yscP*(217-381) Δ*fliK*) and TH16997 (P_{tetA}-*flhD*$^+$ *C*$^+$ P_{araBAD}-*fliK*($\Delta_{aa161\text{-}200}$) Δ*fliK*) in the presence of 15 µg/ml tetracycline. (C) Motility of strains TH3730, TH16791, TH16996 and TH16997 in the presence of 15 µg/ml tetracycline and 0.2% arabinose. (D) Motility of strains TH3730, TH16941 (P_{tetA}-*flhD*$^+$ *C*$^+$ P_{araBAD}-*fliK*$^+$ Δ*fliK flgE*::3xHA), TH17011 (P_{tetA}-*flhD*$^+$ *C*$^+$ P_{araBAD}-*fliK*-*yscP*(217-381) Δ*fliK flgE*::3xHA) and TH17012 (P_{tetA}-*flhD*$^+$ *C*$^+$ P_{araBAD}-*fliK*(Δaa161-200) Δ*fliK flgE*::3xHA) in the presence of 15 µg/ml tetracycline. (E) Motility of strains TH3730, TH16941, TH17011 and TH17012 in the presence of 15 µg/ml tetracycline and 0.2% arabinose.

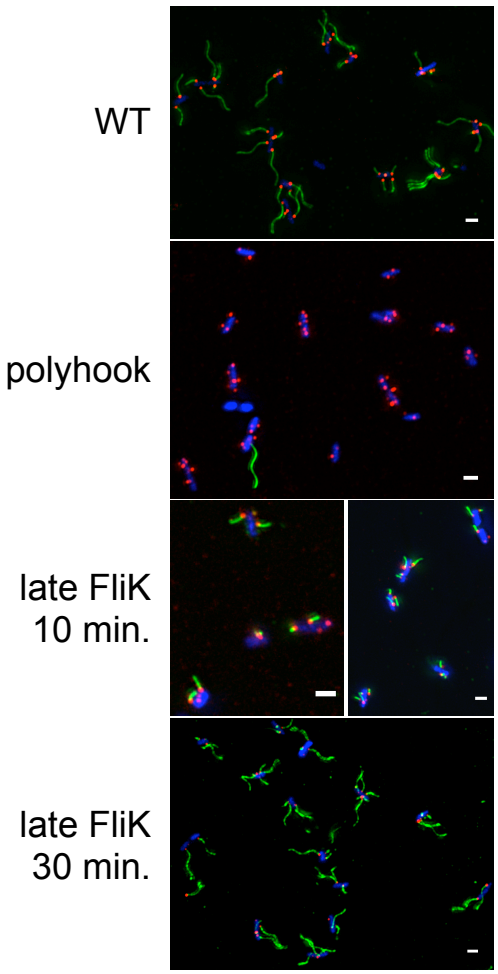

FIGURE 5.3

FliK induces secretion specificity switch in hooks > wt length. 'WT': Simultaneous induction of *fliK* and flagellar genes expression. 'polyhook': Flagellar genes were induced without induction of *fliK*. 'late FliK': Late *fliK* induction after 45 minutes of flagellar genes expression for 10 and 30 minutes, respectively. Tetracycline was not removed prior to addition of arabinose. Representative fluorescent microscopy images of strain TH16941 (P_{tetA}-*flhD*$^+$*C*$^+$ P_{araBAD}-*fliK*$^+$ Δ*fliK* *flgE*::3xHA) are shown. Scale bar = 2 µm.

5.3.2 The switch to late-substrate secretion occurs immediately after FliK induction in hooks greater than the physiological length.

In the absence of FliK, addition of Tc for 45 minutes ensures that hooks polymerize beyond their physiological length. We then induced *fliK* 45 minutes after addition of Tc and followed by an additional 10 or 30 minutes growth, respectively, to determine if FliK could induce the secretion specificity switch in HBBs with elongated hooks. As displayed in Figure 5.3, almost every HBB switched to late, filament-type secretion, as visualized by immunoblotting using hook- and filament-specific antibodies. Importantly, even after only 10 minutes of *fliK* induction, short filaments attached to nearly every HBB were observed. This suggests that the first ruler molecule secreted into HBBs with elongated hooks immediately flipped the specificity switch, as predicted by the Infrequent Ruler hypothesis. In the control sample where *fliK* expression was never induced, rarely a filament was observed (about 5-10% of detected HBBs) (Figure 5.3). This result can be explained by a combination of spontaneous switching of the type III secretion apparatus to late secretion and leaky expression of the P_{araBAD}-*fliK* allele that would result in FliK secretion.

Next, we obtained the hook length distribution of the model strain under different FliK induction conditions (Figure 5.4C). In the first sample, both flagellar genes and *fliK* were induced simultaneously (labeled 'WT' in the figure), in the second sample, only flagellar genes were induced (labeled 'polyhook' in the figure) and in the third sample *fliK* expression was induced only after 45 minutes of flagellar gene expression (labeled 'late FliK' in the figure). In case of simultaneous expression of HBB genes and *fliK*, an average hook length of 43 ± 6 nm was observed (Figure 5.4C left panel). The average hook length is approximately 12 nm shorter as previously observed under wildtype conditions (67). However, this result can be explained by simultaneous and not hierarchical expression of HBB genes and *fliK*, contrary of what is the case under wildtype conditions, and, overproduction of *fliK* expressed from the strong P_{araBAD} promoter. In fact, it has been previously reported that overexpression of *fliK* produced shorter hooks (47 ± 7 nm) (150). When *fliK* was not expressed in the polyhook sample, hook length control was completely abolished with hooks up to 1.2 µm length (Figure 5.4C middle panel). This is consistent with the hook length distribution observed in a *fliK* deletion strain (157). Importantly, in the sample where *fliK* expression was induced late after physiological HBB completion, hook length appears to be partially controlled (Figure 5.4C right panel). Hooks longer than 500 nm were not observed contrary to the polyhook sample (Figure 5.4C middle panel) and additionally the histogram reveals a prominent population of 42 ± 5 nm. In this sample, *fliK* was induced for 30 minutes during which time also the inducer for HBB genes was present.

Accordingly, production of nascent 'wildtype' HBBs accounts for this prominent peak. It is important to stress, however, that the isolation procedure for hook-basal-bodies requires either very long hooks (e.g. as found in a polyhook phenotype) or attached filaments. This explains the prominent 'wildtype' peak at 42 nm and suggests that the longer hooks up to 500 nm length indeed switched to late-substrate secretion and had a filament attached during the HBB preparation. In order to exclude that only

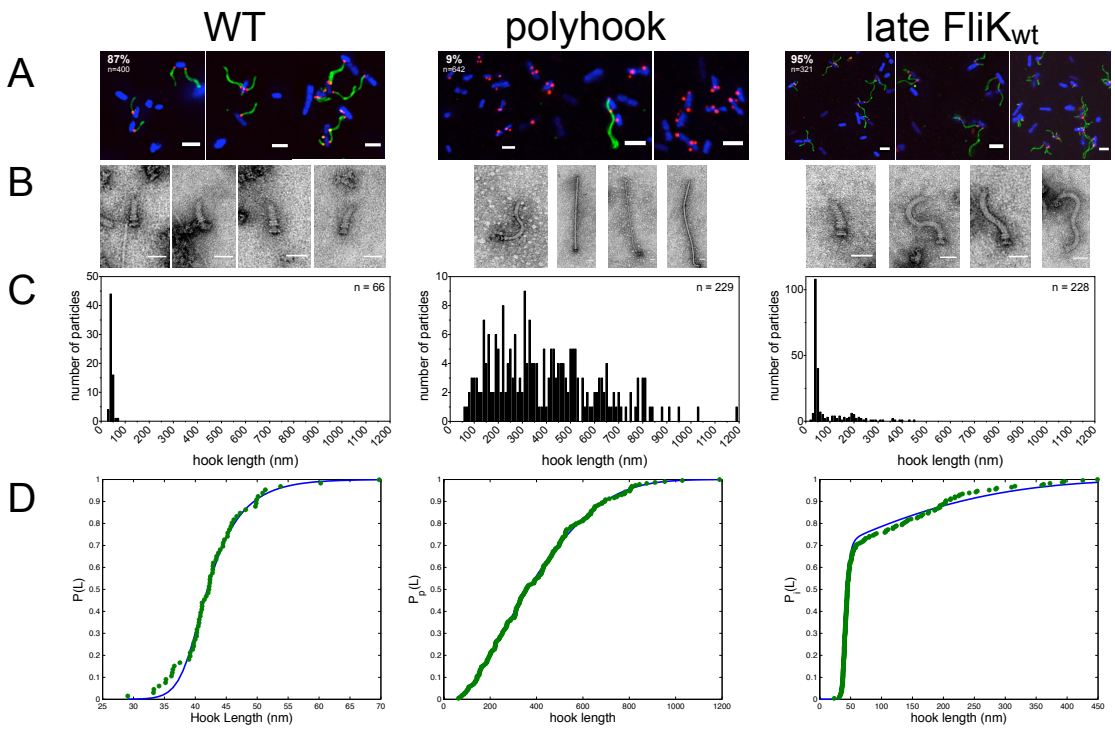

FIGURE 5.4

Late FliK secretion induces secretion specificity switch in elongated hooks. Left panels (WT): Simultaneous induction of *fliK* and flagellar genes expression. Middle panels (polyhook): Flagellar genes were induced without induction of *fliK*. Right panels (late FliK): Late *fliK* induction after 45 minutes of flagellar genes expression. (A) Representative fluorescent microscopy images of strain TH16941 (P_{tetA}-*flhD*$^+$*C*$^+$ P_{araBAD}-*fliK*$^+$ Δ*fliK* *flgE*::3xHA). Tc was removed prior to addition of arabinose to prevent formation of nascent HBBs. Percentage of HBBs with attached filaments (upper left corner). DNA (blue), hooks (red) and filaments (green). Scale bar = 2 µm. (B) Representative electron micrograph images of hooks isolated from strain TH16791 (P_{tetA}-*flhD*$^+$*C*$^+$ P_{araBAD}-*fliK*$^+$ Δ*fliK*). Scale bar = 50 nm. (C) Histogram of measured hooks of strain TH16791. (D) Cumulative distribution function of hooks measured for TH16791.

nascent HBBs switched to filament-type secretion after late FliK induction (e.g. as seen in Figure 5.3), we repeated the late FliK induction experiment under conditions where tetracycline, the inducer of flagellar genes was removed after 45 minutes before the addition of arabinose, the inducer of *fliK* (Figure 5.4A). This ensures that during the following 30 minutes of *fliK* expression no nascent HBBs are produced and FliK is only secreted in old hook-basal-bodies with elongated hooks. Under these conditions approximately 95% of detected HBBs indeed switched to filament-type secretion (Figure 5.4A right panel).

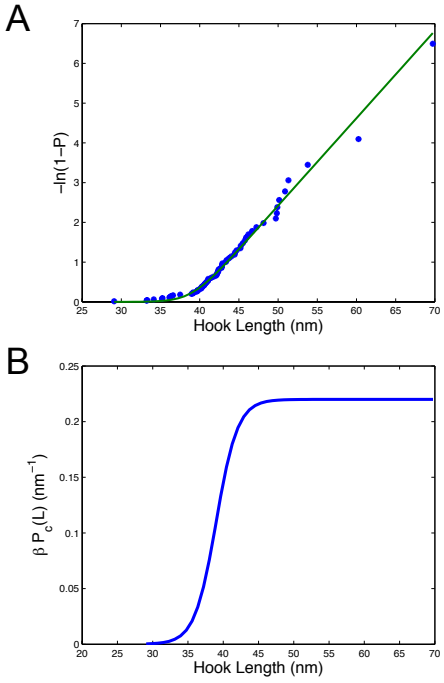

FIGURE 5.5

Data analysis of simultaneous FliK and flagellar genes expression (WT data). (A) Hook length data, shown as asterisks, from Figure 5.4 replotted as $-\ln(1-P(L))$ vs. L, with the solid curve given by $G(L)$ in equation (5.6). (B) The function $P_c(L)$ as estimated from wildtype data in Figure 5.4.

In the Methods section, we present a mathematical model of the Infrequent Ruler mechanism that allows us to use wildtype hook length data and polyhook data to predict the length distribution of hooks produced by late FliK induction. First we use the experimentally obtained hook length data from the wildtype sample (Figure 5.4D, left panel) to estimate the function $P_c(L)$, the probability of FliK interaction with FlhB at hook length L. The CDF (cumulative distribution function) $P(L)$ for this data is shown in Figure 5.4D, with data points shown as asterisks. An estimate of $P_c(L)$ is shown in Figure 5.5B. The second data set is polyhook data, determined from a culture in which there was no FliK induction. The culture was grown for 75 minutes. The histogram of lengths is shown in Figure 5.4C (middle panel) and the CDF $P_p(L)$ for this collection of polyhooks is shown in Figure 5.4D (middle panel). The third type of data is from a

culture grown for 75 minutes, with induction of FliK at time $T_0 = 45$ minutes (Figure 5.4 right panel). In Figure 5.4D (right panel) is shown the CDF of the data (shown as asterisks) and the predicted CDF $P_i(L)$ determined from equation (5.8), using the functions $P_c(L)$ and $P_p(L)$.

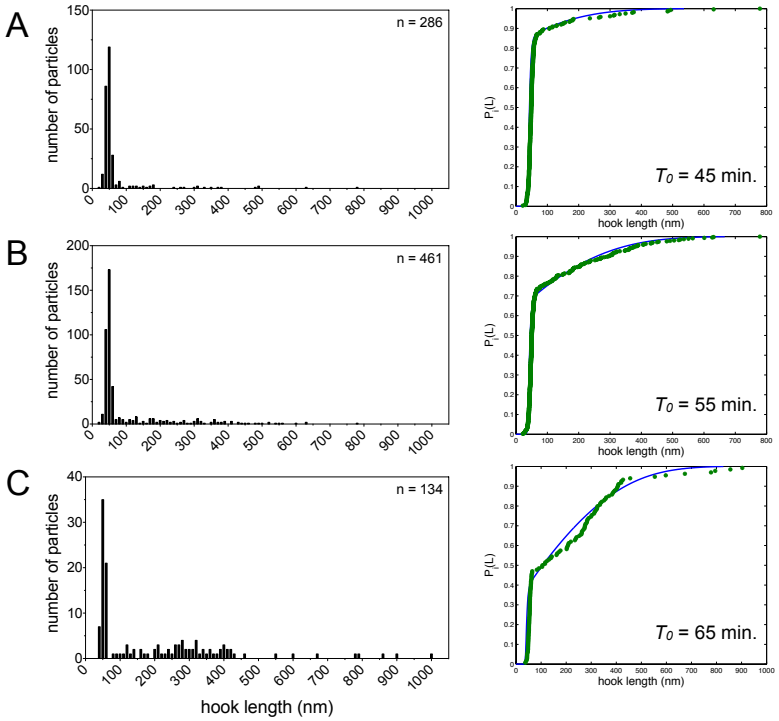

FIGURE 5.6

Late induction of FliK at varying times T_0. Strain TH16791 (P_{tetA}-*flhD*$^+$ *C*$^+$ P_{araBAD}-*fliK*$^+$ Δ*fliK*) was grown in the presence of Tc (inducer of flagellar genes) for (A) 45 minutes, (B) 55 minutes and (C) 65 minutes. Afterwards FliK expression was induced by addition of arabinose for a total sample time of 80 minutes. Left panels: histogram of measured hooks. Right panels: cumulative distribution function of measured hooks, data shown as asterisks and $P_i(L)$ (solid curve) computed from equation (5.8) using $L^* = 600$ nm ($T_0 = 45$ min.), 440 nm ($T_0 = 55$ min.) and 260 nm ($T_0 = 65$ min.).

The agreement between the curve $P_i(L)$ and the data is strikingly good. There is some error, however, which is possibly explained by the fact that in the derivation of equation (5.8), the velocity of hook growth is assumed to be constant, independent of length. A better estimate of the length distribution at the time of induction would require more detailed knowledge of the velocity of hook growth as a function of length. In spite of this caveat, however, the excellent agreement between the late FliK induction data and the prediction based on information from sample 1 (WT) and sample 2 (polyhook) gives strong evidence in favor of the hypothesis that hook length determination is by an Infrequent Ruler mechanism with a switching probability function $P_c(L)$. This analysis was further applied to several datasets with varying induction times T_0. The results with the same agreement are shown in Figure 5.6 ($T_0 = 45$min, 55min and 65 min).

5.3.3 Secretion of FliK deletion and insertion alleles in elongated hooks immediately induce the secretion specificity switch.

To further assess the ability of late FliK secretion in triggering the specificity switch in hooks greater than the physiological length, we engineered FliK deletion and insertion variants and tested their ability to control hook length after late FliK induction. First, a long FliK variant was generated by inserting a 164 amino acid fragment of YscP after amino acid 140 of FliK, resulting in $FliK_{570}$. A short FliK variant was constructed by deleting amino acids 161 through 202 of FliK, resulting in $FliK_{363}$. $FliK_{570}$ (reported hook length 81.6 ± 9.5 nm) and $FliK_{363}$ (reported hook length 43.5 ± 8.0 nm) retain hook length control if expressed from the native P_{fliK} promoter (172). In order to allow for inducible expression, both *fliK* variants were expressed from the chromosomal P_{araBAD} promoter. The ability of the FliK variants to flip the specificity switch to late-substrate secretion was first analyzed by filament immunostaining (Figure 5.7A, 5.8A, 5.9A). Under conditions where nascent HBBs were not produced anymore after FliK induction, late FliK secretion switched 91% ($FliK_{570}$) and 96% ($FliK_{363}$) of the detected hook-basal-bodies to filament-type secretion (Figure 5.7A and 5.8A). Next, the hook length distribution after late FliK induction was determined, albeit because of experimental constrictions under conditions where production of new HBBs was still possible (Figure 5.7B+C, 5.8B+C, 5.9B+C). When flagellar genes and $FliK_{570}$ were expressed simultaneously, the hook length histogram reveals a peak at 79 ± 6 nm (Figure 5.9C first column). Hook length was not regulated with hook lengths up to 960 nm when $FliK_{570}$ was not expressed (Figure 5.9C second column). When $FliK_{570}$ was induced late after 45 minutes of HBB genes expression, hooks longer than 400 nm were not observed with a peak at 78 ± 7 nm that can be attributed to nascent HBBs (Figure 5.7C). For the shorter $FliK_{363}$ variant an average hook length of 38 ± 6 nm was found under conditions where flagellar genes and $FliK_{363}$ were expressed simultaneously (Figure 5.9C third column). When only flagellar genes were expressed, hook length was not controlled with lengths up to 960 nm (Figure 5.9C fourth column). Under conditions where $FliK_{363}$ was expressed late, maximal hook lengths were 380 nm with a peak corresponding to nascent HBBs at 39 ± 6 nm (Figure 5.8C).

The measured hook length data of the polyhook and wildtype samples for both $FliK_{570}$ and $FliK_{363}$ were then used to predict the late $FliK_{570}$ ($FliK_{363}$) hook length distribution $P_i(L)$ computed as described in the Methods Section. As it was the case for late wildtype FliK, we found excellent agreement between the experimental data of late induction of $FliK_{570}$ and $FliK_{363}$ and the prediction of the Infrequent Ruler model.

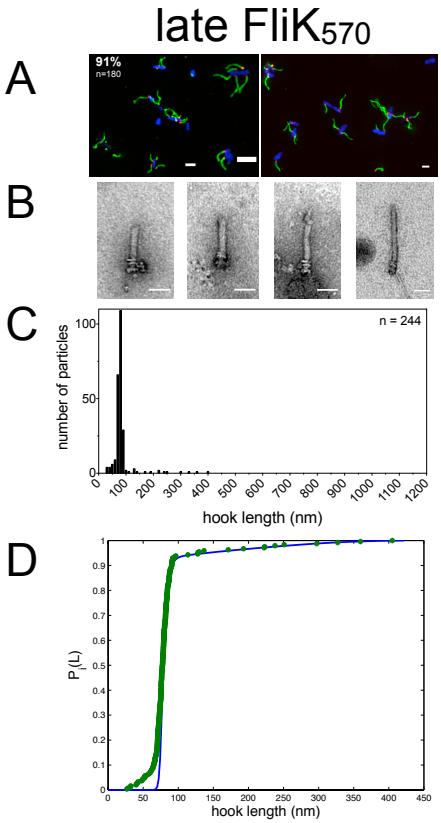

FIGURE 5.7

Late secretion of long FliK$_{570}$ variant. FliK$_{570}$ expression was induced late after 45 minutes of flagellar genes expression. (A) Representative fluorescent microscopy images of strain TH17011 (P$_{tetA}$-*flhD*$^+$ *C*$^+$ P$_{araBAD}$-*fliK*(140'-*yscP*(217-381)-'141*fliK*) Δ*fliK flgE*::3xHA). Tc was removed prior to addition of arabinose to prevent formation of nascent HBBs. Percentage of HBBs with attached filaments (upper left corner). DNA (blue), hooks (red) and filaments (green). Scale bar = 2 µm. (B) Representative electron micrograph images of hooks isolated from strain TH16996 (P$_{tetA}$-*flhD*$^+$ *C*$^+$ P$_{araBAD}$-*fliK*(140'-*yscP*(217-381)-'141*fliK*) Δ*fliK*). Scale bar = 50 nm. (C) Histogram of measured hooks of strain TH16996. (D) Cumulative distribution function of hooks measured for strain TH16996.

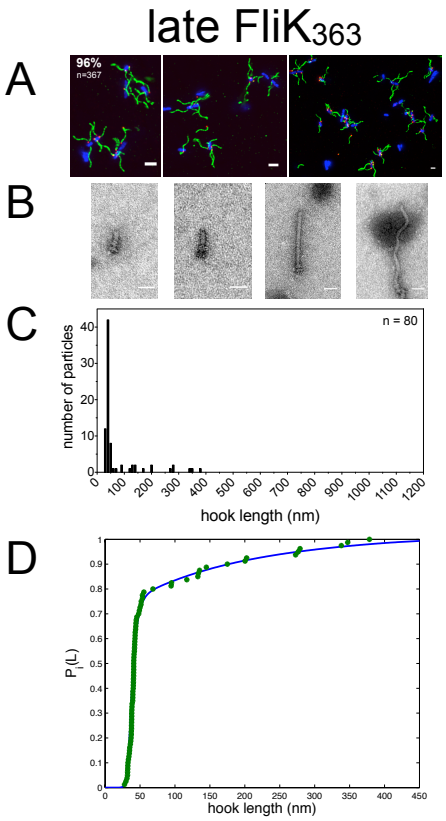

FIGURE 5.8

Late secretion of short FliK$_{363}$ variant. FliK$_{363}$ expression was induced late after 45 minutes of flagellar genes expression. (A) Representative fluorescent microscopy images of strain TH17012 (P$_{tetA}$-*flhD*$^+$ *C*$^+$ P$_{araBAD}$-*fliK*Δ161-202 Δ*fliK* *flgE*::3xHA). Tc was removed prior to addition of arabinose to prevent formation of nascent HBBs. Percentage of HBBs with attached filaments (upper left corner). DNA (blue), hooks (red) and filaments (green). Scale bar = 2 µm. (B) Representative electron micrograph images of hooks isolated from strain TH16997 (P$_{tetA}$-*flhD*$^+$ *C*$^+$ P$_{araBAD}$-*fliK*Δ161-202 Δ*fliK*). Scale bar = 50 nm. (C) Histogram of measured hooks of strain TH16997. (D) Cumulative distribution function of hooks measured for strain TH16997.

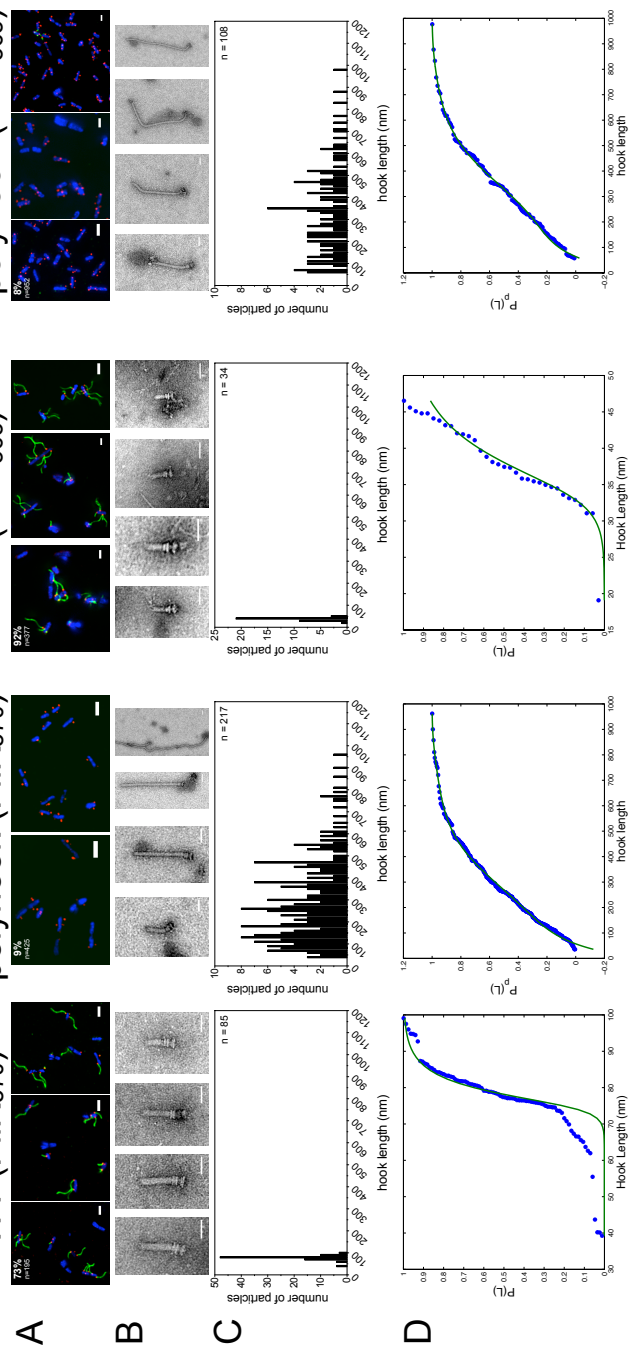

FIGURE 5.9

Long and short FliK variants. Switching to filament secretion and hook length distribution under wildtype and polyhook conditions. 'WT' sample, simultaneous expression of P_{tetA}-*fliD*$^+$ *C*$^+$ and *fliK*. 'Polyhook' sample, only P_{tetA}-*fliD*$^+$ *C*$^+$ was expressed. (A) First and second column: representative fluorescent microscopy images of strain TH17011 (P_{tetA}-*fliD*$^+$ *C*$^+$ P_{araBAD}-*fliK*(140'-*yscP*(217-381)-'141-*fliK*) Δ*fliK flgE*::3xHA). Third and fourth column: strain TH17012 (P_{tetA}-*fliD*$^+$ *C*$^+$ P_{araBAD}-*fliK*Δ161-202 Δ*fliK flgE*::3xHA). Tc was removed prior to addition of arabinose to prevent formation of nascent HBBs. Percentage of HBBs with attached filaments (upper left corner). DNA (blue), hooks (red) and filaments (green). Scale bar = 2 µm. (B) First and second column: representative electron micrograph images of hooks isolated from strain TH16996 (P_{tetA}-*fliD*$^+$ *C*$^+$ P_{araBAD}-*fliK*(140'-*yscP*(217-381)-'141-*fliK*) Δ*fliK*). Third and fourth column: strain TH16997 (P_{tetA}-*fliD*$^+$ *C*$^+$ P_{araBAD}-*fliK*Δ161-202 Δ*fliK*) Scale bar = 50 nm. (C) Histogram of measured hooks of strain TH16996 (first and second column) and TH16997 (third and fourth column). (D) Cumulative distribution function of hooks measured for TH16996 (first and second column) and TH16997 (third and fourth column).

5.3.4 The speed of FliK secretion inversely correlates with hook length.

The Infrequent Ruler model predicts a mechanism for rapid secretion of the FliK ruler molecule in hooks shorter than the physiological length such that the C-terminus of FliK does not interact with FlhB during export. Contrary, in hooks of or longer than the physiological length, the rate of FliK secretion must be slow enough to allow time for a productive interaction of the FliK C-terminus with the secretion apparatus. It has been reported that the FliK N-terminus interacts with the hook cap FlgD or assembled hook subunits (139, 145). More frequent interactions of FliK with hook subunits could explain a slower FliK secretion rate in longer hooks. Additionally, it would be feasible that the nascent FliK N-terminus starts to fold as it exits the secretion channel. When FliK is secreted through hook-basal-bodies with a combined length that is smaller than that of the elongated FliK molecule, initial folding of the FliK N-terminus could act as a Brownian ratchet that rapidly pulls the FliK molecule past the type III secretion apparatus and through the channel (86). We tested the speed of FliK secretion in the model strain where flagellar gene expression can be synchronized and is uncoupled from FliK expression (P_{tetA}-*flhD*$^+$*C*$^+$ P_{araBAD}-*fliK*$^+$ Δ*fliK*). Flagellar genes were expressed for 45 minutes, giving rise to polyhooks, before Tc, the inducer of flagellar genes, was removed. Afterwards, *fliK* was induced and intra- and extracellular FliK protein levels were determined using quantitative Western blot analysis (Figure 5.10A, upper panels).

Cellular FliK protein was detected approximately 25 minutes after induction and detectable levels of secreted FliK were observed at approximately 30 minutes after induction. Next, the shortest possible hook-basal-body structure with defined length was analyzed for the rate of FliK secretion. In a strain background that is deleted for *flgE*, the gene encoding for the hook subunit, flagellar basal-body assembly halts after PL-ring formation, thus resulting in the shortest possible basal-body structure that is capable of extra-cellular secretion. As displayed in Figure 5.10A (lower panels), secreted FliK can be detected approximately 25 minutes after *fliK* induction. Importantly, significantly more FliK is secreted in the hook deletion background if compared to the polyhook sample. Cellular FliK levels were comparable but slightly higher in the polyhook sample because of less secreted FliK. However, one can argue that the lower levels of secreted FliK under polyhook conditions could be explained with the ability of secreted FliK to flip the specificity switch, which would result in cessation of rod-hook-type secretion in the polyhook sample. A switch of secretion specificity to late-substrates would eliminate secretion of FliK resulting in lower levels of secreted FliK. Hence, we repeated the quantitative analysis of FliK secretion in a *flhB*(N269A) background that does not undergo the secretion specificity switch (53). The $FlhB_{N269A}$ allele was introduced into the model strain (P_{tetA}-*flhD*$^+$*C*$^+$ P_{araBAD}-*fliK*$^+$ Δ*fliK* *flhB*(N269A)) and secreted FliK protein was detected after late FliK expression. As presented in Figure 5.10B, intracellular and secreted FliK can be detected roughly at the same time and in comparable quantities as in the *flhB*$^+$ background (Figure 5.10A). This illustrates that the capability of the secretion apparatus to secrete rod-hook-type substrates is not impaired in the $FlhB_{N269A}$ background. The late FliK induction experiment was repeated in the same strain background where additionally the gene encoding for the hook protein was

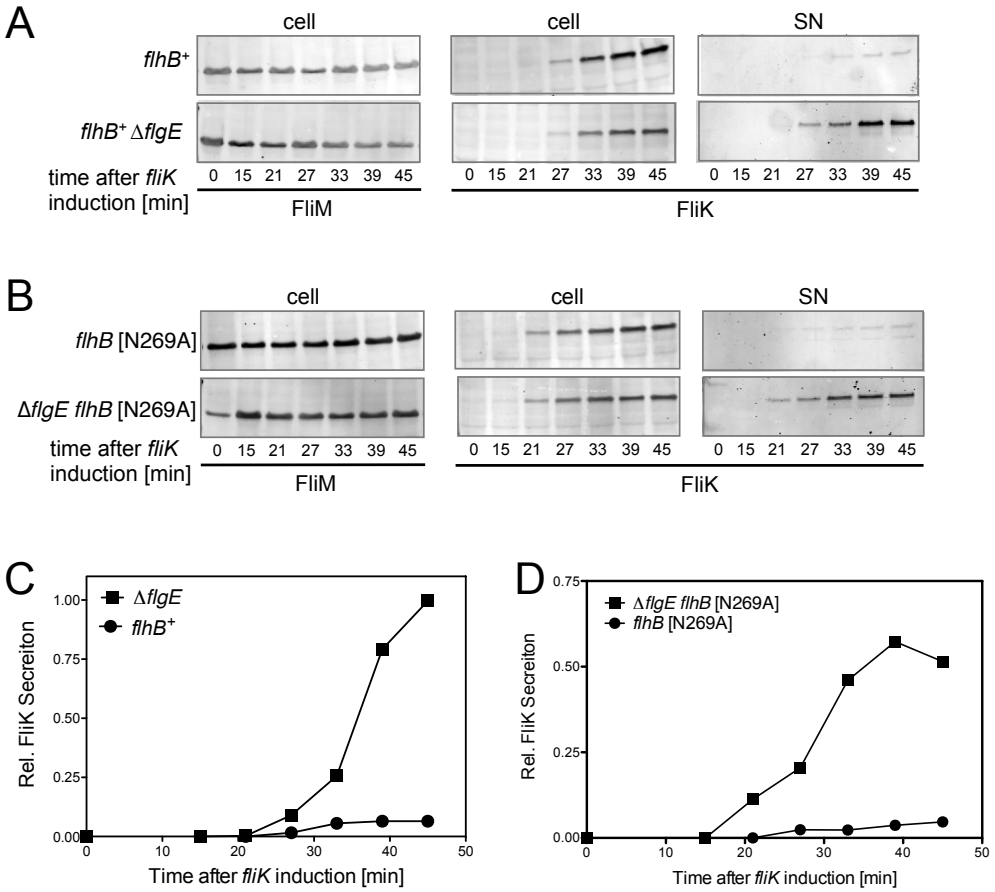

FIGURE 5.10

Speed of FliK secretion is dependent on hook length. Cellular FliM (left panels), cellular FliK (middle panels) and extracellular FliK levels (right panels). Expression of flagellar genes and *fliK* was induced as outlined in Materials and Methods. Residual Tc was washed-out before induction of FliK and samples were taken at the time points indicated. Representative Western blots are shown. (A) Strain TH16791 (P_{tetA}-*flhD*$^+$ *C*$^+$ P_{araBAD}-*fliK*$^+$ Δ*fliK*) and strain TH17069 (P_{tetA}-*flhD*$^+$ *C*$^+$ P_{araBAD}-*fliK*$^+$ Δ*fliK* Δ*flgE*). (B) Strain TH17112 (P_{tetA}-*flhD*$^+$ *C*$^+$ P_{araBAD}-*fliK*$^+$ Δ*fliK* *flhB*(N269A)) and strain TH17076 (P_{tetA}-*flhD*$^+$ *C*$^+$ P_{araBAD}-*fliK*$^+$ Δ*fliK* *flhB*(N269A) Δ*flgE*). (C) Relative levels of secreted FliK normalized against intracellular FliM of TH16791 and TH17069. (D) Relative levels of secreted FliK normalized against intracellular FliM of TH17112 and TH17076.

deleted. Importantly, in this hook deletion mutant the rate and levels of FliK secretion were significantly increased if compared to the polyhook sample in the same $FlhB_{N269A}$ background (Figure 5.10B+D).

These results demonstrate that FliK is secreted at significantly higher levels in the absence of the hook than under polyhook conditions, thus providing evidence for the mechanism suggested above where FliK-FlgE interactions and/or N-terminal folding of the nascent FliK N-terminus determine the rate of FliK secretion.

5.4 Discussion

Here, we present experimental evidence in support of an Infrequent Ruler mechanism for the determination of flagellar hook length. In this model, the molecular ruler FliK is intermittently secreted throughout hook polymerization (Figure 5.11). Hook length is measured by secretion of a FliK molecule and hook polymerization will continue until a secreted FliK molecule is in close proximity and provided with sufficient time for a productive interaction with the FlhB component of the type III secretion apparatus at the base of the flagellum to flip a switch in secretion specificity (43, 86). The Infrequent Ruler model predicts a mechanism of hook length determination in which the probability of a productive FliK interaction with the secretion apparatus is an increasing function of hook length (86).

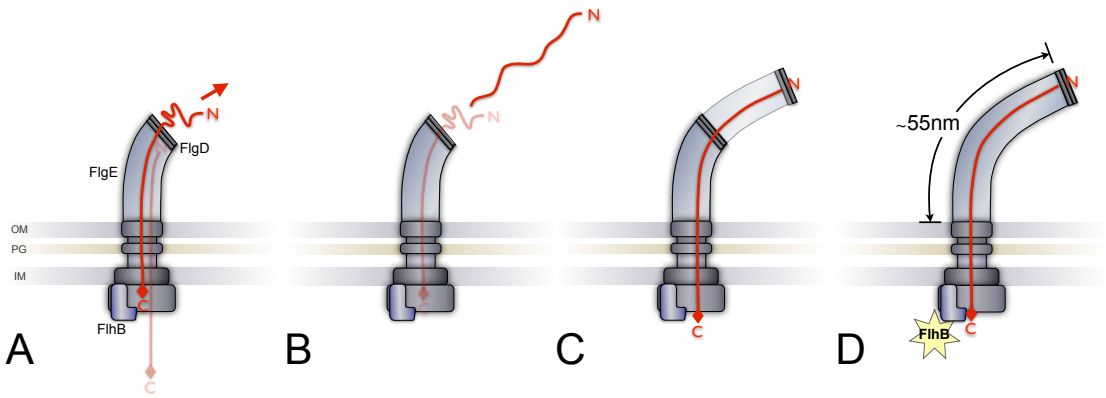

FIGURE 5.11

Model of hook-length determination by the Infrequent Ruler mechanism. (A) FliK is intermittently secreted during hook polymerization. During FliK secretion, hook polymerization temporarily halts and the N-terminus of FliK interacts with assembled FlgE and FlgD subunits during its secretion. The lack of interactions in short hooks or the folding of the secreted FliK N-terminus as it exits the secretion channel rapidly pulls the FliK molecule past FlhB through the channel without induction of the secretion specificity switch (see text for details). (B) FliK is secreted outside of the cell and hook polymerization continues. (C) The hook has grown to the physiological (or longer) length (here: 55 nm). A new FliK molecule is secreted and this time secretion is slower because of more frequent interactions of the FliK N-terminus with assembled hook subunits. Additionally, the N-terminus of FliK is not yet secreted outside of the cell where its folding might enhance secretion. (D) The C-terminus of FliK is now closely aligned to FlhB and the slower rate of FliK secretion allows for sufficient time for a productive FliK-FlhB interaction that induces the secretion specificity switch (indicated by a yellow star; FliK colored in red).

For small hook lengths, induction of the switch is unlikely presumably because FliK is secreted too fast for a productive interaction with FlhB. Likewise, for hooks of physiological or longer length virtually every secreted FliK molecule flips the secretion specificity switch. Here, we show that as predicted by the model, the switch to late-substrate secretion is immediately induced upon FliK secretion in hooks greater than the physiological length. Importantly, the experimental data displayed excellent agreement with the predicted probability curves calculated using mathematical models of the Infrequent Ruler mechanism. We furthermore provide experimental evidence for the suggested mechanism where FliK is secreted faster in shorter hooks than in longer ones thus explaining the greater probability of a productive FliK-induced specificity switch in hooks with increasing length.

It has to be stressed, that the Infrequent Ruler model proposed here accounts for all published data on flagellar hook length control. The Infrequent Ruler model predicts that more frequent measurements of hook length by an increased rate of FliK secretion would result in shorter hook lengths. More frequent measurement would increase the probability of a productive interaction of FliK with the secretion apparatus that would flip the specificity switch. Shorter hooks have indeed been observed under conditions where FliK measures hook length more frequently, e.g. overexpression of FliK (131, 150), underexpression of FlgE (149) or hook length in a hook-polymerization defective mutant (145). Similarly, the model predicts that overexpression of the hook subunit FlgE or under-expression of FliK would result in longer hooks because of less frequent or even only one measurement during hook assembly, and this has also been reported previously (149, 150). Recently, it has been shown that wildtype and FlhB variants had similar kinetic profiles and apparent affinities suggesting that the specificity switch is more complex (146). An increased velocity of FliK secretion in hooks shorter than the physiological length could account for these observations.

However, recent results from the homologous needle length control system in *Yersinia* resulted in an opposing model in which a single, static ruler is attached inside the secretion channel throughout needle polymerization (195). While using an elegant experimental approach employing merodiploid bacteria expressing YscP rulers of different sizes, the conclusions of the authors are not in agreement with previously published data and the results presented here for the flagellar system. It appears likely that, although closely related on a functional level, the actual mechanism of length control could be different in the two systems. It has been shown for the flagellar hook length control system, that the molecular ruler FliK is secreted during hook polymerization (131), thus arguing against a 'static-ruler' mechanism at least for the flagellar system. In addition, the secretion channel of the flagellar system is too narrow to accommodate a static FliK molecule and hook subunits that need to pass by during hook polymerization at the same time (171). A general problem of the 'static-ruler' model is the pre-requisite of an attachment of the ruler molecule to the capping protein of the growing structure. However, up-to-date no capping protein has been identified for the injectisome needle system.

In summary, we believe that the strong agreement between the published data on hook length control by FliK, our experimental results and the mathematical models presented

here provide convincing evidence in favor of the proposed Infrequent Ruler mechanism for flagellar hook length control in *Salmonella*. We note that the proposed Infrequent Ruler model would explain equally well termination of needle length polymerization in *Yersinia* as an alternative to the 'static-ruler' model.

5.5 Materials and Methods

Bacterial strains, plasmids and media

All bacterial strains used in this study are listed in Table 5.1. Cells were cultured in lysogeny broth (LB). A concentration of 100 µg/ml ampicillin, 15 µg/ml tetracycline and 0.2% (w/v) arabinose was supplemented as needed. The generalized transducing phage of *S. typhimurium* P22 HT105/1 *int-201* was used in all transductional crosses (168).

TABLE 5.1 ***Salmonella enterica*** **serovar** ***Typhimurium*** **strains used in this study.**

Strain number	Genotype	Reference
TH3730	$P_{flhDC5451}$::TPOP	(80)
TH6701	Δ*araBAD925*::*tetRA*	lab collection
TH16791	Δ*araBAD7606*::*fliK*$^+$ Δ*fliK6140* $P_{flhDC5451}$::TPOP	this study
TH16941	Δ*araBAD7606*::*fliK*$^+$ *flgE7742*::3xHA Δ*fliK6140* $P_{flhDC5451}$::TPOP	this study
TH16996	Δ*araBAD1089*::*fliK*(*fliK*'140-*yscP*(217-381)-141'*fliK*) Δ*fliK6140* $P_{flhDC5451}$::TPOP	this study
TH16997	Δ*araBAD1090*::*fliK*(Δaa161-200) Δ*fliK6140* $P_{flhDC5451}$::TPOP	this study
TH17011	Δ*araBAD1089*::*fliK*(*fliK*'140-*yscP*(217-381)-141'*fliK*) *flgE7742*::3xHA Δ*fliK6140* $P_{flhDC5451}$::TPOP	this study
TH17012	Δ*araBAD1090*::*fliK*(Δaa161-200) *flgE7742*::3xHA Δ*fliK6140* $P_{flhDC5451}$::TPOP	this study
TH17069	Δ*araBAD7606*::*fliK*$^+$ ΔflgE7599 Δ*fliK6140* $P_{flhDC5451}$::TPOP	this study
TH17076	Δ*araBAD7606*::*fliK*$^+$ *flhB7152*(N269A) Δ*fliK6140* $P_{flhDC5451}$::TPOP	this study
TH17112	Δ*araBAD7606*::*fliK*$^+$ ΔflgE7599 *flhB7152*(N269A) Δ*fliK6140* $P_{flhDC5451}$::TPOP	this study

FliK secretion assay, SDS-PAGE and Western Blotting

Levels of protein secretion were analyzed by Western blot. Overnight cultures were diluted 1:100 in LB media and grown for two hours at 37 ℃. Induction of flagellar genes was performed by addition of 15 µg/ml tetracycline. After an induction period of 60 minutes cells were spun down and washed twice with equal volumes of PBS to remove tetracycline. Subsequently, cells were resuspended in LB media containing 0.2% L-arabinose to induce FliK production. Samples were taken at different time points up to 45 minutes after arabinose induction. The optical density at 600 nm was determined immediately for all samples. 1.5 ml aliquots of the cell culture were centrifuged for 1 min at room temperature and 14,000 rpm to separate pellet and supernatant. The supernatant was filtered through a 0.2 µm low protein binding filter (Acrodisk Syringe Filter, PALL Life Sciences) to remove remaining cells. Secreted proteins in the filtered supernatant were precipitated by addition of final 10% TCA. The supernatant samples were resolved in Laemmli sample buffer (BIO-RAD) and adjusted to 20 OD units per µl. The cellular fraction was pelleted by centrifugation, the remaining supernatant was removed, and the pellet was adjusted to 20 OD units per µl in 2x SDS sample buffer. Expressed FliK and FliM levels of whole-cell lysate and cultural supernatant were subjected to SDS-PAGE on a 4-20% gradient gel (BIO-RAD). Equivalents of 200 and 300 OD units were loaded for the cellular and supernatant fractions, respectively. Protein levels were analyzed by immunoblotting using anti-FliK and anti-FliM antibodies (rabbit) for detection. To visualize antigen-antibody complexes, secondary anti-rabbit-IRDye^{690} antibodies (LI-COR) were used. Densiometric measurements of FliK and FliM bands were performed using the LI-COR Odyssey Infrared Imaging System software.

Isolation of hook-basal bodies, electron microscopy and measurements of hook-length

Hook-basal-body (HBB) isolation was carried out by the methods described in Aizawa et al. (7) with minor modifications. Flagellar samples were not collected by CsCl gradient centrifugation, but were pelleted at 60,000 x g for 1 hour using a Beckman 50.2Ti at 4 ℃. Purified hook-basal body samples were negatively stained with 2% uranyl acetate on copper coated grids. Images were captured using a Hitachi H-7100 electron microscope at an acceleration voltage of 125kV. Hook lengths were measured using NIH ImageJ 1.42q software.

Fluorescent microscopy

For fluorescent microscopy analysis of flagellar hooks and filaments, an overnight culture was diluted 1:100 in fresh media and cells were grown to mid-log phase. Afterwards, flagellar gene expression was induced by addition of 15 µg/ml tetracycline and *fliK* expression from the chromosomal *ara* locus was induced by addition of final 0.2% arabinose. About 30 µl cells were applied to a well formed by a poly-L-lysine treated coverslip separated by a double-sided sticky tape from a microsope slide. After immobilization, cells were fixed by addition of final 2% formaldehyde and 0.2% glutaraldehyde. Flagella were stained using polyclonal anti-FliC antibodies (rabbit) and anti-rabbit conjugated

Alexa Fluor^{488} secondary antibodies (Invitrogen). Hooks were stained using monoclonal anti-hemagglutinin conjugated to Alexa Fluor^{594} (Invitrogen). DNA staining was performed using Hoechst (Invitrogen). Images were collected with optical Z sections every 100 nm using an Applied Precision optical sectioning microscope and deconvolved using softWoRx v.3.4.2 (Applied Precision). The pixel data of individual Z sections of the deconvolved images were projected on a single plane using the Quick Projection tool (settings: maximal intensity) of softWoRx Explorer v1.3 (Applied Precision).

Mathematical model of the Infrequent Ruler hypothesis

The Infrequent Ruler mechanism hypothesis is that FliK is intermittently secreted during hook growth and that the probability of FliK interaction with FlhB leading to hook growth termination is an increasing function of the length of the hook at the time secretion of FliK occurs. We let $P_c(L)$ denote the probability of productive interaction of FliK leading to occurrence of the specificity switch when the hook is length L. The rate at which FliK secretion occurs is $ar(L)$, where $r(L)$ is the rate of secretion of all secretants, and a is the fraction of secreted molecules that are FliK. We let P be the probability that hook growth is terminated at length less than or equal to L. Since the overall rate of productive interaction of FliK is $ar(L)\ P_c(L)$, the time rate of change of P is given by

$$\frac{dP}{dt} = ar(L)P_c(L)(1-P), \tag{5.1}$$

and that of L is

$$\frac{dL}{dt} = br(L)\Delta, \tag{5.2}$$

where b is the fraction of secreted molecules that are FlgE, and Δ is the length increment from polymerization of a single FlgE molecule. It follows (dividing equation (5.1) by equation (5.2)) that

$$\frac{dP}{dL} = \beta P_c(L)(1-P), \tag{5.3}$$

where $\beta = \frac{a}{b\Delta}$.

If testing with FliK begins when the hook is length L_0, then $P(L_0) = 0$. To clarify the notation, we let $P(L|L_0)$ be the probability that a hook is terminated at length L given that testing was initiated at length L_0. Then, solving equation (5.3) subject to $P(L_0|L_0) = 0$ we find

$$P(L|L_0) = 1 - \exp\left(-\beta \int_{L_0}^{L} P_c(\eta)d\eta\right). \tag{5.4}$$

This equation can be used to determine $P_c(L)$ from $P(L|L_0)$ by rewriting it as

$$-\beta \int_{L_0}^{L} P_c(\eta)d\eta = -\ln(1 - P(L|L_0)). \tag{5.5}$$

We can use the experimentally obtained hook length data from the wildtype sample (Figure 5.4D, left panel) to estimate the function $P_c(L)$. The CDF (cumulative distribution function) for this data is shown in Figure 5.4D, with data points shown as asterisks. The data shown in Figure 5.4D are replotted as $-\ln(1-P(L))$ vs. L as shown in Figure 5.5A. The solid curve in this figure is the function

$$G(L) = \frac{1}{\rho}\ln\left(1-\exp(-\alpha\hat{L})+\exp(\alpha(L-\hat{L})\right), \tag{5.6}$$

with $\hat{L} = 39\text{nm}$, $\alpha = 0.66\text{nm}^{-1}$, and $\rho = 3$, determined by a simple visual fit. This allows us to estimate $\beta P_c(L)$ as

$$\beta P_c(L) = \frac{dG}{dL} = \frac{\alpha\exp(\alpha(L-\hat{L}))}{\rho(1-\exp(-\alpha\hat{L})+\exp(\alpha(L-\hat{L}))}, \tag{5.7}$$

shown in Figure 5.5B. The solid curve shown in Figure 5.4D is the CDF $P(L|0)$ as determined from equation (5.4) using the function $P_c(L)$ given in equation (5.7). The second data set is polyhook data, determined from a culture in which there was no FliK induction. The histogram of lengths is shown in Figure 5.4C (middle panel) and the CDF for this collection of polyhooks is shown in Figure 5.4D (middle panel). To use the information provided by this data, we need a representation of the CDF, $P_p(L)$ (subscript p for 'polyhook'). We found an excellent fit of the data using a function of the form $P_p(L) = \exp(f(L))$, where $f(L)$ is a fifth order polynomial. The details of this polynomial are not informative and so are not provided here. A plot of $P_p(L)$ is shown as a curve in Figure 5.4D (middle panel).

The third type of data is from a culture grown for 75 minutes, with induction of FliK at time $T_0 = 45$ minutes (Figure 5.4 right panel). To predict this distribution from $P_c(L)$ and $P_p(L)$, we first note that the function $P_p(L)$ gives information about when hooks were initiated. That is, suppose induction of FliK is started at the time that polyhooks of length L^* in Figure 5.4 (middle panel) are just initiated. This means that at the time of FliK induction $P_p(L^*)$ have yet to be initiated, and the length distribution of hooks already initiated is given by $p_p(L+L^*)$, where $p_p(L) = \frac{d}{dL}P_p(L)$ (with a slight caveat mentioned in Results). It follows that the distribution of hooks lengths produced by late induction of FliK is given by

$$P_i(L) = P(L|0)P_p(L^*) + \int_0^L P(L|L_0)p_p(L_0+L^*)dL_0. \tag{5.8}$$

5.6 Acknowledgements

This work was supported by PHS grant GM056141 (to K.T.H.) from the National Institutes of Health and NSF grant DMS-0718036 (to J.P.K.). We thank Nao Moriya and Tohru Minamino for providing the FliK antibody. We also thank the Hughes lab for discussions of the manuscript. M.E. and H.M.S gratefully acknowledge scholarship support of the Boehringer Ingelheim Fonds.

Concluding Remarks

The bacterial flagellum is a complex nanomachine assembled from dozens of proteins and its construction is coordinated by the coupling of flagellar gene regulation to the state of the assembly process.

At the center of the flagellum resides a specialized type III export system that is responsible for the secretion of most extra-cytoplasmic components of the nanomachine. Although the players involved in type III secretion have been known for some time, the molecular details of the actual export process remained unclear. Perhaps the most significant advance in recent years has been our discovery that the export process *per se* is energized by the means of the proton motive force and does not require ATP hydrolysis by the ATPase FliI. We demonstrated in Chapter 1 that treatment with the protonophore CCCP prevented export of flagellar substrates showing that the type III secretion system of the flagellum functions as a proton-driven protein export machine. Surprisingly, a mutant strain deleted for the flagellar-specific ATPase FliI, and type III injectisome-related ATPases InvJ and SsaN, displayed weak motility and rare formation of flagella. These results indicate a possible alternative role for ATP hydrolysis in type III secretion that is distinct from the actual protein translocation. A reasonable proposal is that the ATPase functions in conjunction with the cargo-delivery complex in substrate delivery, cargo release or unfolding prior to secretion. Furthermore, these results are consistent with the observation that secretion of effector proteins by the type III injectisome of *Yersinia enterocolitica* is inhibited by the addition of uncouplers (200). The use of the proton gradient as an energy source for type III secretion is not surprising given the speed of the export process. Several thousand amino acid residues per second are exported at early stages of filament assembly or translocated into eukaryotic host cell in case of the flagellum and type III injectisome, respectively (74, 170). This rapid translocation process requires a rapid supply of energy, which likely is more easily provided by the PMF than by hydrolysis of ATP.

The surprising discovery that highly conserved proteins, like the type III secretion ATPase FliI appeared not to be required for the export process *per se*, encouraged us to further dissect the minimal protein components of the flagellar type III secretion apparatus. In Chapter 2 we utilized random transposon mutagenesis in conjunction with a positive selection for secretion via the type III secretion apparatus to assess the requirement of the cytoplasmic rotor-switch complex (C-ring) in flagellar type III protein export. A β-lactamase reporter protein was fused to a flagellar type III secretion-specific sub-

strate. If a functional flagellar type III export apparatus is present, the reporter fusion protein translocates into the periplasm where it can confer resistance against ampicillin. Duplications of the *flhDC* operon region and transposon insertions in various flagellar regulatory loci were isolated. We found that any condition that resulted in at least two-fold increase in expression of the flagellar master regulator $FlhD_4C_2$ would overcome the requirement of the C-ring and the ATPase complex FliHIJ in flagellar type III secretion. This was the case if the *flhDC* region was duplicated or if transposons inserted into negative regulators of *flhDC* expression or $FlhD_4C_2$ activity, like *lrhA*, *ecnR* or *ydiV*. The increased expression of $FlhD_4C_2$ coincided with an two-fold increase in number of assembled hook basal body complexes per cell. Increased concentration of the activator of Class II transcription, $FlhD_4C_2$, enhances expression of flagellar secretion substrates and components of the flagellar type III secretion apparatus. The combination of increased substrate concentrations and enhanced numbers of available secretion systems allowed for significant secretion of the reporter protein even in the absence of the cytoplasmic C-ring. These findings suggested that the main role of the C-ring is as the rotor of the flagellum and its function in type III secretion is limited. We proposed that under physiological conditions the C-ring serves as a non-essential affinity cup-like structure that locally increases concentration of substrates prior to export by the type III secretion system.

We next employed the β-lactamase reporter protein fused to the flagellar hook to dissect the functional roles of every component of the flagellar export system. In Chapter 3 we quantified secretion of the reporter protein into the periplasm in mutants deleted for export apparatus components. Consistent with the results in Chapter 1 and 2, the ATPase FliI and other soluble components of the flagellar type III secretion system, as well as the rotor-switch complex (FliGMN) were dispensable for export under conditions where excess substrate was provided. We were also able to measure significant type III export in a mutant strain, where both the cytoplasmic C-ring and the ATPase complex were deleted. The export in this deletion background could be increased by overexpression of membrane components of the secretion apparatus, most prominently FliP, or transposon insertions in negative regulators of flagellar gene expression. These results solidify and extend the above mentioned model, where cytoplasmic components of the flagellar type III secretion system are of secondary importance and not strictly required for the actual export process. A surprising finding was that export could occur even in the absence of the MS-ring that was thought to enclose the type III secretion system. Initially, we performed a random transposon mutagenesis in a strain deleted for *fliF* selecting for export of the reporter protein. We isolated insertions in genes related to *flhDC* regulation that would result in generally elevated flagellar gene expression, similar to our findings in Chapter 2. The overexpression of FliP, FliQ and FlhA also greatly increased export in the absence of the MS-ring indicating that these membrane components were able to nucleate independently of the MS-ring if expressed at high enough levels. Overexpression of FliP was most effective in all deletion backgrounds, which could be explained with the interpretation that FliP forms the core channel of the flagellar type III secretion apparatus. These findings prompted us to test export in a strain deleted for all flagellar genes. We could indeed show that export of the reporter protein

is possible if only FliP is present to catalyze substrate translocation. Model building of the transmembrane domains of FliP revealed that a possible channel of appropriate diameter could be formed by three FliP molecules (Figure 3.9). In this hypothetical channel, the transmembrane segments of the FliP subunits are orientated in a way that large hydrophobic residues form a substrate-enfolding gasket near the periplasmic side that would have striking similarity to the 'phenylalanine-clamp' inside the anthrax-toxin channel (97). In our hypothesis for the mechanism of type III secretion, multiple copies of FliP form the substrate channel, FliQ and FliR have a structural role in stabilizing the channel and FlhA and FlhB are arranged around the pore, where their cytoplasmic domains interact with the substrate or cargo-delivery complex. FlhA has several invariant acidic and basic residues that could function in proton binding and conduction. In this model, the proton movement in FlhA would energize the substrate translocation by cyclic conformational changes of its cytoplasmic domain. A dynamic domain motion of the C-terminal domain of FlhA is possible based on the recently solved structure of the cytoplasmic domain of FlhA and mutational analysis (162).

The discovery that a single flagellar membrane protein, FliP, can catalyze translocation of a flagellar substrate has important evolutionary implications. It has been suggested by intelligent designers that the bacterial flagellum is of irreducible complexity because it would have required co-evolution of numerous components, and thus its natural evolution would have been highly improbable (16). However, our results show that a rudimentary channel, formed by an ancestral FliP protein, might have provided some useful transport activity on which selection could have acted to stepwise add other components eventually resulting in the present day, highly specialized and highly evolved flagellum.

A flexible coupling structure, the hook, connects the flagellar basal body with the rigid filament. Length of the flagellar hook is highly regulated in *Salmonella enterica* and hook polymerization is terminated at a length of 55 $\pm$ 6 nm (67). Termination of hook growth coincides with a switch in substrate specificity of the flagellar type III secretion apparatus at the base of the structure. After the switch, the secretion system ceases export of rod-hook-type substrates and secretes late secretion substrates, like the filament subunits. A cleavage of the C-terminal, cytoplasmic domain of the FlhB component of the export apparatus is the pre-requisite for the specificity switch. For an efficient switch, however, a productive interaction of the C-terminus of FliK with FlhB must occur. This interaction presumably induces a conformational change in FlhB and results in the secretion substrate specificity switch. The FliK protein is considered to function as a molecular ruler, similar to the Yop secretion protein P (YscP) of *Yersinia* that has been demonstrated to control length of injectisome needles (78).

The fundamental question has been, how the cell determines the correct length of the external hook structure and how this information is transferred back to the secretion apparatus that is embedded in the inner membrane. Several models of how flagellar hook length is regulated have been proposed, including 'measuring cup', 'static ruler' or 'infrequent ruler' mechanisms (see INTRODUCTION for more details). In this work, we provide experimental evidence that refute the 'measuring cup' model for hook length determination and support a mechanism for flagellar hook length control by an infrequent,

molecular ruler.

In the flagellar hook length control system, a molecular ruler mechanism was initially discarded because intramolecular deletions of FliK resulted in hooks of uncontrolled length instead of shorter ones (84). As an alternative model, it was proposed that the cytoplasmic rotor-switch complex (C-ring) functions as a measuring cup that would fill up with the appropriate number of hook subunits needed to build a hook of correct length (120). In Chapter 4 we demonstrated normal hook length control even in the complete absence of the C-ring, thus refuting the 'measuring cup' model. We found that the mutants of the C-ring components that were reported by Kawagishi et al. to produce shorter hooks (84) are in fact deficient in hook-basal-body assembly. As discussed later, an 'infrequent ruler' mechanisms would account for shorter hooks in an assembly-deficient mutant because this would coincide with more frequent measurements of hook length in the time needed to assemble a hook of physiological length. In a previous study, FliK deletion variants were constructed that retain hook length control, but were apparently not secreted (172). Using an optimized detection method, we showed in Chapter 4 that these FliK deletion variants are in fact secreted, thus demonstrating that secreted FliK directly measures hook length, similar to the mechanism of needle length control.

Our suggested 'Infrequent Ruler' model accounts for all published data on hook length control. In this model, FliK is intermittently secreted during hook polymerization. Shorter hooks will be made if FliK measures hook length more frequently during the time it takes for completion of the hook-basal-body. This is the case if the ruler is overexpressed or hook subunits are less expressed, while contrary the overexpression of hook subunits or underexpression of FliK would result in longer hooks and in fact all this has been published (131, 149, 150). The 'Infrequent Ruler' model for hook length determination can be described by a mathematical model. This model predicts that the probability of a productive FliK interaction with the secretion apparatus is an increasing function of hook length (86).

In a next step, we sought experimental evidence in favor of the 'Infrequent Ruler' hypothesis. In this model, hook length is measured by intermittent secretion of FliK ruler molecules and hook polymerization will continue until a secreted FliK molecule is in close proximity and provided with sufficient time for a productive interaction with the FlhB component of the export apparatus. This interaction would then result in the specificity switch. Possible molecular mechanisms that would allow sufficient time for this interaction include the possibility that the velocity of FliK secretion is dependent on hook length. Interactions of the FliK N-terminus with assembled hook subunits and the hook cap could slow-down FliK secretion in elongated hooks (139, 145). Alternatively, and not mutually exclusive, the nascent N-terminus of the secreted FliK molecule could start to fold as the molecule exits the secretion channel in short hooks. This folding could act as a Brownian ratchet that would rapidly pull the C-terminus of the ruler molecule past the secretion apparatus without time for a productive interaction with FlhB (86).

Accordingly, FliK secretion in short hooks should be unlikely to induce a secretion specificity switch. However, every secreted FliK molecule should flip the secretion speci-

ficity switch in hooks of physiological length or longer. In Chapter 5 we demonstrated that indeed the first FliK molecule that is secreted in elongated hooks induced the switch to late-substrate secretion as predicted by the model. Importantly, the experimental hook length data showed excellent agreement with the above mentioned mathematical model of the hook termination process by the 'Infrequent Ruler' mechanism. Additionally, the 'Infrequent Ruler' model predicts that FliK is secreted faster in short hooks than in elongated hooks. We tested the velocity of FliK secretion in synchronized cells where FliK was either secreted through a elongated hook structure or through a basal-body missing the hook completely. We found that FliK was secreted at significantly higher levels through a basal-body structure missing the hook than through an elongated hook structure. These results provide experimental evidence for the mechanism where the velocity of FliK secretion determines its probability for a productive interaction with the secretion apparatus.

Taken together, the proposed 'Infrequent Ruler' model for hook length determination does not only account for all published data on flagellar hook length control, but also explains equally well termination of needle polymerization in *Yersinia* where currently a 'static ruler' model is favored. Future research should test if the needle length regulator YscP is also intermittently secreted and able to induce the switch to late-substrate secretion in elongated needles, like it is the case in the flagellar hook length control system.

Future perspectives

In the past decades significant progress has been made in the visualization of the overall flagellar structure and function. High-resolution structures of several key components, like the cytoplasmic ATPase (76), the rotor-switch complex proteins (25, 26, 155, 188), the flagellar hook (166, 171) and the flagellar filament (165, 209) are now available. In addition with 3D-EM image reconstructions of the flagellar hook-basal-body we now have a relatively comprehensive picture of the overall structure of this fascinating nanomachine (40, 188). The assembly of the flagellum is a highly regulated and coordinated process. Many sub-structures have the ability for self-assembly while the assembled flagellum still retains a uniform shape. This is partially made possible by unique length control mechanisms, as for example for the length control of the hook. Many competing models for the mechanisms of hook length determination have been proposed. As illustrated above, we described in this work a unifying model that accounts for all published data on hook length control (43). We present experimental data that provide strong evidence in favor of this 'Infrequent Ruler' mechanism for hook length determination in which FliK takes measurements of hook length while being intermittently secreted during the assembly process of the hook-basal-body complex. The three-dimensional structure of FliK is missing and if eventually obtained should provide much of the still needed information how the ruler can transmit length informations of the hook back to the export components embedded in the inner membrane. Future research should accordingly focus on the mechanisms of the secretion specificity switch. A cleavage of the cytoplasmic C-terminal domain of FlhB is a pre-requisite for the specificity switch, however nothing

is known about the nature of the conformational change that ultimately constitutes the switch within the type III secretion system.

On related matters, we know now that the export of flagellar substrates via the flagellar type III secretion apparatus is in fact energized using the proton motive force and not by ATP hydrolysis as previously thought (140, 158). In addition, we accumulated evidence suggesting that many components of the export apparatus have a supporting role in facilitating the actual secretion process, but are dispensable under certain conditions. The cytoplasmic C-ring, for example, appears to have a primary function as the rotor of the flagellum and only in a secondary role acts as an affinity-cup like structure to facilitate efficient substrate delivery to the export system (44). In fact, we obtained evidence that suggested that the membrane protein FliP forms the central proton-conducting channel of the flagellar type III secretion apparatus. Unfortunately, structural informations about the membrane components is lacking and further mechanistic data is limited. Accordingly, obtaining structural and mechanistic informations about how proton influx is coupled to the protein export process remains the most challenging goal in the field of type III secretion.

References

(1) **Aberg, A., Fernández-Vázquez, J., Cabrer-Panes, J. D., Sánchez, A. and Balsalobre, C.** (2009); Similar and divergent effects of ppGpp and DksA deficiencies on transcription in *Escherichia coli*; *Journal of Bacteriology*; **191** (10): 3226–36. (cited on page 33)

(2) **Abramoff, M., Magelhaes, P. J. and Ram, S. J.** (2004); Image Processing with ImageJ; *Biophotonics International*; **11** (7): 36–42. (cited on pages 57 und 89)

(3) **Adler, J. and Templeton, B.** (1967); The effect of environmental conditions on the motility of *Escherichia coli*; *Journal of General Microbiology*; **46** (2): 175–184. (cited on page 1)

(4) **Agrain, C., Callebaut, I., Journet, L., Sorg, I., Paroz, C., Mota, L. J. and Cornelis, G. R.** (2005); Characterization of a Type III secretion substrate specificity switch (T3S4) domain in YscP from *Yersinia enterocolitica*; *Molecular Microbiology*; **56** (1): 54–67. (cited on pages 15, 101 und 124)

(5) **Aizawa, S. I.** (1996); Flagellar assembly in *Salmonella typhimurium*; *Molecular Microbiology*; **19** (1): 1–5. (cited on page 2)

(6) **Aizawa, S. I.** (2009); What is essential for flagellar assembly?; *Jarrell K, editor. Pili and Flagella: Current Research and Future Trends*; (p. 238). (cited on page 63)

(7) **Aizawa, S. I., Dean, G. E., Jones, C. J., Macnab, R. M. and Yamaguchi, S.** (1985); Purification and characterization of the flagellar hook-basal body complex of *Salmonella typhimurium*; *Journal of Bacteriology*; **161** (3): 836–49. (cited on page 141)

(8) **Aizawa, S. I., Vonderviszt, F., Ishima, R. and Akasaka, K.** (1990); Termini of *Salmonella* flagellin are disordered and become organized upon polymerization into flagellar filament; *Journal of Molecular Biolology*; **211** (4): 673–7. (cited on page 63)

(9) **Akeda, Y. and Galan, J. E.** (2005); Chaperone release and unfolding of substrates in type III secretion; *Nature*; **437** (7060): 911–5. (cited on pages 9, 13, 18, 25 und 30)

(10) **Aldridge, P., Karlinsey, J. E., Becker, E., Chevance, F. F. V. and Hughes, K. T.** (2006); Flk prevents premature secretion of the anti-σ factor FlgM into the periplasm; *Molecular Microbiology*; **60** (3): 630–643. (cited on page 27)

(11) **Aldridge, P. D., Karlinsey, J. E., Aldridge, C., Birchall, C., Thompson, D., Yagasaki, J. and Hughes, K. T.** (2006); The flagellar-specific transcription factor, σ^{28}, is the Type III secretion chaperone for the flagellar-specific anti-σ^{28} factor FlgM; *Genes & Development*; **20** (16): 2315–2326. (cited on pages 7 und 63)

(12) **Anderson, R. P. and Roth, J. R.** (1978); Tandem genetic duplications in *Salmonella typhimurium*: amplification of the histidine operon; *Journal of Molecular Biology*; **126** (1): 53–71. (cited on page 34)

(13) **Arnam, J. S. V., McMurry, J. L., Kihara, M. and Macnab, R. M.** (2004); Analysis of an engineered *Salmonella* flagellar fusion protein, FliR-FlhB; *Journal of Bacteriology.*; **186** (8): 2495–2498. (cited on page 82)

(14) **Bakker, E. P. and Mangerich, W. E.** (1983); The effects of weak acids on potassium uptake by *Escherichia coli* K-12 inhibition by low cytoplasmic pH; *Biochimica et Biophysica Acta*; **730** (2): 379–86. (cited on page 26)

(15) **Barker, C. S., Meshcheryakova, I. V., Kostyukova, A. S. and Samatey, F. A.** (2010); FliO Regulation of FliP in the Formation of the *Salmonella enterica* Flagellum; *PLoS Genetics*; **6** (9). (cited on pages 65 und 66)

(16) **Behe, M. J.**; Darwin's Black Box: The Biochemical Challenge to Evolution (New York: Free Press, 1996). (cited on pages 84 und 147)

(17) **Berg, H.** (2003); The rotary motor of bacterial flagella; *Annual Review of Biochemistry*; **72**: 19–54. (cited on pages 30 und 63)

(18) **Berg, H. C. and Anderson, R. A.** (1973); Bacteria swim by rotating their flagellar filaments; *Nature*; **245** (5425): 380–382. (cited on pages 1, 30, 63, 98 und 122)

(19) **Blair, D. F.** (2006); Fine structure of a fine machine; *Journal of Bacteriology*; **188** (20): 7033–5. (cited on page 2)

(20) **Blair, D. F.** (2009); Structure and mechanism of the flagellar rotary motor; *Jarrell K, ed.. Pili and Flagella: Current Research and Future Trends*; (p. 238). (cited on page 63)

(21) **Blair, D. F. and Berg, H. C.** (1990); The MotA protein of *E. coli* is a proton-conducting component of the flagellar motor; *Cell*; **60** (3): 439–49. (cited on page 5)

(22) **Blocker, A., Komoriya, K. and Aizawa, S.** (2003); Type III secretion systems and bacterial flagella: insights into their function from structural similarities; *Proc Natl Acad Sci USA*; **100** (6): 3027–30. (cited on pages 11, 18, 63 und 122)

(23) **Brown, J., Faulds-Pain, A. and Aldridge, P.** (2009); The coordination of flagellar gene expression and the flagellar assembly pathway; *Jarrell K, editor. Pili and Flagella: Current Research and Future Trends*; (p. 238). (cited on page 63)

(24) **Brown, J. D., Saini, S., Aldridge, C., Herbert, J., Rao, C. V. and Aldridge, P. D.** (2008); The rate of protein secretion dictates the temporal dynamics of flagellar gene expression; *Molecular Microbiology*; **70** (4): 924–37. (cited on pages 105 und 119)

(25) **Brown, P., Hill, C. and Blair, D.** (2002); Crystal structure of the middle and C-terminal domains of the flagellar rotor protein FliG.; *EMBO Journal*; **21** (13): 3225–34. (cited on page 149)

(26) **Brown, P., Mathews, M., Joss, L., Hill, C. and Blair, D.** (2005); Crystal structure of the flagellar rotor protein FliN from *Thermotoga maritima.*; *Journal of Bacteriology.*; **187** (8): 2890–902. (cited on page 149)

(27) **Chevance, F. F. V. and Hughes, K. T.** (2008); Coordinating assembly of a bacterial macromolecular machine; *Nature Reviews Microbiology*; **6** (6): 455–65. (cited on pages 1, 5, 9, 15, 30, 32, 63, 99, 100 und 122)

(28) **Chevance, F. F. V., Takahashi, N., Karlinsey, J. E., Gnerer, J., Hirano, T., Samudrala, R., Aizawa, S.-I. and Hughes, K. T.** (2007); The mechanism of outer membrane penetration by the eubacterial flagellum and implications for spirochete evolution; *Genes & Development*; **21** (18): 2326–35. (cited on page 99)

(29) **Chun, S. Y. and Parkinson, J. S.** (1988); Bacterial motility: membrane topology of the *Escherichia coli* MotB protein; *Science*; **239** (4837): 276–8. (cited on page 5)

(30) **Claret, L., Calder, S. R., Higgins, M. and Hughes, C.** (2003); Oligomerization and activation of the FliI ATPase central to bacterial flagellum assembly; *Molecular Microbiology*; **48** (5): 1349–55. (cited on pages 9 und 65)

(31) **Clegg, S. and Hughes, K. T.** (2002); FimZ is a molecular link between sticking and swimming in *Salmonella enterica* serovar *Typhimurium*; *Journal of Bacteriology*; **184** (4): 1209–13. (cited on page 32)

(32) **Cornelis, G. R.** (2006); The type III secretion injectisome; *Nature Reviews Microbiology*; **4** (11): 811–25. (cited on pages 1, 11, 13, 18, 63, 101, 113 und 122)

(33) **Cornelis, G. R. and Gijsegem, F. V.** (2000); Assembly and function of type III secretory systems; *Annu Rev Microbiol*; **54**: 735–74. (cited on page 1)

(34) **Datsenko, K. A. and Wanner, B. L.** (2000); One-step inactivation of chromosomal genes in *Escherichia coli* K-12 using PCR products; *Proc Natl Acad Sci USA*; **97** (12): 6640–6645. (cited on page 84)

(35) **Davis, R. W., Botstein, D. and Roth, J. R.**; Advanced bacterial genetics (Cold Spring Harbor, New York: Cold Spring Harbor Laboratory, 1980). (cited on page 25)

(36) **Deane, J. E., Roversi, P., Cordes, F. S., Johnson, S., Kenjale, R., Daniell, S., Booy, F., Picking, W. D., Picking, W. L., Blocker, A. J. and Lea, S. M.** (2006); Molecular model of a type III secretion system needle: Implications for host-cell sensing; *Proc Natl Acad Sci USA*; **103** (33): 12,529–33. (cited on page 13)

(37) **Delalez, N. J., Wadhams, G. H., Rosser, G., Xue, Q., Brown, M. T., Dobbie, I. M., Berry, R. M., Leake, M. C. and Armitage, J. P.** (2010); Signal-dependent turnover of the bacterial flagellar switch protein FliM; *Proc Natl Acad Sci USA*; **107** (25): 11,347–51. (cited on page 2)

(38) **DePamphilis, M. L. and Adler, J.** (1971); Fine structure and isolation of the hook-basal body complex of flagella from *Escherichia coli* and *Bacillus subtilis*; *Journal of Bacteriology.*; **105** (1): 384–395. (cited on page 1)

(39) **DePamphilis, M. L. and Adler, J.** (1971); Purification of intact flagella from *Escherichia coli* and *Bacillus subtilis.*; *Journal of Bacteriology.*; **105** (1): 376–383. (cited on page 1)

(40) **Derosier, D.** (2006); Bacterial flagellum: visualizing the complete machine *in situ*; *Current Biology*; **16** (21): R928–30. (cited on pages 10 und 149)

(41) **Dreyfus, G., Williams, A. W., Kawagishi, I. and Macnab, R. M.** (1993); Genetic and biochemical analysis of *Salmonella typhimurium* FliI, a flagellar protein related to the catalytic subunit of the F_0F_1 ATPase and to virulence proteins of mammalian and plant pathogens; *Journal of Bacteriology*; **175** (10): 3131–8. (cited on page 25)

(42) **Ellermeier, C. D. and Slauch, J. M.** (2003); RtsA and RtsB coordinately regulate expression of the invasion and flagellar genes in *Salmonella enterica* serovar *Typhimurium*; *Journal of Bacteriology*; **185** (17): 5096–108. (cited on page 33)

(43) **Erhardt, M., Hirano, T., Su, Y., Paul, K., Wee, D. H., Mizuno, S., Aizawa, S.-I. and Hughes, K. T.** (2010); The role of the FliK molecular ruler in hook-length control in *Salmonella enterica*; *Molecular Microbiology*; **75** (5): 1272–1284. (cited on pages 15, 16, 65, 66, 69, 124, 138 und 149)

(44) **Erhardt, M. and Hughes, K. T.** (2010); C-ring requirement in flagellar type III secretion is bypassed by FlhDC upregulation; *Molecular Microbiology*; **75** (2): 376–393. (cited on pages 66, 69, 79, 90, 103, 105 und 150)

(45) **Erhardt, M., Namba, K. and Hughes, K. T.** (2010); Bacterial Nanomachines: The Flagellum and Type III Injectisome; *Cold Spring Harbor Perspectives in Biology.* (cited on pages 10 und 12)

(46) **Evans, L. D. B., Stafford, G. P., Ahmed, S., Fraser, G. M. and Hughes, C.** (2006); An escort mechanism for cycling of export chaperones during flagellum assembly; *Proc Natl Acad Sci USA*; **103** (46): 17,474–9. (cited on pages 22 und 65)

(47) **Fan, F. and Macnab, R. M.** (1996); Enzymatic characterization of FliI. An ATPase involved in flagellar assembly in *Salmonella typhimurium*; *The Journal of Biological Chemistry*; **271** (50): 31,981–31,988. (cited on pages 9, 18, 25 und 63)

(48) **Ferris, H. U., Furukawa, Y., Minamino, T., Kroetz, M. B., Kihara, M., Namba, K. and Macnab, R. M.** (2005); FlhB regulates ordered export of flagellar components via autocleavage mechanism; *The Journal of Biological Chemistry*; **280** (50): 41,236–42. (cited on pages 13, 99, 100 und 105)

(49) **Ferris, H. U. and Minamino, T.** (2006); Flipping the switch: bringing order to flagellar assembly.; *Trends Microbiol.*; **14** (12): 519–526. (cited on pages 5 und 9)

(50) **Francis, N. R., Irikura, V. M., Yamaguchi, S., DeRosier, D. J. and Macnab, R. M.** (1992); Localization of the *Salmonella typhimurium* flagellar switch protein FliG to the cytoplasmic M-ring face of the basal body; *Proc Natl Acad Sci USA*; **89** (14): 6304–8. (cited on pages 2 und 65)

(51) **Francis, N. R., Sosinsky, G. E., Thomas, D. and DeRosier, D. J.** (1994); Isolation, characterization and structure of bacterial flagellar motors containing the switch complex; *Journal of Molecular Biolology*; **235** (4): 1261–70. (cited on page 65)

(52) **Fraser, G. M., González-Pedrajo, B., Tame, J. R. H. and Macnab, R. M.** (2003); Interactions of FliJ with the *Salmonella* type III flagellar export apparatus; *Journal of Bacteriology*; **185** (18): 5546–54. (cited on page 22)

(53) **Fraser, G. M., Hirano, T., Ferris, H. U., Devgan, L. L., Kihara, M. and Macnab, R. M.** (2003); Substrate specificity of type III flagellar protein export in *Salmonella* is controlled by subdomain interactions in FlhB; *Molecular Microbiology*; **48** (4): 1043–57. (cited on pages 13, 124 und 136)

(54) **Frye, J., Karlinsey, J. E., Felise, H. R., Marzolf, B., Dowidar, N., McClelland, M. and Hughes, K. T.** (2006); Identification of new flagellar genes of *Salmonella enterica* serovar *Typhimurium.*; *Journal of Bacteriology*; **188** (6): 2233–2243. (cited on page 5)

(55) **Galán, J. and Collmer, A.** (1999); Type III secretion machines: bacterial devices for protein delivery into host cells; *Science*; **284** (5418): 1322–8. (cited on page 1)

(56) **Galán, J. E. and Wolf-Watz, H.** (2006); Protein delivery into eukaryotic cells by type III secretion machines; *Nature*; **444** (7119): 567–73. (cited on pages 1, 11 und 101)

(57) **Galperin, M. Y., Dibrov, P. A. and Glagolev, A. N.** (1982); $\Delta\mu H^+$ is required for flagellar growth in *Escherichia coli*; *FEBS Letters.*; **143** (2): 319–322. (cited on page 25)

(58) **Gillen, K. L. and Hughes, K. T.** (1991); Molecular characterization of *flgM*, a gene encoding a negative regulator of flagellin synthesis in *Salmonella typhimurium*; *Journal of Bacteriology.*; **173** (20): 6453–9. (cited on pages 25 und 54)

(59) **Gillen, K. L. and Hughes, K. T.** (1991); Negative regulatory loci coupling flagellin synthesis to flagellar assembly in *Salmonella typhimurium*; *Journal of Bacteriology.*; **173** (7): 2301–10. (cited on pages 20 und 25)

(60) **González-Pedrajo, B., Minamino, T., Kihara, M. and Namba, K.** (2006); Interactions between C ring proteins and export apparatus components: a possible mechanism for facilitating type III protein export; *Molecular Microbiology*; **60** (4): 984–98. (cited on pages 2, 30, 32, 65, 66 und 79)

(61) **Goodier, R. I. and Ahmer, B. M.** (2001); SirA orthologs affect both motility and virulence; *Journal of Bacteriology*; **183** (7): 2249–58. (cited on pages 105, 118 und 119)

(62) **Gophna, U., Ron, E. Z. and Graur, D.** (2003); Bacterial type III secretion systems are ancient and evolved by multiple horizontal-transfer events; *Gene*; **312**: 151–63. (cited on page 13)

(63) **Hensel, M., Shea, J. E., Raupach, B., Monack, D., Falkow, S., Gleeson, C., Kubo, T. and Holden, D. W.** (1997); Functional analysis of *ssaJ* and the *ssaK/U* operon, 13 genes encoding components of the type III secretion apparatus of *Salmonella* Pathogenicity Island 2; *Molecular Microbiology*; **24** (1): 155–67. (cited on page 25)

(64) **Hirano, T., Minamino, T. and Macnab, R. M.** (2001); The role in flagellar rod assembly of the N-terminal domain of *Salmonella* FlgJ, a flagellum-specific muramidase; *Journal of Molecular Biology*; **312** (2): 359–69. (cited on page 2)

(65) **Hirano, T., Mizuno, S., Aizawa, S.-I. and Hughes, K. T.** (2009); Mutations in Flk, FlgG, FlhA, and FlhE That Affect the Flagellar Type III Secretion Specificity Switch in *Salmonella enterica*; *Journal of Bacteriology*; **191** (12): 3938–49. (cited on pages 16 und 116)

(66) **Hirano, T., Shibata, S., Ohnishi, K., Tani, T. and Aizawa, S.-I.** (2005); N-terminal signal region of FliK is dispensable for length control of the flagellar hook; *Molecular Microbiology*; **56** (2): 346–60. (cited on pages 16 und 115)

(67) **Hirano, T., Yamaguchi, S., Oosawa, K. and Aizawa, S.** (1994); Roles of FliK and FlhB in determination of flagellar hook length in *Salmonella typhimurium*; *Journal of Bacteriology.*; **176** (17): 5439–5449. (cited on pages 2, 5, 13, 63, 82, 100, 101, 102, 103, 107, 109, 120, 122, 124, 128 und 147)

(68) **Hodgkinson, J., Horsley, A., Stabat, D., Simon, M., Johnson, S., da Fonseca, P., Morris, E., Wall, J., Lea, S. and Blocker, A.** (2009); Three-dimensional reconstruction of the *Shigella* T3SS transmembrane regions reveals 12-fold symmetry and novel features throughout; *Nature Structural & Molecular Biology*; **16** (5): 477–85. (cited on page 11)

(69) **Homma, M., DeRosier, D. J. and Macnab, R. M.** (1990); Flagellar hook and hook-associated proteins of *Salmonella typhimurium* and their relationship to other axial components of the flagellum; *Journal of Molecular Biolology*; **213** (4): 819–832. (cited on page 5)

(70) **Homma, M., Komeda, Y., Iino, T. and Macnab, R. M.** (1987); The *flaFIX* gene product of *Salmonella typhimurium* is a flagellar basal body component with a signal peptide for export; *Journal of Bacteriology.*; **169** (4): 1493–1498. (cited on page 5)

(71) **Homma, M., Kutsukake, K., Hasebe, M., Iino, T. and Macnab, R. M.** (1990); FlgB, FlgC, FlgF and FlgG. A family of structurally related proteins in the flagellar basal body of *Salmonella typhimurium*; *Journal of Molecular Biolology*; **211** (2): 465–77. (cited on page 84)

(72) **Hueck, C.** (1998); Type III protein secretion systems in bacterial pathogens of animals and plants; *Microbiology and Molecular Biology Reviews*; **62** (2): 379–433. (cited on pages 13, 63 und 122)

(73) **Hughes, K. T., Gillen, K. L., Semon, M. J. and Karlinsey, J. E.** (1993); Sensing structural intermediates in bacterial flagellar assembly by export of a negative regulator; *Science*; **262** (5137): 1277–80. (cited on pages 5, 7, 13, 26, 32 und 63)

(74) **Iino, T.** (1969); Polarity of flagellar growth in *Salmonella*; *Journal of General Microbiology*; **56** (2): 227–39. (cited on pages 9 und 145)

(75) **Iino, T.** (1974); Assembly of *Salmonella* flagellin *in vitro* and *in vivo*.; *J. Supramol. Struct.*; **2** (2-4): 372–84. (cited on pages 18 und 63)

(76) **Imada, K., Minamino, T., Tahara, A. and Namba, K.** (2007); Structural similarity between the flagellar type III ATPase FliI and F1-ATPase subunits; *Proc Natl Acad Sci USA*; **104** (2): 485–90. (cited on pages 13 und 149)

(77) **Jensen, P. R. and Michelsen, O.** (1992); Carbon and energy metabolism of *atp* mutants of *Escherichia coli*; *Journal of Bacteriology*; **174** (23): 7635–41. (cited on page 66)

(78) **Journet, L., Agrain, C., Broz, P. and Cornelis, G. R.** (2003); The needle length of bacterial injectisomes is determined by a molecular ruler; *Science*; **302** (5651): 1757–60. (cited on pages 13, 15, 101, 112, 122, 124 und 147)

(79) **Journet, L., Hughes, K. T. and Cornelis, G. R.** (2005); Type III secretion: a secretory pathway serving both motility and virulence; *Molecular Membrane Biology*; **22** (1-2): 41–50. (cited on page 11)

(80) **Karlinsey, J. E., Tanaka, S., Bettenworth, V., Yamaguchi, S., Boos, W., Aizawa, S. I. and Hughes, K. T.** (2000); Completion of the hook-basal body complex of the *Salmonella typhimurium* flagellum is coupled to FlgM secretion and *fliC* transcription; *Molecular Microbiology*; **37** (5): 1220–31. (cited on pages 5, 105, 119, 123, 125 und 140)

(81) **Karlinsey, J. E., Tsui, H. C., Winkler, M. E. and Hughes, K. T.** (1998); Flk couples *flgM* translation to flagellar ring assembly in *Salmonella typhimurium*; *Journal of Bacteriology.*; **180** (20): 5384–5397. (cited on page 25)

(82) **Katsura, I.** (1987); Determination of bacteriophage λ tail length by a protein ruler; *Nature*; **327** (6117): 73–5. (cited on page 15)

(83) **Katsura, I. and Hendrix, R. W.** (1984); Length determination in bacteriophage λ tails; *Cell*; **39** (3 Pt 2): 691–8. (cited on page 15)

(84) **Kawagishi, I., Homma, M., Williams, A. W. and Macnab, R. M.** (1996); Characterization of the flagellar hook length control protein *fliK* of *Salmonella typhimurium* and *Escherichia coli*; *Journal of Bacteriology*; **178** (10): 2954–9. (cited on pages 15, 100, 124 und 148)

(85) **Kazetani, K., Minamino, T., Miyata, T., Kato, T. and Namba, K.** (2009); ATP-induced FliI hexamerization facilitates bacterial flagellar protein export; *Biochem Biophys Res Commun*; **388** (2): 323–7. (cited on page 65)

(86) **Keener, J. P.** (2010); A molecular ruler mechanism for length control of extended protein structures in bacteria; *Journal of Theoretical Biology*; **263** (4): 481–9. (cited on pages 16, 124, 136, 138 und 148)

(87) **Kelly, A., Goldberg, M. D., Carroll, R. K., Danino, V., Hinton, J. C. D. and Dorman, C. J.** (2004); A global role for Fis in the transcriptional control of metabolism and type III secretion in *Salmonella enterica* serovar *Typhimurium*; *Microbiology*; **150** (Pt 7): 2037–53. (cited on page 32)

(88) **Khan, I. H., Reese, T. S. and Khan, S.** (1992); The cytoplasmic component of the bacterial flagellar motor; *Proc Natl Acad Sci USA*; **89** (13): 5956–60. (cited on page 65)

(89) **Khan, S., Zhao, R. and Reese, T. S.** (1998); Architectural features of the *Salmonella typhimurium* flagellar motor switch revealed by disrupted C-rings; *Journal of Structural Biology*; **122** (3): 311–9. (cited on page 65)

(90) **Kimbrough, T. G. and Miller, S. I.** (2000); Contribution of *Salmonella typhimurium* type III secretion components to needle complex formation; *Proc Natl Acad Sci USA*; **97** (20): 11,008–13. (cited on page 11)

(91) **Kojima, S. and Blair, D. F.** (2004); The bacterial flagellar motor: structure and function of a complex molecular machine; *International Review of Cytology*; **233**: 93–134. (cited on pages 1, 5 und 98)

(92) **Komeda, Y., Suzuki, H., Ishidsu, J. I. and Iino, T.** (1976); The role of cAMP in flagellation of *Salmonella typhimurium*; *Molecular and General Genetics*; **142** (4): 289–98. (cited on page 32)

(93) **Komoriya, K., Shibano, N., Higano, T., Azuma, N., Yamaguchi, S. and Aizawa, S. I.** (1999); Flagellar proteins and type III-exported virulence factors are the predominant proteins secreted into the culture media of *Salmonella typhimurium*; *Molecular Microbiology*; **34** (4): 767–79. (cited on page 20)

(94) **Konishi, M., Kanbe, M., McMurry, J. L. and Aizawa, S. I.** (2009); Flagellar formation in C-ring-defective mutants by overproduction of FliI, the ATPase specific for flagellar type III secretion; *Journal of Bacteriology*; **191** (19): 6186–91. (cited on pages 15, 32, 65, 66, 79, 104 und 124)

(95) **Koroyasu, S., Yamazato, M., Hirano, T. and Aizawa, S. I.** (1998); Kinetic analysis of the growth rate of the flagellar hook in *Salmonella typhimurium* by the population balance method; *Biophysical Journal*; **74** (1): 436–43. (cited on pages 100, 110 und 111)

(96) **Koster, M., Bitter, W., de Cock, H., Allaoui, A., Cornelis, G. R. and Tommassen, J.** (1997); The outer membrane component, YscC, of the Yop secretion machinery of *Yersinia enterocolitica* forms a ring-shaped multimeric complex; *Molecular Microbiology*; **26** (4): 789–97. (cited on page 11)

(97) **Krantz, B. A., Melnyk, R. A., Zhang, S., Juris, S. J., Lacy, D. B., Wu, Z., Finkelstein, A. and Collier, R. J.** (2005); A phenylalanine clamp catalyzes protein translocation through the anthrax toxin pore; *Science*; **309** (5735): 777–81. (cited on pages 81, 83 und 147)

(98) **Kubori, T., Matsushima, Y., Nakamura, D., Uralil, J., Lara-Tejero, M., Sukhan, A., Galán, J. E. and Aizawa, S. I.** (1998); Supramolecular structure of the *Salmonella typhimurium* type III protein secretion system; *Science*; **280** (5363): 602–5. (cited on pages 11 und 63)

(99) **Kubori, T., Shimamoto, N., Yamaguchi, S., Namba, K. and Aizawa, S.** (1992); Morphological pathway of flagellar assembly in *Salmonella typhimurium*; *Journal of Molecular Biology*; **226** (2): 433–46. (cited on page 32)

(100) **Kubori, T., Sukhan, A., Aizawa, S. I. and Galán, J. E.** (2000); Molecular characterization and assembly of the needle complex of the *Salmonella typhimurium* type III protein secretion system; *Proc Natl Acad Sci USA*; **97** (18): 10,225–30. (cited on pages 11 und 13)

(101) **Kubori, T., Yamaguchi, S. and Aizawa, S.** (1997); Assembly of the switch complex onto the MS ring complex of *Salmonella typhimurium* does not require any other flagellar proteins; *Journal of Bacteriology*; **179** (3): 813–7. (cited on page 2)

(102) **Kugelberg, E., Kofoid, E., Reams, A. B., Andersson, D. I. and Roth, J. R.** (2006); Multiple pathways of selected gene amplification during adaptive mutation; *Proc Natl Acad Sci USA*; **103** (46): 17,319–24. (cited on page 36)

(103) **Kutsukake, K.** (1997); Autogenous and global control of the flagellar master operon, *flhD*, in *Salmonella typhimurium*; *Molecular and General Genetics*; **254** (4): 440–8. (cited on pages 7, 32, 42, 45 und 52)

(104) **Kutsukake, K., Minamino, T. and Yokoseki, T.** (1994); Isolation and characterization of FliK-independent flagellation mutants from *Salmonella typhimurium*; *Journal of Bacteriology*; **176** (24): 7625–9. (cited on pages 13 und 100)

(105) **Laemmli, U. K. and Favre, M.** (1973); Maturation of the head of bacteriophage T4. I. DNA packaging events.; *J Mol. Biol.*; **80** (4): 575–599. (cited on page 26)

(106) **Larsen, S. H., Adler, J., Gargus, J. J. and Hogg, R. W.** (1974); Chemomechanical coupling without ATP: the source of energy for motility and chemotaxis in bacteria; *Proc Natl Acad Sci USA*; **71** (4): 1239–1243. (cited on page 63)

(107) **Lee, C., Wozniak, C. E., Karlinsey, J. E. and Hughes, K. T.** (2007); Genomic screening for regulatory genes using the T-POP transposon; *Methods in Enzymology*; **421**: 159–67. (cited on pages 34, 57 und 90)

(108) **Lee, H. J. and Hughes, K. T.** (2006); Posttranscriptional control of the *Salmonella enterica* flagellar hook protein FlgE.; *Journal of Bacteriology*; **188** (9): 3308–3316. (cited on pages 22, 24, 26, 30, 33, 51, 54, 69, 89, 107 und 116)

(109) **Lehnen, D., Blumer, C., Polen, T., Wackwitz, B., Wendisch, V. F. and Unden, G.** (2002); LrhA as a new transcriptional key regulator of flagella, motility and chemotaxis genes in *Escherichia coli*; *Molecular Microbiology*; **45** (2): 521–32. (cited on pages 33, 41, 44, 52 und 53)

(110) **Libby, S. J., Goebel, W., Ludwig, A., Buchmeier, N., Bowe, F., Fang, F. C., Guiney, D. G., Songer, J. G. and Heffron, F.** (1994); A cytolysin encoded by *Salmonella* is required for survival within macrophages; *Proc Natl Acad Sci USA*; **91** (2): 489–93. (cited on page 32)

(111) **Liu, X. and Matsumura, P.** (1994); The FlhD/FlhC complex, a transcriptional activator of the *Escherichia coli* flagellar class II operons; *Journal of Bacteriology*; **176** (23): 7345–51. (cited on pages 7, 32 und 63)

(112) **Livak, K. J. and Schmittgen, T. D.** (2001); Analysis of relative gene expression data using real-time quantitative PCR and the $2^{-\Delta\Delta CT}$ Method; *Methods*; **25** (4): 402–8. (cited on pages 37, 47 und 58)

(113) **Lloyd, S. A., Tang, H., Wang, X., Billings, S. and Blair, D. F.** (1996); Torque generation in the flagellar motor of *Escherichia coli*: evidence of a direct role for FliG but not for FliM or FliN; *Journal of Bacteriology*; **178** (1): 223–31. (cited on pages 2, 5 und 118)

(114) **Macnab, R.** (1999); The bacterial flagellum: reversible rotary propellor and type III export apparatus; *Journal of Bacteriology.*; **181** (23): 7149–7153. (cited on page 63)

(115) **Macnab, R.** (2003); How bacteria assemble flagella; *Annual Review of Microbiology*; **57**: 77–100. (cited on pages 1, 5, 11, 18, 20, 30, 63, 98 und 122)

(116) **Macnab, R. M.**; Flagella and motility.; vol. 1 (Neidhardt, F.C., Curtiss, R., III, Ingraham, J.L., Lin, E.C.C., Low, K.B., Magasanik, B. et al. (eds). Washington, DC: ASM Press, 1996). (cited on page 98)

(117) **Macnab, R. M.** (2004); Type III flagellar protein export and flagellar assembly; *Biochim. Biophys. Acta.*; **1694** (1-3): 207–217. (cited on pages 11, 13, 63, 65 und 98)

(118) **Magdalena, J., Hachani, A., Chamekh, M., Jouihri, N., Gounon, P., Blocker, A. and Allaoui, A.** (2002); Spa32 regulates a switch in substrate specificity of the type III secreton of *Shigella flexneri* from needle components to Ipa proteins; *Journal of Bacteriology*; **184** (13): 3433–41. (cited on page 124)

(119) **Majdalani, N. and Gottesman, S.** (2005); The Rcs phosphorelay: a complex signal transduction system; *Annu Rev Microbiol*; **59**: 379–405. (cited on page 32)

(120) **Makishima, S., Komoriya, K., Yamaguchi, S. and Aizawa, S. I.** (2001); Length of the flagellar hook and the capacity of the type III export apparatus; *Science*; **291** (5512): 2411–3. (cited on pages 15, 99, 100, 107, 108, 109, 113, 114, 124 und 148)

(121) **Malakooti, J., Ely, B. and Matsumura, P.** (1994); Molecular characterization, nucleotide sequence, and expression of the *fliO*, *fliP*, *fliQ*, and *fliR* genes of *Escherichia coli*; *Journal of Bacteriology*; **176** (1): 189–97. (cited on pages 66 und 77)

(122) **Maloy, S. R. and Nunn, W. D.** (1981); Selection for loss of tetracycline resistance by *Escherichia coli.*; *Journal of Bacteriology.*; **145** (2): 1110–1111. (cited on page 84)

(123) **Manson, M., Tedesco, P., Berg, H., Harold, F. and der Drift, C. V.** (1977); A protonmotive force drives bacterial flagella; *Proc Natl Acad Sci USA*; **74** (7): 3060–3064. (cited on page 5)

(124) **Marlovits, T. C., Kubori, T., Sukhan, A., Thomas, D. R., Galán, J. E. and Unger, V. M.** (2004); Structural insights into the assembly of the type III secretion needle complex; *Science*; **306** (5698): 1040–2. (cited on pages 10, 11 und 63)

(125) **Mathews, M. A., Tang, H. L. and Blair, D. F.** (1998); Domain analysis of the FliM protein of *Escherichia coli*; *Journal of Bacteriology*; **180** (21): 5580–90. (cited on pages 118 und 119)

(126) **Matsuura, A., Shioi, J. I. and Imae, Y.** (1977); Motility in *Bacillus subtilis* driven by an artificial protonmotive force; *FEBS Letters.*; **82**: 187–190. (cited on page 5)

(127) **McMurry, J. L., Murphy, J. W. and González-Pedrajo, B.** (2006); The FliN-FliH interaction mediates localization of flagellar export ATPase FliI to the C ring complex; *Biochemistry*; **45** (39): 11,790–8. (cited on page 2)

(128) **Miller, J.**; Assay of β-Galactosidase (Cold Spring Harbor, New York: Cold Spring Harbor Laboratory, 1972). (cited on page 58)

(129) **Minamino, T., Chu, R., Yamaguchi, S. and Macnab, R. M.** (2000); Role of FliJ in flagellar protein export in *Salmonella*; *Journal of Bacteriology*; **182** (15): 4207–15. (cited on page 65)

(130) **Minamino, T., Ferris, H. U., Moriya, N., Kihara, M. and Namba, K.** (2006); Two parts of the T3S4 domain of the hook-length control protein FliK are essential for the substrate specificity switching of the flagellar type III export apparatus; *Journal of Molecular Biolology*; **362** (5): 1148–1158. (cited on pages 5, 7, 13, 15, 100, 110 und 124)

(131) **Minamino, T., González-Pedrajo, B., Yamaguchi, K., Aizawa, S. I. and Macnab, R. M.** (1999); FliK, the protein responsible for flagellar hook length control in *Salmonella*, is exported during hook assembly; *Molecular Microbiology*; **34** (2): 295–304. (cited on pages 15, 16, 101, 115, 124, 139 und 148)

(132) **Minamino, T., Iino, T. and Kutuskake, K.** (1994); Molecular characterization of the *Salmonella typhimurium flhB* operon and its protein products; *Journal of Bacteriology*; **176** (24): 7630–7. (cited on page 100)

(133) **Minamino, T., Imada, K. and Namba, K.** (2008); Mechanisms of type III protein export for bacterial flagellar assembly; *Molecular Biosystems*; **4** (11): 1105–15. (cited on page 9)

(134) **Minamino, T., Imada, K. and Namba, K.** (2008); Molecular motors of the bacterial flagella; *Current Opinion in Structural Biology*; **18** (6): 693–701. (cited on page 4)

(135) **Minamino, T., Imae, Y., Oosawa, F., Kobayashi, Y. and Oosawa, K.** (2003); Effect of intracellular pH on rotational speed of bacterial flagellar motors; *Journal of Bacteriology.*; **185** (4): 1190–1194. (cited on page 20)

(136) **Minamino, T. and Macnab, R. M.** (1999); Components of the *Salmonella* flagellar export apparatus and classification of export substrates; *Journal of Bacteriology.*; **181** (5): 1388–1394. (cited on pages 9, 30, 32, 63 und 65)

(137) **Minamino, T. and Macnab, R. M.** (2000); Domain structure of *Salmonella* FlhB, a flagellar export component responsible for substrate specificity switching; *Journal of Bacteriology*; **182** (17): 4906–14. (cited on pages 13, 82, 100 und 105)

(138) **Minamino, T. and Macnab, R. M.** (2000); FliH, a soluble component of the type III flagellar export apparatus of *Salmonella*, forms a complex with FliI and inhibits its ATPase activity; *Molecular Microbiology*; **37** (6): 1494–503. (cited on pages 9, 22 und 65)

(139) **Minamino, T., Moriya, N., Hirano, T., Hughes, K. and Namba, K.** (2009); Interaction of FliK with the bacterial flagellar hook is required for efficient export specificity switching; *Molecular Microbiology*; **74** (1): 239–51. (cited on pages 15, 16, 101, 136 und 148)

(140) **Minamino, T. and Namba, K.** (2008); Distinct roles of the FliI ATPase and proton motive force in bacterial flagellar protein export; *Nature*; **451** (7177): 485. (cited on pages 2, 9, 13, 30, 38, 51, 65, 66, 69, 79 und 150)

(141) **Minamino, T. and Pugsley, A. P.** (2005); Measure for measure in the control of type III secretion hook and needle length; *Molecular Microbiology*; **56** (2): 303–8. (cited on pages 99, 101, 113 und 114)

(142) **Minamino, T., Saijo-Hamano, Y., Furukawa, Y., González-Pedrajo, B., Macnab, R. M. and Namba, K.** (2004); Domain organization and function of *Salmonella* FliK, a flagellar hook-length control protein; *Journal of Molecular Biology*; **341** (2): 491–502. (cited on page 15)

(143) **Minamino, T., Shimada, M., Okabe, M., Saijo-Hamano, Y., Imada, K., Kihara, M. and Namba, K.** (2010); Role of the C-terminal cytoplasmic domain of FlhA in bacterial flagellar type III protein export; *Journal of Bacteriology*; **192** (7): 1929–3. (cited on page 82)

(144) **Minamino, T., Yamaguchi, S. and Macnab, R. M.** (2000); Interaction between FliE and FlgB, a proximal rod component of the flagellar basal body of *Salmonella*; *Journal of Bacteriology.*; **182** (11): 3029–3036. (cited on page 5)

(145) **Moriya, N., Minamino, T., Hughes, K. T., Macnab, R. M. and Namba, K.** (2006); The type III flagellar export specificity switch is dependent on FliK ruler and a molecular clock; *Journal of Molecular Biolology*; **359** (2): 466–477. (cited on pages 15, 99, 102, 104, 105, 106, 113, 114, 115, 136, 139 und 148)

(146) **Morris, D. P., Roush, E. D., Thompson, J. W., Moseley, M. A., Murphy, J. W. and McMurry, J. L.** (2010); Kinetic characterization of

Salmonella FliK-FlhB interactions demonstrates complexity of the Type III secretion substrate-specificity switch; *Biochemistry*; **49** (30): 6386–93. (cited on page 139)

(147) **Morrissey, J. H.** (1981); Silver stain for proteins in polyacrylamide gels: a modified procedure with enhanced uniform sensitivity; *Analytical Biochemistry*; **117** (2): 307–10. (cited on page 115)

(148) **Mueller, C. A., Broz, P., Müller, S. A., Ringler, P., Erne-Brand, F., Sorg, I., Kuhn, M., Engel, A. and Cornelis, G. R.** (2005); The V-antigen of *Yersinia* forms a distinct structure at the tip of injectisome needles; *Science*; **310** (5748): 674–6. (cited on page 13)

(149) **Muramoto, K., Makishima, S., Aizawa, S. and Macnab, R. M.** (1999); Effect of hook subunit concentration on assembly and control of length of the flagellar hook of *Salmonella*; *Journal of Bacteriology*; **181** (18): 5808–13. (cited on pages 16, 115, 139 und 148)

(150) **Muramoto, K., Makishima, S., Aizawa, S. I. and Macnab, R. M.** (1998); Effect of cellular level of FliK on flagellar hook and filament assembly in *Salmonella typhimurium*; *Journal of Molecular Biology*; **277** (4): 871–82. (cited on pages 16, 115, 128, 139 und 148)

(151) **Namba, K. and Vonderviszt, F.** (1997); Molecular architecture of bacterial flagellum; *Quarterly Reviews of Biophysics*; **30** (1): 1–65. (cited on pages 1 und 2)

(152) **Ohnishi, K., Fan, F., Schoenhals, G. J., Kihara, M. and Macnab, R. M.** (1997); The FliO, FliP, FliQ, and FliR proteins of *Salmonella typhimurium*: putative components for flagellar assembly; *Journal of Bacteriology.*; **179** (19): 6092–6099. (cited on pages 66 und 77)

(153) **Ohnishi, K., Kutsukake, K., Suzuki, H. and Iino, T.** (1990); Gene *fliA* encodes an alternative σ factor specific for flagellar operons in *Salmonella typhimurium*; *Molecular and General Genetics*; **221** (2): 139–47. (cited on page 32)

(154) **Ohnishi, K., Ohto, Y., Aizawa, S., Macnab, R. M. and Iino, T.** (1994); FlgD is a scaffolding protein needed for flagellar hook assembly in *Salmonella typhimurium*; *Journal of Bacteriology*; **176** (8): 2272–81. (cited on page 2)

(155) **Park, S.-Y., Lowder, B., Bilwes, A. M., Blair, D. F. and Crane, B. R.** (2006); Structure of FliM provides insight into assembly of the switch complex in the bacterial flagella motor; *Proc Natl Acad Sci USA*; **103** (32): 11,886–91. (cited on page 149)

(156) **Parsot, C., Hamiaux, C. and Page, A.-L.** (2003); The various and varying roles of specific chaperones in type III secretion systems; *Curr Opin Microbiol*; **6** (1): 7–14. (cited on page 63)

(157) **Patterson-Delafield, J., Martinez, R. J., Stocker, B. A. and Yamaguchi, S.** (1973); A new *fla* gene in *Salmonella typhimurium–flaR–*and its mutant phenotype-superhooks; *Archives of Microbiology*; **90** (2): 107–20. (cited on pages 5, 13, 100, 110, 124 und 128)

(158) **Paul, K., Erhardt, M., Hirano, T., Blair, D. F. and Hughes, K. T.** (2008); Energy source of flagellar type III secretion; *Nature*; **451** (7177): 489–92. (cited on pages 2, 9, 13, 30, 31, 33, 38, 51, 65, 66, 69, 79, 88, 102 und 150)

(159) **Paul, K., Harmon, J. G. and Blair, D. F.** (2006); Mutational analysis of the flagellar rotor protein FliN: identification of surfaces important for flagellar assembly and switching; *Journal of Bacteriology*; **188** (14): 5240–8. (cited on pages 2, 65, 66, 79, 118 und 119)

(160) **Rappleye, C. A. and Roth, J. R.** (1997); A *Tn*10 derivative (T-POP) for isolation of insertions with conditional (tetracycline-dependent) phenotypes; *Journal of Bacteriology*; **179** (18): 5827–34. (cited on page 34)

(161) **Rosu, V. and Hughes, K. T.** (2006); σ^{28}-dependent transcription in *Salmonella enterica* is independent of flagellar shearing; *Journal of Bacteriology*; **188** (14): 5196–5203. (cited on pages 24 und 27)

(162) **Saijo-Hamano, Y., Imada, K., Minamino, T., Kihara, M., Shimada, M., Kitao, A. and Namba, K.** (2010); Structure of the cytoplasmic domain of FlhA and implication for flagellar type III protein export; *Molecular Microbiology*; **76** (1): 260–8. (cited on pages 82 und 147)

(163) **Saijo-Hamano, Y., Minamino, T., Macnab, R. M. and Namba, K.** (2004); Structural and functional analysis of the C-terminal cytoplasmic domain of FlhA, an integral membrane component of the type III flagellar protein export apparatus in Salmonella; *Journal of Molecular Biolology*; **343** (2): 457–66. (cited on page 82)

(164) **Saini, S., Brown, J. D., Aldridge, P. D. and Rao, C. V.** (2008); FliZ Is a posttranslational activator of $FlhD_4C_2$-dependent flagellar gene expression; *Journal of Bacteriology*; **190** (14): 4979–88. (cited on page 41)

(165) **Samatey, F., Imada, K., Nagashima, S., Vonderviszt, F., Kumasaka, T., Yamamoto, M. and Namba, K.** (2001); Structure of the bacterial flagellar protofilament and implications for a switch for supercoiling; *Nature*; **410** (6826): 331–7. (cited on page 149)

(166) **Samatey, F., Matsunami, H., Imada, K., Nagashima, S., Shaikh, T., Thomas, D., Chen, J., DeRosier, D., Kitao, A. and Namba, K.** (2004); Structure of the bacterial flagellar hook and implication for the molecular universal joint mechanism; *Nature*; **431** (7012): 1062–8. (cited on pages 98 und 149)

(167) **Samatey, F. A.**; Flagella structure (Norfolk: Caister Academic Press, 2009). (cited on page 63)

(168) **Sanderson, K. E. and Roth, J. R.** (1983); Linkage map of *Salmonella typhimurium*, Edition VI.; *Microbiol. Rev.*; **47** (3): 410–453. (cited on pages 54, 84, 115 und 140)

(169) **Sarkar, M. K., Paul, K. and Blair, D.** (2010); Chemotaxis signaling protein CheY binds to the rotor protein FliN to control the direction of flagellar rotation in *Escherichia coli*; *Proc Natl Acad Sci USA*; **107** (20): 9370–5. (cited on page 65)

(170) **Schlumberger, M. C., Müller, A. J., Ehrbar, K., Winnen, B., Duss, I., Stecher, B. and Hardt, W.-D.** (2005); Real-time imaging of type III secretion: *Salmonella* SipA injection into host cells; *Proc Natl Acad Sci USA*; **102** (35): 12,548–53. (cited on pages 9 und 145)

(171) **Shaikh, T. R., Thomas, D. R., Chen, J. Z., Samatey, F. A., Matsunami, H., Imada, K., Namba, K. and DeRosier, D. J.** (2005); A partial atomic structure for the flagellar hook of *Salmonella typhimurium*; *Proc Natl Acad Sci USA*; **102** (4): 1023–8. (cited on pages 16, 101, 139 und 149)

(172) **Shibata, S., Takahashi, N., Chevance, F. F. V., Karlinsey, J. E., Hughes, K. T. and Aizawa, S.-I.** (2007); FliK regulates flagellar hook length as an internal ruler; *Molecular Microbiology*; **64** (5): 1404–15. (cited on pages 15, 99, 101, 112, 113, 116, 122, 124, 132 und 148)

(173) **Silverman, M. and Simon, M.** (1974); Flagellar rotation and the mechanism of bacterial motility; *Nature*; **249** (452): 73–74. (cited on pages 1 und 63)

(174) **Simm, R., Remminghorst, U., Ahmad, I., Zakikhany, K. and Römling, U.** (2009); A role for the EAL-like protein STM1344 in regulation of CsgD expression and motility in *Salmonella enterica* serovar *Typhimurium*; *Journal of Bacteriology*; **191** (12): 3928–37. (cited on page 58)

(175) **Sorg, I., Wagner, S., Amstutz, M., Müller, S. A., Broz, P., Lussi, Y., Engel, A. and Cornelis, G. R.** (2007); YscU recognizes translocators as export substrates of the *Yersinia* injectisome; *EMBO Journal*; **26** (12): 3015–24. (cited on pages 122 und 124)

(176) **Soutourina, O., Kolb, A., Krin, E., Laurent-Winter, C., Rimsky, S., Danchin, A. and Bertin, P.** (1999); Multiple control of flagellum biosynthesis in *Escherichia coli*: role of H-NS protein and the cyclic AMP-catabolite activator protein complex in transcription of the *flhDC* master operon; *Journal of Bacteriology*; **181** (24): 7500–8. (cited on page 32)

(177) **Spaeth, K. E., Chen, Y.-S. and Valdivia, R. H.** (2009); The *Chlamydia* Type III Secretion System C-ring Engages a Chaperone-Effector Protein Complex; *PLoS Pathogens*; **5** (9): e1000,579. (cited on page 54)

(178) **Spory, A., Bosserhoff, A., von Rhein, C., Goebel, W. and Ludwig, A.** (2002); Differential regulation of multiple proteins of *Escherichia coli* and *Salmonella enterica* serovar *Typhimurium* by the transcriptional regulator SlyA; *Journal of Bacteriology*; **184** (13): 3549–59. (cited on pages 32, 41, 44, 52 und 53)

(179) **Stojiljkovic, I., Bäumler, A. J. and Hantke, K.** (1994); Fur regulon in gram-negative bacteria. Identification and characterization of new iron-regulated *Escherichia coli* genes by a Fur titration assay; *Journal of Molecular Biology*; **236** (2): 531–45. (cited on page 32)

(180) **Stolz, B. and Berg, H. C.** (1991); Evidence for interactions between MotA and MotB, torque-generating elements of the flagellar motor of *Escherichia coli*; *Journal of Bacteriology*; **173** (21): 7033–7. (cited on page 5)

(181) **Suzuki, T. and Komeda, Y.** (1981); Incomplete flagellar structures in *Escherichia coli* mutants; *Journal of Bacteriology*; **145** (2): 1036–41. (cited on page 66)

(182) **Suzuki, T., Murakami, T., Iino, R., Suzuki, J., Ono, S., Shirakihara, Y. and Yoshida, M.** (2003); F_0F_1-ATPase/synthase is geared to the synthesis mode by conformational rearrangement of ϵ subunit in response to proton motive force and ADP/ATP balance; *The Journal of Biological Chemistry*; **278** (47): 46,840–6. (cited on page 20)

(183) **Takahashi, N., Mizuno, S., Hirano, T., Chevance, F., Hughes, K. and Aizawa, S.** (2009); Autonomous and FliK-dependent length control of the flagellar rod in *Salmonella enterica*; *Journal of Bacteriology*; **191** (20): 6469–72. (cited on page 5)

(184) **Takaya, A., Matsui, M., Tomoyasu, T., Kaya, M. and Yamamoto, T.** (2006); The DnaK chaperone machinery converts the native $FlhD_2C_2$ heterotetramer into a functional transcriptional regulator of flagellar regulon expression in *Salmonella*; *Molecular Microbiology*; **59** (4): 1327–40. (cited on page 33)

(185) **Tampakaki, A., Fadouloglou, V., Gazi, A., Panopoulos, N. and Kokkinidis, M.** (2004); Conserved features of type III secretion; *Cellular Microbiology*; **6** (9): 805–16. (cited on page 11)

(186) **Tang, H., Braun, T. F. and Blair, D. F.** (1996); Motility protein complexes in the bacterial flagellar motor; *Journal of Molecular Biology*; **261** (2): 209–21. (cited on page 119)

(187) **Thomas, D., Morgan, D. G. and DeRosier, D. J.** (2001); Structures of bacterial flagellar motors from two FliF-FliG gene fusion mutants; *Journal of Bacteriology*; **183** (21): 6404–12. (cited on page 2)

(188) **Thomas, D. R., Francis, N. R., Xu, C. and DeRosier, D. J.** (2006); The three-dimensional structure of the flagellar rotor from a clockwise-locked mutant of *Salmonella enterica* serovar *Typhimurium*; *Journal of Bacteriology*; **188** (20): 7039–48. (cited on pages 100 und 149)

(189) **Toker, A. S. and Macnab, R. M.** (1997); Distinct regions of bacterial flagellar switch protein FliM interact with FliG, FliN and CheY; *Journal of Molecular Biology*; **273** (3): 623–34. (cited on page 2)

(190) **Tomoyasu, T., Takaya, A., Isogai, E. and Yamamoto, T.** (2003); Turnover of FlhD and FlhC, master regulator proteins for *Salmonella* flagellum biogenesis, by the ATP-dependent ClpXP protease; *Molecular Microbiology*; **48** (2): 443–52. (cited on pages 33 und 41)

(191) **Vandesompele, J., Preter, K. D., Pattyn, F., Poppe, B., Roy, N. V., Paepe, A. D. and Speleman, F.** (2002); Accurate normalization of real-time quantitative RT-PCR data by geometric averaging of multiple internal control genes; *Genome Biology*; **3** (7): research 0034.1–0034.11. (cited on pages 37, 47 und 58)

(192) **Vogler, A. P., Homma, M., Irikura, V. M. and Macnab, R. M.** (1991); *Salmonella typhimurium* mutants defective in flagellar filament regrowth and sequence similarity of FliI to F_0F_1, vacuolar, and archaebacterial ATPase subunits; *Journal of Bacteriology.*; **173** (11): 3564–3572. (cited on pages 18 und 63)

(193) **Wagner, S., Königsmaier, L., Lara-Tejero, M., Lefebre, M., Marlovits, T. C. and Galán, J. E.** (2010); Organization and coordinated assembly of the type III secretion export apparatus; *Proc Natl Acad Sci USA*; **107** (41): 17,745–50. (cited on page 11)

(194) **Wagner, S., Sorg, I., Degiacomi, M., Journet, L., Peraro, M. D. and Cornelis, G. R.** (2009); The helical content of the YscP molecular ruler determines the length of the *Yersinia* injectisome; *Molecular Microbiology*; **71** (3): 692–701. (cited on page 101)

(195) **Wagner, S., Stenta, M., Metzger, L. C., Peraro, M. D. and Cornelis, G. R.** (2010); Length control of the injectisome needle requires only one molecule of Yop secretion protein P (YscP); *Proc Natl Acad Sci USA*; **107** (31): 13,860–5. (cited on pages 15 und 139)

(196) **Wang, Q., Zhao, Y., McClelland, M. and Harshey, R. M.** (2007); The RcsCDB signaling system and swarming motility in *Salmonella enterica* serovar *Typhimurium*: dual regulation of flagellar and SPI-2 virulence genes; *Journal of Bacteriology*; **189** (23): 8447–57. (cited on pages 32, 41, 52 und 53)

(197) **Wang, S., Fleming, R. T., Westbrook, E. M., Matsumura, P. and McKay, D. B.** (2006); Structure of the *Escherichia coli* FlhDC complex, a

prokaryotic heteromeric regulator of transcription; *Journal of Molecular Biology*; **355** (4): 798–808. (cited on pages 5 und 32)

(198) **Waters, R. C., O'Toole, P. W. and Ryan, K. A.** (2007); The FliK protein and flagellar hook-length control; *Protein Science*; **16** (5): 769–80. (cited on page 5)

(199) **Wei, B. L., Brun-Zinkernagel, A. M., Simecka, J. W., Prüss, B. M., Babitzke, P. and Romeo, T.** (2001); Positive regulation of motility and *flhDC* expression by the RNA-binding protein CsrA of *Escherichia coli*; *Molecular Microbiology*; **40** (1): 245–56. (cited on page 33)

(200) **Wilharm, G., Lehmann, V., Krauss, K., Lehnert, B., Richter, S., Ruckdeschel, K., Heesemann, J. and Trulzsch, K.** (2004); *Yersinia enterocolitica* type III secretion depends on the proton motive force but not on the flagellar motor components MotA and MotB.; *Infection and Immunity*; **72** (7): 4004–4009. (cited on pages 13, 18, 20, 25, 65 und 145)

(201) **Williams, A. W., Yamaguchi, S., Togashi, F., Aizawa, S. I., Kawagishi, I. and Macnab, R. M.** (1996); Mutations in *fliK* and *flhB* affecting flagellar hook and filament assembly in *Salmonella typhimurium*; *Journal of Bacteriology*; **178** (10): 2960–70. (cited on pages 13, 82, 100 und 122)

(202) **Wozniak, C. E. and Hughes, K. T.** (2008); Genetic dissection of the consensus sequence for the class 2 and class 3 flagellar promoters; *Journal of Molecular Biology*; **379** (5): 936–52. (cited on pages 84 und 90)

(203) **Wozniak, C. E., Lee, C. and Hughes, K. T.** (2009); T-POP array identifies EcnR and PefI-SrgD as novel regulators of flagellar gene expression; *Journal of Bacteriology*; **191** (5): 1498–508. (cited on pages 7, 33, 41, 42, 52, 53, 54, 57 und 69)

(204) **Yamaguchi, S., Aizawa, S., Kihara, M., Isomura, M., Jones, C. J. and Macnab, R. M.** (1986); Genetic evidence for a switching and energy-transducing complex in the flagellar motor of *Salmonella typhimurium*; *Journal of Bacteriology*; **168** (3): 1172–9. (cited on page 65)

(205) **Yamaguchi, S., Fujita, H., Ishihara, A., Aizawa, S. and Macnab, R. M.** (1986); Subdivision of flagellar genes of *Salmonella typhimurium* into regions responsible for assembly, rotation, and switching; *Journal of Bacteriology*; **166** (1): 187–93. (cited on page 65)

(206) **Yamamoto, S. and Kutsukake, K.** (2006); FliT acts as an anti-$FlhD_2C_2$ factor in the transcriptional control of the flagellar regulon in *Salmonella enterica* serovar *Typhimurium*; *Journal of Bacteriology*; **188** (18): 6703–8. (cited on pages 7, 41 und 69)

(207) **Yanagihara, S., Iyoda, S., Ohnishi, K., Iino, T. and Kutsukake, K.** (1999); Structure and transcriptional control of the flagellar master operon of *Salmonella typhimurium*; *Genes & Genetic Systems*; **74** (3): 105–11. (cited on pages 32 und 46)

(208) **Yonekura, K., Maki, S., Morgan, D., DeRosier, D., Vonderviszt, F., Imada, K. and Namba, K.** (2000); The bacterial flagellar cap as the rotary promoter of flagellin self-assembly.; *Science*; **290** (5499): 2148–2152. (cited on page 5)

(209) **Yonekura, K., Maki-Yonekura, S. and Namba, K.** (2003); Complete atomic model of the bacterial flagellar filament by electron cryomicroscopy.; *Nature*; **424** (6949): 643–650. (cited on pages 2, 98, 101 und 149)

(210) **Zarivach, R., Deng, W., Vuckovic, M., Felise, H. B., Nguyen, H. V., Miller, S. I., Finlay, B. B. and Strynadka, N. C. J.** (2008); Structural analysis of the essential self-cleaving type III secretion proteins EscU and SpaS; *Nature*; **453** (7191): 124–7. (cited on page 110)

(211) **Zarivach, R., Vuckovic, M., Deng, W., Finlay, B. B. and Strynadka, N. C. J.** (2007); Structural analysis of a prototypical ATPase from the type III secretion system; *Nature Structural & Molecular Biology*; **14** (2): 131–7. (cited on page 13)

(212) **Zhang, X. and Bremer, H.** (1995); Control of the *Escherichia coli rrnB* P1 promoter strength by ppGpp; *The Journal of Biological Chemistry*; **270** (19): 11,181–9. (cited on page 58)

(213) **Zhao, R., Amsler, C. D., Matsumura, P. and Khan, S.** (1996); FliG and FliM distribution in the *Salmonella typhimurium* cell and flagellar basal bodies; *Journal of Bacteriology*; **178** (1): 258–65. (cited on page 2)

(214) **Zhao, R., Pathak, N., Jaffe, H., Reese, T. S. and Khan, S.** (1996); FliN is a major structural protein of the C-ring in the *Salmonella typhimurium* flagellar basal body; *Journal of Molecular Biology*; **261** (2): 195–208. (cited on page 2)

(215) **Zhu, K., González-Pedrajo, B. and Macnab, R. M.** (2002); Interactions among membrane and soluble components of the flagellar export apparatus of *Salmonella*; *Biochemistry*; **41** (30): 9516–24. (cited on page 82)

List of Abbreviations

aa	amino acid
Ab	antibodies
Amp, amp	ampicillin
Ap^R	ampicillin-resistant
Ap^S	ampicillin-sensitive
Ara	L-arabinose
ATP	adenosine-5'-triphosphate
Bla	β-lactamase
bp	base pair
C-terminal	carboxyl-terminal
CCCP	Carbonylcyanide *m*-chlorophenylhydrozone
cDNA	complementary DNA
Cm	Chloramphenicol
CTAB	hexadecyl-trimethylammonium bromide
DAPI	4',6-diamidino-2-phenylindole
DNA	deoxyribonucleic acid
DTT	1,4-Dithio-DL-threitol
EDTA	ethylenediamine-tetraaceticacid
EM	electron microscopy
FM-64	*N*-(3-triethylammoniumpropyl)-4-(6-(4-(diethylamino)phenyl) hexatrienyl)pyridinium dibromide
GFP	green fluorescent protein
GST	glutathione S-transferase
HA	hemagglutinin
HBB	hook-basal-body
HSP	heat-shock protein
IM	inner (cytoplasmic) membrane
IPTG	Isopropyl-β-D-thiogalactopyranoside
kDa	kilodaltons
LB	lysogeny broth
MIC	minimum inhibitory concentration
min	minutes
MOPS	3-(N-morpholino)propanesulfonic acid

mot	motility
mRNA	messenger ribonucleic acid
N-terminal	amino-terminal
o/n	overnight
o/p	over-expression
OD	optical density
OM	outer membrane
ONPG	*o*-nitrophenyl-β-D-Galactoside
P_{araBAD}	*araBAD* promoter
P_{tetA}	*tetA* promoter
PCR	polymerase chain reaction
PG	peptidoglycan
PMF, pmf	proton motive force
PPBS	peptone/protease-peptone/bile-salts
qPCR	quantitative PCR
RLU	relative light units
RNA	ribonucleic acid
SD, s.d.	standard deviation
SDS-PAGE	sodium-dodecyl-sulfate polyacrylamide gel electrophoresis
T3S	type III secretion
TB	tryptone broth
Tc	Tetracycline
TCA	trichloroacetic acid
TM	trans-membrane
w/v	weight/volume percentage solution
wt, WT	wildtype
X-Gal	5-Bromo-4-chloro-3-indolyl-β-D-galactopyranoside

List of amino acids

Alanine	Ala	A
Arginine	Arg	R
Asparagine	Asn	N
Aspartic acid	Asp	D
Cysteine	Cys	C
Glutamine	Gln	Q
Glutamic acid	Glu	E
Glycine	Gly	G
Histidine	His	H
Isoleucine	Ile	I
Leucine	Leu	L
Lysine	Lys	K
Methionine	Met	M
Phenylalanine	Phe	F
Proline	Pro	P
Serine	Ser	S
Threonine	Thr	T
Tryptophane	Trp	W
Tyrosine	Tyr	Y
Valine	Val	V

Declaration of Contributions

K. Paul†, **M. Erhardt**†, T. Hirano, D. F. Blair†[1], K. T. Hughes[1]. Energy source of flagellar type III secretion. (2008) *Nature* vol. 451 (7177) pp. 489-92

I designed and performed experiments, analyzed data and partly wrote the paper. Figure 1.2A-C and Figure 1.3B have been published in a modified form in my diploma thesis 'Genetic Structure and Function Analysis of the Conserved Integral Membrane Components (FliOPQR) of the Flagellar Type III Secretion Apparatus of *Salmonella enterica*' (20^{th} December, 2006)

M. Erhardt[1], K. T. Hughes. C-ring requirement in flagellar type III secretion is bypassed by FlhDC upregulation. (2010) *Molecular Microbiology* vol. 75 (2) pp. 376-393

I designed and performed experiments, analyzed data and wrote the paper.

M. Erhardt†, M. K. Sarkar†, K. Paul, T. Hirano, K. T. Hughes[1], D. F. Blair[1]. Genetic Dissection of the Bacterial Type III Secretion Apparatus Reveals Minimal Components Essential for Export. (2010) *in preparation*

I designed and performed experiments, analyzed data and partly wrote the paper.

M. Erhardt†, T. Hirano†, Y. Su, K. Paul, D. H. Wee, S. Mizuno, S.-I. Aizawa, K. T. Hughes[1]. The Role of the FliK Molecular Ruler in Hook-length Control in *Salmonella enterica*. (2010) *Molecular Microbiology* vol. 75 (5) pp. 1272-1284

I designed and performed experiments, analyzed data and partly wrote the paper.

M. Erhardt, H. M. Singer†, D. H. Wee†, J. P. Keener[1], K. T. Hughes[1]. An Infrequent Molecular Ruler Controls Flagellar Hook Length in *Salmonella enterica*. (2010) *in preparation*

I designed and performed experiments, analyzed data and wrote the paper.

---

†These authors contributed equally to this work

[1]Corresponding author